

INTERACTION OF LIGHTNING
WITH POWER DISTRIBUTION LINES

By

CARLOS T. MATA

A DISSERTATION PRESENTED TO THE GRADUATE SCHOOL
OF THE UNIVERSITY OF FLORIDA IN PARTIAL FULFILLMENT
OF THE REQUIREMENTS FOR THE DEGREE OF
DOCTOR OF PHILOSOPHY

UNIVERSITY OF FLORIDA

2000

Copyright 2000

by

Carlos T. Mata

To my wife Aixa, and my parents Angel and Teresa.

ACKNOWLEDGMENTS

The contents and results of this work would not have been possible without the help and guidance of Dr. V.A. Rakov and Dr. M.A. Uman, who kept me very busy with the research as well as correcting draft after draft of this dissertation. They certainly asked the most interesting questions, for some of which I have not found answers yet.

Thanks to Keith Rambo for always being there and providing anything that was needed for the experiments. Special thanks to Dr. D. Carroll for guiding me with the ATP/EMTP, and for those relaxing fishing days I needed so desperately while working on the experiments. I would also like to thank Dr. L. Vu-Quoc for introducing me to the world of L^AT_EX and Linux. Thanks to Dr. G. Bosman for introducing me to the lightning laboratory research group, and guiding me throughout my indescribable experience as a graduate student at UF.

The experimental part of this dissertation would not have been possible without the collaboration of many people among whom I should mention: Gena Bronsted, Asdrubal Mata, Alonso Guarisma, Rafael Sutil, and Michael Stapleton who worked summer after summer under the hot Camp Blanding sun, and to whom I give special thanks for sharing with me all those “wonderful” long summer days. I should thank also Angel G. Mata for virtually taking over my work at Blanding when I had to work on this manuscript. He did an excellent job conducting the experiments, working with the video records, and creating many figures presented in this document. Thanks go also to George Schnetzer for his technical help on designing, implementing, and

installing sensors on the test distribution lines.

I would like to thank my parents, family, and friends for their support, encouragement, and hope, and especially my wife for her “patience” during those long summer days I spent working at Blanding, and the long working nights I spent seated at my computer.

CONTENTS

| | |
|--|------|
| ACKNOWLEDGMENTS | iv |
| LIST OF TABLES | x |
| LIST OF FIGURES..... | xxix |
| ABSTRACT | xxxv |
| CHAPTERS | |
| 1 INTRODUCTION | 1 |
| 2 LITERATURE REVIEW | 5 |
| 2.1 Lightning..... | 5 |
| 2.1.1 Natural lightning | 5 |
| 2.1.2 Artificially-Initiated Lightning | 12 |
| 2.2 Lightning's Interaction with Power Systems | 16 |
| 2.2.1 Experimental Data | 16 |
| 2.2.2 Modeling | 20 |
| 3 EXPERIMENTAL FACILITIES | 22 |
| 3.1 Rocket Launcher..... | 26 |
| 3.2 Distribution Lines | 27 |
| 3.2.1 Grounding | 29 |
| 3.2.2 Arresters | 32 |
| 3.3 Instrumentation | 34 |
| 3.3.1 Sensors | 36 |
| 3.3.2 Voltage Attenuators | 41 |
| 3.3.3 Data Recording Equipment | 41 |
| 4 VOLTAGE MEASURING TECHNIQUES | 52 |
| 4.1 Conventional Measuring Techniques | 52 |
| 4.2 Magnetic-Flux-Compensated Voltage Divider | 56 |

| | | |
|------------|---|-----|
| 5 | REPRESENTATION OF SOURCE AND SYSTEM ELEMENTS IN EMTP | 62 |
| 5.1 | Lightning Current Model | 62 |
| 5.2 | Transmission Line Model | 64 |
| 5.3 | Arrester Models and Equivalent Circuits | 66 |
| 5.4 | Leads Connecting the Neutral to Ground Rods | 72 |
| 5.5 | Ground Rod Model | 73 |
| 6 | DATA PRESENTATION, ANALYSIS, AND MODELING | 77 |
| 6.1 | 1996 Experiments..... | 77 |
| 6.1.1 | Currents to Ground: Cases 1, 2 and 3 | 79 |
| 6.1.2 | Voltages Across the Arresters: Case 3 | 82 |
| 6.2 | 1999 Experiments..... | 82 |
| 6.2.1 | Flash UF-9904 | 84 |
| 6.2.2 | Flash UF-9911 | 86 |
| 6.2.3 | Flash UF-9912 | 86 |
| 6.2.4 | Flash UF-9914 | 87 |
| 6.2.5 | Flash UF-9915 | 88 |
| 6.2.6 | Flash UF-9916 | 88 |
| 6.2.7 | Summary of the 1999 Experiments | 90 |
| 6.3 | 2000 Experiments..... | 91 |
| 6.3.1 | Flash FPL0011 | 98 |
| 6.3.2 | Flash FPL0014 | 99 |
| 6.3.3 | Flash FPL0018 | 102 |
| 6.3.4 | Flash FPL0032 | 106 |
| 6.3.5 | Flash FPL0033 | 107 |
| 6.3.6 | Flash FPL0034 | 108 |
| 6.3.7 | Flash FPL0036 | 110 |
| 6.3.8 | Flash FPL0036, Data and EMTP Modeling | 114 |
| 6.3.9 | Flash FPL0037 | 129 |
| 6.3.10 | Summary of the 2000 Experiments | 135 |
| 7 | SUMMARY | 140 |
| 7.1 | 1996 Experiments..... | 140 |
| 7.2 | 1999 Experiments..... | 141 |
| 7.3 | 2000 Experiments..... | 141 |
| 8 | RECOMMENDATIONS FOR FUTURE RESEARCH | 149 |
| APPENDICES | | |
| A | MEASURING STATIONS ON POWER DISTRIBUTION LINES (DRAWINGS) | 151 |

| | |
|--|-----|
| B SENSORS | 162 |
| B.1 Voltage Dividers | 162 |
| B.1.1 Resistive Voltage Dividers | 162 |
| B.1.2 Mixed Dividers | 164 |
| B.2 Anti-Aliasing Filters | 166 |
| C CONFIGURATIONS AND INSTRUMENTATION SETTINGS | 169 |
| C.1 1999 Configurations | 169 |
| C.1.1 Configuration FPL-A-99 | 169 |
| C.1.2 Configuration FPL-B-99 | 170 |
| C.1.3 Configuration FPL-C-99 | 170 |
| C.1.4 Configuration FPL-D-99 | 170 |
| C.2 2000 Configurations | 171 |
| C.2.1 Configuration FPL-A-00 | 171 |
| C.2.2 Configuration FPL-B-00 | 172 |
| C.2.3 Configuration FPL-C-00 | 172 |
| D DESCRIPTION OF THE ELECTROMAGNETIC TRANSIENT PROGRAM (EMTP) | 203 |
| D.1 Lumped and Distributed Elements in EMTP | 203 |
| D.1.1 Resistor | 204 |
| D.1.2 Inductor | 204 |
| D.1.3 Capacitor | 205 |
| D.1.4 Lossless Transmission Line | 206 |
| D.2 Rigorous Frequency-Dependent Transmission Line Models | 208 |
| D.2.1 J. Marti Frequency-Dependent Transmission Line Model | 209 |
| D.2.2 Noda Frequency-Dependent Transmission Line Model | 215 |
| D.3 Type 1 Source | 218 |
| D.4 EMTP Algorithm | 219 |
| E ATP FILES | 221 |
| E.1 Transmission Line Models | 221 |
| E.2 Arresters Equivalent Circuits | 224 |
| E.3 Leads Connecting the Neutral to Ground Rods | 232 |
| E.4 Ground Rods | 234 |
| F FREQUENCY RESPONSE OF GROUND RODS | 243 |
| G WAVEFORMS ARITHMETIC | 250 |
| H 1999 AND 2000 DATA PRESENTATION | 252 |

| | |
|--|-----|
| I CHARACTERISTICS OF CURRENT WAVEFORMS FOR THE 2000 EXPERIMENTS..... | 311 |
| BIBLIOGRAPHY..... | 376 |
| BIOGRAPHICAL SKETCH | 385 |

LIST OF TABLES

| | | |
|------|--|----|
| 3.1 | Measured grounding resistances of the horizontal and vertical line configurations. | 31 |
| 3.2 | V-I characteristic of the ABB type MVK 10-kV MOV arrester. | 32 |
| 3.3 | V-I characteristic of the Ohio Brass PDV 100 18-kV MOV arrester. | 33 |
| 3.4 | V-I characteristic of the Cooper Power Systems UltraSIL Housed VariSTAR Heavy Duty 18 kV arrester. | 34 |
| 3.5 | Parameters for the Pearson Electronics, Inc. current transformers. | 39 |
| 3.6 | Parameters for the T&M Research Products, Inc. CVRs (shunts). | 40 |
| 3.7 | Parameters of the voltage dividers (VD) used in the 1996, 1999, and 2000 experiments. | 41 |
| 3.8 | Typical settings for the four-channel Nicolet Pro 90 digitizing oscilloscopes. | 44 |
| 3.9 | Camera locations and objects in their fields of view for the summer of 1999 experiments (See Figure C.5). | 49 |
| 3.10 | Camera locations and objects in their fields of view for configuration FPL-A-00, Section C.2.1 (See Figure C.9 and C.10). | 50 |
| 3.11 | Camera locations and objects in their fields of view for the summer of 2000 experiments for configuration FPL-B-00, Section C.2.2 (See Figure C.11 and C.12). | 51 |
| 5.1 | V-I characteristics of A_0 and A_1 | 69 |
| 6.1 | Summary of launches and strikes to the horizontal framing configuration distribution line during the months of August and September of 1999. | 83 |
| 6.2 | Summary of the 1999 experiments. | 92 |

| | | |
|------|---|-----|
| 6.3 | Summary of launches and strikes to the horizontal framing configuration distribution line during July of 2000. | 93 |
| 6.4 | Summary of launches and strikes to the horizontal and vertical framing configuration distribution line during August of 2000. | 94 |
| 6.5 | Parameters of strokes triggered at ICLRT during summer 2000 (a time window of 1 ms was used to calculate the charge). | 96 |
| 6.6 | Section numbers of Mata et al. [2000b] containing waveforms displayed on different time scales for Flash FPL0011. | 99 |
| 6.7 | Section numbers of Mata et al. [2000c] containing waveforms displayed on different time scales for Flash FPL0014. | 101 |
| 6.8 | Section numbers of Mata et al. [2000d] containing waveforms displayed on different time scales for Flash FPL0018. | 105 |
| 6.9 | Section numbers of Mata et al. [2000e] containing waveforms displayed on different time scales for Flash FPL0032. | 107 |
| 6.10 | Section numbers of Mata et al. [2000f] containing waveforms displayed on different time scales for Flash FPL0033. | 108 |
| 6.11 | Section numbers of Mata et al. [2000g] containing waveforms displayed on different time scales for Flash FPL0034. | 109 |
| 6.12 | Calculated dissipated arrester energy by the phase C arrester at pole 11 for the five strokes of flash FPL0036. Also shown are the arrester transferred charge and peak current. Value in parenthesis indicate the time window of integration. | 127 |
| 6.13 | Section numbers of Mata et al. [2000h] containing waveforms displayed on different time scales for Flash FPL0037. | 129 |
| 6.14 | Summary of the 2000 experiments. | 139 |
| B.1 | Measured frequency response of the anti-aliasing filters in volts for a 2-V input signal. | 167 |
| C.1 | Instrumentation settings for flash UF-9904; strike to Phase C of the horizontal configuration distribution line, mid-point between poles 9 and 10. | 175 |
| C.2 | Instrumentation settings for flashes UF-9911 and UF-9912; strike to Phase C of the horizontal configuration distribution line, mid-point between poles 9 and 10, no termination resistors. | 177 |

| | | |
|------|--|-----|
| C.3 | Instrumentation settings for flashes UF-9914 and UF-9915, strike to Phase <i>B</i> of the horizontal configuration distribution line with termination resistors and inductors; mid-point between poles 9 and 10. | 179 |
| C.4 | Instrumentation settings for flashes UF-9916 and UF-9917, strike to Phase <i>B</i> of the horizontal configuration distribution line with termination resistors and inductors; mid-point between poles 9 and 10. | 182 |
| C.5 | Instrumentation summary for flashes FPL0011 and FPL0014, strike to phase <i>C</i> of the horizontal configuration distribution line with high power termination resistors; mid-point between poles 9 and 10 (see also Table C.6) | 185 |
| C.6 | Instrumentation settings for flashes FPL0011 and FPL0014 (see also Table C.5 and Figure C.6). | 187 |
| C.7 | Instrumentation summary for flash FPL0018, strike to phase <i>C</i> of the horizontal configuration distribution line with high power termination resistors; mid-point between poles 9 and 10 (see also Table C.8) | 188 |
| C.8 | Instrumentation settings for flash FPL0018 (see also Table C.7 and Figure C.6). | 190 |
| C.9 | Instrumentation summary for flashes FPL0032, FPL0033, FPL0034, and FPL0036, strike to phase <i>C</i> of the horizontal configuration distribution line with high power termination resistors; mid-point between poles 9 and 10 | 191 |
| C.10 | Instrumentation settings for flashes FPL0032, FPL0033, FPL0034, and FPL0036 (see also Table C.9 and Figure C.6). | 193 |
| C.11 | Instrumentation summary for flash FPL0037, strike to phase <i>C</i> of the horizontal configuration distribution line with high power termination resistors; pole 9 (see also Table C.12) | 195 |
| C.12 | Instrumentation settings for flash FPL0037 (see also Table C.11 and Figure C.7). | 197 |
| I.1 | Peak current and charge transferred at different points in the system calculated at three different instants of time (100 μ s, 500 μ s, and 1 ms) for stroke 1 of flash FPL0011. | 312 |
| I.2 | Peak current and charge transferred at different points in the system calculated at three different instants of time (100 μ s, 500 μ s, and 1 ms) for stroke 2 of flash FPL0011. | 313 |

| | | |
|------|--|-----|
| I.3 | Peak current and charge transferred at different points in the system calculated at three different instants of time (100 μ s, 500 μ s, and 1 ms) for stroke 3 of flash FPL0011. | 314 |
| I.4 | Peak current and charge transferred at different points in the system calculated at three different instants of time (100 μ s, 500 μ s, and 1 ms) for stroke 4 of flash FPL0011. | 315 |
| I.5 | Peak current and charge transferred at different points in the system calculated at three different instants of time (100 μ s, 500 μ s, and 1 ms) for stroke 5 of flash FPL0011. | 316 |
| I.6 | Peak current and charge transferred at different points in the system calculated at three different instants of time (100 μ s, 500 μ s, and 1 ms) for stroke 1 of flash FPL0014. | 317 |
| I.7 | Power spectrum density of measured current waveforms integrated over four different frequency ranges as a percentage of its power spectrum density integrated over the bandwidth of the measurement for stroke 1 of flash FPL0014. | 318 |
| I.8 | Peak current and charge transferred at different points in the system calculated at three different instants of time (100 μ s, 500 μ s, and 1 ms) for stroke 2 of flash FPL0014. | 319 |
| I.9 | Power spectrum density of measured current waveforms integrated over four different frequency ranges as a percentage of its power spectrum density integrated over the bandwidth of the measurement for stroke 2 of flash FPL0014. | 320 |
| I.10 | Peak current and charge transferred at different points in the system calculated at three different instants of time (100 μ s, 500 μ s, and 1 ms) for stroke 3 of flash FPL0014. | 321 |
| I.11 | Power spectrum density of measured current waveforms integrated over four different frequency ranges as a percentage of its power spectrum density integrated over the bandwidth of the measurement for stroke 3 of flash FPL0014. | 322 |
| I.12 | Peak current and charge transferred at different points in the system calculated at three different instants of time (100 μ s, 500 μ s, and 1 ms) for stroke 1 of flash FPL0018. | 323 |

| | | |
|------|---|-----|
| I.13 | Power spectrum density of measured current waveforms integrated over four different frequency ranges as a percentage of its power spectrum density integrated over the bandwidth of the measurement for stroke 1 of flash FPL0018. | 324 |
| I.14 | Peak current and charge transferred at different points in the system calculated at three different instants of time (100 μ s, 500 μ s, and 1 ms) for stroke 2 of flash FPL0018. | 325 |
| I.15 | Power spectrum density of measured current waveforms integrated over four different frequency ranges as a percentage of its power spectrum density integrated over the bandwidth of the measurement for stroke 2 of flash FPL0018. | 326 |
| I.16 | Peak current and charge transferred at different points in the system calculated at three different instants of time (100 μ s, 500 μ s, and 1 ms) for stroke 3 of flash FPL0018. | 327 |
| I.17 | Power spectrum density of measured current waveforms integrated over four different frequency ranges as a percentage of its power spectrum density integrated over the bandwidth of the measurement for stroke 3 of flash FPL0018. | 329 |
| I.18 | Peak current and charge transferred at different points in the system calculated at three different instants of time (100 μ s, 500 μ s, and 1 ms) for stroke 4 of flash FPL0018. | 330 |
| I.19 | Power spectrum density of measured current waveforms integrated over four different frequency ranges as a percentage of its power spectrum density integrated over the bandwidth of the measurement for stroke 4 of flash FPL0018. | 331 |
| I.20 | Peak current and charge transferred at different points in the system calculated at three different instants of time (100 μ s, 500 μ s, and 1 ms) for stroke 5 of flash FPL0018. | 332 |
| I.21 | Power spectrum density of measured current waveforms integrated over four different frequency ranges as a percentage of its power spectrum density integrated over the bandwidth of the measurement for stroke 5 of flash FPL0018. | 334 |
| I.22 | Peak current and charge transferred at different points in the system calculated at three different instants of time (100 μ s, 500 μ s, and 1 ms) for stroke 6 of flash FPL0018. | 335 |

| | | |
|------|---|-----|
| I.23 | Power spectrum density of measured current waveforms integrated over four different frequency ranges as a percentage of its power spectrum density integrated over the bandwidth of the measurement for stroke 6 of flash FPL0018. | 336 |
| I.24 | Peak current and charge transferred at different points in the system calculated at three different instants of time (100 μ s, 500 μ s, and 1 ms) for stroke 1 of flash FPL0032. | 337 |
| I.25 | Peak current and charge transferred at different points in the system calculated at three different instants of time (100 μ s, 500 μ s, and 1 ms) for stroke 2 of flash FPL0032. | 339 |
| I.26 | Peak current and charge transferred at different points in the system calculated at three different instants of time (100 μ s, 500 μ s, and 1 ms) for stroke 3 of flash FPL0032. | 340 |
| I.27 | Peak current and charge transferred at different points in the system calculated at three different instants of time (100 μ s, 500 μ s, and 1 ms) for stroke 4 of flash FPL0032. | 341 |
| I.28 | Peak current and charge transferred at different points in the system calculated at three different instants of time (100 μ s, 500 μ s, and 1 ms) for stroke 5 of flash FPL0032. | 342 |
| I.29 | Peak current and charge transferred at different points in the system calculated at three different instants of time (100 μ s, 500 μ s, and 1 ms) for stroke 6 of flash FPL0032. | 343 |
| I.30 | Peak current and charge transferred at different points in the system calculated at three different instants of time (100 μ s, 500 μ s, and 1 ms) for stroke 7 of flash FPL0032. | 344 |
| I.31 | Peak current and charge transferred at different points in the system calculated at three different instants of time (100 μ s, 500 μ s, and 1 ms) for stroke 1 of flash FPL0033. | 345 |
| I.32 | Peak current and charge transferred at different points in the system calculated at three different instants of time (100 μ s, 500 μ s, and 1 ms) for stroke 1 of flash FPL0034. | 346 |
| I.33 | Power spectrum density of measured current waveforms integrated over four different frequency ranges as a percentage of its power spectrum density integrated over the bandwidth of the measurement for stroke 1 of flash FPL0034. | 347 |

| | |
|--|-----|
| I.34 Peak current and charge transferred at different points in the system calculated at three different instants of time (100 μ s, 500 μ s, and 1 ms) for stroke 2 of flash FPL0034. | 348 |
| I.35 Power spectrum density of measured current waveforms integrated over four different frequency ranges as a percentage of its power spectrum density integrated over the bandwidth of the measurement for stroke 2 of flash FPL0034. | 349 |
| I.36 Peak current and charge transferred at different points in the system calculated at three different instants of time (100 μ s, 500 μ s, and 1 ms) for stroke 3 of flash FPL0034. | 350 |
| I.37 Power spectrum density of measured current waveforms integrated over four different frequency ranges as a percentage of its power spectrum density integrated over the bandwidth of the measurement for stroke 3 of flash FPL0034. | 352 |
| I.38 Peak current and charge transferred at different points in the system calculated at three different instants of time (100 μ s, 500 μ s, and 1 ms) for stroke 4 of flash FPL0034. | 353 |
| I.39 Power spectrum density of measured current waveforms integrated over four different frequency ranges as a percentage of its power spectrum density integrated over the bandwidth of the measurement for stroke 4 of flash FPL0034. | 354 |
| I.40 Peak current and charge transferred at different points in the system calculated at three different instants of time (100 μ s, 500 μ s, and 1 ms) for stroke 5 of flash FPL0034. | 355 |
| I.41 Power spectrum density of measured current waveforms integrated over four different frequency ranges as a percentage of its power spectrum density integrated over the bandwidth of the measurement for stroke 5 of flash FPL0034. | 358 |
| I.42 Peak current and charge transferred at different points in the system calculated at three different instants of time (100 μ s, 500 μ s, and 1 ms) for stroke 1 of flash FPL0036. | 359 |
| I.43 Power spectrum density of measured current waveforms integrated over four different frequency ranges as a percentage of its power spectrum density integrated over the bandwidth of the measurement for stroke 1 of flash FPL0036. | 360 |

| | |
|---|-----|
| I.44 Peak current and charge transferred at different points in the system calculated at three different instants of time (100 μ s, 500 μ s, and 1 ms) for stroke 2 of flash FPL0036. | 361 |
| I.45 Power spectrum density of measured current waveforms integrated over four different frequency ranges as a percentage of its power spectrum density integrated over the bandwidth of the measurement for stroke 2 of flash FPL0036. | 362 |
| I.46 Peak current and charge transferred at different points in the system calculated at three different instants of time (100 μ s, 500 μ s, and 1 ms) for stroke 3 of flash FPL0036. | 363 |
| I.47 Power spectrum density of measured current waveforms integrated over four different frequency ranges as a percentage of its power spectrum density integrated over the bandwidth of the measurement for stroke 3 of flash FPL0036. | 364 |
| I.48 Peak current and charge transferred at different points in the system calculated at three different instants of time (100 μ s, 500 μ s, and 1 ms) for stroke 4 of flash FPL0036. | 365 |
| I.49 Power spectrum density of measured current waveforms integrated over four different frequency ranges as a percentage of its power spectrum density integrated over the bandwidth of the measurement for stroke 4 of flash FPL0036. | 366 |
| I.50 Peak current and charge transferred at different points in the system calculated at three different instants of time (100 μ s, 500 μ s, and 1 ms) for stroke 5 of flash FPL0036. | 367 |
| I.51 Power spectrum density of measured current waveforms integrated over four different frequency ranges as a percentage of its power spectrum density integrated over the bandwidth of the measurement for stroke 5 of flash FPL0036. | 370 |
| I.52 Peak current and charge transferred at different points in the system calculated at three different instants of time (100 μ s, 500 μ s, and 1 ms) for stroke 1 of flash FPL0037. | 371 |
| I.53 Power spectrum density of measured current waveforms integrated over four different frequency ranges as a percentage of its power spectrum density integrated over the bandwidth of the measurement for stroke 1 of flash FPL0037. | 372 |

| | |
|--|-----|
| I.54 Peak current and charge transferred at different points in the system calculated at three different instants of time (100 μ s, 500 μ s, and 1 ms) for stroke 2 of flash FPL0037. | 373 |
| I.55 Power spectrum density of measured current waveforms integrated over four different frequency ranges as a percentage of its power spectrum density integrated over the bandwidth of the measurement for stroke 2 of flash FPL0037. | 374 |

LIST OF FIGURES

| | | |
|-----|--|----|
| 2.1 | General distribution of charge in a cumulonimbus (thunderstorm) cloud as determined in England. Arrows indicate air current flow. Adapted from Simpson and Scrase [1937]. | 6 |
| 2.2 | Schematic of the basic charge structure in the convective region of a thunderstorm (adapted from Stolzenburg et al. 1998). | 7 |
| 2.3 | The four categories of cloud-to-ground lightning depending on leader propagation direction and polarity of charge transferred to ground. Adapted from Berger and Vogelsanger [1966]. | 8 |
| 2.4 | Streak-camera photograph of a 12-return stroke flash. Increasing time goes from left to right. New Mexico Institute of Mining and Technology photograph. Adapted from Uman [1987]. | 10 |
| 2.5 | A photograph of lightning triggered at the ICLRT on Summer of 1999. | 12 |
| 2.6 | Sequence of events involved in the formation of the first return stroke in classical (grounded-wire) triggered lightning. Adapted from Rakov et al. [1998]. | 13 |
| 2.7 | Sequence of events involved in the formation of the first return stroke in altitude (ungrounded-wire) triggered lightning, (adapted from Rakov et al. [1998]). | 15 |
| 2.8 | Okushishiku test transmission line tower. Adapted from Matsumoto et al. [1996]. | 17 |
| 3.1 | Overview of the International Center for Lightning Research and Testing (ICLRT) at Camp Blanding, Florida, July 1996 (boldface indicates poles supporting arresters). | 23 |
| 3.2 | Overview of the Lightning Research and Testing (ICLRT) at Camp Blanding, Florida, July 1999 (boldface indicates poles supporting arresters). | 24 |

| | | |
|------|--|----|
| 3.3 | Overview of the International Center for Lightning Research and Testing (ICLRT) at Camp Blanding, Florida, July 2000 (boldface indicates poles supporting arresters). | 25 |
| 3.4 | Layout of the 568 concentric-lay-stranded aluminum conductor, aluminum-alloy reinforced. | 28 |
| 3.5 | Illustration of the fall-of-potential method for measuring apparent ground resistance. | 30 |
| 3.6 | V-I characteristic of the ABB type MVK 10-kV MOV arresters. | 32 |
| 3.7 | V-I characteristic of the Ohio Brass PDV 100 18-kV MOV arresters. | 33 |
| 3.8 | V-I characteristic of the Cooper Power Systems UltraSIL Housed VariSTAR Heavy Duty 18kV arrester. | 34 |
| 3.9 | Diagram of connections at Pole 5 of the horizontal configuration distribution line, summer 2000. | 35 |
| 3.10 | Connection diagram of the Pearson Electronics, Inc. Coils. | 40 |
| 3.11 | Connection diagram of the shunts. | 40 |
| 3.12 | Connection of sensors, ISOBE 3000, filters, and oscilloscopes. | 43 |
| 4.1 | a) Conventional connections of the voltage divider; b) Coaxial connection of the voltage divider (adapted from Schmidt et al. [1989]). | 53 |
| 4.2 | Different voltage waveforms across an arrester. | 54 |
| 4.3 | Principle of a differential voltage divider (adapted from Drilling et al. [1998]). | 56 |
| 4.4 | Magnetically Compensated Voltage Divider. The direction of the arrows in voltages V_1 , V_2 , V_3 , and V_4 represents the polarity of the measurement. | 57 |
| 4.5 | a) Flux of \mathbf{B} through a surface S with a contour C ; b) Geometrical relations between the volume current density and the magnetic induction it produces. | 59 |
| 4.6 | Summing box configuration (resistors for summing four voltage signals) used in the Magnetic-Flux-Compensated Voltage Divider. | 60 |

| | | |
|-----|---|----|
| 5.1 | Processing of the measured lightning channel current waveform to eliminate quantization noise for subsequent use in the EMTP. The dotted line represents the measured current waveform, circles indicate manually-picked points that represents nodes to perform the cubic interpolation, and the solid line represents the interpolated waveform: a) 100 μ s time window, b) rising portion of the incident current, and c) decaying portion of the incident current. | 65 |
| 5.2 | Equivalent circuit developed by Schmidt et al. [1989]. | 66 |
| 5.3 | Frequency-dependent model proposed by IEEE Working Group 3.4.11 [1992]..... | 67 |
| 5.4 | Simplified frequency-dependent model proposed by Pinceti and Giannettini [1999]. | 68 |
| 5.5 | Induced voltage in the measuring loop when measuring the voltage across an arrester. | 70 |
| 5.6 | Calculation of C and L to be used in the circuit model for downleads. | 73 |
| 5.7 | Calculated C and L for a downlead of 6 m composed of 20 sections. The total equivalent C and L are $\sum_{i=1}^n C(i) = 49.94 \text{ pF}$ and $\sum_{i=1}^n L(i) = 8.21 \mu\text{H}$ | 74 |
| 5.8 | Distributed-circuit model of ground rods: a) Schematic representation of current flow and magnetic field lines; b) Equivalent circuit of the ground rod shown in a), where n represents the number of sections. Adapted from Imece et al. [1996]. | 75 |
| 6.1 | ATP/MATLAB minimization algorithm to estimate optimum grounding resistances. | 78 |
| 6.2 | Current to ground at pole 1 versus time displayed on a 100- μ s scale, for flash 9621. | 79 |
| 6.3 | Current to ground at pole 9 versus time displayed on a 100- μ s scale, for flash 9621. | 79 |
| 6.4 | Current to ground at pole 10 versus time displayed on a 100- μ s scale, for flash 9621. | 80 |
| 6.5 | Current to ground at pole 15 versus time displayed on a 100- μ s scale, for flash 9621. | 80 |
| 6.6 | Voltage across the arrester at pole 9 displayed on a 100- μ s scale, for flash 9621. | 81 |

| | | |
|------|--|-----|
| 6.7 | Voltage across the arrester at pole 9 displayed on a 10- μ s scale, for flash 9621. | 81 |
| 6.8 | Event UF-9911 on a 1.25 s time scale (data taken from the Magnetic Tape Recorder) a) Total lightning current [I_i]; b) Voltage across arrester of phase B at pole 8 [V_{BNS}]. | 85 |
| 6.9 | Event UF-9916 on a 1.25 s time scale (data taken from the Magnetic Tape Recorder) a) Total lightning current [I_i]; b) Voltage across arrester of phase B at pole 8 [V_{BNS}]. | 89 |
| 6.10 | Measured peak current to ground for strokes 1 and 3 (in ascending order from left to right) of flash FPL0014 (See Tables I.6 and I.10). Lightning strike point is between poles 9 and 10. | 100 |
| 6.11 | Percentage of total charge transferred to ground at different poles, calculated at three different instants of time (100 μ s, 500 μ s, and 1 ms from the beginning of the return stroke), for stroke 1 of flash FPL0014 (See Table I.6). Lightning strike point is between poles 9 and 10. | 103 |
| 6.12 | Percentage of total charge transferred to ground at different poles, calculated at three different instants of time (100 μ s, 500 μ s, and 1 ms from the beginning of the return stroke), for stroke 2 of flash FPL0014 (See Table I.8). Lightning strike point is between poles 9 and 10. | 103 |
| 6.13 | Percentage of total charge transferred to ground at different poles, calculated at three different instants of time (100 μ s, 500 μ s, and 1 ms from the beginning of the return stroke), for stroke 3 of flash FPL0014 (See Table I.10). Lightning strike point is between poles 9 and 10. | 104 |
| 6.14 | Measured peak current to ground for strokes 1 through 6 (in ascending order from left to right) of flash FPL0018 (See Tables I.12, I.14, I.16, I.18, I.20, and I.22). Lightning strike point is between poles 9 and 10. | 104 |
| 6.15 | Measured peak current to ground for strokes 1 through 5 (in ascending order from left to right) of flash FPL0034 (See Tables I.32, I.34, I.36, I.38, and I.40). Lightning strike point is between poles 9 and 10. | 110 |
| 6.16 | Measured peak current through arresters for strokes 1 through 5 (in ascending order from left to right) of flash FPL0036 (See Tables I.42, I.44, I.46, I.48, and I.50). Lightning strike point is between poles 9 and 10. | 111 |
| 6.17 | Measured peak current to ground for strokes 1 through 5 (in ascending order from left to right) of flash FPL0036 (See Tables I.42, I.44, I.46, I.48, and I.50). Lightning strike point is between poles 9 and 10. | 111 |

| | |
|--|-----|
| 6.18 Flash FPL0036, stroke 1. | 112 |
| 6.19 Percentage of total charge transferred through phase C arresters at different poles and terminating resistor at pole 1, calculated at three different instants of time (100 μ s, 500 μ s, and 1 ms from the beginning of the return stroke), for stroke 1 of flash FPL0036 (See Table I.42). Lightning strike point is between poles 9 and 10. | 115 |
| 6.20 Percentage of total charge transferred to ground at different poles, calculated at three different instants of time (100 μ s, 500 μ s, and 1 ms from the beginning of the return stroke), for stroke 1 of flash FPL0036 (See Table I.42). Lightning strike point is between poles 9 and 10. | 115 |
| 6.21 Percentage of total charge transferred through phase C arresters at different poles and terminating resistor at pole 1, calculated at three different instants of time (100 μ s, 500 μ s, and 1 ms from the beginning of the return stroke), for stroke 4 of flash FPL0036 (See Table I.48). Lightning strike point is between poles 9 and 10. | 116 |
| 6.22 Percentage of total charge transferred to ground at different poles, calculated at three different instants of time (100 μ s, 500 μ s, and 1 ms from the beginning of the return stroke), for stroke 4 of flash FPL0036 (See Table I.48). Lightning strike point is between poles 9 and 10. | 116 |
| 6.23 Illustration of possible compensation on current waveforms when running the optimization algorithm. | 118 |
| 6.24 Current to ground at pole 1 (I_{G1}) versus time displayed on a 100- μ s scale, for stroke 1 of flash FPL0036. | 119 |
| 6.25 Current to ground at pole 2 (I_{G2}) versus time displayed on a 100- μ s scale, for stroke 1 of flash FPL0036. | 119 |
| 6.26 Current to ground at pole 5 (I_{G5}) versus time displayed on a 100- μ s scale, for stroke 1 of flash FPL0036. | 119 |
| 6.27 Current to ground at pole 8 (I_{G8}) versus time displayed on a 100- μ s scale, for stroke 1 of flash FPL0036. | 120 |
| 6.28 Current to ground at pole 11 (I_{G11}) versus time displayed on a 100- μ s scale, for stroke 1 of flash FPL0036. | 120 |
| 6.29 Current to ground at pole 14 (I_{G14}) versus time displayed on a 100- μ s scale, for stroke 1 of flash FPL0036. | 120 |
| 6.30 Current to ground at pole 8 (I_{G8}) versus time displayed on a 10- μ s scale, for stroke 1 of flash FPL0036. | 121 |

| | |
|---|-----|
| 6.31 Current to ground at pole 11 (I_{G11}) versus time displayed on a 10- μ s scale, for stroke 1 of flash FPL0036. | 121 |
| 6.32 Current to ground at pole 14 (I_{G14}) versus time displayed on a 10- μ s scale, for stroke 1 of flash FPL0036. | 121 |
| 6.33 Current to ground at pole 17 (I_{G17}) versus time displayed on a 100- μ s scale, for stroke 1 of flash FPL0036. | 122 |
| 6.34 Current to ground at pole 18 (I_{G18}) versus time displayed on a 100- μ s scale, for stroke 1 of flash FPL0036. | 122 |
| 6.35 Terminating resistor current at pole 1 (I_{CN1}) versus time displayed on a 100- μ s scale, for stroke 1 of flash FPL0036. | 123 |
| 6.36 Phase C arrester current at pole 2 (I_{CN2}) versus time displayed on a 100- μ s scale, for stroke 1 of flash FPL0036. | 123 |
| 6.37 Phase C arrester current at pole 5 (I_{CN5}) versus time displayed on a 100- μ s scale, for stroke 1 of flash FPL0036. | 123 |
| 6.38 Phase C arrester current at pole 11 (I_{CN11}) versus time displayed on a 100- μ s scale, for stroke 1 of flash FPL0036. | 125 |
| 6.39 Phase C arrester current at pole 14 (I_{CN14}) versus time displayed on a 100- μ s scale, for stroke 1 of flash FPL0036. | 125 |
| 6.40 Phase C arrester current at pole 17 (I_{CN17}) versus time displayed on a 100- μ s scale, for stroke 1 of flash FPL0036. | 125 |
| 6.41 Correlation between the arrester's dissipated energy and: a) the arrester transferred charge, and b) the arrester peak current. | 128 |
| 6.42 Flash FPL0037, stroke 1, displayed on a 1-ms scale (some current waveforms are saturated, see Table I.52). | 130 |
| 6.43 Measurement of return-stroke peak current, RS peak, and two measurements of M-component current, $\max(M)_1$ and $\max(M)_2$. The current waveform was recorded at the launcher (at the channel base). | 131 |
| 6.44 Measured and calculated conductances in percent of the total conductance of the grounding system. | 132 |
| 6.45 Measured stroke peak current, M component peak current $\max(M)_1$, and M component peak current $\max(M)_2$ for flash FPL0037 (See Figure 6.43). Arrows indicate saturated current waveforms (See Table I.52). Lightning strike point was at Pole 9, phase C. | 132 |

| | |
|---|-----|
| 6.46 Measured stroke peak current, M component peak current $\max(M)_1$, and M component peak current $\max(M)_2$ for flash FPL0037 in percent of their respective maximums at the channel base (See Figure 6.43). Arrows indicate saturated current waveforms (See Table I.52). Lightning strike point was at Pole 9, phase C. | 132 |
| 6.47 a) Incident lightning channel current and current through arrester at pole 11 (I_{LS} and I_{CN11S} , respectively), b) measured arrester voltage and current at pole 8 (V_{CN8S} and I_{CN8S}), c) computed energy for the arrester at pole 8 which failed during flash FPL0037. | 134 |
| 6.48 Measured peak current to ground in percent of the total lightning peak current as a function of distance from the strike point. Dots represent measured peak current to ground for all strokes triggered in 2000 with no severe saturation, circles indicate mean values, and the solid line is the exponential function that fits the mean values. | 136 |
| 7.1 Measured peak current to ground versus measured incident peak current for the 2000 experiment. | 145 |
| 7.2 Calculated charge transferred to ground at different poles versus calculated stroke charge, on a $100\mu s$ window, for the 2000 experiment. .. | 146 |
| 7.3 Calculated charge transferred to ground at different poles versus calculated stroke charge, on a $500\mu s$ window, for the 2000 experiment. .. | 147 |
| 7.4 Calculated charge transferred to ground at different poles versus calculated stroke charge, on a 1 ms window, for the 2000 experiment. ... | 148 |
| A.1 Conductor's layout and clearance distances of the distribution line with horizontal phase conductor arrangement. | 151 |
| A.2 Distribution line with horizontal configuration, distance between poles and location of arresters. | 152 |
| A.3 Horizontal and vertical line changes from 1999 to 2000 (bold-pole labels represent arrester poles). Distance between poles on the horizontal line are about 47 m on average, except for distances from Pole 12 to 13, 13 to 14, and 14 to 15 of the horizontal line which are 61 m, 72 m, and 65 m, respectively. Distance between poles on the vertical line are about 58 m on average. | 153 |
| A.4 Diagram of connections at Pole 1 of the horizontal configuration distribution line, summer 2000. | 154 |

| | | |
|------|--|-----|
| A.5 | Diagram of connections at Pole 2 of the horizontal configuration distribution line, summer 2000. | 155 |
| A.6 | Diagram of connections at Pole 8 of the horizontal configuration distribution line, summer 2000. | 156 |
| A.7 | Diagram of connections at Pole 9 of the horizontal configuration distribution line, summer 2000. | 157 |
| A.8 | Diagram of connections at Pole 11 of the horizontal configuration distribution line, summer 2000. | 158 |
| A.9 | Diagram of connections at Pole 14 of the horizontal configuration distribution line, summer 2000. | 159 |
| A.10 | Diagram of connections at Pole 17 of the horizontal configuration distribution line, summer 2000. | 160 |
| A.11 | Diagram of connections at Pole 18 of the horizontal configuration distribution line, summer 2000. | 161 |
| B.1 | High frequency circuit diagram of a resistive voltage divider | 163 |
| B.2 | Capacitive-Compensated Voltage Divider | 164 |
| B.3 | Circuit diagram of the 5 MHz anti-aliasing filters. | 167 |
| B.4 | Theoretical frequency response of the 5 MHz anti-aliasing filters. | 168 |
| C.1 | Locations of measurements for Flash UF-9904, strike to phase C of the horizontal configuration at the middle of the line, between poles 9 and 10. | 174 |
| C.2 | Locations of measurements for Flashes UF-9911 and UF-9912, strikes to phase C of the horizontal configuration at the middle of the line, between poles 9 and 10. | 176 |
| C.3 | Locations of measurements for Flashes UF-9914 and UF-9915, strikes to phase B of the horizontal configuration at the middle of the line, between poles 9 and 10. | 178 |
| C.4 | Locations of measurements for Flashes UF-9916 and UF-9917, strikes to phase B of the horizontal configuration at the middle of the line, between poles 9 and 10. | 181 |

| | |
|---|-----|
| C.5 Still and video camera locations for the summer of 1999 experiments. The directions of the arrows indicate the field of view of the devices (See Table 3.9). | 183 |
| C.6 Locations of measurements for flashes FPL0011 and FPL0014, strike to phase C of the horizontal configuration at the middle of the line, between poles 9 and 10. | 184 |
| C.7 Locations of measurements for flash FPL0037, strike to phase C of the horizontal configuration at pole 9. | 194 |
| C.8 Flash FPL0039 and FPL0040 to the vertical configuration distribution line, no measurements installed, strike to phase A at pole 8. | 198 |
| C.9 Video cameras locations for the summer of 2000 experiments for config- uration FPL-A-00, Section C.2.1. The directions of the arrows indicate the field of view of the devices (see Table 3.10). | 199 |
| C.10 Still cameras location for the summer of 2000 experiments for config- uration FPL-A-00, Section C.2.1. The directions of the arrows indicate the field of view of the devices (see Table 3.10). | 200 |
| C.11 Video cameras location for the summer of 2000 experiments for config- uration FPL-B-00, Section C.2.2 The directions of the arrows indicate the field of view of the devices (see Table 3.11). | 201 |
| C.12 Still cameras location for the summer of 2000 experiments for config- uration FPL-B-00, Section C.2.2. The directions of the arrows indicate the field of view of the devices (see Table 3.11). | 202 |
| D.1 Equivalent impedance network for: a) resistor; b) inductor; c) capacitor. | 205 |
| D.2 a) Lossless line of length d ; b) Equivalent impedance network (adapted from Dommel [1969]). | 208 |
| D.3 Equivalent circuit used for lossy transmission lines. | 208 |
| D.4 Frequency dependent line representation seen from line end k ; a) with $R - C$ network; b) with equivalent resistance after applying implicit integration (adapted from Dommel [1986]). | 213 |
| F.1 Frequency response of a vertically driven ground electrode of 24.4 m, with $\epsilon_r = 1$, and a low-frequency low-current resistance of 10Ω for different number of $R - L - C$ sections n (see Figure 5.8). | 243 |

| | | |
|------|--|-----|
| F.2 | Frequency response of a vertically driven ground electrode of 24.4 m, with $\epsilon_r = 1$, and a low-frequency low-current resistance of 100Ω for different number of $R - L - C$ sections n (see Figure 5.8). | 244 |
| F.3 | Frequency response of a vertically driven ground electrode of 24.4 m, with $\epsilon_r = 1$, and a low-frequency low-current resistance of 1000Ω for different number of $R - L - C$ sections n (see Figure 5.8). | 245 |
| F.4 | Frequency response of a vertically driven ground electrode of 24.4 m, with $\epsilon_r = 10$, and a low-frequency low-current resistance of 10Ω for different number of $R - L - C$ sections n (see Figure 5.8). | 245 |
| F.5 | Frequency response of a vertically driven ground electrode of 24.4 m, with $\epsilon_r = 10$, and a low-frequency low-current resistance of 100Ω for different number of $R - L - C$ sections n (see Figure 5.8). | 246 |
| F.6 | Frequency response of a vertically driven ground electrode of 24.4 m, with $\epsilon_r = 10$, and a low-frequency low-current resistance of 1000Ω for different number of $R - L - C$ sections n (see Figure 5.8). | 246 |
| F.7 | Frequency response of a vertically driven ground electrode of 2.4 m, with $\epsilon_r = 1$, and a low-frequency low-current resistance of 10Ω for different number of $R - L - C$ sections n (see Figure 5.8). | 247 |
| F.8 | Frequency response of a vertically driven ground electrode of 2.4 m, with $\epsilon_r = 1$, and a low-frequency low-current resistance of 100Ω for different number of $R - L - C$ sections n (see Figure 5.8). | 247 |
| F.9 | Frequency response of a vertically driven ground electrode of 2.4 m, with $\epsilon_r = 1$, and a low-frequency low-current resistance of 1000Ω for different number of $R - L - C$ sections n (see Figure 5.8). | 248 |
| F.10 | Frequency response of a vertically driven ground electrode of 2.4 m, with $\epsilon_r = 10$, and a low-frequency low-current resistance of 10Ω for different number of $R - L - C$ sections n (see Figure 5.8). | 248 |
| F.11 | Frequency response of a vertically driven ground electrode of 2.4 m, with $\epsilon_r = 10$, and a low-frequency low-current resistance of 100Ω for different number of $R - L - C$ sections n (see Figure 5.8). | 249 |
| F.12 | Frequency response of a vertically driven ground electrode of 2.4 m, with $\epsilon_r = 10$, and a low-frequency low-current resistance of 1000Ω for different number of $R - L - C$ sections n (see Figure 5.8). | 249 |
| G.1 | Re-sampling and interpolating digitally recorded data to sum or subtract waveforms. | 251 |

| | |
|---|-----|
| H.1 Total lightning current [I_i] for the first return stroke of flash UF-9916, displayed on three different time scales. a) 10 ms; b) 200 μ s; c) 50 μ s. | 254 |
| H.2 Phase current versus time waveforms at Pole 9 for the first return stroke of flash UF-9916, displayed on a 10 ms scale. a) Phase A current [I_{A9}]; b) Phase B current [I_{B9}]; c) Phase C current [I_{C9}]. | 255 |
| H.3 Phase current versus time waveforms at Pole 9 for the first return stroke of flash UF-9916, displayed on a 200 μ s scale. a) Phase A current [I_{A9}]; b) Phase B current [I_{B9}]; c) Phase C current [I_{C9}]. | 256 |
| H.4 Phase current versus time waveforms at Pole 9 for the first return stroke of flash UF-9916, displayed on a 50 μ s scale. a) Phase A current [I_{A9}]; b) Phase B current [I_{B9}]; c) Phase C current [I_{C9}]. | 257 |
| H.5 Phase current versus time waveforms at Pole 8 for the first return stroke of flash UF-9916, displayed on a 10 ms scale. a) Phase A current [I_{A8}]; b) Phase B current [I_{B8}]; c) Phase C current [I_{C8}]. | 258 |
| H.6 Phase current versus time waveforms at Pole 8 for the first return stroke of flash UF-9916, displayed on a 200 μ s scale. a) Phase A current [I_{A8}]; b) Phase B current [I_{B8}]; c) Phase C current [I_{C8}]. | 259 |
| H.7 Phase current versus time waveforms at Pole 8 for the first return stroke of flash UF-9916, displayed on a 50 μ s scale. a) Phase A current [I_{A8}]; b) Phase B current [I_{B8}]; c) Phase C current [I_{C8}]. | 260 |
| H.8 Phase A arrester at Pole 8 current and voltage versus time waveforms for the first return stroke of flash UF-9916, displayed on a 10 ms scale. a) Current through the arrester [I_{AN8}]; b) Voltage across the arrester [V_{AN8}]; | 261 |
| H.9 Phase A arrester at Pole 8 current and voltage versus time waveforms for the first return stroke of flash UF-9916, displayed on a 200 μ s scale. a) Current through the arrester [I_{AN8}]; b) Voltage across the arrester [V_{AN8}]; | 262 |
| H.10 Phase A arrester at Pole 8 current and voltage versus time waveforms for the first return stroke of flash UF-9916, displayed on a 50 μ s scale. a) Current through the arrester [I_{AN8}]; b) Voltage across the arrester [V_{AN8}]; | 263 |
| H.11 Phase B arrester at Pole 8 current and voltage versus time waveforms for the first return stroke of flash UF-9916, displayed on a 10 ms scale. a) Current through the arrester [I_{BN8}]; b) Voltage across the arrester [V_{BN8}]; | 264 |

| | |
|--|-----|
| H.12 Phase B arrester at Pole 8 current and voltage versus time waveforms for the first return stroke of flash UF-9916, displayed on a $200\ \mu s$ scale. a) Current through the arrester [I_{BNS}]; b) Voltage across the arrester [V_{BNS}]; | 265 |
| H.13 Phase B arrester at Pole 8 current and voltage versus time waveforms for the first return stroke of flash UF-9916, displayed on a $50\ \mu s$ scale. a) Current through the arrester [I_{BNS}]; b) Voltage across the arrester [V_{BNS}]; | 266 |
| H.14 Phase C arrester at Pole 8 current and voltage versus time waveforms for the first return stroke of flash UF-9916, displayed on a 10 ms scale. a) Current through the arrester [I_{CNS}]; b) Voltage across the arrester [V_{CNS}]; | 267 |
| H.15 Phase C arrester at Pole 8 current and voltage versus time waveforms for the first return stroke of flash UF-9916, displayed on a $200\ \mu s$ scale. a) Current through the arrester [I_{CNS}]; b) Voltage across the arrester [V_{CNS}]; | 268 |
| H.16 Phase C arrester at Pole 8 current and voltage versus time waveforms for the first return stroke of flash UF-9916, displayed on a $50\ \mu s$ scale. a) Current through the arrester [I_{CNS}]; b) Voltage across the arrester [V_{CNS}]; | 269 |
| H.17 Phase to phase voltage versus time waveform at Pole 8 [V_{BAS}] for the first return stroke of Flash UF-9916, displayed on different time windows. a) 10 ms; b) $200\ \mu s$; c) $50\ \mu s$ | 270 |
| H.18 Phase current versus time waveforms at Pole 7 for the first return stroke of flash UF-9916, displayed on a 10 ms scale. a) Phase A current [I_{A7}]; b) Phase B current [I_{B7}]; c) Phase C current [I_{C7}]. | 271 |
| H.19 Phase current versus time waveforms at Pole 7 for the first return stroke of flash UF-9916, displayed on a $200\ \mu s$ scale. a) Phase A current [I_{A7}]; b) Phase B current [I_{B7}]; c) Phase C current [I_{C7}]. | 272 |
| H.20 Phase current versus time waveforms at Pole 7 for the first return stroke of flash UF-9916, displayed on a $50\ \mu s$ scale. a) Phase A current [I_{A7}]; b) Phase B current [I_{B7}]; c) Phase C current [I_{C7}]. | 273 |
| H.21 Currents to ground versus time waveforms at Poles 7, 8, 11, and 12 for the first return stroke of Flash UF-9916, displayed on a 10 ms scale. a) Current to ground at pole 7 [I_{G7}]; b) Current to ground at pole 8 [I_{G8}]; c) Current to ground at pole 11 [I_{G11}]; d) Current to ground at pole 12 [I_{G12}]. | 274 |

| | |
|---|-----|
| H.22 Currents to ground versus time waveforms at Poles 7, 8, 11, and 12 for the first return stroke of Flash UF-9916, displayed on a $200\mu s$ scale. a) Current to ground at pole 7 [I_{G7}]; b) Current to ground at pole 8 [I_{G8}]; c) Current to ground at pole 11 [I_{G11}]; d) Current to ground at pole 12 [I_{G12}]. | 275 |
| H.23 Currents to ground versus time waveforms at Poles 7, 8, 11, and 12 for the first return stroke of Flash UF-9916, displayed on a $50\mu s$ scale. a) Current to ground at pole 7 [I_{G7}]; b) Current to ground at pole 8 [I_{G8}]; c) Current to ground at pole 11 [I_{G11}]; d) Current to ground at pole 12 [I_{G12}]. | 276 |
| H.24 Comparison of the sum of currents to ground ($\sum I_G = I_{G7} + I_{G8} + I_{G11} + I_{G12}$) and the total lightning current (I_i) for the first return stroke of Flash UF-9916, displayed on $200\mu s$ and $50\mu s$. The dashed line is the sum of currents to ground ($\sum I_G$) and the solid line is the lightning channel current. a) $200\mu s$; b) $50\mu s$; c) Percent difference between currents to ground and lightning channel current. | 277 |
| H.25 Comparison of computed difference between measured voltages (V_{BNS} and V_{ANS}) and measured voltage [V_{BA8}] for the first return stroke of Flash UF-9916, displayed in different time windows. The dashed line is the calculated voltage ($V_{BNS} - V_{ANS}$) that was obtained by subtracting the measurements of [V_{BNS}] and [V_{ANS}]. a) $200\mu s$. b) $50\mu s$. c) $20\mu s$. . | 278 |
| H.26 Flash FPL0011, stroke 1. | 279 |
| H.27 Flash FPL0011, stroke 2. | 280 |
| H.28 Flash FPL0011, stroke 3. | 281 |
| H.29 Flash FPL0011, stroke 4. | 282 |
| H.30 Flash FPL0011, stroke 5. | 283 |
| H.31 Flash FPL0014, stroke 1. | 284 |
| H.32 Flash FPL0014, stroke 2. | 285 |
| H.33 Flash FPL0014, stroke 3. | 286 |
| H.34 Flash FPL0018, stroke 1. | 287 |
| H.35 Flash FPL0018, stroke 2. | 288 |
| H.36 Flash FPL0018, stroke 3. | 289 |

| | |
|---|-----|
| H.37 Flash FPL0018, stroke 4 | 290 |
| H.38 Flash FPL0018, stroke 5 | 291 |
| H.39 Flash FPL0018, stroke 6 | 292 |
| H.40 Flash FPL0032, stroke 1 | 293 |
| H.41 Flash FPL0032, stroke 2 | 294 |
| H.42 Flash FPL0032, stroke 3 | 295 |
| H.43 Flash FPL0032, stroke 4 | 296 |
| H.44 Flash FPL0032, stroke 5 | 297 |
| H.45 Flash FPL0032, stroke 6 | 298 |
| H.46 Flash FPL0032, stroke 7 | 299 |
| H.47 Flash FPL0033, stroke 1 | 300 |
| H.48 Flash FPL0034, stroke 1 | 301 |
| H.49 Flash FPL0034, stroke 2 | 302 |
| H.50 Flash FPL0034, stroke 3 | 303 |
| H.51 Flash FPL0034, stroke 4 | 304 |
| H.52 Flash FPL0036, stroke 2 | 305 |
| H.53 Flash FPL0036, stroke 3 | 306 |
| H.54 Flash FPL0036, stroke 4 | 307 |
| H.55 Flash FPL0036, stroke 5 | 308 |
| H.56 Flash FPL0037, stroke 1 | 309 |
| H.57 Flash FPL0037, stroke 2 | 310 |
| I.1 Percentage of total charge transferred to ground at different poles, calculated at three different instants of time (100 μ s, 500 μ s, and 1 ms from the beginning of the return stroke), for stroke 1 of flash FPL0018 (See Table I.12). Lightning strike point is between poles 9 and 10. | 328 |

I.2 Percentage of total charge transferred to ground at different poles, calculated at three different instants of time (100 μ s, 500 μ s, and 1 ms from the beginning of the return stroke), for stroke 2 of flash FPL0018 (See Table I.14). Lightning strike point is between poles 9 and 10. ... 328

I.3 Percentage of total charge transferred to ground at different poles, calculated at three different instants of time (100 μ s, 500 μ s, and 1 ms from the beginning of the return stroke), for stroke 3 of flash FPL0018 (See Table I.16). Lightning strike point is between poles 9 and 10. ... 333

I.4 Percentage of total charge transferred to ground at different poles, calculated at three different instants of time (100 μ s, 500 μ s, and 1 ms from the beginning of the return stroke), for stroke 4 of flash FPL0018 (See Table I.18). Lightning strike point is between poles 9 and 10. ... 333

I.5 Percentage of total charge transferred to ground at different poles, calculated at three different instants of time (100 μ s, 500 μ s, and 1 ms from the beginning of the return stroke), for stroke 5 of flash FPL0018 (See Table I.20). Lightning strike point is between poles 9 and 10. ... 338

I.6 Percentage of total charge transferred to ground at different poles, calculated at three different instants of time (100 μ s, 500 μ s, and 1 ms from the beginning of the return stroke), for stroke 6 of flash FPL0018 (See Table I.22). Lightning strike point is between poles 9 and 10. ... 338

I.7 Percentage of total charge transferred to ground at different poles, calculated at three different instants of time (100 μ s, 500 μ s, and 1 ms from the beginning of the return stroke), for stroke 1 of flash FPL0034 (See Table I.32). Lightning strike point is between poles 9 and 10. ... 351

I.8 Percentage of total charge transferred to ground at different poles, calculated at three different instants of time (100 μ s, 500 μ s, and 1 ms from the beginning of the return stroke), for stroke 2 of flash FPL0034 (See Table I.34). Lightning strike point is between poles 9 and 10. ... 351

I.9 Percentage of total charge transferred to ground at different poles, calculated at three different instants of time (100 μ s, 500 μ s, and 1 ms from the beginning of the return stroke), for stroke 3 of flash FPL0034 (See Table I.36). Lightning strike point is between poles 9 and 10. ... 356

I.10 Percentage of total charge transferred to ground at different poles, calculated at three different instants of time (100 μ s, 500 μ s, and 1 ms from the beginning of the return stroke), for stroke 4 of flash FPL0034 (See Table I.38). Lightning strike point is between poles 9 and 10. ... 356

I.11 Percentage of total charge transferred to ground at different poles, calculated at three different instants of time (100 μ s, 500 μ s, and 1 ms from the beginning of the return stroke), for stroke 5 of flash FPL0034 (See Table I.40). Lightning strike point is between poles 9 and 10. ... 357

I.12 Percentage of total charge transferred to ground at different poles, calculated at three different instants of time (100 μ s, 500 μ s, and 1 ms from the beginning of the return stroke), for stroke 2 of flash FPL0036 (See Table I.44). Lightning strike point is between poles 9 and 10. ... 368

I.13 Percentage of total charge transferred to ground at different poles, calculated at three different instants of time (100 μ s, 500 μ s, and 1 ms from the beginning of the return stroke), for stroke 3 of flash FPL0036 (See Table I.46). Lightning strike point is between poles 9 and 10. ... 368

I.14 Percentage of total charge transferred to ground at different poles, calculated at three different instants of time (100 μ s, 500 μ s, and 1 ms from the beginning of the return stroke), for stroke 5 of flash FPL0036 (See Table I.50). Lightning strike point is between poles 9 and 10. ... 369

I.15 Percentage of total charge transferred to ground at different poles, calculated at three different instants of time (100 μ s, 500 μ s, and 1 ms from the beginning of the return stroke), for stroke 1 of flash FPL0037 (See Table I.52). Lightning strike point was at pole 9. 375

I.16 Percentage of total charge transferred to ground at different poles, calculated at three different instants of time (100 μ s, 500 μ s, and 1 ms from the beginning of the return stroke), for stroke 2 of flash FPL0037 (See Table I.54). Lightning strike point was at pole 9. 375

Abstract of Dissertation Presented to the Graduate School
of the University of Florida in Partial Fulfillment of the
Requirements for the Degree of Doctor of Philosophy

INTERACTION OF LIGHTNING
WITH POWER DISTRIBUTION LINES

By

Carlos T. Mata

December 2000

Chairman: Dr. Vladimir A. Rakov

Major Department: Electrical and Computer Engineering

Triggered-lightning experiments were conducted in 1996, 1999, and 2000 to study the responses of overhead power distribution lines to lightning at the International Center for Lightning Research and Testing (ICLRT) at Camp Blanding, Florida. The lightning was artificially initiated (triggered) from natural thunderclouds using the rocket-and-wire technique, and its current was directed to a phase conductor at mid-span or at a pole near the center of the line. Experimental results and associated EMTP modeling are presented in this dissertation for the following line configurations: 1) a two-conductor, 740-m overhead distribution line with 2 arrester stations in 1996; 2) a four-conductor, 245-m overhead distribution line with 2 arrester stations in 1999; and 3) a four-conductor, 829-m overhead distribution line with 6 arrester stations in 2000. The three-phase lines tested in 1999 and 2000 were standard designs of a major Florida power company. Lightning peak currents injected into the lines ranged from 7 to 57 kA. Voltages and currents were measured at various locations along the line.

Video and photographic cameras were used to image lightning channels and detect line flashovers.

The significant results of the research are 1) flashovers between conductors were observed, both accompanied and not accompanied by arrester failures, 2) an arrester failed on seven of eight direct lightning strikes to the line in 2000, 3) arcing between conductors may prevent failures of arresters connected to the struck phase, 3) the bulk of the lightning current flows from the struck phase to neutral through the arresters closest to the strike point, 4) the withstand energy of the arresters can be exceeded due to the contribution from multiple strokes and/or relatively low-level, long-lasting current components, 6) the distribution of charge transferred to ground among multiple neutral grounds, which is determined by low-frequency, low-current grounding resistances is different from the distribution of peak currents to ground, which is characterized by a rapid decrease of current with increasing distance from the strike point, 7) EMTP allows one to model the observed line behavior with reasonable accuracy, 8) overall, the standard lightning protection of the distribution lines tested does not appear to be adequate.

CHAPTER 1 INTRODUCTION

With the deregulation of the power industry, the ability to provide continuous, high quality electric power service has become increasingly important for the power utilities. With the increasing use of computers and sophisticated electronics in residences and industry, utility customers have become much less tolerant of service interruptions and outages. The importance of lightning research to the power industry becomes clear if we consider statements made and reports written on this subject. A Joint IEEE-EEI Committee studying outages on EHV lines stated, “lightning is the greatest single cause of outages . . . , accounting for about 26 % of the outages on 230 kV circuits and about 65 % of the outages on 345 kV” (IEEE-EEI [1967]). This conclusion was reached after analyzing data obtained over a 14-year period from 42 operating companies in the USA and Canada. In Japan, lightning is also a problem: “most transmission line outages in Japan are caused by lightning” (Motoyama et al. 1998). Over 50,000 fault reports on distribution lines were analyzed in the United Kingdom over a period of 14 years for circuits up to 33 kV, and it was found that 47 % of all these incidents were caused by lightning (Connor and Parkins 1966). The number of service interruptions due to lightning strikes is a significant fraction of the total number of interruptions experienced by power utilities in Florida, despite utility efforts to minimize outages due to lightning. More than 25 % of the outages in the Florida Power & Light (FPL) distribution system are attributed to lightning.

Lightning presents a problem for distribution lines because voltage surges from direct and nearby lightning can exceed the lines’ basic insulation level (BIL) resulting

in a flashover that is often sustained by the 60 Hz follow current, potentially leading to long-duration service interruptions. Additionally, lightning can damage distribution line equipment such as transformers, lightning arresters, and insulators. Over the years, Florida Power & Light (FPL) has used several different distribution-line designs. Although the lightning susceptibility of these distribution lines has been tested to some degree both in laboratory experiments and using computer models, “the lightning performance characteristics of these designs have not been determined to a high level of confidence” (I. Ares, FPL, Distribution Reliability Support Services).

There are a few places in the world where researchers are able to initiate (trigger) lightning, with the International Center for Lightning Research and Testing (ICLRT) at Camp Blanding, Florida, being the only such facility that is continuously operated for studying various aspects of lightning and its effects. This unique outdoor laboratory enables researchers to study *real electric system responses* to artificially initiated lightning from natural thunderstorms.

In the summer of 1996, in a project sponsored by the Electrical Power Research Institute (EPRI), a two-conductor experimental transmission line was subjected to triggered lightning, and its responses (current and voltages) were measured.

In the summer of 1999, a study sponsored by Florida Power and Light (FPL) began at the ICLRT. In this project, two FPL standard distribution-line framing configurations were built at the ICLRT, and experiments were performed to examine their responses to direct lightning strikes. One framing configuration was tested in the summer of 1999, and two more in the summer of 2000. The 2000 framing configurations were longer-versions of two framing configurations built in 1999.

The objectives of testing these distribution line configurations using triggered lightning are as follows:

- To determine the relative susceptibility of different line configurations to lightning-caused flashovers or other failures.

- To study the mechanism of lightning damage to distribution lines in order to improve their lightning withstanding capability.
- To determine the distribution of currents to ground through the multiple grounding electrodes from the neutral to earth at different distances from the strike point.
- To determine the distribution of the lightning channel current through lightning arresters connected between phase and neutral at different distances from the strike point.
- To *develop an EMTP-based¹ computer model* that can reproduce the field test results.
- To develop recommendations to improve existing framing configuration thereby minimizing the number of interruptions in the electric service of the utility company.

The primary experimental data for this dissertation were obtained during the summer of 2000, although data from previous experiments in 1996 and 1999 (Mata et al. 1998a, Fernandez et al. 1998, Mata et al. 1998b, Mata et al. 1999a, Mata et al. 1999b, Mata et al. 2000a, Rakov et al. 2000, Mata et al. 2000i) are presented as well.

The author of this dissertation, with the guidance of his faculty advisors, was in charge of the design, installation, and calibration of the measuring equipment on the distribution lines in 1999 and 2000. The author also wrote a series of computer-oscilloscope interface programs for data acquisition automation, control, plotting, and analysis of the acquired data.

¹The EMTP is a computer program designed to solve Electromagnetic transients in lumped and/or distributed circuits (Alternative Transient Program (ATP) Rule Book [1987-1998]).

A review of the pertinent literature on lightning and lightning interaction with power systems is presented in Chapter 2. In Chapter 3 we describe the experimental facility and experimental setup for the tests. In Chapter 4 we discuss conventional techniques used to measure voltage across arresters and the design of a novel *magnetic-flux-compensated voltage divider* used to reduce the influence of magnetic coupling to the measuring circuit. Modeling of transients using EMTP is presented in Chapter 5, and a comparison of model-predicted waveforms and acquired data is presented in Chapter 6.

CHAPTER 2 LITERATURE REVIEW

The literature reviewed in this chapter primarily concerns two subjects: (2.1) *lightning* and (2.2) *lightning's interaction with power systems*. The former includes a brief review of the processes involved in both natural lightning and lightning artificially-initiated using the rocket-and-wire technique. The latter includes a review of previous experiments concerned with lightning's interaction with power systems.

2.1 Lightning

2.1.1 Natural lightning

Lightning is a natural electrical discharge that is most often produced by cumulonimbus (thunderstorm) clouds. An idealized distribution of electrical charge in such a cloud was presented first by Simpson and Scrase [1937] (illustrated in Figure 2.1) from measurements made in England but thought to be generally valid worldwide. A more recent distribution of electrical charge in thunderstorm clouds was presented by Stolzenburg et al. [1998] (illustrated in Figure 2.2). Basically, the charged cloud can be viewed as a vertical electrical dipole whose negative-charge center is located near an altitude where the ambient air temperature is about -10° to -20° C, which is about 7 km or so for summer thunderstorms in Florida, and whose positive-charge center is situated above the negative charge region in the upper levels of the cloud and can extend up to 12 km to 15 km in altitude in Florida. This primary charge structure

is often supplemented by a second, smaller region of positive charge located in the lower levels of the cloud beneath the negative charge center. In Florida, the visual base (lower boundary) for cumulonimbus clouds is at about 1-2 km above ground.

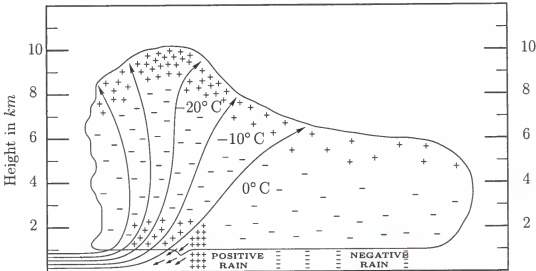


Figure 2.1: General distribution of charge in a cumulonimbus (thunderstorm) cloud as determined in England. Arrows indicate air current flow. Adapted from Simpson and Scrase [1937].

The onset of lightning activity usually occurs about 20 min after precipitation forms in the cumulonimbus cloud (Uman 1987). Less than half of the lightning flashes produced during the active part of a thunderstorm in Florida actually strike ground, and this fraction is even less during the final stages of a storm. The majority of lightning are intra-cloud discharges. However, it is the minority, cloud-to-ground lightning, that is of more practical concern.

Downward cloud-to-ground lightning is initiated by an extending plasma channel called a *leader*, which originates from a charge source inside the cumulonimbus cloud and progresses downward toward ground. Upward lightning is initiated by a leader that originates from a high metallic structure or high geographic structure such as a

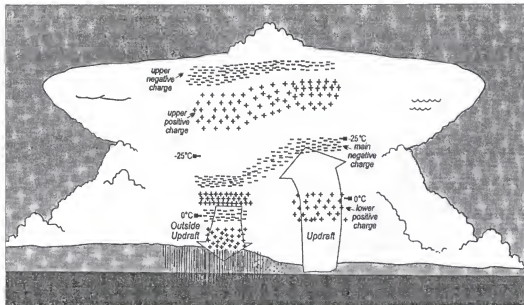


Figure 2.2: Schematic of the basic charge structure in the convective region of a thunderstorm (adapted from Stolzenburg et al. 1998).

mountain top on earth and extends upwards.

There are four categories of cloud-to-ground lightning, illustrated in Figure 2.3, depending on the polarity of charge transferred to ground and direction of propagation of the initial leader: ① downward negative lightning, ② upward negative lightning, ③ downward positive lightning, and ④ upward positive lightning. Types ① and ② result in the lowering of negative charge to Earth; types ③ and ④ result in the lowering of positive charge to Earth.

Category ① is the most common form, accounting for over 90 % of all cloud-to-ground lightning worldwide. Category ② is characteristic of tall structures and moderate-height structures on mountain tops. These two types of lightning discharges serve to neutralize a fraction of the negative charge in the cloud. The result is often phrased “as effectively lowering negative charge to ground” (Uman 1987).

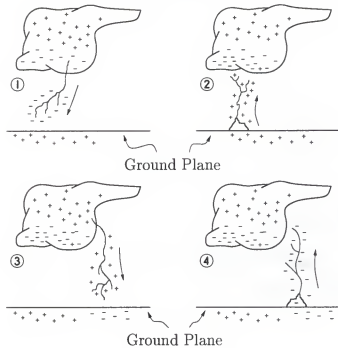


Figure 2.3: The four categories of cloud-to-ground lightning depending on leader propagation direction and polarity of charge transferred to ground. Adapted from Berger and Vogelsanger [1966].

2.1.1.1 Downward negative lightning

The initial leader in downward negative lightning progresses in a stepped manner and therefore is called *stepped* leader. The steps are discrete advancements in the length of the leader, that have been observed with high-speed photographic cameras. Steps have been reported to be from as short as 3 m in length to as long as 200 m, and the time interval between steps can range from 5 to 50 μ s. It is generally observed that the longer intervals correspond to longer steps, with the longer steps (for a downward-moving leader) usually occurring at higher altitudes and shorter steps occurring at lower altitudes. Electric and magnetic field pulses corresponding to individual steps have been observed, prior to the return-stroke field pulse. As the stepped leader advances, branches usually develop, and this can sometimes bias the interstep interval measurements measured from field pulse rates. The average propagation speed of the

stepped leader is about $2 \times 10^5 \text{ ms}^{-1}$, and the total leader duration is typically about 35 ms (Uman 1987; Rakov et al. 1994).

The stepped-leader stage of the downward negative lightning discharge ends when the leader attaches to earth (or some grounded object). Lightning attachment to a grounded object involves an upward connecting discharge, developing from the grounded object or from ground in response to the descending stepped leader. The upward connecting discharges are usually on the order of tens of meters in length and are oppositely charged with respect to the descending leader. After the junction between the stepped leader and the upward connecting discharge, a return stroke ensues which effectively neutralizes the negative charges in the leader channel via a current wave propagating from earth toward the cloud at about 10^8 ms^{-1} (Uman 1987). Both leader and return stroke participate in lowering negative charge from cloud to ground.

After the cessation of the first return stroke current, subsequent leaders may be initiated in the cloud. Typically, there are 3 to 5 leader/return-stroke sequences in a lightning flash, and the geometric mean inter-stroke interval is 60 ms (Rakov et al. 1994). Subsequent downward leaders usually do not exhibit stepping like the first leader since they tend to follow the previously formed channel (such leaders are referred to as dart leaders), although this is not always the case as is evident from the existence of dart-stepped leaders and new ground strike points created by subsequent leaders (Rakov et al. 1994). The propagation speed of dart leaders is faster than stepped leaders, about 10^7 ms^{-1} (Uman 1987). Upward connecting discharges, emitted from grounded objects in response to descending dart leaders are relatively short, of meter length, and their duration is of the order of some hundreds of nanoseconds (Wang et al. 1999).

Return strokes produce the spectacular luminosity and the loud thunder associated with lightning (see the streak camera picture in Figure 2.4). From the tower



Figure 2.4: Streak-camera photograph of a 12-return stroke flash. Increasing time goes from left to right. New Mexico Institute of Mining and Technology photograph. Adapted from Uman [1987].

measurements of Berger et al. [1975] the median peak current of the first return stroke in natural lightning is about 30 kA, with less than 1 % of all first return stroke currents exceeding 200 kA. The median rise-time of the current pulse, measured from 2 kA to peak, is $5.5 \mu\text{s}$; and the median width of the pulse, measured from 2 kA to half-peak value, is $75 \mu\text{s}$. The median peak current for subsequent return strokes in natural lightning is about 12 kA. The rise-time of the current pulse for subsequent strokes, measured from 2 kA to peak, is $1.1 \mu\text{s}$ although this value is near the time resolution ($\approx 0.2 \mu\text{s}$) of the measurement of Berger et al. [1975]; and the median width of the pulse, measured from 2 kA to half-peak value, is $32 \mu\text{s}$. Tower studies other than those of Berger et al. [1975] and triggered lightning studies (Fisher et al. 1993; Leteinturier et al. 1991) have shown subsequent strokes rise time of a few hundred of nanoseconds and maximum $\partial i / \partial t$ of $4 \times 10^{11} \text{ As}^{-1}$.

Approximately 30 to 50 % of all flashes contain a so-called long continuing current

(Rakov and Uman 1990). Long continuing current is defined as current of duration longer than 40 ms with magnitude of tens to hundreds of amperes that can flow in the lightning channel (for up to hundreds of milliseconds) after the return-stroke current peak. Current pulses, called *M* component pulses, may be superimposed on the continuing current (Thottappillil et al. 1995). *M* components current pulses differ from return stroke pulses in their wave-shape characteristics. According to Thottappillil et al. [1995], the geometric mean current peak-value for *M* components is 117 A; the geometric mean 10–90 % rise-time is 422 μ s; the geometric mean half-peak width is 816 μ s; the geometric mean time interval between *M* components is 4.9 ms; and, most significantly, the preceding continuing current has a geometric mean value of 177 A (return strokes occur only after no-current intervals).¹

2.1.1.2 Upward negative lightning

The initial leader in upward negative lightning is positively charged and extends from ground toward the cloud. Unlike the case of a downward negative lightning, there is no return stroke when the leader enters a negative charge source within the cumulonimbus cloud (at a height of 7 km or so in Florida). Instead, an initial continuous current (ICC) flows between the cloud and the earth for some tens to some hundreds of milliseconds. The initial upward leader and ICC constitute the initial stage of an upward lightning flash. After a no-current interval following the ICC, downward-moving negative dart leaders may (although not necessarily) start inside the cloud and traverse the same path as the ICC, resulting in an upward return stroke upon attachment to earth. The dart leaders and return strokes in this type of flash are similar to subsequent strokes in downward negative lightning described in previous subsection. Nearly all lightning strikes to very tall structures (hundreds of meters in

¹The 10–90 % rise-time is defined as the time on the wave front between 10 % of the peak value and 90 % of the peak value, and the half-peak width is the time between 50 % of the peak value on the wave front and 50 % of the peak value on the wave tail.

height) are initiated by upward positive leaders (Eriksson 1978).

2.1.2 Artificially-Initiated Lightning

Lightning can be artificially initiated (see Figure 2.5) from a cumulonimbus cloud by using a small rocket equipped with a spool of metallic wire (e.g., Uman et al. 1997; Rakov et al. 1998). The presence of sufficient charge inside the cloud is inferred from the vertical electric field measured at ground. In experiments at the ICLRT, when the field is in the range of 5 kVm^{-1} to 9 kVm^{-1} at ground, a rocket is launched toward the cloud. The rocket ascends with a speed of about 200 ms^{-1} and is trailed by the unspooling wire.



Figure 2.5: A photograph of lightning triggered at the ICLRT on Summer of 1999.

In the case of the common “classical” technique for initiating (triggering) lightning, illustrated in Figure 2.6, the triggering wire is a continuous conductor, typically

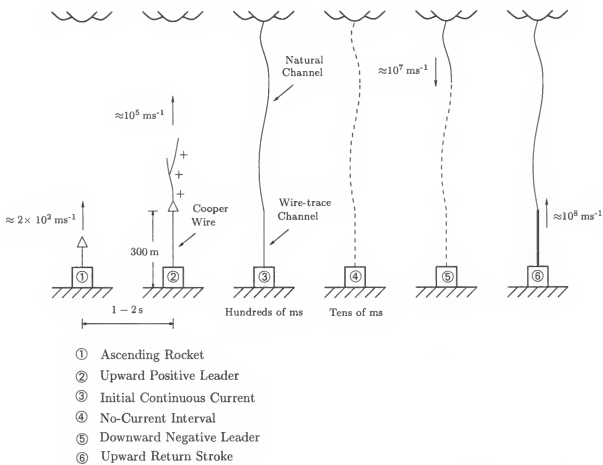


Figure 2.6: Sequence of events involved in the formation of the first return stroke in classical (grounded-wire) triggered lightning. Adapted from Rakov et al. [1998].

a copper filament reinforced for strength by a kevlar sheath, that is about 500 m to 700 m long and electrically connected to the grounded rocket-launching unit. As the rocket ascends to a height of about 150 m to 300 m, electric field enhancement at the tip of the rocket often results in a positive upward-moving leader (the polarity stated is for the typical conditions when the negative-charge center is at the bottom of the cloud). The upward positive leader is followed by an initial continuous current (ICC), when the leader reaches a negative charge source in the cloud. The triggering wire is destroyed during the upward-leader stage. The upward positive leader and ICC constitute the initial stage of a classical triggered lightning. After a no-current in-

terval following the ICC, negative downward-moving dart leaders may develop in the cloud. The dart-leader/return-stroke sequences usually follow the previously formed channel and are statistically similar (Fisher et al. 1993) to subsequent strokes in natural lightning. Dart leaders, though, do not always occur, in which case the flashes are composed of the initial stage only and are commonly referred to as “wireburns” or “wireburn-only discharges”. The designation is misleading, since wireburns can transfer many coulombs of charge and is equivalent to upward lightning from tall structures (Section 2.1.1.2), causing damage to power systems.

The processes involved in classical triggered lightning are similar to those described for natural upward negative lightning discharges initiated from tall structures, the only difference being that, in the triggered lightning case, the “tall structure” is erected in a few seconds and quickly replaced by a plasma channel. Note that the initial downward stepped-leader and first return stroke are not present in classical triggered lightning, the natural first return stroke being on average larger than subsequent return strokes.

A triggering technique developed to yield a downward-moving stepped leader is the altitude or ungrounded-wire triggering technique (e.g., Uman et al. 1997; Rakov et al. 1998) as illustrated in Figure 2.7. In this case, the wire is not a continuous, grounded conductor, but rather is separated near ground by an insulating section. A commonly-used design has some hundreds of meters of copper wire (triggering wire) attached to the rocket followed by 400 m of insulation with an additional 50-m copper section (intercepting wire) attached to the rocket-launching unit. A positive upward leader is elicited from the upper end of the triggering wire at some altitude, and some time later a downward negative stepped leader is initiated from the lower-end of the elevated triggering wire. The strike point of the downward stepped leader is very unpredictable and does not always attach to the lowermost 50-m section of copper wire. Upon attachment of the downward leader to ground, an upward return

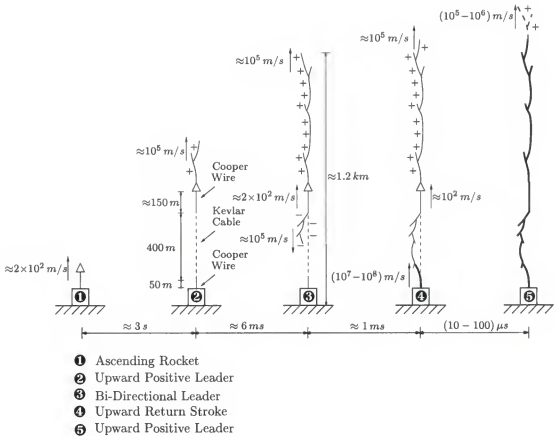


Figure 2.7: Sequence of events involved in the formation of the first return stroke in altitude (ungrounded-wire) triggered lightning, (adapted from Rakov et al. [1998]).

stroke ensues. The return stroke is relatively short-lived because, at a propagation speed 100-1000 times faster than the upward leader, it soon catches up to the leader, reaching the end of the channel. Another feature of the first return stroke resulting from this technique is that the lowermost section of copper wire may be still intact when the return stroke wave is initiated. If so, the wire explodes and the return stroke current, measured at the rocket-launching unit, is interrupted for some microseconds before recovering and rising to peak (Rakov et al. 1998). The first return stroke in altitude triggered lightning can, therefore, exhibit a peculiar double-pulse and serves to establish a low impedance path between the upward leader tip and ground.

The processes that follow are similar to those previously described for the classical technique. No data from altitude triggered lightning are presented in this dissertation.

2.2 Lightning's Interaction with Power Systems

Lightning is a major cause of power distribution system failures in regions of appreciable thunderstorm activity. Several research efforts have been undertaken in the past to determine the responses of distribution systems to direct and nearby lightning strikes. Although many researchers have calculated the responses of transmission and distribution systems, only a few have compared model predictions with responses of such systems to real lightning.

2.2.1 Experimental Data

In 1978, a project was funded by the U.S. Department of Energy (DoE) to study the responses to lightning of power distribution systems in the Tampa Bay area of Florida (Schneider and Stillwell 1979; Master et al. 1984, 1986). A research group from General Electric recorded waveforms of arrester discharge currents for two natural lightning strikes to a 7.62-kV, single-phase, overhead distribution line at unknown distances (although probably very close) from the arresters (Schneider and Stillwell 1979). One event was a single-stroke flash that lowered negative charge to ground. The arrester discharge current had a peak amplitude of 15 kA, a rise-time of about $2\ \mu\text{s}$, and decayed to half of the peak value in about $36\ \mu\text{s}$. The other event was a three-stroke flash that lowered positive charge to ground. The peak amplitudes of the arrester discharge current were 42 kA, 32 kA, and 40 kA for the three strokes, respectively, with rise-times of $5.6\ \mu\text{s}$ for the first event and about $1\ \mu\text{s}$ for the second and third events. The time to half value of each event was about $60\ \mu\text{s}$, $9\ \mu\text{s}$, and $5\ \mu\text{s}$, respectively (Schneider and Stillwell 1979). In a separate part of the DoE study,

a research group from the University of Florida measured voltages on an unenergized, 460-m overhead distribution line, simulating a standard 7.62-kV, single-phase line, with both ends open-circuited (Master et al. 1984, 1986). The majority of the lightning activity during the experiment was between 4 km and 12 km away (Master et al. 1984).

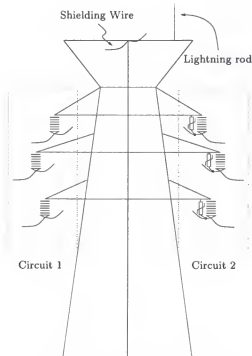


Figure 2.8: Okushishiku test transmission line tower. Adapted from Matsumoto et al. [1996].

In South Africa, an 11-kV, three-phase, overhead distribution line (with no shield wire) was constructed as part of a joint project between the Electricity Supply Commission (Johannesburg, South Africa) and the National Electrical Engineering Research Institute (Pretoria, South Africa), to study the interaction between lightning and overhead lines (Eriksson et al. 1982). The line was 9.9 km long, with the western end of the line grounded to a buried counterpoise and the eastern end open-circuited. Arrester discharge currents from each phase were measured at the east end of the

line. Voltages on each phase conductor were measured near the midpoint of the line, as well as on one phase at the east end. The measured arrester discharge currents were from natural lightning striking ground near the line. The largest arrester current recorded had a peak value of about 1 kA. Voltage waveforms were obtained at the midpoint of the line for a larger data set than the current waveforms, including 281 cases in which the peak value exceeded 12 kV. The majority of the voltages were unipolar with a positive polarity and were due to nearby lightning, lowering negative charge to ground. A total of 12 of the 281 events were from direct strikes to the line. The maximum voltage recorded during two years of the project was 300 kV (Eriksson et al. 1982).

In Japan, the shielding wire of a double-circuit, 275-kV, "Okushishiku" test transmission line, was subject to rocket-triggered and natural lightning, from 1987 to 1996 (Matsumoto et al. 1996, Motoyama et al. 1998, Kobayashi et al. 1998). The test transmission line was 2.15 km long, having a total of seven transmission towers, double insulator strings with arcing horn gaps, three gapless 154-kV MOV arresters, a single shielding wire, and 500Ω termination resistors. Arresters were connected on each phase of one of the circuits of the transmission line, at the suspension steel tower being struck from 1987 to 1993, and they were removed in 1994. At one end of the transmission line 500Ω termination resistors (182 m from the strike point) were connected. At the other end, the phase conductors were connected directly to the metallic crossarms, which was grounded. From 1993 to 1996, the tower was struck 10 times, eight with triggered lightning, and two with natural lightning (Motoyama et al. 1998). The lightning channel peak current measured for the two natural strikes were 132 kA and 159 kA, in 1993 and 1994, respectively. Lightning channel currents, shielding wire currents, tower bottom currents, arrester currents, and insulator strings voltages were measured simultaneously. The maximum recorded peak voltage across the insulator strings that were not protected by MOV arresters in 1993 was 935 kV,

and the maximum arrester peak current and voltage measured were 3 kA and 293 kV, respectively (Matsumoto et al. 1996). In 1994, a back flashover in the line was observed, and a maximum peak of approximately 2.5 MV was measured across a string insulator, where back flashover took place (Motoyama et al. 1998). Although the authors claimed that “*The increase of the voltages just before the flashover . . . might be due to the malfunction of the measuring device*”, referring to the spike seen with the resistive voltage divider used, this spike might have been the effect of magnetic coupling to the measuring loop, as observed in measuring the voltage across an arrester in our experiments (Mata et al. 2000a).

In 1985 and 1986, the University of Florida was funded by the U.S. Department of Energy, under contract with Martin Marietta Energy Systems, to set up an unenergized, 448-m long, overhead distribution line on a triggered-lightning research facility at the NASA Kennedy Space Center in Florida (Georgiadis et al. 1992; Rubinstein et al. 1994). The line consisted of three conductors, only one of which was terminated at both ends with the line’s characteristic impedance of about 600Ω . Voltages were measured at either end of the matched conductor. Georgiadis et al. [1992] describes the voltages induced on the line from distant natural lightning. Additionally, lightning was artificially initiated, using the rocket-and-wire technique, and the lightning current was directed to ground 20 m from the eastern end of the line. Voltages induced on the line were obtained for three lightning flashes, containing eleven strokes, lowering negative charge to ground, as described by Rubinstein et al. [1994]. The voltage waveforms were grouped into two categories, oscillatory and impulsive, both with almost an equal number of occurrences. For both cases, the waveforms were initially bipolar, with the positive crest being about 40 % of the amplitude of the negative crest following it. The oscillatory waveforms averaged negative crests of 47 kV (standard deviation of 9 kV) at the east end of the line and 72 kV (standard deviation of 20 kV) at the west end followed by damped oscillations at both ends with average

periods of $3.3\ \mu\text{s}$ (standard deviation of $0.3\ \mu\text{s}$). These periods are consistent with reflections on the line for a wave with a propagation speed slightly less than the speed of light. The impulsive waveforms averaged negative crests of $354\ \text{kV}$ (standard deviation of $44\ \text{kV}$) at the east end of the line and $870\ \text{kV}$ (standard deviation of $102\ \text{kV}$) at the west end. The impulsive waveforms corresponded to lightning return strokes that produced larger vertical electric field changes than the strokes associated with the oscillatory waveforms. Modeling of the data has been presented by Rubinstein et al. [1994] and Rachidi et al. [1997].

From 1993 to 1997, a series of studies were conducted by the University of Florida at the International Center for Lightning Research and Testing (ICLRT) at Camp Blanding, Florida funded by the Electric Power Research Institute (EPRI). Over these five years, the responses of a single phase unenergized test power distribution system to direct and nearby lightning (artificially initiated and natural) strikes were studied (Fernandez 1997; Fernandez et al. 1997a 1997b, 1998; Mata et al. 1998a). During the 1995-1996 experiments, the first simultaneously measured arrester discharge current and voltage waveforms during very close, direct lightning strikes to an unenergized power distribution system were obtained (Fernandez et al. 1997b). Two EPRI final reports summarizing experiments from 1993-1997 including a discussion of damage to underground cables, tests on a residential service entrance, and tests on an overhead distribution line are presented by Fernandez et al. [1998] and Mata et al. [1998a].

2.2.2 Modeling

Matsumoto et al. [1996] presented an EMTP model of a natural lightning strike to a rod installed on the top of a steel tower of the Okushishiku test transmission line. It is not clear how good the EMTP model presented was, since even though the authors claimed that their model “*could simulate actual waveforms and peak values of lightning surges accurately*”, Motoyama et al. [1998] stated: “*We found some*

mistakes in the calculation of surge response on the previous paper".

Motoyama et al. [1998] presented an EMTP model that intended to reproduce the responses of the Okushishiku test transmission line to a natural lightning strike during which back flashovers at four phases were observed. The authors presented 2 cases for which certain parameters were optimized to fit better the measured waveforms. Although the authors claimed that: "*case 2 gave the best fit for peak values and the breakdown time of the observed and calculated voltages and currents*", up to 60% discrepancy is observed in current peaks, and up to 135 % discrepancy is observed in voltage peaks for what they call the best model. Despite of the large currents injected into ground for the two events presented by Matsumoto et al. [1996] and Motoyama et al. [1998], grounding impedances were assumed to be linear and pure resistive in their models, an assumption not likely to be valid.

CHAPTER 3 EXPERIMENTAL FACILITIES

The International Center for Lightning Research and Testing (ICLRT) is an outdoor facility, occupying about 100 acres of land at the Camp Blanding, Florida Army National Guard Base, located approximately midway between Gainesville and Jacksonville, Florida, and is used for triggering lightning artificially from natural overhead thunderclouds using the rocket-and-wire technique (e.g., Uman et al. 1997; Rakov et al. 1998). In 1996, the ICLRT consisted of rocket-launching units, an unenergized test power distribution system, an office trailer, launch trailers, and several storage trailers. The test power distribution system was comprised of a single phase overhead distribution line and an underground distribution system, including three underground cables, four padmount transformers (each located in one of four instrument stations), a street light, and a simulated house service entrance. During the 1996 experiments at ICLRT, lightning arresters were installed on the overhead line (for some of the tests), across the transformer primaries, and at the service entrance (a detailed description of the ICLRT and the 1996, and 1997 experiments, is found in Fernandez et al. 1998 and Mata et al. 1998a). An overview of ICLRT in 1996 is shown (in more detail) in Figure 3.1. In 1999, two different distribution line sections (see Section 3.2) were built by FPL to test their lightning withstand capability. An overview of ICLRT in 1999 is shown in Figure 3.2. In 2000, the previously built test power distribution lines were extended in length as shown in Figure 3.3 (see Section 3.2).

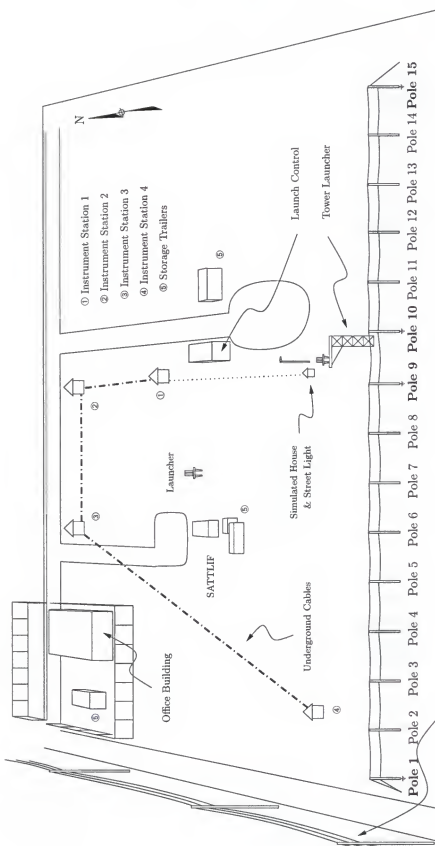


Figure 3.1: Overview of the International Center for Lightning Research and Testing (ICLRT) at Camp Blanding, Florida., July 1996 (boldface indicates poles supporting arresters).

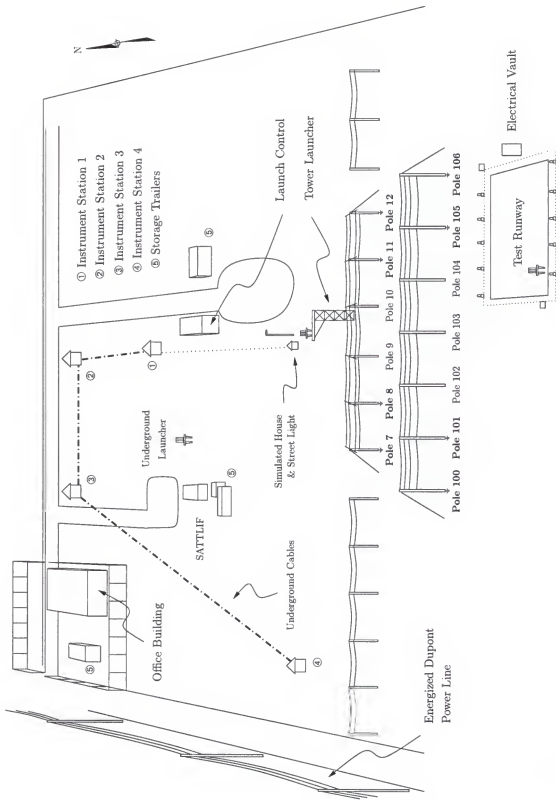


Figure 3.2: Overview of the Lightning Research and Testing (ICLRT) at Camp Blanding, Florida, July 1999 (boldface indicates poles supporting arresters).

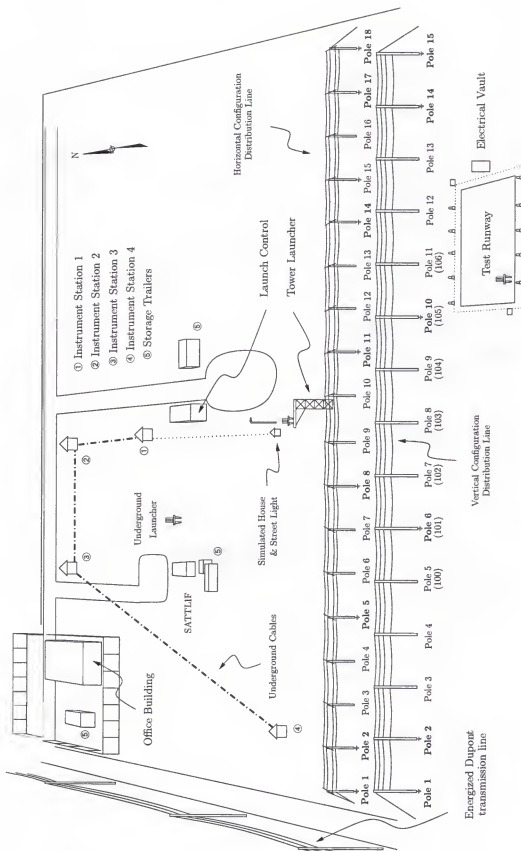


Figure 3.3: Overview of the International Center for Lightning Research and Testing (ICLRT) at Camp Blanding, Florida, July 2000 (boldface indicates poles supporting arresters).

3.1 Rocket Launcher

The Tower Launcher (see Figure 3.3) is employed to initiate (trigger) lightning to the test line using the classical rocket-and-wire technique (see Section 2.1.2). The rocket launcher is mounted atop an 11-m tower located 20 m north of the overhead line, near its midpoint.

In 1996, experiments involving the tower launcher were conducted by M. I. Fernandez, C. T. Mata, K. J. Rambo, and M. V. Stapleton. The triggered-lightning current was measured at the launcher with a T&M Research Products, Inc. shunt, model R-7000-10, and three current transformers (Section 3.3.1.1, page 36). Multiple sensors were used to increase the dynamic range of the measurements and for redundancy. The current was directed from the UF Launcher via a metallic lead to the overhead line between Poles 9 and 10 (Fernandez et al. 1997a; Mata et al. 1998a).

In 1999, experiments involving the tower launcher were conducted by C. T. Mata, K. J. Rambo and M. V. Stapleton. The triggered-lightning current was measured at the launcher with a T&M Research Products, Inc. shunt, model R-7000-10 (Section 3.3.1.2). The current was directed from the Tower Launcher via a metallic lead to desired points on the distribution line under test.

In 2000, experiments involving the tower launcher were conducted by C. T. Mata, K. J. Rambo, M. V. Stapleton, and A. G. Mata. The triggered-lightning current was measured at the launcher with a T&M Research Products, Inc. shunt, model R-5600-8 (See Section 3.3.1.3). Multiple fiber optic transmitters were used to increase the dynamic range of the measurements and for redundancy. The current was directed from the Tower Launcher via a metallic lead to desired points on the distribution lines under test.

The Tower Launcher is operated from the Launch Control trailer remotely via fiber optic links and pneumatic hoses. The fiber optics and pneumatics are used to select

the rocket to be launched and to actuate ignition of the rocket's motor, respectively.

3.2 Distribution Lines

Distribution lines, summer 1996 In 1996, the test line was approximately 740-m long and terminated at both ends in an impedance of 500Ω (see Figure 3.1). The distance between the fifteen poles varied from 47 to 73 m. Both the phase and the neutral were "Azuza", seven-strand conductors. They were mounted on insulators having a critical flashover voltage (CFO) of 500 kV and separated by 1.8 m. MOV arresters were installed at poles 1, 9, 10, and 15 (Section 3.2.2). Grounding of the line's neutral at these four poles was accomplished by means of 24.4-m cooper vertically-driven rods (Section 3.2.1).

Distribution lines, summer 1999 and 2000 Two distribution line sections were built by FPL in summer 1999. These transmission line sections were built according to FPL's standards (FPL 1996):

- *Typical crossarm with 2T conductor.*¹ This line consisted of six *wooden* poles, two arrester stations with Ohio Brass PDV-100 MOV (Section 3.2.2) installed at the second pole from each end, and different termination impedances that were used in different stages of the experiment (see C.1 for a detailed description) connected between phase conductors and neutral at each termination pole to match the characteristic impedance of the line and simulate to some extent a real-life electric power system. The line had a length of 245 m approximately. This was the only line tested in 1999. See the conductor's layout in Figure A.1, page 151, and the overall line in Figure A.2, page 152. Phase conductors were

¹The "Typical crossarm with 2T conductor" line is referred here as the horizontal configuration distribution line and the "Typical modified vertical with 568 conductor" line is referred here as the vertical configuration distribution line.

AWG #2, seven-strand conductors with an equivalent diameter of 0.7417 cm (0.292 in), and a dc-20° resistance of 0.9954 Ω/km (1.602 Ω/mi). The neutral conductor was AWG 1/0, seven-strand conductor with an equivalent diameter of 0.9347 cm (0.368 in), and a dc-20° resistance of 0.6263 Ω/km (1.008 Ω/mi).

- *Typical modified vertical with 568 conductor.* This line consists of seven *wooden* poles, two arrester stations with Ohio Brass PDV-100 MOV (Section 3.2.2) installed at the second pole from each end. It runs parallel to an 5 m south of the horizontal configuration distribution line (see Figures 3.2). The line had a length of 365 m approximately. Phase conductors were 568, (which are concentric-lay-stranded aluminum conductors, aluminum-alloy reinforced) 587.2 MCM, nineteen-strand conductors (15/4) with an equivalent diameter of 2.2327 cm (0.879 in), and a dc-20° resistance of 0.0994 Ω/km (0.1599 Ω/mi). The conductor consists of four wires type 6201-TB1 and fifteen wires type 1350-H19 (see Figure 3.4) with the diameter of each wire being 0.4465 cm (0.1758 in). The neutral conductor was AWG 3/0, seven-strand conductor with an equiva-

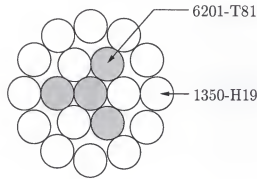


Figure 3.4: Layout of the 568 concentric-lay-stranded aluminum conductor, aluminum-alloy reinforced.

lent diameter of 1.17856 cm (0.464 in), and a dc-20° resistance of 0.3380 Ω/km (0.5441 Ω/mi).

The transmission line sections during 2000 differ from the transmission line sections of summer 1999, on the length, termination resistors (Section C.2), number of arrester stations, and types of arresters (Section 3.2.2). The differences between the 1999 distribution lines, and their 2000 extended versions can be seen in Figure A.3, page 153. The length of the extended horizontal configuration distribution line was approximately 856 m, while the length of the extended vertical configuration distribution line was approximately 812 m.

3.2.1 Grounding

In 1996, the neutral was grounded, by means of vertical ground rods, at poles 1, 9, 10, and 15 (see Figure 3.1).

In 1999, the neutral of the horizontal configuration distribution line was grounded, by means of vertical ground rods, at poles 7, 8, 11, and 12. The neutral of vertical configuration distribution line was grounded similarly at poles 100, 101, 105, and 106 (see Figure 3.2).

In 2000, the neutral of the horizontal configuration distribution line was grounded, by means of vertical ground rods, at poles 2, 5, 14, 17, and 18, and similarly, the neutral of the vertical configuration distribution line was grounded at poles 1, 2, 6, 10, 14 and 15 (see Figure 3.3). Ground resistances of the grounding rods were measured by FPL (in 1999) using a clamp-on meter and by UF (in 1996, 1999 and 2000) using the fall-of-potential method. The fall-of-potential technique is illustrated in Figure 3.5. Although long-term variation of grounding resistance should be small, short-term variation could be significant due to sporadic rainfall in Florida, particularly during the summer months (Fernandez et al. 1998). A current source is connected between the rod under test and a remote ground rod, which are *both disconnected from the test system* and separated by distance D . A third rod is used as a voltage probe. The potential difference between the probe and the rod under test is measured at

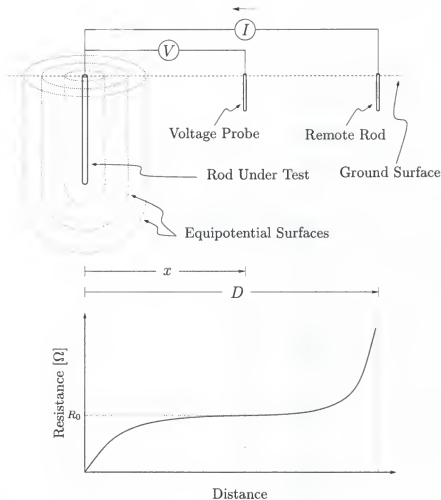


Figure 3.5: Illustration of the fall-of-potential method for measuring apparent ground resistance.

different separation distances, x . When the probe is moved away from the rod under test toward the remote ground rod, the voltage between the probe and the rod under test at some distances becomes relatively insensitive to further increase in distance. The ground resistance is then found as the ratio of the relatively constant voltage to the current supplied by the current source (IEEE 1983). The values of grounding resistance measured by UF and FPL are given in Table 3.1.

Table 3.1: Measured grounding resistances of the horizontal and vertical line configurations.

| Horizontal Configuration, Resistances in Ω | | | | | | | | | | | | | |
|---|------|------|------|------|------|------|-----|------|------|------|------|------|-----|
| Date | P1 | P2 | P5 | P7 | P8 | P9 | P10 | P11 | P12 | P14 | P15 | P17 | P18 |
| 08-05-96 ^a | 56 | | | | | 26 | 50 | | | | | 41 | |
| 06-15-99 ^b | | | | 41.4 | 41.6 | | | 51.0 | 42.6 | | | | |
| 06-19-99 ^a | | | | | | | | 44.4 | 35.6 | | | | |
| 06-21-99 ^a | | | | 24.6 | 31.0 | | | | | | | | |
| 07-03-00 ^a | | | | | | | | | | 46.4 | 10.6 | 27.3 | |
| 07-04-00 ^a | 40.7 | 46.8 | 27.7 | | | 51.6 | | 54.9 | | | | | |
| 09-18-00 ^a | | | | | | | | | | | 37.1 | 22.1 | |

Vertical Configuration, Resistances in Ω

| Date | Pole 1 | Pole 2 | Pole 5 | Pole 6 | Pole 10 | Pole 11 | Pole 14 | Pole 15 |
|-----------------------|--------|--------|--------|--------|---------|---------|---------|---------|
| 06-14-99 ^b | | | 31.3 | 37.5 | 31.0 | 39.1 | | |
| 06-19-99 ^a | | | | | 39.5 | 53.6 | | |
| 06-21-99 ^a | | | 23.2 | 41.2 | | | | |

^a Values measured by UF using the fall of potential method.

^b Values measured by FPL using a clamp-on resistance meter.

3.2.2 Arresters

1996 Experiments: the MOV distribution arresters that were used in 1996 were manufactured by ABB. These are the ABB Type MVK with rated voltage of 10 kV. The manufacturer specified V-I characteristic, in response to an 8/20 μ s wave, is given in Table 3.2.

Table 3.2: V-I characteristic of the ABB type MVK 10-kV MOV arrester.

| Discharge Voltage [kV] | Discharge Current [kA] |
|------------------------|------------------------|
| 29.7 | 1 |
| 31.6 | 2.5 |
| 32.5 | 5 |
| 36.4 | 10 |
| 39.7 | 20 |

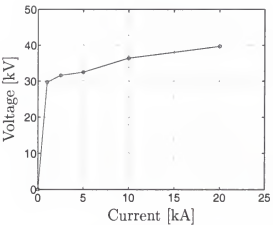


Figure 3.6: V-I characteristic of the ABB type MVK 10-kV MOV arresters.

1999 Experiments: the MOV distribution arresters that were used during the 1999 experiments, were manufactured by Ohio Brass. The Ohio Brass arresters are the PDV-100 with rated voltage of 18 kV. The PDV-100 is a polymer-housed arrester that was introduced in 1986 as the first U.S. non-ceramic arrester for heavy duty applications. It complies with ANSI standards for heavy duty arresters. The manufacturer specified V-I characteristic, in response to an 8/20 μ s wave, is given in Table 3.3. Other data provided by the manufacturer and useful for modeling purposes are: 0.5 μ s, 10 kA maximum IR of 68 kV; and 500 A switching surge maximum IR of 45 kV.

Arresters were installed at the second pole from each end, and replaced after each

storm day when the line was struck by lightning. They were labeled and sent to FPL for laboratory testing.

Table 3.3: V-I characteristic of the Ohio Brass PDV 100 18-kV MOV arrester.

| Discharge Voltage [kV] | Discharge Current [kA] |
|------------------------|------------------------|
| 49 | 1.5 |
| 52 | 3 |
| 55 | 5 |
| 60 | 10 |
| 70 | 20 |
| 82 | 40 |

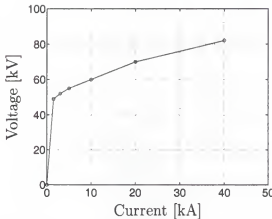


Figure 3.7: V-I characteristic of the Ohio Brass PDV 100 18-kV MOV arresters.

2000 Experiments: In the 2000 experiments, arresters manufactured by Ohio Brass (the same as used in the 1999 experiments) and Cooper Power Systems were used. The Cooper Power Systems arresters are the UltraSIL Housed VariSTAR Heavy Duty with a rated voltage of 18 kV. The UltraSIL series has a silicone rubber housing with an optional insulated mounting bracket, made of glass filled polyester, designed to provide needed mechanical strength for installation and severe loading conditions. The manufacturer specified V-I characteristic, in response to an 8/20 μ s wave, is given in Table 3.4. Other data provided by the manufacturer and useful for modeling purposes is: 0.5 μ s, 10 kA maximum IR of 64.9 kV.

Arresters were installed at Poles 2, 5, 8, 11, 14, and 17 of the horizontal configuration distribution line and at Poles 2, 6, 10, and 14 on the vertical configuration distribution line (see Figure 3.3). Ohio Brass arresters were only installed at Poles 8 and 11 of the horizontal configuration distribution line and Poles 6 and 10 of the vertical configuration distribution line. Phase C arresters at Poles 8 and 11 of the

horizontal configuration distribution line were replaced after each storm-day when the line was struck by lightning. They were labeled and stored at the ICLRT.

Table 3.4: V-I characteristic of the Cooper Power Systems UltraSIL Housed VariSTAR Heavy Duty 18 kV arrester.

| Discharge Voltage [kV] | Discharge Current [kA] |
|------------------------|------------------------|
| 48.5 | 1.5 |
| 51.6 | 3 |
| 53.9 | 5 |
| 58.8 | 10 |
| 65.0 | 20 |
| 73.2 | 40 |

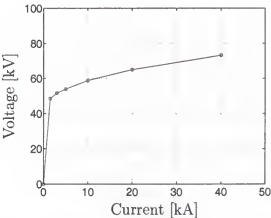


Figure 3.8: V-I characteristic of the Cooper Power Systems UltraSIL Housed VariSTAR Heavy Duty 18 kV arrester.

3.3 Instrumentation

Different line configurations, tested during the 1996, 1999, and 2000 experiments, are described in Section 3.2. The four different configurations of the 1999 experiments are shown in Figures C.1, C.2, C.3, and C.4 (see Mata et al. 1999b, for more details). The three different configurations of the 2000 experiments, are shown in Figures C.6, C.7, and C.8. Instrumentation settings are also shown in Appendix C. Different sensors were used throughout the experiments, and they are described in this section.

The installation of instrumentation on the transmission lines was crucial for the success of the experiments. Since very high voltage were expected to develop on the transmission lines, the instrumentation had to be carefully installed so that the BIL of the line was not affected by the installation of sensors, boxes, or coaxial

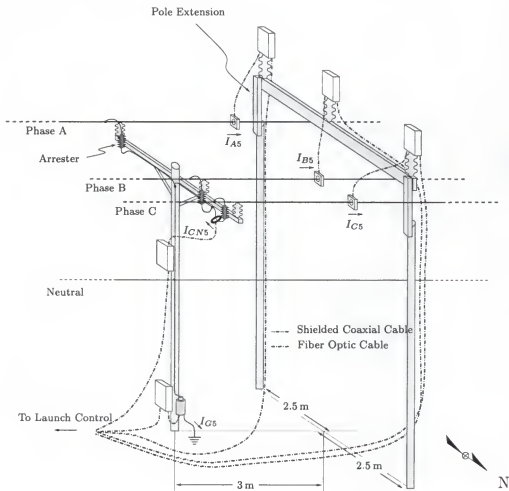


Figure 3.9: Diagram of connections at Pole 5 of the horizontal configuration distribution line, summer 2000.

cables. If there were going to occur any flashovers on the line, we did not want the instrumentation to be involved with them. This was achieved by carefully installing sensors, boxes, and coaxial cables, maintaining always the distance between different instrumentation equipment connected to different phases greater than the distance between phases. Also, no equipment was installed between the phases and the neutral conductors at poles without arresters. Pearson coils measuring phase currents were physically connected to those phases, avoiding any floating points in the system. As an example, the diagram of installation of instrumentation at pole 5 can be seen in

Figure 3.9. The diagrams for all other poles are shown from Pages 154 to 161.

3.3.1 Sensors

3.3.1.1 1996 sensors

Current Transformers (CTs): CTs, also called Pearson coils, used during the 1996 experiments were manufactured by Pearson Electronics, Inc. (PEI). Three different models were used to measure the lightning channel current:² 1330, 3025, and 3419 (see Table 3.5 for a summary of the parameters of these coils).

Current viewing resistors (CVRs): CVRs used during the 1996 experiments were low-inductance shunts manufactured by the University of Florida (UF), by Power Technologies, Inc. (PTI), and by T&M Research Products, Inc. UF shunts and PTI Standard shunts were used to measure currents at multiple locations throughout the test power distribution system and a T&M Research Products, Inc. model R-7000-10 was used to measure the lightning channel current (see Table 3.6).

Voltage dividers: Voltage dividers used during the 1995 and 1996 experiments were 400-kV resistive dividers manufactured by Lightning Technologies, Inc. Table 3.7 contains a summary of the average parameters for each voltage divider. The 400-kV dividers were used in 1996 to measure voltage on the overhead line at Poles 1, 9, and 15. In this year, it was experimentally determined by Mr. K. J. Rambo and Mr. M. V. Stapleton of the Department of Electrical and Computer Engineering at UF that the actual division ratios for the 400-kV dividers differed significantly from the manufacturer's division ratio given in Table 3.7. Two experimental procedures were conducted, each procedure repeated several times in order to arrive at some

²Multiple sensors were used to increase the dynamic range of the measurements and for redundancy.

average experimental value. The experimentally found divider ratio was about 1200:1 (see Fernandez et al. 1997a; Mata et al. 1998a).

3.3.1.2 1999 sensors

Current transformers (CTs): CTs used during the 1999 experiments were manufactured by Pearson Electronics, Inc. The CTs used in these experiments were 110A and 3525 (clamp on) models, whose parameters are summarized in Table 3.5.

Current viewing resistors (CVRs): CVRs (or shunts) used during the 1999 experiments were low-inductance shunts manufactured by T&M Research Products, Inc. model R-7000-10 (see Table 3.6 for a summary of the parameters of these CVRs). These shunts were used to measured current to ground and the lightning channel current.

Voltage Dividers: Voltage dividers used during the 1999 experiments were 75-kV magnetic-flux-compensated voltage dividers (see section 4.2), and 300-kV and 1.41-MV capacitive-compensated resistive dividers (see section B.1.2), all designed and built by the University of Florida (see Table 3.7 for a summary of the parameters of the voltage dividers). The components used to built these dividers were 47 k Ω , 80 J (single impulse), 3 W, 20 % rated Ohmite resistors connected in parallel to 30 kV DC, 500 pF, 20 % rated Cera-mite capacitors. The 75-kV *magnetic-flux-compensated voltage dividers* were used to measure voltage across arresters (as explained in section B.1.2). The 300-kV capacitive-compensated resistive divider was used to measure phase-to-phase voltage at the arrester pole, and the 1.41-MV capacitive-compensated resistive dividers were used to measure the phase-to-phase and phase-to-neutral voltages at pole 9, 25 m from the strike point, although voltage measurements at pole 9 were not successfully recorded (Mata et al. 1999b). On December 8, 1999, the voltage dividers were taken to the high voltage laboratory of FPL (located in West

Palm Beach) and calibrated using a Hipotronic voltage divider owned by the FPL high voltage laboratory as a reference. In spring of 2000, after further testings on the magnetic-flux compensated voltage dividers, it was found that the resistors used on the high voltage arm of the device were dynamically changing their ohmic value at high voltages. This resulted in distorted waveforms that did not reproduced the actual voltage across the arresters.

See Appendix C, Section C.1, for the configuration tables that indicate where 1999 sensors were used.

3.3.1.3 2000 sensors

Current Transformers (CTs): CTs used during the 2000 experiments were manufactured by Pearson Electronics, Inc. Three different models were used in these experiments: 110A, 3525, and a clamp-on version of the 3025 Pearson coil.

Current viewing resistors (CVRs): CVRs (or shunts) used during the 2000 experiments were low-inductance shunts manufactured by T&M Research Products, Inc. models R-7000-10 and R-5600-8 (see Table 3.6 for a summary of the parameters of these CVRs). A total of nine shunts were used in these experiments, and they were labeled as MS #n (where $n = 1, \dots, 9$). Shunts 1 through 4 are model R-7000-10, and shunts 5 through 9 are model R-5600-8. These shunts were used to measured currents to ground and the lightning channel current .

Voltage Dividers: new 175-kV magnetic-flux-compensated and 350-kV capacitive-compensated voltage dividers (see Section 4.2 and B.1.2) were built, using higher voltage-rated resistors ($1\text{ M}\Omega$, 35 kV, 9 W, 10 % rated Ohmite resistors connected in parallel to two 15 V DC, 100 pF, 20 % rated Cera-mite capacitors). The design was the same as the ones used in the 1999 experiments (see Table 3.7 for a summary of the parameters of the voltage dividers).

See Appendix C, Section C.2, for the configuration tables that indicate where the 2000 sensors were used.

Table 3.5 contains a summary of the CT parameters which are listed by model number. The *Peak Current* values are based on the maximum voltage output of each sensor. The *I-t Product* is the total charge that can be transferred without saturating the core of the current transformer. Exceeding the I-t product may cause a distortion of the output signal. The *Usable Rise Time* refers to the minimum 10 to 90 % rise-time of the input signal that will not cause overshoot or ringing in the output signal. The frequency response values are based on the -3dB points. Each of the CTs has a $50\text{-}\Omega$ output impedance; thus, a $50\text{-}\Omega$ termination will reduce the sensor output by a factor of two, as shown in Figure 3.10. Table 3.6 contains a summary of the parameters of CVRs³.

Table 3.5: Parameters for the Pearson Electronics, Inc. current transformers.

| Current Transformer | Output [V/A] | Peak Current [kA] | I-t Product [C] | Usable Rise Time [ns] | Frequency Response |
|---------------------|--------------|-------------------|-----------------|-----------------------|--------------------|
| 110A | 0.1 | 10 | 0.5 | 20 | 1 Hz - 20 MHz |
| 1330 | 0.005 | 100 | 65.0 | 0.25 | 0.9 Hz - 1.5 MHz |
| 3025 | 0.025 | 20 | 3.0 | 100 | 7 Hz - 4 MHz |
| 3025C ^b | 0.025 | 20 | 3.0 | 100 | 7 Hz - 5 MHz |
| 3525 ^a | 0.1 | 10 | 0.5 | 25 | 5 Hz - 15 MHz |
| 3419 | 0.002 | 250 | 30.0 | 250 | 1.7 Hz - 1.5 MHz |

^a These are custom built devices; the regular 3525 CT has a maximum peak current of 5 kA.

^b These are a clamp-on version of the 3025 model, with an wider bandwidth.

³A $50\text{-}\Omega$ resistor is connected to the output of the device to avoid a very low impedance (about $1\text{ m}\Omega$) at the ISOBE transmitter input (see Figure 3.11).

⁵HV and LV stand for High Voltage and Low Voltage, respectively.

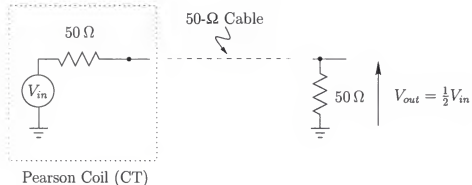


Figure 3.10: Connection diagram of the Pearson Electronics, Inc. Coils.

Table 3.6: Parameters for the T&M Research Products, Inc. CVRs (shunts).

| Model | V/A [Ω] | Energy Rating [J] | Power Rating [W] | Usable Rise Time [ns] | Output Imp. [Ω] | Freq. Resp. |
|-----------|------------|----------------------|---------------------|--------------------------|--------------------|----------------|
| R-5600-8 | 0.00125 | 5200 | - | 13 | 0.00125 | 0 - 12 MHz |
| R-7000-10 | 0.001 | 7000 | 225 | 45 | 0.001 | 0 - 9 MHz |

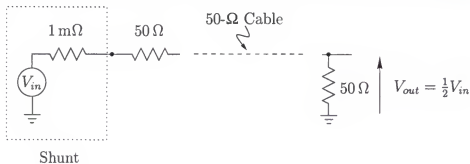


Figure 3.11: Connection diagram of the shunts.

Table 3.7: Parameters of the voltage dividers (VD) used in the 1996, 1999, and 2000 experiments.⁵

| VD Rating | HV Resistor [$k\Omega$] | HV Capacitor [pF] | LV Resistor [Ω] | LV Capacitor [nF] | Nominal VD Ratio |
|---------------------|---------------------------|-------------------|--------------------------|-------------------|-------------------------|
| 75 kV ^a | 5×47 | 100 / 5 | 50 ^b | 94 | 3.2816×10^{-5} |
| 175 kV ^a | 5×1000 | 100 / 10 | 50 ^b | 1000 | 1.9011×10^{-6} |
| 300 kV | 10×47 | 500 / 10 | 50 ^b | 470 | 1.0637×10^{-4} |
| 350 kV | 10×1000 | 100 / 20 | 50 ^b | 1000 | 1.0×10^{-6} |
| 400 kV | 1×5 | - | 5 | - | 1.0×10^{-3} |
| 1.41 MV | 47×47 | 500 / 47 | 50 ^b | 470 | 2.2634×10^{-5} |

^a Parameters for this divider correspond to each of the four sections of the device (see Figure 4.4).

^b The 50- Ω resistor corresponds to the characteristic impedance of a coaxial cable terminated into 50 Ω .

3.3.2 Voltage Attenuators

Voltage attenuators are used, when needed, to lower the gain of the measuring system. The attenuators have voltage ratios of $\sqrt{2}:1$, 2:1, 5:1, 10:1. All attenuators have 50 Ω input and output impedances.

3.3.3 Data Recording Equipment

In 1996, Nicolet Pro 90 Digitizing Oscilloscopes (Section 3.3.3.2) and Macrodyne Lightning Transient Recorders (LTR, Section 3.3.3.1) were used to record voltage and current waveforms, respectively.

In 1999, three different digitizing oscilloscopes were used: Nicolet Pro 90 (Section 3.3.3.2), Nicolet Multipro (Section 3.3.3.3), and LeCroy 9354 (Section 3.3.3.4). Also, a Honeywell 101 tape recorder/reproducer (Section 3.3.3.8) was used to record important measurements in parallel with the digitizing scopes.

In 2000, seven LeCroy Waverunners LT344L (Section 3.3.3.5), one LeCroy 9354 (Section 3.3.3.4), one LeCroy LC574AL (Section 3.3.3.6), and one LeCroy 9384AL

(Section 3.3.3.7) digitizing scopes were used. Also, a Honeywell 101 tape recorder/producer was used to record important measurements in parallel with the digitizing scopes. The interconnection of sensors, ISOBE 3000, filters, and oscilloscopes is shown in Figure 3.12.

3.3.3.1 Macrodyne lightning transient recorders (LTR)

LTRs have 7-bit amplitude resolution (128 quantization levels) and 5 MHz sampling rate. The LTR stores the digitized input signal into memory only if the input signal changes by more than two quantization levels. This effectively reduces the amplitude resolution by a factor of two, down to 6 bits (64 quantization levels). Furthermore, the LTR's effective sampling rate (the sampling rate at which data are actually stored into memory) is variable, depending on the rate of change of the input signal. Portions of the signal with higher rates of change will have a higher effective sampling rate, up to 5 MHz, while portions of the signal with lower rates of change will be stored in memory at a lower rate. When the input signal is zero or nearly dc, the effective sampling rate is a minimal 76 Hz. Overall, the number of samples required to store a given event is reduced via this memory-saving mode of operation, allowing many lightning events to be stored before the data are read out. When the LTR is sampling at its minimal rate and a fast transient occurs, the LTR records the new point. Since data points are connected by straight lines, this sometimes results in a long ramp (up to 13.16 ms) connecting the two points. To avoid this ramp created by the LTR signal processing algorithm, we insert a point in the data one minimum sampling time ($0.2\ \mu\text{s}$) before the fast transient.

3.3.3.2 Nicolet Pro 90 digitizing oscilloscope

Nicolet Pro 90 digitizing oscilloscopes are four-channel recorders with a data capacity of 258,816 samples per channel. Channels 1 and 2 have 8-bit amplitude reso-

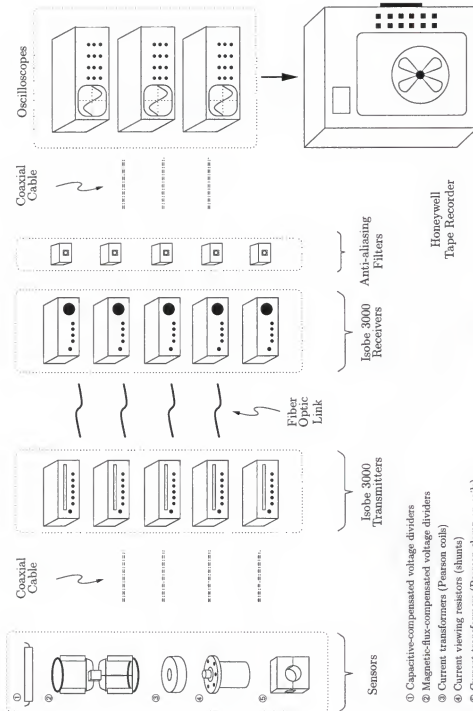


Figure 3.12: Connection of sensors, ISOBE 3000, filters, and oscilloscopes.

- ① Capacitive-compensated voltage dividers
- ② Magnetic-flux-compensated voltage dividers
- ③ Current transformers (Pearson coils)
- ④ Current viewing resistors (shunts)
- ⑤ Current transformers (Pearson clamp on coils)

lution (256 quantization levels) with up to 200 MHz sampling rate. Channels 3 and 4 have 12-bit amplitude resolution (4096 quantization levels) with up to 10 MHz sampling rate. The sampling rate used for channels 1, 2, 3 and 4 was 10 MHz limiting the record lengths to 25.8816 ms per channel. The Nicolet Pro 90 has a programmable pre-trigger memory which was set to 500 μ s. Also, post-trigger delay was used to set two channels to record sequentially. For most measurements, channels 3 and 1, and channels 4 and 2 were used in tandem (see Appendix C for more details). This setup is summarized in Table 3.8. The Nicolet Pro 90 oscilloscopes were housed in the Launch Control trailer and were powered by APS 500 uninterruptable power supply (UPS) units.

Table 3.8: Typical settings for the four-channel Nicolet Pro 90 digitizing oscilloscopes.

| Channels | Amplitude Resolution | Sampling Rate | Record Length per Channel [ms] | Combined Record Length [ms] |
|----------|----------------------|---------------|--------------------------------|-----------------------------|
| 3 and 1 | 12-bit and 8-bit | 10 MHz | 25.8816 | 51.7632 |
| 4 and 2 | 12-bit and 8-bit | 10 MHz | 25.8816 | 51.7632 |

3.3.3.3 Nicolet Multipro digitizing system

The Nicolet Multipro digitizing oscilloscope is a four-card recorder, each card having 4 channels, with data capacity of 517,632 samples per channel. All channels have 12-bit amplitude resolution (4096 quantization levels) with up to 100 MHz sampling rate. The sampling rate used for all channels was 10 MHz, limiting the record length to 51.7632 ms per channel. The Nicolet Multipro has a programmable pre-trigger memory which was set to 500 μ s. Also, post-trigger delay was used to set two channels to record sequentially for some measurements (see Appendix C for more details). The Multipro oscilloscope was housed in the Launch Control trailer and was powered

by UPS.

3.3.3.4 LeCroy 9354 digitizing oscilloscope

The LeCroy 9354 digitizing oscilloscope has an input bandwidth of 500 MHz, four segmentable 8 bit channels and a digitization rate of up to 2 GHz. There was one 9354 used in the experiment until September 6, 1999, at which time a second 9354 was added to the experiment. The first 9354 had a 500 Mb PCMCIA hard drive; the second unit had only a floppy disk drive for data collection. All channels were set to sample at 10 MHz rate with a pre-trigger of 500 μ s. The maximum data storage for each channel is 400,000 points at a sampling rate of 10 MHz. Each channel was set to record a maximum of eight segments with a data storage of 50,000 points per segment for the first scope and a maximum of eight segments with a data storage of 20,000 points per segment for the second scope. The reduction of data storage on the second scope is due to the limitation of data space on the floppy disk drive on the second scope. The record length for each segment was 5 ms on the first scope and 2 ms on the second scope. In the 2000 experiments, a LeCroy 9354 was setup to measure low-level, slow current and voltage waveforms from August 2 to August 22. These scopes were housed in the Launch Control trailer and were each powered by UPS.

3.3.3.5 LeCroy Waverunner LT344L digitizing oscilloscope

The LeCroy Waverunner digitizing oscilloscopes have an input bandwidth of 500 MHz and four segmentable 8 bit channels. These oscilloscopes had a 500 Mb PCMCIA hard drive. All channels were set to sample at 20 MHz rate (for most of the flashes) with a pre-trigger of 500 μ s. The maximum data storage for each channel is 1,000,000 points. Each channel was set to record a maximum of five segments with a data storage of 200,000 points per segment. The record length for each segment

was 10 ms. These scopes were housed in the Launch Control trailer and were each powered by UPS.

3.3.3.6 LeCroy LC574AL digitizing oscilloscope

This LeCroy LC574AL was lent by NASA to the Lightning Laboratory for the 2000 summer experiments. This digitizing oscilloscope has an input bandwidth of 1 GHz, four segmentable 8 bit channels and a digitization rate of up to 4 GHz, with a 500 Mb PCMCIA hard drive. All channels were set to sample at 25 MHz rate with a pre-trigger of 500 μ s. The maximum data storage for each channel is 2,000,000 points. Each channel was set to record a maximum of five segments with a data storage of 250,000 points per segment. The record length for each segment was 10 ms.

3.3.3.7 LeCroy 9384AL digitizing oscilloscope

This digitizing oscilloscope has an input bandwidth of 1 GHz, four segmentable 8 bit channels and a digitization rate of up to 4 GHz, with a 500 Mb PCMCIA hard drive. All channels were set to sample at 25 MHz rate with a pre-trigger of 500 μ s. The maximum data storage for each channel is 2,000,000 points. Each channel was set to record a maximum of five segments with a data storage of 250,000 points per segment. The record length for each segment was 10 ms.

3.3.3.8 Honeywell 101 tape recorder/reproducer

The Honeywell model 101 is a high-performance IRIG portable magnetic tape recorder/reproducer with microcomputer control. The recorder card contains both a recorder amplifier and a head driver amplifier. The recorder amplifier conditions external data input signals, and the head driver amplifier provides gain for a bias signal internal to the Model 101. The two signals are linearly mixed in the recorder head. The reproducer cards allow the data recorded into the magnetic tape to be

played back. The recorder has 16 analog channels, 5 direct record channels and 8 FM record channels. Direct record allows selectable input data voltage magnitude range of 0.1-1 volt or 1-7.1 volts, with a bandwidth of 100 Hz to 2 MHz and a source impedance of 75Ω maximum to meet specifications, or 600Ω maximum with some degradation in frequency responses (direct record is used to record audio and time). The FM recording allows selectable input data voltage magnitude range of ± 10 V peak with $20\text{ k}\Omega$ input impedance or ± 4.24 V peak with 75Ω input impedance, with a bandwidth of dc to 500 kHz.

3.3.3.9 Nicolet Isobe 3000 fiber optic link

The recorders (Nicolet Pro 90, Nicolet Multipro, LeCroy 9354 and Honeywell 101) measured the sensor outputs (Section 3.3.1) remotely via Nicolet 3000 fiber optic links, each composed of an Isobe transmitter, a fiber optic cable, and an Isobe receiver. The Isobe transmitters are battery operated and mounted in shielded containers at the sensor location. The transmitter has three input settings: ± 10 V, ± 1 V, and ± 0.1 V. Its output signal is relayed via fiber optic cables to the Isobe receiver which has an output voltage range of ± 2 V and is housed with the oscilloscopes in the Launch Control trailer. The propagation delay of the Isobe pair (transmitter and receiver) combined with the first one meter of fiber optic cable is approximately 70 ns, plus an additional delay of 5 ns per meter of optical cable beyond the first meter. Fiber optic cables were assigned to Isobes transmitter and receiver pairs, and delays were determined experimentally. These delays are summarized in the tables of Appendix C. The receivers have a $50\text{-}\Omega$ output impedance; thus, a $50\text{-}\Omega$ termination will reduce the receiver output by a factor of two.

3.3.3.10 Anti-aliasing filters

A total of 25 anti-aliasing filters⁶ were built and used to avoid aliasing when sampling the signals with the digitizing oscilloscopes. Each filter was assigned to a specific ISOBE (see section B.2). Since the sampling frequency for all recording channels was set to 10 MHz, the anti-aliasing filters were designed to have a -3dB attenuation at 5 MHz (half the sampling rate). The circuit diagram of the filters is shown in Figure B.3. Each anti-aliasing filter was tested to obtain its frequency response (see section B.2, page 166). The interconnection of sensors, ISOBE 3000, filters, and oscilloscopes is shown in Figure 3.12.

3.3.3.11 Video and photographic equipment

Video and photographic equipment used in the 1999 experiments consists of three Panasonic SVHS, two Sony Hi8 Hi-Fi Video Cameras, and four Nikon 35-mm Cameras. In 2000, three Sony DV (digital video cameras, model DCR-TVR900) were added to the experiment. The cameras were located at various positions throughout the ICLRT. The video cameras (Panasonic SVHS, Sony Hi8, and Sony DV) were started manually at the beginning of the storm with tapes that hold up to two hours (Panasonic SVHS and Sony Hi8) and ninety minutes (Sony DV) of video. The Nikon 35-mm cameras are triggered synchronously via a fiber optic relay system. The camera triggering system is located in the Launch Control trailer. When the 35-mm cameras are activated, the camera shutters are set to remain open until a flash (or sufficient light input) is detected. A summary of the camera locations and objects in their field of view for the 1999 experiments appear in Table 3.9 and their locations are shown in Figure C.5 on page 183. A summary of the camera locations and objects in their field of view for the 2000 experiments, configuration FPL-A-00 (Section C.2.1),

⁶Anti-aliasing filters are used to bandlimit the continuous time signals before they are sampled (see Cartinhour [1998]).

appear in Table 3.10 and their locations are shown in Figure C.9 on page 199 (video cameras) and Figure C.10 on page 200 (still cameras). A summary of the camera locations for configuration FPL-B-00 (Section C.2.2) appear in Table 3.11 and their locations are shown in Figure C.11 on page 201 (video cameras) and Figure C.12 on page 202 (still cameras).

Table 3.9: Camera locations and objects in their fields of view for the summer of 1999 experiments (See Figure C.5).

| Camera | Location | Objects in the Field of View |
|----------------------|--|--------------------------------|
| Video 1 ^a | Launch Trailer | Tower Launcher close-up |
| Video 2 ^a | IS3 | Wide distribution line view |
| Video 3 ^a | Field (between IS1 and distribution line) | Current injection point |
| Video 4 ^b | Tower Launcher | East view of distribution line |
| Video 5 ^b | Tower Launcher | West view of distribution line |
| Photo 1 | Launch Trailer | Tower Launcher close-up |
| Photo 2 | IS1 | Current injection point |
| Photo 3 | IS3 | Wide distribution line view |
| Photo 4 | Field (between IS1 and distribution line) | Current injection point |

^a Panasonic SVHS

^b Sony Hi8

Table 3.10: Camera locations and objects in their fields of view for configuration FPL-A-00, Section C.2.1 (See Figure C.9 and C.10).

| Camera | Location | Objects in the Field of View |
|----------------------|--|-------------------------------------|
| S-VHS-1 ^a | Launch Trailer | Tower Launcher close-up |
| S-VHS-2 ^a | Tower Launcher | Current injection point |
| S-VHS-3 ^a | Simulated House | Current injection point |
| DV-1 ^c | Tower Launcher | Pole 9, Horizontal Configuration |
| DV-2 ^c | Tower Launcher | West view of distribution line |
| DV-3 ^c | Tower Launcher | Pole 10, Horizontal Configuration |
| Hi-8-1 ^b | Tower Launcher | East view of distribution line |
| Hi-8-2 ^b | Field (South of the Tower Launcher) | Current injection point |
| Hi-8-3 ^b | IS3 | Wide distribution line view |
| Still 1 | Tower Launcher | Current injection point |
| Still 2 | Launch Trailer | Tower Launcher close-up |
| Still 3 | Simulated House | Current injection point |
| Still 4 | IS3 | Wide distribution line view |
| Still 5 | Field (South of the Tower Launcher) | Current injection point |

^a Panasonic SVHS

^b Sony Hi8

^c Sony Digital Video Camera

Table 3.11: Camera locations and objects in their fields of view for the summer of 2000 experiments for configuration FPL-B-00, Section C.2.2 (See Figure C.11 and C.12).

| Camera | Location | Objects in the Field of View |
|----------------------|--|-------------------------------------|
| S-VHS-1 ^a | Launch Trailer | Tower Launcher close-up |
| S-VHS-2 ^a | Tower Launcher | Midpoint (between pole 9 and 10) |
| S-VHS-3 ^a | Simulated House | Current injection point |
| DV-1 ^c | Tower Launcher | Current injection point |
| DV-2 ^c | Tower Launcher | West view of distribution line |
| DV-3 ^c | Tower Launcher | Pole 10, Horizontal Configuration |
| Hi-8-1 ^b | Tower Launcher | East view of distribution line |
| Hi-8-2 ^b | Field (South of the Tower Launcher) | Current injection point |
| Hi-8-3 ^b | IS3 | Wide distribution line view |
| Still 1 | Tower Launcher | Midpoint (between pole 9 and 10) |
| Still 2 | Launch Trailer | Tower Launcher close-up |
| Still 3 | Simulated House | Current injection point |
| Still 4 | IS3 | Wide distribution line view |
| Still 5 | Field (South of the Tower Launcher) | Current injection point |

^a Panasonic SVHS

^b Sony Hi8

^c Sony Digital Video Camera

CHAPTER 4

VOLTAGE MEASURING TECHNIQUES

In this chapter we describe conventional techniques used to measure voltages across arresters (Section 4.1), and we present a new technique in which a novel device, the magnetic-flux-compensated voltage divider, is used (Section 4.2).

4.1 Conventional Measuring Techniques

Although a significant distortion of the voltage waveform may result depending on the magnitude and waveshape of the current waveform (Mata et al. 2000a), the most common practice for voltage measurement is to connect a voltage divider in parallel with the object under test (Schwab 1972; Bowdler 1973; Kuffel 1984; Creed 1989; Khalifa 1990; Ryan 1994; Naidu and Kamaraju 1995; IEEE 1995; Kim et al. 1996; Mis 1999). While this might be acceptable for cases when currents involved in the measurement are fairly slow, small, or both, this practice may lead to considerable errors and voltage-waveforms distortions for large and fast currents because of an induced $\partial i / \partial t$ component in the measuring loop (Section 4.2). It is based on this conventional technique (voltage divider in parallel with the object under test) that High Voltage Laboratories test arresters, and arrester's manufacturers provide their characteristic curves. No standards are available on this subject, and the technique for arrester voltage measurement seems to be left to the judgment of each High Voltage Laboratory director. Yet, waveforms obtained using the *conventional voltage measurement technique* are still being used to develop sophisticated arrester models (Durbak 1985; Petit et al. 1991; Soler et al. 1991; Lucas and McLaren 1991; IEEE

Working Group 3.4.11 1992; Pereira et al. 1995; Kim et al. 1996; Hagiwara et al. 1997; Pinceti and Giannettoni 1999; da Costa et al. 1999) and to compare different models presented in the literature (Stockum 1994; Kim et al. 1996).

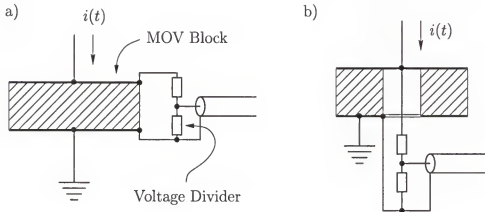


Figure 4.1: a) Conventional connections of the voltage divider; b) Coaxial connection of the voltage divider (adapted from Schmidt et al. [1989]).

The most significant distortion on the voltage waveform when large and fast currents are involved is the presence of a spike at the beginning of the voltage waveform (Dang et al. 1986; Mukae et al. 1987; IEEE Working Group 3.4.11 1992; Mata et al. 2000a)¹. Schmidt et al. [1989] presented detailed and interesting systematic research on this subject. In this work, the test objects were MOV blocks with *cylindrical hole*², as seen in Figure 4.1b. The source of the voltage spike was identified by comparing voltage measurements with two voltage divider arrangements (Figure 4.1); “the arrangement of the voltage divider adjacent to the blocks results in a voltage spike of about 85 % because of the magnetic coupling from the current ($\partial i / \partial t$) in

¹In Dang et al. [1986] and Mukae et al. [1987] a voltage spike (or voltage overshoot) of up to 50 to 100 % was reported, while in Mata et al. [2000a] voltage spikes of about 300 % (with respect to the residual voltage) were observed.

²According to this work, comparative measurements with and without hole showed the same behavior in principle.

the voltage measuring loop" (see Figure 4.1a). On the other hand, measurements obtained using the configuration shown in Figure 4.1b, resulted in a voltage spike of about 20 % (with respect to the residual voltage) for the same current impulse.³

Three typical arrester voltage waveforms (summarized in Figure 4.2) where identified in the work of Schmidt et al. [1989]. The first voltage waveform (Figure 4.2a) corresponds to a fast current using the test connection shown in Figure 4.1a, where a spike of about 50-80 ns wide was identified. Figure 4.2b shows the voltage waveform response to a fast current obtained when using the "coaxial" connection (Figure 4.1b), where a spike of about 10-50 ns wide was observed. The last voltage waveform (see Figure 4.2c) corresponds to a slow current with either of the configurations shown in Figure 4.1. Note that the amplitude of the initial peak depends on the current waveform.

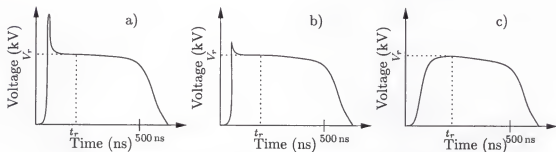


Figure 4.2: Different voltage waveforms across an arrester.

Other important findings in Schmidt et al. [1989] were that: (i) The residual voltage (V_r) increased with shorter front times in the current. (ii) The initial peak in the voltage waveform becomes larger than the residual voltage for current front times less than 30 ns. (iii) A voltage overshoot of *only* about 30 % can be related to the characteristics of the material. (iv) Voltage spikes could be considerable when testing

³The residual voltage ($V_{R/20\mu s, 10 kA}$) is defined as the discharge voltage for the nominal 8/20 μ s wave with an amplitude of 10 kA (Schmidt et al. 1989), while the residual voltage (V_r) is defined as the clamping voltage of the arrester.

arresters (of the order of 200 % of the residual voltage for a 30-to-90 % front time of about 1 μs).

Although the “coaxial” connection presented in this work (Figure 4.1b) reduces significantly the magnetic coupling to the measuring circuit, this technique is not practical when measuring voltages across commercial arresters.

An interesting “differential voltage divider” was introduced by Drilling et al. [1998] to measure *low voltage* surge arrester and spark gap voltages during the application of high rate of rise current impulses. The device is based on the conventional technique with an additional loop to compensate for the $\partial i/\partial t$ component. Although the equivalent circuit they analyze for the conventional technique is incorrect (since they assumed the $\partial i/\partial t$ to be the result of only the stray inductance of the arrester), the new differential divider presented seems very promising. The principle of operation of the differential voltage divider is shown in Figure 4.3. Here, ① is the high voltage divider connected to the surge arrester so that the area of the loop made by the divider, its leads and the arrester is ③. This divider measured the voltage across the arrester in the conventional way. A second identical divider ② with a shorted compensation loop ④ is placed next to the first divider and signals are sent to the differential amplifier. Both areas are penetrated by the magnetic flux originated from the current in the surge arrester. The induced voltage in the compensation loop ④ is adjustable and it is calibrated as follows: (i) the arrester under test is replaced by a short circuit, (ii) the same surge current (at which the arrester will be tested) is applied, (iii) the output voltage of the differential divider is adjusted to zero.

The weakness and limitations of the differential voltage divider are:

- The device does not provide any compensation for a possible non-symmetric current density on the nonlinear material (Mata et al. 1999a and 1999b; Andoh et al. 2000).
- The operation of this device is limited to low voltages where the second loop (④

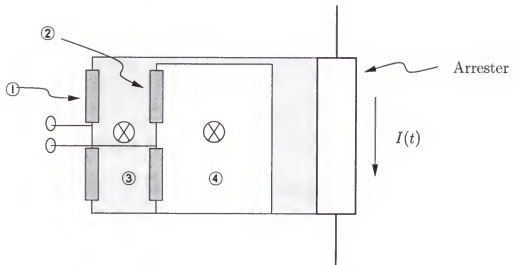


Figure 4.3: Principle of a differential voltage divider (adapted from Drilling et al. [1998]).

in Figure 4.3) does not present a potential hazard for a flashover to the upper lead of ①.

- This device cannot be used to measure voltages across arrester on real distribution systems because loop ③ needs to be fairly large to accommodate for the compensation loop ④.
- The compensation technique requires calibration with the same current as that at which the arrester will be exposed. In reality, different lightning events will have different currents.

4.2 Magnetic-Flux-Compensated Voltage Divider

In order to measure the “actual” voltage across an arrester, that is, to minimize induction effects, a novel voltage divider was designed and implemented: *the magnetic-flux-compensated voltage divider*.⁴ The idea of the *magnetic-flux-compensated voltage*

⁴The Disclosure of Invention was submitted to the Licensing Office on fall of 1999 to patent this device.

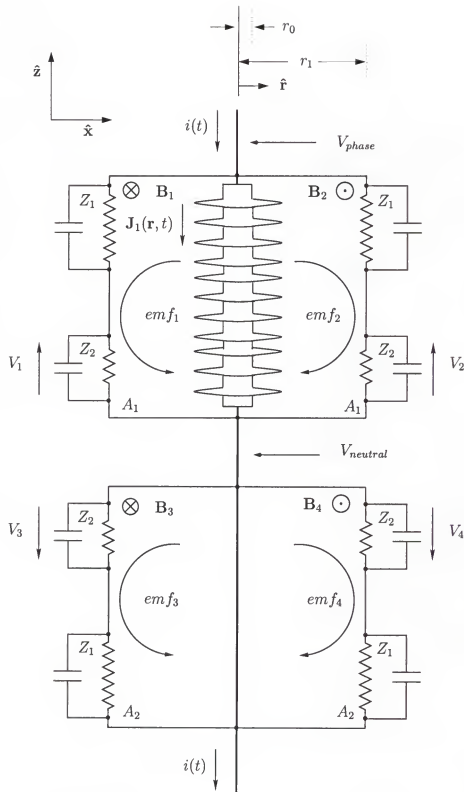


Figure 4.4: Magnetically Compensated Voltage Divider. The direction of the arrows in voltages V_1 , V_2 , V_3 , and V_4 represents the polarity of the measurement.

divider is to cancel out the induced voltage in the measuring loop (see Section 4.1), by using four mixed dividers (see Figure 4.4)⁵.

Recall that the induced electromotive force due to a time varying magnetic field derives from Maxwell's equations (Wangness 1986):

$$emf = \oint_C \mathbf{E} \cdot d\mathbf{l} = - \int_S \frac{\partial \mathbf{B}}{\partial t} \cdot d\mathbf{a} \quad (4.1)$$

where the magnetic induction \mathbf{B} is given by (see Figure 4.5):

$$\mathbf{B}(\mathbf{r}, t) = \int_{V'} d\mathbf{B}(\mathbf{r}, t) dv' = \frac{\mu_0}{4\pi} \int_{V'} \frac{\mathbf{J}'(\mathbf{r}', t) \times \hat{\mathbf{R}}}{R^2} dv' \quad (4.2)$$

and then, combining (4.1) and (4.2),

$$emf = - \frac{\partial \Phi}{\partial t} = - \frac{\partial}{\partial t} \int_S \left[\frac{\mu_0}{4\pi} \int_{V'} \frac{\mathbf{J}'(\mathbf{r}', t) \times \hat{\mathbf{R}}}{R^2} dv' \right] \cdot d\mathbf{a} \quad (4.3)$$

It was found (Mata et al., Mata et al. 1999a, 1999b) that with the proper connection of several voltage dividers, the induction coupling would be minimized. The connection is such that two mixed dividers (parallel connection) are connected parallel to the arrester in the same plane (upper part). The electromotive forces emf_1 and emf_2 might not be equal, due to a possible non-symmetric (with respect to vertical axis $\hat{\mathbf{z}}$) current distribution \mathbf{J}_1 (see Figure 4.4) although the device is designed so that the area A_1 is the same in both sides.⁶ With two voltage dividers the effect of a non-symmetric current distribution \mathbf{J}_1 in the arrester is minimized since by compensating emf_1 and emf_2 we average the induced voltages. The bottom part of the

⁵For this invention, parallel-mixed dividers are used, these are described in Section B.1.2

⁶A non-symmetric current distribution \mathbf{J}_1 would imply a non-symmetric magnetic induction \mathbf{B} (and therefore $\mathbf{B}_1 \neq \mathbf{B}_2$), which would result in different electromotive forces according to (4.3).

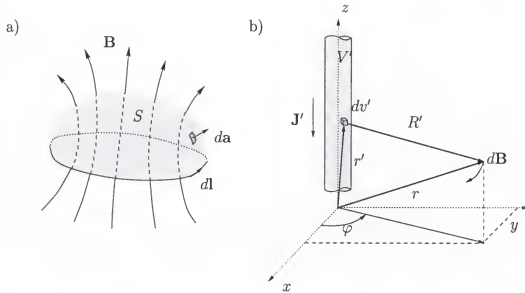


Figure 4.5: a) Flux of \mathbf{B} through a surface S with a contour C ; b) Geometrical relations between the volume current density and the magnetic induction it produces.

device is similar to the top part, connected upside down across a short circuit below the arrester. The area (A_2) is the same in both sides, therefore the electromotive force is the same ($emf_4 = emf_3$). The four outputs (V_1 , V_2 , V_3 and V_4) are then added. If we define the proportionality constant k_p as:

$$k_p = \frac{R_2}{R_1 + R_2} \quad (4.4)$$

then we can express V_1 , V_2 , V_3 and V_4 as follows:

$$V_1 = k_p (V_{phase} - V_{neutral} + emf_1) \quad (4.5)$$

$$V_2 = k_p (V_{phase} - V_{neutral} + emf_2) \quad (4.6)$$

$$V_3 = -k_p emf_3 \quad (4.7)$$

$$V_4 = -k_p emf_4 \quad (4.8)$$

These voltages are added by means of an electronic summing box built into the device

(see Figure 4.6). By adding (4.5), (4.6), (4.7), and (4.8) (note that by symmetry V_3 and V_4 are equal) we minimize the induced electromotive force component on the output voltage of the device (4.9).

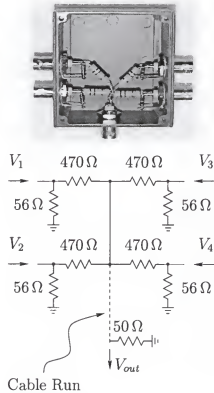


Figure 4.6: Summing box configuration (resistors for summing four voltage signals) used in the Magnetic-Flux-Compensated Voltage Divider. All grounds at 56Ω resistors are local grounds in the electronics box. Ground for the 50Ω resistor is at the end of the coaxial cable carrying the voltage signals.

$$V_{out} \propto V_1 + V_2 + V_3 + V_4 = k_p [2(V_{phase} - V_{neutral}) + (emf_1 + emf_2 - emf_3 - emf_4)] \quad (4.9)$$

where

$$emf_1 + emf_2 - emf_3 - emf_4 \approx 0 \quad (4.10)$$

The assumptions for this voltage divider to provide the actual voltage across a device

are the following:

- ① The device is connected to the distribution line such that the **B** fields from the distribution line conductors are perpendicular to the normal of the areas.
- ② Other sources of time-varying magnetic fields such as the tortuous lightning channel above the distribution line or currents flowing in phase or ground wires are insignificant or are distant enough that they affect equally the four loops.
- ③ The geometry shown in Figure 4.4 is such that $A_1 = A_2$.

CHAPTER 5

REPRESENTATION OF SOURCE AND SYSTEM ELEMENTS IN EMTP

Network sections (such as transmission line sections, downleads, ground rods, etc.) in the EMTP model for the 1996 and 2000 experiments were modularized by using the Data Base Module (DBM) feature of EMTP (Alternative Transient Program (ATP) Rule Book [1987-1998]). The processed DBM can be included in the model as many times as needed.

5.1 Lightning Current Model

A Type 1 (user defined) current source can be used in the EMTP simulation, where the user specifies the value of the source at each time step (see Section D.3 on page 218). Therefore, an ideal current source can be defined in the EMTP to represent the measured lightning channel current.

The measured lightning channel current waveforms exhibit discontinuities (due to sampling and quantization noise) that must be removed before using that current waveform as an input to the EMTP program. These discontinuities cause relatively large $\partial i/\partial t$ and/or $\partial v/\partial t$ spikes. Depending on the digitizer used to measure the lightning channel current (resolution and sampling rate) different algorithms are used to process data to be used as an input to the EMTP program. Quantization noise (caused by the digitizing oscilloscope) is a serious problem since small (but fast) oscillations in the source current cause large oscillations in the model responses. In the following we describe processing of measured current waveforms to be used as sources for EMTP.

In 1996, the lightning channel current was measured using a LTR (see Fernández 1997). Here, the LTR record (+/- 13 kA range) of the total triggered-lightning current was up-sampled (using a linear interpolation algorithm) and then filtered by a first order Butterworth digital filter with a cutoff frequency of 700 kHz to smooth out the discontinuities in the waveform. These discontinuities are a result of LTR's limited vertical resolution. The algorithm used to upsample, filter, and write the signal to a formatted ASCII file follows:

```
____ Processing LTR data ____  

% Uses LTR '0216' with a range of 13 kA  

%  

% Create the Source file to be used in the ATP simulation.  

% Source type 1, the user specifies the value of the source  

% at each time step  

%  

load ..../data/07-31-96/AS021601.001  

tp=0:5e-9:100e-6;  

%  

AS021601(:,1)=AS021601(:,1) - 1.9;  

AS021601(4,2)=0; % assign zeros so the source start with 0 magnitude  

AS021601(4,1)=0;  

%  

%      Use interpolation to upsample the LTR waveform  

%      In this case, the time step is 5 ns (200 MHz).  

%  

out=interp1(AS021601(:,1)*1e-6,AS021601(:,2)*130,tp,'linear');  

%           us          range 13 kA  

%  

% BUTTER Butterworth digital and analog filter design.  

% [B,A] = BUTTER(N,Wn) designs an Nth order lowpass digital  

% Butterworth filter and returns the filter coefficients in length  

% N+1 vectors B (numerator) and A (denominator). The coefficients  

% are listed in descending powers of z. The cut-off frequency  

% Wn must be 0.0 < Wn < 1.0, with 1.0 corresponding to  

% half the sample rate.  

%  

[b,a] = butter(1,.007); % Determine the filter parameters  

sour = filter(b,a,out); % filter signal "out", ans store it in "sour"  

% b = 0.01087642013487  0.01087642013487  

% a = 1.000000000000000 -0.97824715973025  

% plot(AS021601(:,1),-AS021601(:,2)*.130,'k*-'),axis([0 100 -15 0])  

% LTR Source.  

%  

% create an ASCII file called source.txt that has the current waveform  

% to be used from the main atm data case.  

% This is the LTR file, up-sampled and filtered.  

fid=fopen('source.txt','w'); % open the file source.txt
```

```
fprintf(fid,'%7.1f\n',-sour');           % write formatted data to file  
fclose(fid);                            % close the file
```

In 2000, when the incident current was acquired with LeCroy oscilloscopes, a different approach was used. Few points are manually selected from the incident current waveform, and points in between are estimated using cubic interpolation. This approach is better than conventional filtering, since quantization noise is removed instead of being smoothed down. Figure 5.1 illustrates this procedure. Notice how the estimated current follows the measured incident current on the fast portion of the waveform (Figure 5.1b) and how effective the algorithm is at the decay portion of the waveform where the quantization noise is maximum (Figure 5.1c).

5.2 Transmission Line Model

The transmission line sections were represented by using the J. Marti frequency-dependent transmission line model (Section D.2.1), using the subroutine LINE CONSTANTS, as described in Alternative Transient Program (ATP) Rule Book [1987-1998], to specify the line and conductors parameters. The J. Marti model was preferred over the Noda frequency-dependent transmission line model (Section D.2.2) because the former requires less computation time which is very valuable when running the optimization algorithms (Section 6.1). The J. Marti source file using the LINE CONSTANTS subroutine, the DBM source, and the datacase files of a 24-m transmission line section are presented in Section E.1.

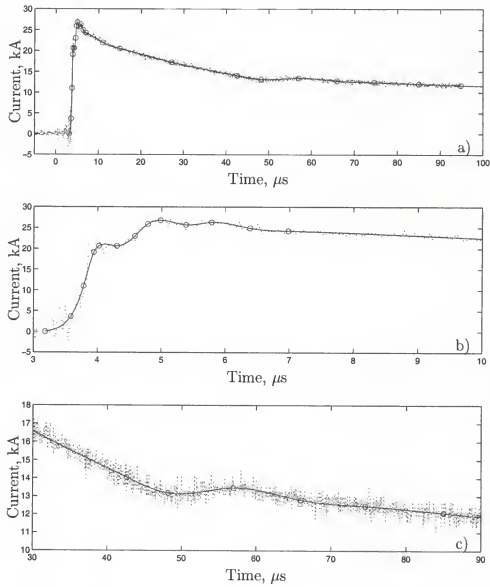


Figure 5.1: Processing of the measured lightning channel current waveform to eliminate quantization noise for subsequent use in the EMTP. The dotted line represents the measured current waveform, circles indicate manually-picked points that represent nodes to perform the cubic interpolation, and the solid line represents the interpolated waveform: a) $100\ \mu\text{s}$ time window, b) rising portion of the incident current, and c) decaying portion of the incident current.

5.3 Arrester Models and Equivalent Circuits

Metal oxide surge arresters were developed in the late 1970s, and ever since they have been the subject of studies and continuous testing.¹ Yet, it is not completely understood how these devices behave when subjected to fast transients, since the models available in the literature are based on measurements made with techniques that are not adequate for large and high-frequency current processes. In this section we present equivalent circuits found in the literature, *conventional* techniques used to measure voltages across arresters, and a proposed *novel* technique to measure *actual* arrester voltages.

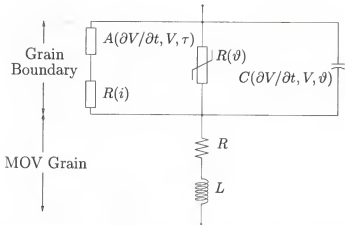


Figure 5.2: Equivalent circuit developed by Schmidt et al. [1989].

In Schmidt et al. [1989], an arrester model that would take into account their findings was developed (see Figure 5.2). Here, $R(i)$ is the non-linear effect of the MOV grain boundary, R is the linear resistance of the MOV grain, $A(\partial V / \partial t, V, \tau)$ is the turn-on element that reflects the dynamic charge distribution at the grain boundary, $C(\partial V / \partial t, V, \vartheta)$ is the capacitance of the arrester block, $R(\vartheta)$ is the high

¹See Woodworth and Thallam [1993] and Thallam et al. [1995] for a complete list of references on metal oxide surge arresters from 1980 to 1992.

ohmic resistance that depends on the temperature and is only of interest at relative low currents ($< 1 \text{ A}$), ϑ is the temperature of the MOV grain, and L is the inductance that constitutes internal and external magnetic fields.²

Most of these parameters were taken from curves they obtained in their experiments.

IEEE Working Group 3.4.11 [1992] proposed a frequency-dependent model, based on data collected by them, supplied by arrester manufacturers, and obtained from test laboratories on arresters, using the *conventional voltage measuring technique*, this model is known as the IEEE model. This model consisted of two non-linear resistors and two $R - L$ filters, as seen in Figure 5.3, although “more sophisticated versions of this model can be made by adding more sections of non-linear resistance separated by $R - L$ filters”. For slow front surges, this $R - L$ filter has very little

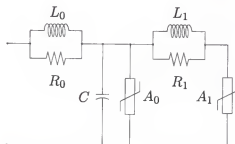


Figure 5.3: Frequency-dependent model proposed by IEEE Working Group 3.4.11 [1992].

impedance and the two non-linear resistors are practically in parallel. For fast surges this impedance becomes more significant and more current is drained in A_0 than in A_1 . Since A_0 has a higher voltage for a given current than A_1 , the arrester model generates higher voltages for faster surges. Its parameters are adjusted by trial-and-error.

²The assumed inductance was of $1\mu\text{H m}^{-1}$ and for the case of coaxial configuration (Figure 4.1b) the inductance was neglected.

A non-linear inductance model, which consists of a non-linear inductance in series with a non-linear resistor, was proposed by Kim et al. [1996], claiming that their model's parameters would be easier to calculate than those of the IEEE model (although it is not clearly stated how to calculate these parameters). The measured waveforms they used to develop their model were obtained also using the *conventional voltage measurement technique*. They proposed a V-I characteristic that consists of a hysteresis loop, which is obtained using the peak voltage of a steep front impulse response (this last could be affected by magnetic coupling to the measuring loop). Their voltage waveforms look unrealistic, since they decay very rapidly and do not exhibit initial spikes (not even for steep front currents).

A simplified model for zinc oxide surge arrester was presented in Pinceti and Giannettoni [1999], based on the IEEE model (IEEE Working Group 3.4.11 1992). The main innovation introduced by the model lays in the simplicity of the criteria proposed for the model's parameter specification (see Figure 5.4). The model can be completely specified starting from the standard manufacturer's data-sheets that report the residual voltages for different current pulses.

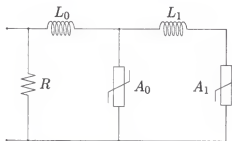


Figure 5.4: Simplified frequency-dependent model proposed by Pinceti and Giannettoni [1999].

In Figure 5.4, R is approximately $1\text{M}\Omega$, L_0 and L_1 are given by:

$$L_0 = \frac{1}{4} \left[\frac{V_{r1/T_2} - V_{r8/20}}{V_{r8/20}} \right] V_n \quad [\mu\text{H}] \quad (5.1)$$

$$L_1 = \frac{1}{12} \left[\frac{V_{r1/T_2} - V_{r8/20}}{V_{r8/20}} \right] V_n \quad [\mu\text{H}] \quad (5.2)$$

where V_n is the arrester rated voltage, V_{r1/T_2} is the residual voltage at 10kA fast front surge ($1/T_2 \mu\text{s}$)³, and $V_{r8/20}$ is the residual voltage at 10kA current surge with a $8/20 \mu\text{s}$ shape. The V-I characteristics of the nonlinear resistors A_0 and A_1 are given in Table 5.1 in p.u. referred to $V_{r8/20}$.

Table 5.1: V-I characteristics of A_0 and A_1 .

| Current [kA] | Voltage A_0 [p.u.] | Voltage A_1 [p.u.] |
|--------------------|----------------------|----------------------|
| 2×10^{-6} | 0.810 | 0.623 |
| 0.1 | 0.974 | 0.788 |
| 1 | 1.052 | 0.866 |
| 3 | 1.108 | 0.922 |
| 10 | 1.195 | 1.009 |
| 20 | 1.277 | 1.091 |

Mata et al. [2000a] proposed an arrester model taking into account magnetic coupling of the current through the arrester to the measuring circuit. This model allowed them to reproduce a voltage spike of about 300 % (with respect to the residual voltage, in that case of 36.4 kV) observed in experimental data. The model is illustrated in Figure 5.5, where the $\text{emf} = \frac{\partial}{\partial t} \iint_A \mathbf{B} \cdot d\mathbf{a}$, and $d\mathbf{a}$ is a differential of area in the loop. The non-linear element $R(t)$ was modeled using a Type 92 non-linear resistors

³The decay time T_2 is not explicitly written because different manufacturers may use different values. According to Pinceti and Giannettoni [1999], "This fact does not cause any trouble, since the peak value of the residual voltage appears on the rising front of the impulse."

(Alternative Transient Program (ATP) Rule Book [1987-1998]). The authors found the initial voltage spike to be an effect of the contribution of the mutual inductance and the stray inductance of the arrester (5.10), and not only of the stray inductance as it is found in the literature (Schmidt et al. 1989; IEEE Working Group 3.4.11 1992). The equivalent circuit shown in Figure 5.5 is also hard to implement in EMTP due

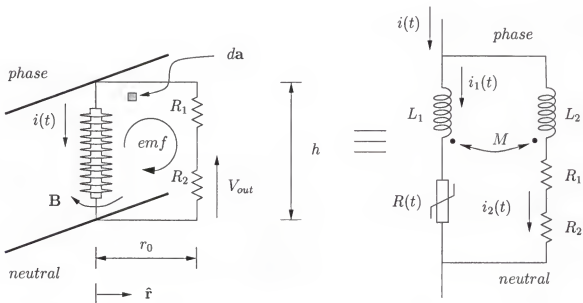


Figure 5.5: Induced voltage in the measuring loop when measuring the voltage across an arrester.

to convergence problems when connecting non-linear elements in series with coupled branches. Therefore, the authors neglected the voltage divider branch in their model, since this is a relatively high impedance compared to the impedance of the arrester. So, the only branch included into the model was the arrester branch (considering only the arrester self-inductance (L_1)), the mutual inductance (M) was taken into account afterwards in the signal processing algorithm). This approximation is valid

if we consider the equation of the equivalent circuit shown in Figure 5.5.

$$\begin{aligned} V_{phase} - V_{neutral} &= V_{R(t)} + L_1 \frac{\partial i_1(t)}{\partial t} - M \frac{\partial i_2(t)}{\partial t} \\ &= V_{R_1} + V_{R_2} + L_2 \frac{\partial i_2(t)}{\partial t} - M \frac{\partial i_1(t)}{\partial t} \end{aligned} \quad (5.3)$$

if we assume that M and L_1 differ by at least one order in magnitude and that:⁴

$$i_2(t) \ll i_1(t)$$

then it follows that:

$$\frac{\partial i_2(t)}{\partial t} \ll \frac{\partial i_1(t)}{\partial t}, \quad \text{and } \therefore i_1(t) \approx i(t)$$

and we can rewrite (5.3) as:

$$\begin{aligned} V_{phase} - V_{neutral} &\approx V_{R(t)} + L_1 \frac{\partial i(t)}{\partial t} \\ &\approx V_{R_1} + V_{R_2} - M \frac{\partial i(t)}{\partial t} \end{aligned} \quad (5.4)$$

From (5.4) we isolate $V_{R_1} + V_{R_2}$, then

$$V_{R_1} + V_{R_2} \approx V_{phase} - V_{neutral} + M \frac{\partial i(t)}{\partial t} \quad (5.5)$$

we also know that,

$$V_{R_2} \approx (V_{R_1} + V_{R_2}) \frac{R_2}{R_1 + R_2} \quad (5.6)$$

and combining (5.5) and (5.6) we obtain:

$$V_{R_2} \approx \frac{R_2}{R_1 + R_2} \left(V_{phase} - V_{neutral} + M \frac{\partial i(t)}{\partial t} \right) \quad (5.7)$$

⁴In Mata et al. [2000a] $M = 6 \mu\text{H}$, $L_1 = 0.5 \mu\text{H}$ and L_2 was neglected.

or expressed in terms of the *actual* voltage across the arrester:

$$V_{R_2} \approx \frac{R_2}{R_1 + R_2} \left(V_{R(t)} + L_1 \frac{\partial i_1(t)}{\partial t} + M \frac{\partial i(t)}{\partial t} \right) \quad (5.8)$$

$$\approx \frac{R_2}{R_1 + R_2} \left(V_{R(t)} + L_1 \frac{\partial i(t)}{\partial t} + M \frac{\partial i(t)}{\partial t} \right) \quad (5.9)$$

$$\approx \frac{R_2}{R_1 + R_2} \left(V_{R(t)} + (L_1 + M) \frac{\partial i(t)}{\partial t} \right) \quad (5.10)$$

where $V_{R_2} = V_{out}$ (the output voltage of the voltage divider seen in Figure 5.5). Note also that the *emf* induced is proportional to $(L_1 + M)$, where L_1 represents the stray and leads inductances of the arrester, and M the magnetic coupling to the measuring loop. This *new approach* reproduces fairly well experimental results as shown by Mata et al. [2000a] (see Section 6.1).

5.4 Leads Connecting the Neutral to Ground Rods

The capacitance and inductance each per unit length of a vertical wire above ground in the absence of other conductors nearby are given by Bazelyan et al. [1978]:

$$C = \frac{2\pi\epsilon_0}{\ln(2h/r)} \quad [F/m] \quad (5.11)$$

$$L = \frac{\mu_0}{2\pi} \ln(2h/r) \quad [H/m] \quad (5.12)$$

where h is the height above ground and r is the conductor's radius. To calculate C and L from (5.11) and (5.12) we have to choose first the number of sections n that will represent the downleads. The vector h is then constructed by dividing the length of the downlead L by the number of sections n and assigning to h the midpoint value of each section. This way we avoid an infinite value when trying to evaluate either (5.11) or (5.12) at $h = 0$. This algorithm is represented in Figure 5.6. If we define $\Delta h = L/n$, from Figure 5.6, h has n terms with increments of Δh , being $h(1) = \Delta h/2$.

Since (5.11) and (5.12) give C and L per unit length we multiply these equations by Δh to obtain (5.13) and (5.14) which give C and L (in F and H respectively) for each section i at a height of $h(i)$.

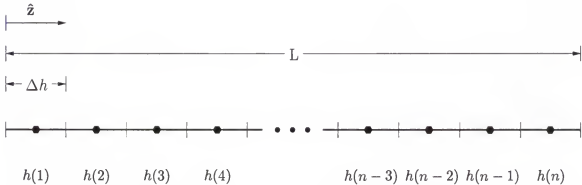


Figure 5.6: Calculation of C and L to be used in the circuit model for downleads.

$$C(i) = \frac{2\pi\epsilon_0}{\ln(2h(i)/r)} \times \Delta h \quad [F] \quad \forall i = 1, 2, \dots, n \quad (5.13)$$

$$L(i) = \frac{\mu_0}{2\pi} \ln(2h(i)/r) \times \Delta h \quad [H] \quad \forall i = 1, 2, \dots, n \quad (5.14)$$

Figure 5.7 shows the values of C and L when representing a downlead of 6 m by 20 $L-C$ sections. The DBM source and datacase files are presented in Section E.3.

5.5 Ground Rod Model

Grounding electrodes can be modeled as distributed R-L-C circuits, as shown in Figure 5.8. In Mata et al. [2000a], it was found (by trial and error) that 30 sections were sufficient for adequate modeling of a 24-m vertical driven rod, where the low-frequency low-current resistances varied from 10 to 60 Ω approximately (See Appendix F for grounding electrodes frequency response for different number of sections used).

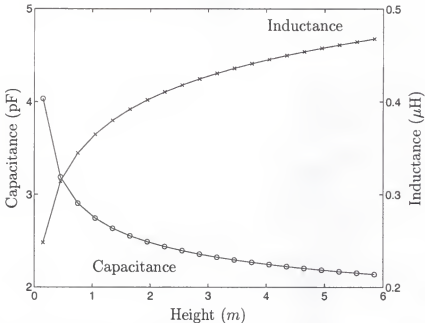


Figure 5.7: Calculated C and L for a downlead of 6 m composed of 20 sections. The total equivalent C and L are $\sum_{i=1}^n C(i) = 49.94 \text{ pF}$ and $\sum_{i=1}^n L(i) = 8.21 \mu\text{H}$.

The capacitance and inductance of the ground rod are given by Imece et al. [1996]:

$$C = \frac{\epsilon_r l}{18 \ln(4l/d)} \times 10^{-9} [\text{F}] \quad (5.15)$$

$$L = 2l \ln\left(\frac{4l}{d}\right) \times 10^{-7} [\text{H}] \quad (5.16)$$

where ϵ_r is the relative permittivity of the soil, l is the length, and d is the diameter of the ground rod.

The nonlinear resistance of the ground rod is usually expressed as a function of current through the rod CIGRE [1991]:

$$R_t(t) = \frac{R_0}{\sqrt{1 + i(t)/I_g}} \quad (5.17)$$

where R_0 is the measured low-frequency, low-current grounding resistance, $i(t)$ is the

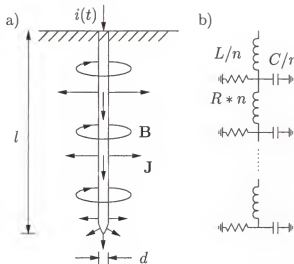


Figure 5.8: Distributed-circuit model of ground rods: a) Schematic representation of current flow and magnetic field lines; b) Equivalent circuit of the ground rod shown in a), where n represents the number of sections. Adapted from Imece et al. [1996].

current through the rod, and I_g is given by:

$$I_g = \frac{E_0 \rho}{2\pi R_0^2} \quad (5.18)$$

In (5.18), E_0 is the critical electric field intensity (approximately 300 kV m^{-1} Imece et al. [1996]), and ρ is the ground resistivity. In 1996, using measured values of R_0 , 26 to 56Ω , $\rho = 4000 \Omega \cdot \text{m}$, we find that I_g is greater than 60 kA . Both measured and calculated currents to ground range from 2 to 8 kA , and hence they are considerably smaller than the computed value of I_g . As a result, the second term under the radical in (5.17) is negligible compared to unity and therefore $R_t \approx R_0$. Based on the above, we modeled ground rods as linear elements. Equations (5.17) and (5.18) imply that in our system the relatively high value of ρ , relatively low values of R_0 , and relatively low values of currents through the rods make the ionization of soil in the vicinity of rods unlikely. However, (5.17) apparently does not account for electrical arcs that can develop radially from the ground rod along the ground surface and reduce the

value of ground resistance with respect to R_0 (e.g., Rakov et al. 1998). The DBM source and datacase files are presented in Section E.4.

CHAPTER 6

DATA PRESENTATION, ANALYSIS, AND MODELING

In this chapter, we present selected measurements made in 1996, 1999, and 2000, and compare the measurements to model predictions for the 1996 and 2000 data. Selected experimental data for the 1996, 1999, and 2000 experiments are presented in Sections 6.1, 6.2, and 6.3, respectively. Additional data for the 1996, 1999, and 2000 experiments are found in Fernandez [1997], Mata et al. [1999b], and Mata et al. [2000i], respectively.

6.1 1996 Experiments

The 1996 experiments are described in Fernandez [1997], Mata et al. [1998a], and Fernandez et al. [1998]. EMTP modeling of the two-conductor distribution line that was exposed to triggered lightning in summer 1996 has been performed by Mata et al. [2000a]. Three different cases were considered, as outlined below.

Case 1. Simple model with measured grounding resistances, 56, 26, 50, and 41Ω , for poles 1, 9, 10, and 15, respectively.

Case 2. Simple model with adjusted values of grounding resistances. These values were 30, 13, 60, and 56Ω for poles 1, 9, 10, and 15, respectively.

Case 3. Complex model using the adjusted values of grounding resistances from *Case 2*.

The adjusted values of grounding resistances were obtained by running an optimization *open-loop* algorithm (using the Nelder-Mead simplex direct search method) in which EMTP was run from MATLAB to compare and minimize the area between

the measured and calculated current-to-ground waveforms for *Case 1*. This algorithm is outlined in Figure 6.1.

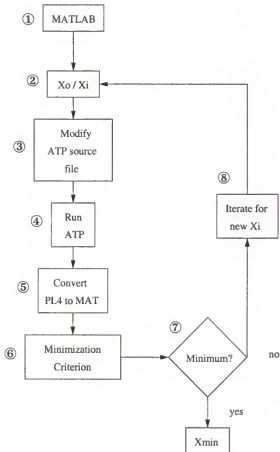


Figure 6.1: ATP/MATLAB minimization algorithm to estimate optimum grounding resistances.

Overall, for *Case 3*, measured and calculated current waveforms showed better agreement than for *Cases 1* and *2* (see Mata et al. [2000a] for more details). Currents to ground are shown in Figures 6.2, 6.3, 6.4, and 6.5.

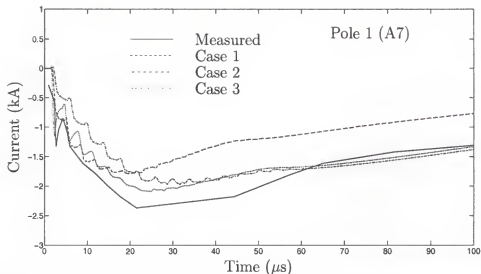


Figure 6.2: Current to ground at pole 1 versus time displayed on a 100- μ s scale, for flash 9621.

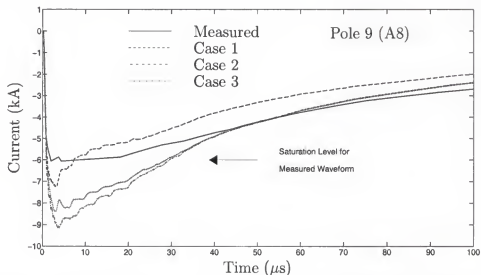


Figure 6.3: Current to ground at pole 9 versus time displayed on a 100- μ s scale, for flash 9621.

6.1.1 Currents to Ground: Cases 1, 2 and 3

The measured and calculated currents to ground at pole 1, shown in 6.2, are in good agreement. Model-predicted waveforms at poles 9, 10, and 15 (Figs. 6.3, 6.4, and 6.5, respectively) for *case 1* show systematic difference of the order of 1 kA with respect to measured waveforms at later times. Overall, it seems that the system allows more

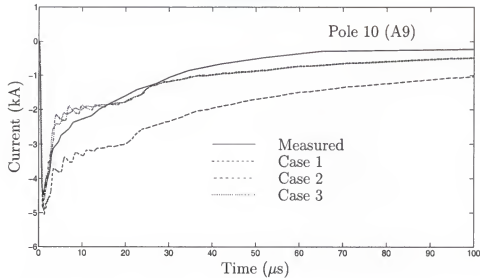


Figure 6.4: Current to ground at pole 10 versus time displayed on a $100\text{-}\mu\text{s}$ scale, for flash 9621.

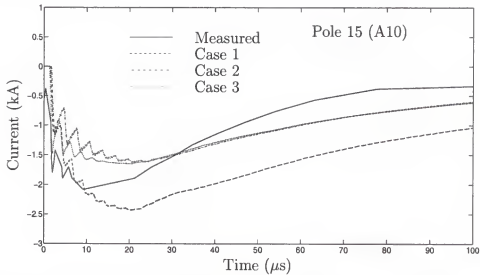


Figure 6.5: Current to ground at pole 15 versus time displayed on a $100\text{-}\mu\text{s}$ scale, for flash 9621.

current to be drained to ground at poles 1 and 9 than at poles 10 and 15. We assumed that the discrepancies are due to the lack of knowledge of the grounding resistances at the time of this experiment, and we adjusted these resistances so that the model-predicted and measured waveforms match better (*case 2*). Note that the distribution of currents to ground is mainly determined by the grounding impedances, and it is relatively insensitive to variations of the failed arrester's impedance at pole 10.

The recomputed currents to ground for *case 3* are presented in the same figures (Figures 6.2, 6.3, 6.4, and 6.5). For this last case, the measured and calculated current waveforms show better agreement than *cases 1 and 2*.

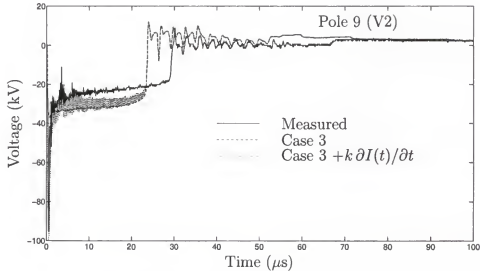


Figure 6.6: Voltage across the arrester at pole 9 displayed on a $100\text{-}\mu\text{s}$ scale, for flash 9621.

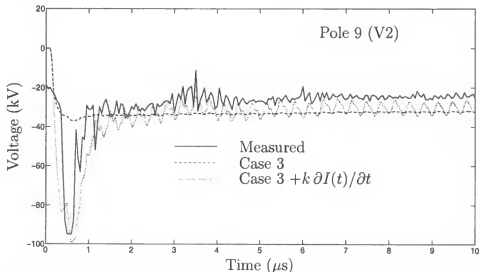


Figure 6.7: Voltage across the arrester at pole 9 displayed on a $10\text{-}\mu\text{s}$ scale, for flash 9621.

6.1.2 Voltages Across the Arresters: Case 3

Measured and calculated voltages at pole 9 are shown in Figures 6.6 and 6.7. The measured voltage waveform at pole 9 shows an initial negative spike clamped at 95 kV (saturation level), followed by damped oscillations superimposed on a plateau that decays slowly from 30 kV to 17 kV for about 29 μ s. After the plateau, the voltage waveform crosses zero sharply and shows damped oscillations superimposed on a small positive overshoot. The initial spike is reproduced when the calculated voltage across the arrester includes the contribution from magnetic coupling to the measuring circuit. The proportionality constant k (see Section 5.3, page 66) determines the magnitudes of the spike and the damped oscillations that follow. Overall, the calculated voltages with magnetic coupling accounted for show better agreement with measurements than voltages computed for the other cases considered here.

6.2 1999 Experiments

In this section we present general information on the 1999 experiments, and we presented the complete set of data (presented in Appendix H) for flash UF-9916 (Section 6.2.6). The 1999 experiments are described in detail in Mata et al. [1999b]. There were a total of 17 rockets fired from the launch tower adjacent to the FPL horizontal distribution line configuration during the period from 08/08/99 to 09/10/99. A summary of launches is given in Table 6.1, where the configuration for each flash and the phase being struck are specified, and the number of return strokes (RS) for each flash was obtained from magnetic tape records. In all tests, lightning current was injected into either phase conductors B or C of the horizontal configuration. The rocket launches resulted in triggering 7 lightning flashes, each with two or more return strokes. Three flashes were directed to phase C of the horizontal configuration (UF-9904, UF-9911, and UF-9912), and four flashes were directed to phase B (UF-9914,

Table 6.1: Summary of launches and strikes to the horizontal framing configuration distribution line during the months of August and September of 1999.

| Date | Time ^a | Flash ID | Result | Number of RS | Struck Phase | Configuration |
|----------|-------------------|----------|------------|--------------|--------------|-----------------------|
| 08-08-99 | 19:07 | UF-9901 | No trigger | | | FPL-A-99 ^b |
| | 19:20 | UF-9902 | No trigger | | | |
| 08-16-99 | 17:07 | UF-9903 | No trigger | | | FPL-A-99 ^b |
| | 17:09 | UF-9904 | Trigger | 5 | C | |
| 08-22-99 | 16:11 | UF-9905 | No trigger | | | FPL-B-99 ^c |
| | 20:07 | UF-9906 | No trigger | | | |
| | 20:09 | UF-9907 | No trigger | | | |
| 08-24-99 | 20:37 | UF-9908 | No trigger | | | FPL-B-99 ^c |
| | 20:38 | UF-9909 | No trigger | | | |
| | 20:50 | UF-9910 | No trigger | | | |
| | 21:01 | UF-9911 | Trigger | 2 | C | |
| | 21:05 | UF-9912 | Trigger | 2 | C | |
| 09-06-99 | 19:03 | UF-9913 | No trigger | | | FPL-C-99 ^d |
| | 19:23 | UF-9914 | Trigger | 2 | B | |
| | 19:25 | UF-9915 | Trigger | 4 | B | |
| 09-10-99 | 19:25 | UF-9916 | Trigger | 7 | B | FPL-D-99 ^e |
| | 19:35 | UF-9917 | Trigger | 4 | B | |

^a EDT (Eastern Daylight Saving Time).

^b Section C.1.1

^c Section C.1.2

^d Section C.1.3

^e Section C.1.4

UF-9915, UF-9916, and UF-9917).

The experience gained in the 1999 experiments was a major factor in the design of the 2000 experiments. It is believed that arrester failures occurred less frequently

in 1999 than in 2000 due to a number of factors including the presence in 1999 of terminating impedances (inductors in parallel with terminating resistors) in some of the tests, relatively small return strokes, arcing between conductors (including that facilitated by the presence of nylon cords between the line conductors and residual triggering wires), and terminating resistor and voltage divider failures (see Section 6.2.7). A brief description of the results for each triggered flash is given next.

6.2.1 Flash UF-9904

The configuration for this event is given in Section C.1.1, page 169. The electrical diagram showing voltage and current measurement locations for this strike is shown in Figure C.1, and the corresponding instrumentation settings are given in Table C.1. Lightning current was injected in phase C. The 433Ω terminating resistors (Section C.1.1) connected between phase C and neutral burned at both ends of the line during the initial continuous current of this flash. A trailing wire left by UF-9903 (an unsuccessful trigger) had fallen across the distribution line, and apparently served to cause arcing from phase C to phase B (from video, there appears to be an arc between phases B and C for every return stroke of the flash). From the high resolution picture taken from IS3 it is observed that the trailing wire illuminates, but it appears to be far from the point where the arc took place, presumably, at or near the location of the nylon cord (See Section C.1.1). Because of the arcs, a relatively large current flowed in the conductor of phase B, burning (at both ends) the 433Ω terminating resistors connected between phase B and neutral during the subsequent strokes.

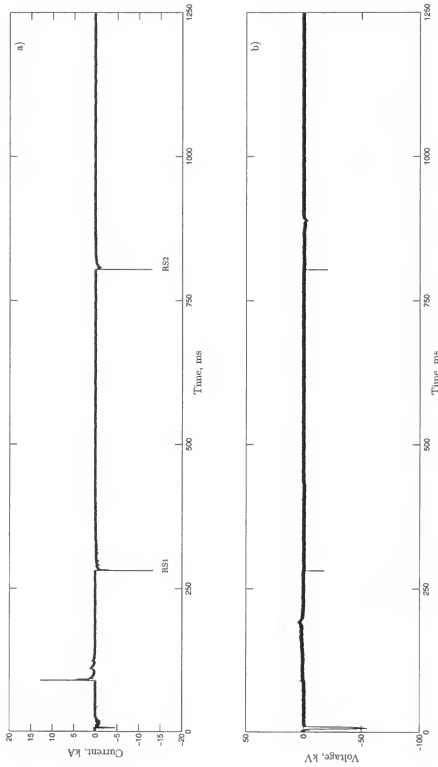


Figure 6.8: Event UF-9911 on a 1.25 s time scale (data taken from the Magnetic Tape Recorder) a) Total lightning current [I_t]; b) Voltage across arrester of phase B at pole 8 [V_{BN8}].

6.2.2 Flash UF-9911

The configuration for this event is given in Section C.1.2, page 170, the electrical diagram is shown in Figure C.2, and the corresponding settings are shown in Table C.2. No terminating resistors were used, so that the line was open-circuited at either end. Lightning current was injected into phase C. For this particular flash, the recorders triggered on the initial stage current, which *damaged the arrester* connected to phase C at pole 8. The total lightning current and the measured voltage across the arrester on phase C at Pole 8 are shown in Figure 6.8 on a 1.25 s time scale. This flash is of particular interest because of the positive continuous current at the beginning of the incident current record (Figure 6.8a). Notice that the arrester failed previous to this large positive continuous current, see the voltage waveform in Figure 6.8b. The collapse of the discharge voltage across the arrester in Figure 6.8b is the point at which the arrester fails, at about 10 ms.

6.2.3 Flash UF-9912

The electrical diagram for this strike is shown in Figure C.2, and the corresponding settings are shown in Table C.2. The configuration was the same as for flash UF-9911 (Section C.1.2, page 170). Lightning current was injected into phase C. The arrester connected to phase C at pole 8 was damaged from the previous strike (UF-9911) on the same day. The oscilloscopes triggered on the first return stroke. No additional damage was evident on the line. The failed arrester from the previous strike (UF-9911) apparently flashed over on both the first and the second stroke, allowing the bulk of the current to flow to the neutral, and from there to ground. Arcs were observed at two different points between phase C and phase B (probably where the nylon cords separate these phases).

6.2.4 Flash UF-9914

The configuration for this event is given in Section C.1.3, page 170. The electrical diagram giving voltage and current measurement locations for this strike is shown in Figure C.3, and the corresponding instrumentation settings are given in Table C.3. For this flash additional measurements were made of the voltage between phases, phase to neutral voltages, and phase currents near the center of the line that were not made for the previous 3 flashes. Lightning current was injected into phase B. Additionally, 16 mH inductors were placed in parallel with the 500Ω , 25 kJ -rated terminating resistors on the line. The purpose of the inductors was to reduce the magnitude of relatively low frequency current components forced through the two line-end arresters that on an actual line might be shared by other arresters and diverted to ground by system transformers. The triggering circuit of the oscilloscopes failed, and only tape recorder data are available. Two of the 1.41 MV rated voltage dividers placed near the center of the line between phases were damaged by the first stroke whose current was near 8 kA, which indicates that a current of such relatively small magnitude would produce a voltage at the middle of the line in excess of 1.5 MV.¹ Arcs were observed on the line between phases B and C, close to the injection point. The failure of the 1.41 MV rated voltage dividers, the arcs observed on the line between phases B and C, and the inductors connected in parallel with the terminating resistors, may have drained enough current from the phase conductor to neutral, so that the energy withstand of the arresters was not exceeded during the flash.

¹Since only tape recorded data are available for this event, we cannot estimate with certainty the rise-time of any of the two return strokes of this flash, which from tape recorded data appears to be of the order of $2\mu s$ for both return strokes.

6.2.5 Flash UF-9915

The configuration of this event was the same as for flash UF-9914 (Section C.1.3, page 170). The electrical diagram for this strike is shown in Figure C.3, and the corresponding settings are given in Table C.3. Since the triggering circuit was not functioning properly on the day this flash occurred, only tape recorder data are available for this flash. This event produced a flashover at the middle of the line from phase B to neutral, although the wire carrying the current from the launcher to phase B might have been involved in the flashover since, as explained in Section C.1.3, there was a nylon cord connected between the downlead from the tower and the neutral, and an examination performed on this nylon cord after this event showed burn marks. For the first return stroke, a flash-over is seen between phase B and phase C (probably at the location of the nylon cord). For the second return stroke an arc was observed from phase C to phase B. From still pictures we see arcs on the clamp-on current sensor connected to phase B. There was also a flash-over from the coaxial cable of this sensor to the neutral. Also, flashovers across the voltage divider connected from phase B to neutral and possibly from phase C to neutral occurred. As in the previous event, it is believed that inductors connected in parallel with terminating resistors, and arcs may have drained enough current from phase B to adjacent phases and/or neutral so that the energy withstand of any arrester connected to this phase was not exceeded during this flash.

6.2.6 Flash UF-9916

The configuration for this event is given in Section C.1.4, page 170. Lightning current was injected into phase B. The electrical diagram for this strike is shown in Figure C.4, and the corresponding settings are given in Table C.4. There was no visually observed flashover, and all instruments recorded data with no obvious

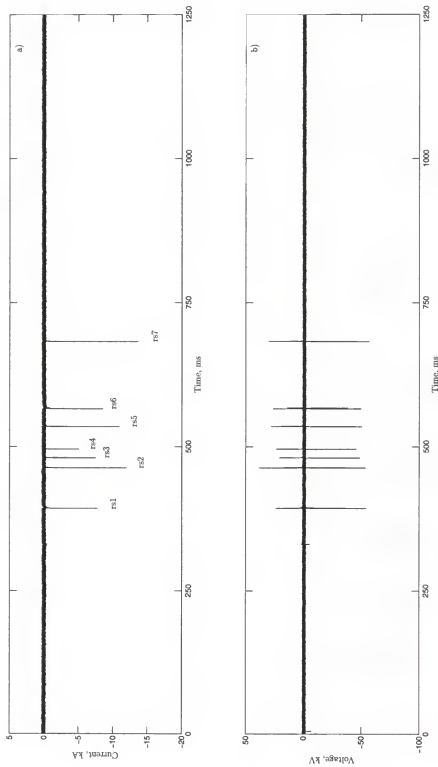


Figure 6.9: Event UF-9916 on a 1.25 s time scale (data taken from the Magnetic Tape Recorder) a) Total lightning current [I_t]; b) Voltage across arrester of phase B at pole 8 [V_{Bx8}].

failures.

The total lightning current and the measured voltage across the arrester on phase C at Pole 8 are shown in Figure 6.9 on a 1.25 s time scale. This flash had a total of seven return strokes. The current that corresponds to the first return stroke is shown on different time scales in Figure H.1. The peak current was about -7 kA, having a rise-time of about 2 μ s. Phase currents arriving at Pole 9 are shown in Figures H.2, H.3, and H.4 on 1 ms, 200 μ s, and 50 μ s time scales, respectively. Phase currents arriving at Pole 8 are shown in Figures H.5, H.6, and H.7 on 1 ms, 200 μ s, and 50 μ s time scales, respectively. Phase A arrester current and voltage at Pole 8 are shown in Figures H.8, H.9, and H.10 on 1 ms, 200 μ s, and 50 μ s time scales, respectively. Phase B arrester current and voltage at Pole 8 are shown in Figures H.11, H.12, and H.13 on 1 ms, 200 μ s, and 50 μ s time scales, respectively. Phase C arrester current and voltage at Pole 8 are shown in Figures H.14, H.15, and H.16 on 1 ms, 200 μ s, and 50 μ s time scales, respectively. Phase to phase voltage at pole 8 is shown in Figure H.17 on different time scales. Phase currents at Pole 7 (currents through the terminating resistors) are shown in Figures H.18, H.19, and H.20 on 1 ms, 200 μ s, and 50 μ s time scales, respectively. Currents to ground at poles 7, 8, 11, and 12 are shown in Figures H.21, H.22, and H.23, on 1 ms, 200 μ s, and 50 μ s time scales, respectively.

6.2.7 Summary of the 1999 Experiments

Table 6.2 summarizes damages (if any) observed during the 1999 experiments. We believe that arresters did not fail as frequently as they did in the 2000 experiments due to several factors including the presence of inductors in parallel with terminating resistors in some of the 1999 tests, relatively small return strokes, arcing between conductors (including that facilitated by the presence of nylon cords between the line conductors and residual triggering wires), and failures of terminating resistors and voltage dividers. Notice from Table 6.2 that for the last three flashes (UF-9914,

UF-9915, and UF-9916) when terminating resistors in parallel with inductors were installed on the line, no arrester failures were observed. Notice also that the current flowed from the struck phase to neutral (and possibly to other phases) through failed voltage dividers and arcs observed in video records at various points in the line. The last flash (UF-9916) was the only flash for which terminating resistors in parallel with inductors were installed on the line and no arcs or voltage divider failures were observed. Yet, the arresters managed to survive. This may have been because UF-9916, although a seven-stroke flash, had relatively small return strokes (see Figure 6.9) and/or enough energy was drained from the struck phase to neutral by the terminating resistors in parallel with the inductors so that the energy withstand of the arresters connected to the struck phase was not exceeded. Notice that no arresters failed on phases adjacent to the struck phase. Figure H.24 shows a comparison of the sum of currents to ground and the total lightning current. Note that the sum of currents to ground is larger than the incident current. This might be due to the fact that in 1999 no end-to-end calibration factors were experimentally obtained for current sensors, whereas for the 2000 experiments, end-to-end calibration factors were obtained. The comparison of computed difference between measured voltages (V_{BN8} and V_{AN8}) and measured voltage [V_{BAS}] is shown in Figure H.25, and their difference was attributed to the nonlinear behavior of the resistors used on the voltage dividers in the 1999 experiments when exposed to high voltages.

6.3 2000 Experiments

During the experiments conducted at the ICLRT in 2000, the distribution line having a horizontal configuration was struck a total of eight times during the period July 11 to August 6 resulting in a total of thirty-four return strokes, and the distri-

Table 6.2: Summary of the 1999 experiments.

| Flash ID | Section | Observations |
|----------|---------|---|
| UF-9904 | 6.2.1 | Terminating resistors connected between phase C and neutral, and phase B and neutral failed. No arresters were damaged. |
| UF-9911 | 6.2.2 | No terminating resistors on the line. Phase C arrester at pole 8 was damaged during the initial stage current. |
| UF-9912 | 6.2.3 | No terminating resistors on the line. Phase C arrester at pole 8 was damaged during previous flash. |
| UF-9914 | 6.2.4 | Terminating resistors in parallel with inductors were installed on the line. Voltage dividers connected between phase B and neutral, and between phase C and neutral failed at the middle of the line. No arresters were damaged. |
| UF-9915 | 6.2.5 | Terminating resistors in parallel with inductors were installed on the line. The voltage divider connected between phase B and neutral failed at the middle of the line. Arcs were observed at various points on the line. No arresters were damaged. |
| UF-9916 | 6.2.6 | Terminating resistors in parallel with inductors were installed on the line. No arresters were damaged. |

bution line having a vertical configuration was struck twice on August 25². Table 6.3 contains a summary of launches and strikes for the month of July, and Table 6.4 gives a summary of launches and strikes for the month of August. Table 6.5 shows the parameters of all recorded strokes triggered during summer 2000. Note that these parameters were calculated by filtering the raw data with a two-point averaging anti-causal zero-phase filter (MATLAB 1996). Further analysis of the data should confirm the return stroke parameters given in Table 6.5. Two levels of saturation of acquired

²The triggering circuit failed, but data for this flash might still be available on magnetic tape. The tape recorder is in need of repair before this determination can be made.

Table 6.3: Summary of launches and strikes to the horizontal framing configuration distribution line during July of 2000.

| Date | Time ^a | Flash ID | Result | Number of RS | Struck Phase | Configuration (Subsection) |
|----------|-------------------|----------|------------|--------------|--------------|----------------------------|
| 07-11-00 | 20:49 | FPL0001 | No Trigger | | | FPL-A-00 |
| | 20:56 | FPL0002 | No Trigger | | | |
| | 20:58 | FPL0003 | No Trigger | | | |
| | 21:07 | FPL0004 | No Trigger | | | |
| 07-12-00 | 12:41 | FPL0005 | No Trigger | | | FPL-A-00 |
| | 13:17 | FPL0006 | No Trigger | | | |
| 07-16-00 | 12:15 | FPL0007 | No Trigger | | | FPL-A-00 |
| | 12:18 | FPL0008 | No Trigger | | | |
| | 12:20 | FPL0009 | No Trigger | | | |
| | 12:21 | FPL0010 | No Trigger | | | |
| | 12:22 | FPL0011 | Trigger | ≥5 | C | (6.3.1) |
| | 12:23 | FPL0012 | No Trigger | | | |
| | 12:24 | FPL0013 | No Trigger | | | |
| | 12:24 | FPL0014 | Trigger | 3 | C | (6.3.2) |
| | 12:32 | FPL0015 | No Trigger | | | |
| | 18:32 | FPL0016 | No Trigger | FPL-A-00 | | |
| 7-20-00 | 18:35 | FPL0017 | No Trigger | | | |
| | 19:04 | FPL0018 | Trigger | ≥6 | C | (6.3.3) |
| | 19:04 | FPL0019 | No Trigger | FPL-A-00 | | |
| 07-25-00 | 19:10 | FPL0020 | No Trigger | | | |
| | 18:06 | FPL0021 | No Trigger | | | FPL-A-00 |
| | 18:08 | FPL0022 | No Trigger | | | FPL-A-00 |
| | 18:09 | FPL0023 | No Trigger | | | |
| | 18:10 | FPL0024 | No Trigger | | | FPL-A-00 |
| 07-28-00 | 18:14 | FPL0025 | Wireburn | | | FPL-A-00 |
| | | | | | | |

^a EDT (Eastern Daylight Saving Time).

Trigger: lightning flash containing return strokes

Wireburn: lightning flash composed of the initial stage only (no return strokes)

Table 6.4: Summary of launches and strikes to the horizontal and vertical framing configuration distribution line during August of 2000.

| Date | Time ^a | Flash ID | Result | Number of RS | Struck Phase | Configuration (Subsection) |
|----------|-------------------|----------|------------|--------------|--------------|----------------------------|
| 08-01-00 | 19:40 | FPL0026 | No Trigger | | | FPL-A-00 |
| | 19:54 | FPL0027 | No Trigger | | | |
| | 20:13 | FPL0028 | No Trigger | | | |
| | 20:14 | FPL0029 | No Trigger | | | |
| 08-02-00 | 17:22 | FPL0030 | No Trigger | | | FPL-A-00 |
| | 17:35 | FPL0031 | No Trigger | | | |
| | 17:47 | FPL0032 | Trigger | ≥ 7 | C | (6.3.4) |
| | 17:54 | FPL0033 | Trigger | 1 | C | (6.3.5) |
| | 17:57 | FPL0034 | Trigger | ≥ 5 | C | (6.3.6) |
| 08-03-00 | 16:11 | FPL0035 | Wireburn | | | FPL-A-00 |
| | 16:12 | FPL0036 | Trigger | ≥ 8 | C | (6.3.7) |
| 08-06-00 | 17:48 | FPL0037 | Trigger | 2 | C | FPL-B-00 (6.3.3) |
| 08-25-00 | 18:10 | FPL0038 | No Trigger | | | FPL-C-00 |
| | 18:16 | FPL0039 | Trigger | ? | A | |
| | 18:21 | FPL0040 | Wireburn | | | |

^a EDT (Eastern Daylight Saving Time)

Trigger: lightning flash containing return strokes

Wireburn: lightning flash composed of the initial stage only (no return strokes)

data are defined:

1. *Severe saturation*: when either the oscilloscope saturated or 140 % of the ISOBE range was exceeded. The oscilloscopes saturation is represented by a dashed line in the data plots.
2. *Slight saturation*: when the scope did not saturate and the waveform peak value is greater than 100 % but less than 140 % of the ISOBE range. The 100 % ISOBE range is represented by a dotted line in the data plots.

There were three unusually large return strokes: stroke 4 of FPL0011 (severely saturated), the single return stroke of FPL0033, and the first return stroke of FPL0037 (these last two slightly saturated). Also, calculated transferred charges for some of the strokes were unusually large (see Table 6.5).

In this section, we present properties of current waveforms for typical flashes, taken from the time and frequency domain tables presented in Appendix I, and measured waveforms compared to model predictions for the first stroke of flash FPL0036 (Section 6.3.8). The time domain tables contain information about the peak current and charge transferred (calculated from current waveforms) in three different time windows ($100\ \mu\text{s}$, $500\ \mu\text{s}$, and $1\ \text{ms}$). The frequency domain tables show the power spectrum density (PSD) of each current measurement integrated over a frequency band (a measure of the power of the signal in that frequency band) in percent with respect to the PSD integrated over the bandwidth of the measurement according to (6.1):

$$PSD_{\Delta f}^{x(n)} = \frac{\int_{0}^{\Delta f} \hat{S}_{xx}(k) df}{\int_0^{Fs} \hat{S}_{xx}(k) df} 100 = \frac{\int_{0}^{\Delta f} X(k) \times X^*(k) df}{\int_0^{Fs} X(k) \times X^*(k) df} 100 [\%] \quad (6.1)$$

where Fs is the sampling frequency, Δf is the frequency band, $x(n)$ is a sequence (measured waveform) of the form of (6.2), $X(k)$ is the discrete Fourier transform (DFT) of $x(n)$, and $\hat{S}_{xx}(k)$ is an estimate (Cartinhour 1998) of the power spectrum

Table 6.5: Parameters of strokes triggered at ICLRT during summer 2000 (a time window of 1 ms was used to calculate the charge).

| Flash ID | RS | Peak [kA] | 10-90% Rise Time [μs] | 50%-decay time [μs] | $\max(\partial i/\partial t)$ [kA/ μs] | Charge [C] |
|-----------|----|--------------|------------------------------------|----------------------------------|--|-------------|
| FPL0011 | 1 | 17.22 | 0.68 | 84.64 | 228.23 | 2.88 |
| | 2 | ≥ 27.71 | - | - | - | ≥ 6.24 |
| | 3 | 19.51 | 1.00 | 13.04 | 81.45 | 3.02 |
| | 4 | ≥ 31.93 | - | - | - | ≥ 5.76 |
| | 5 | 12.68 | 0.24 | 7.92 | 88.61 | 0.88 |
| FPL0014 | 1 | 11.11 | 1.00 | 17.12 | 22.38 | 0.79 |
| | 2 | 25.14 | 0.56 | 25.92 | 59.97 | 2.17 |
| | 3 | 13.29 | 1.04 | 7.76 | 36.70 | 0.70 |
| FPL0018 | 1 | 13.47 | 1.00 | 7.92 | 44.75 | 0.96 |
| | 2 | 8.74 | 0.92 | 14.60 | 26.85 | 0.34 |
| | 3 | 7.45 | 1.04 | 7.32 | 37.59 | 0.51 |
| | 4 | 9.92 | 0.36 | 6.76 | 40.28 | 0.72 |
| | 5 | 7.09 | 0.36 | 7.08 | 35.80 | 0.64 |
| | 6 | 12.39 | 0.32 | 6.64 | 61.76 | 0.98 |
| FPL0032 | 1 | 11.06 | - | 21.92 | 148.22 | 0.46 |
| | 2 | 11.56 | - | 20.12 | 82.15 | 1.03 |
| | 3 | 8.35 | 0.76 | 12.88 | 28.57 | 0.34 |
| | 4 | 18.85 | 0.84 | 18.08 | 66.07 | 1.91 |
| | 5 | 17.21 | 0.60 | 13.68 | 55.36 | 1.43 |
| | 6 | 9.78 | - | 16.72 | 46.43 | 0.46 |
| | 7 | 9.21 | 0.64 | 18.96 | 44.64 | 0.50 |
| FPL0033 | 1 | 56.45 | 0.36 | 50.44 | 439.30 | 10.16 |
| FPL0034 | 1 | 29.03 | 1.04 | 38.04 | 82.15 | 3.47 |
| | 2 | 19.67 | 1.08 | 25.00 | 57.14 | 1.36 |
| | 3 | 19.32 | 1.08 | 24.84 | 51.79 | 1.34 |
| | 4 | 19.32 | 1.08 | 12.76 | 80.36 | 1.41 |
| | 5 | 27.60 | 1.24 | 12.84 | 80.36 | 3.07 |
| FPL0036 | 1 | 27.15 | 1.28 | 56.84 | 128.58 | 3.71 |
| | 2 | 27.58 | 0.36 | 35.92 | 108.93 | 3.95 |
| | 3 | 24.94 | 1.04 | 41.04 | 83.93 | 2.64 |
| | 4 | 7.73 | 1.08 | 17.92 | 16.07 | 0.42 |
| | 5 | 9.08 | 1.12 | 18.12 | 32.14 | 0.53 |
| FPL0037 | 1 | 48.08 | 1.24 | 27.48 | 139.29 | 11.07 |
| | 2 | 21.01 | 1.20 | 11.64 | 112.50 | 1.76 |
| Mean | | 18.16 (32) | 0.85 (29) | 21.94 (32) | 82.76 (32) | 2.05 (32) |
| Geo. Mean | | 15.64 (32) | 0.77 (29) | 17.51 (32) | 63.79 (32) | 1.29 (32) |

Numbers in parentheses are sample sizes. Note that saturated waveforms were not used in computing mean or geometric mean values.

density function $S_{xx}(k)$:

$$x(n) = \begin{cases} \text{possible nonzero values, } & n = 0, 1, \dots, N - 1 \\ 0, & \text{otherwise} \end{cases} \quad (6.2)$$

$$X(k) = \sum_{n=0}^{N-1} x(n) e^{-j \frac{2\pi}{N} kn}, \quad k = 0, 1, \dots, N - 1 \quad (6.3)$$

$$\hat{S}_{xx}(k) = \frac{1}{(2N + 1)} X(k) \times X^*(k) \quad (6.4)$$

Also, incident current, currents to ground, neutral currents, and phase C arresters and phase currents for each stroke of all flashes (except for stroke 1 of flash FPL0036 which is presented in Figure 6.18, page 112) are presented in Appendix H on a 100- μs . Note that saturation levels (tabulated in Appendix I) are not shown in these figures. Additionally, 3-D bar plots, showing the charge transferred to ground at different points on the line, are presented for the flashes when no triggering wires (from previous launches) were laying over the distribution lines. The contents of these tables and the 3-D plots are explained below. We define the **ground charge transfer matrix** which is created as follows.

First, we define a row matrix tw that contains the three different integration upper limits used to calculate the charge:

$$tw_{1 \times m} = [100 \mu s, 500 \mu s, 1 ms] \quad (6.5)$$

The components of the *ground charge transfer matrix* are given by (6.6):

$$GC(k, l) = \sum_j \frac{\int_0^{tw(l)} I_{Gj}^{(k)} dt}{\int_0^{tw(l)} I_i^{(k)} dt} \times 100 \quad (6.6)$$

where k is the stroke order, l indicates the element of the row matrix tw (6.5), j takes the values of 1, 2, 5, 8, 11, 14, 17, and 18, $I_i^{(k)}$ is the measured incident current³ of stroke k , and $I_{Gj}^{(k)}$ is the measured current to ground at pole j of stroke k . The ground charge transfer matrix is then given by (6.7):

$$\mathbf{GC}_{XX} = [GC(k, l)]_{n \times m} = \begin{pmatrix} GC(1, 1) & \dots & GC(1, m) \\ \vdots & \ddots & \vdots \\ GC(n, 1) & \dots & GC(n, m) \end{pmatrix} \quad (6.7)$$

where XX are the last two digits of the flash ID, and n is the maximum number of strokes for which data are available. Ideally, all elements of (6.7) should be equal to 100 %. Values smaller than 100 % might result from saturated current waveforms, calibration errors (overestimation of the incident current and/or underestimation of currents to ground), significant capacitive and resistive leakage currents, and/or measurements resolution.

6.3.1 Flash FPL0011

The configuration for this event is given in Section C.2.1, page 171. The electrical diagram showing voltage and current measurement locations for this strike is shown in Figure C.6. The instrumentation summary is given in Table C.5, and instrumentation settings in Table C.6.

Data for flash FPL0011 are presented in Mata et al. [2000b] which is divided into six sections. Section 1 presents plots for all data available for this flash. As stated above, whenever present in the plots, dashed lines represent the saturation level of the digital oscilloscopes, and dotted lines represent 100 % of the ISOBE range. Strokes 1, 2, 3, 4, and 5 are presented in Sections 2, 3, 4, 5, and 6, respectively. Each section is

³Note that the incident current used to perform the calculations was I_{Mi} , except for those strokes when this measurement was saturated or was not available, in which case I_i was used.

divided into subsections which contain plots of the waveforms on different time scales. The structure of Mata et al. [2000b] is outlined in Table 6.6.

Phase C arrester at pole 8 failed presumably during the second return stroke of this flash. Several trailing wires were laying over the two distribution lines at the time this flash occurred. Arcs are observed in video records at different points on the line.

I_{CN2} and I_{B5} waveforms were lost (oscilloscope failure and ISOBE failure, respectively) and I_{CN11} and V_{CB8} are not reliable (coaxial connector problems).

Peak values and calculated charges of all measured current waveforms available for this flash are given in Tables I.1-I.5 for strokes 1-5.

Table 6.6: Section numbers of Mata et al. [2000b] containing waveforms displayed on different time scales for Flash FPL0011.

| Return Stroke Number | Section numbers for different time windows | | | |
|----------------------|--|------|-------------|------------|
| | 10 ms | 1 ms | 100 μ s | 10 μ s |
| 1 | 2.1 | 2.2 | 2.3 | 2.4 |
| 2 | 3.1 | 3.2 | 3.3 | 3.4 |
| 3 | 4.1 | 4.2 | 4.3 | 4.4 |
| 4 | 5.1 | 5.2 | 5.3 | 5.4 |
| 5 | 6.1 | 6.2 | 6.3 | 6.4 |

6.3.2 Flash FPL0014

The configuration for this event is given in Section C.2.1, page 171. The electrical diagram showing voltage and current measurement locations for this strike is shown in Figure C.6. The instrumentation summary is given in Table C.5, and instrumentation settings in Table C.6.

Data for flash FPL0014 are presented in Mata et al. [2000c], which is divided into

four sections. Section 1 presents plots for all data available for this flash. Whenever present in the plots, dashed lines represent the saturation level of the digital oscilloscopes, and dotted lines represent 100% of the ISOBE range. Strokes 1, 2, and 3 are presented in Sections 2, 3, and 4, respectively. Each section is divided into subsections which contain plots of the waveforms on different time scales. The structure of Mata et al. [2000c] is outlined in Table 6.7.

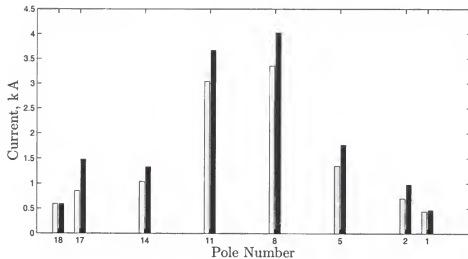


Figure 6.10: Measured peak current to ground for strokes 1 and 3 (in ascending order from left to right) of flash FPL0014 (See Tables I.6 and I.10). Lightning strike point is between poles 9 and 10.

The previous flash (FPL0011) burned all trailing wires from previous launches. Phase C arrester at pole 8 had previously failed (on flash FPL0011, and it had not been replaced when flash FPL0014 occurred) and *flashovers across the damaged arrester were observed on video records. Also, a three-phase and a two-phase flashovers were observed* in video records close to the strike point, separated by several meters. From phase currents I_{B9} and I_{A9} , and arrester current I_{BN8} records, we infer the occurrence of: i) a phase C to phase B flashover for strokes 1, 2, and possibly 3; ii) a presumably phase B to phase A flashover for stroke 2; and iii) a phase C to phase B flashover

at some point between pole 9 and 8 for stroke 3 of this flash. For this stroke, the phase B arrester current at pole 8 I_{BN8} is unusually large and unipolar, while phase B currents at pole 9 I_{B9} is relatively small, making us believe that the flashover occurred somewhere between where phase current measurement instruments were installed at pole 9 and pole 8 (most likely this occurred at pole 8, since burn marks were found on coaxial connectors installed at the phase B arrester at pole 8).

Measurements V_{CB8} and I_{CN11} are not reliable due to coaxial connectors problems. Also, measurement I_{B5} was lost due to an ISOBE failure. Measurements I_{Mi} , I_{AN8} , and V_{AN8} are not available for the second stroke of this flash due to an oscilloscope malfunction. Also, due to a failure on the Honeywell tape recorder (Section 3.3.3.8) data are not available on magnetic tape. Peak values and calculated charges of all

Table 6.7: Section numbers of Mata et al. [2000c] containing waveforms displayed on different time scales for Flash FPL0014.

| Return Stroke Number | Section numbers for different time windows | | | |
|----------------------|--|------|-------------|------------|
| | 10 ms | 1 ms | 100 μ s | 10 μ s |
| 1 | 2.1 | 2.2 | 2.3 | 2.4 |
| 2 | 3.1 | 3.2 | 3.3 | 3.4 |
| 3 | 4.1 | 4.2 | 4.3 | 4.4 |

measured current waveforms available for this flash are tabulated in Tables I.6, I.8, and I.10 for strokes 1, 2, and 3 respectively. Figure 6.10 shows peak values of currents to ground for strokes 1 and 3 (peak values for stroke 2 are not presented due to severe saturation on I_{G17} , see Table I.8). Note that current to ground peaks are larger close to the strike point (at the middle of the line) and relatively smaller at distant poles. Charges transferred to ground (as a percentage of the total stroke charge) are shown in Figures 6.11, 6.12, and 6.13, for strokes 1, 2, and 3 respectively. Note that distant poles (1, 2, 17, and 18) seem to transfer a larger percentage of the total charge for

larger time windows (this effect is more pronounced at poles 17 and 18). Also, from (6.8) we see that 20 % of the charge seems to be lost for all three time windows.

Also, the power spectrum density integrated over four different frequency bands for each current measurement are presented in Tables I.7, I.9, and I.11 for strokes 1, 2, and 3 respectively. The ground charge transfer matrix for three-stroke flash FPL0014 is given by 6.8:

$$\text{GC}_{14} = \begin{pmatrix} 81 & 81 & 82 \\ 77 & 77 & 78 \\ 75 & 76 & 77 \end{pmatrix} \% \quad (6.8)$$

6.3.3 Flash FPL0018

The configuration for this event is given in Section C.2.1, page 171. The electrical diagram showing voltage and current measurement locations for this strike is shown in Figure C.6. The instrumentation summary is given in Table C.7, and instrumentation settings in Table C.8. Data for flash FPL0018 are presented in Mata et al. [2000d] which is divided into seven sections. Section 1 presents plots for all data available for this flash. Strokes 1, 2, 3, 4, 5, and 6 are presented in Sections 2, 3, 4, 5, 6, and 7, respectively. Each section is divided into subsections which contain plots of the waveforms on different time scales. The structure of Mata et al. [2000d] is outlined in Table 6.8.

Phase C arrester at pole 8 burned presumably during the ICC of this flash. A total of six return strokes were recorded in the five segments of the oscilloscopes (two of them being in the first segment). The conditions to trigger arrived late in the storm when the digital video cameras were out of tape. Therefore, for this flash, only video records of SVHF and Hi 8 cameras are available, in which no relevant information is

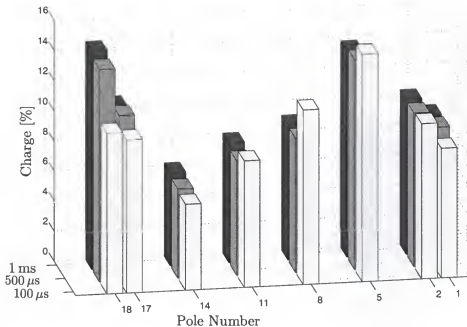


Figure 6.11: Percentage of total charge transferred to ground at different poles, calculated at three different instants of time ($100\ \mu s$, $500\ \mu s$, and $1\ ms$ from the beginning of the return stroke), for stroke 1 of flash FPL0014 (See Table I.6). Lightning strike point is between poles 9 and 10.

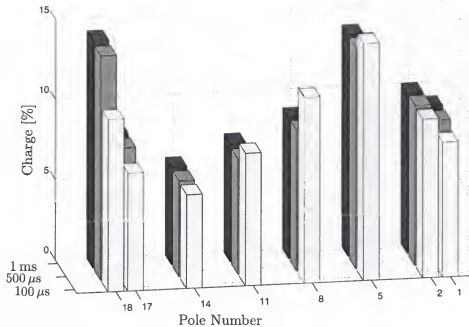


Figure 6.12: Percentage of total charge transferred to ground at different poles, calculated at three different instants of time ($100\ \mu s$, $500\ \mu s$, and $1\ ms$ from the beginning of the return stroke), for stroke 2 of flash FPL0014 (See Table I.8). Lightning strike point is between poles 9 and 10.

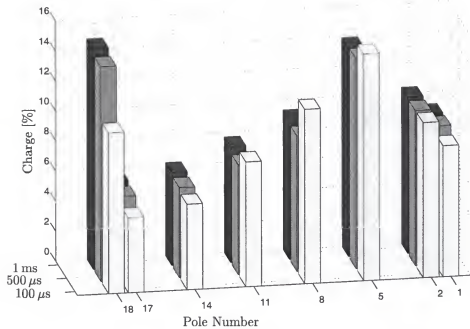


Figure 6.13: Percentage of total charge transferred to ground at different poles, calculated at three different instants of time ($100\ \mu s$, $500\ \mu s$, and $1\ ms$ from the beginning of the return stroke), for stroke 3 of flash FPL0014 (See Table I.10). Lightning strike point is between poles 9 and 10.

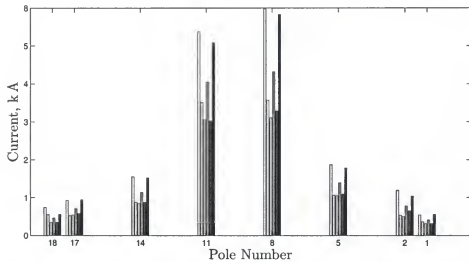


Figure 6.14: Measured peak current to ground for strokes 1 through 6 (in ascending order from left to right) of flash FPL0018 (See Tables I.12, I.14, I.16, I.18, I.20, and I.22). Lightning strike point is between poles 9 and 10.

Table 6.8: Section numbers of Mata et al. [2000d] containing waveforms displayed on different time scales for Flash FPL0018.

| Return Stroke Number | Section numbers for different time windows | | | |
|-------------------------|--|------|-------------|------------|
| | 10 ms | 1 ms | 100 μ s | 10 μ s |
| 1 | 2.1 | 2.2 | 2.3 | 2.4 |
| 2 | | 3.1 | 3.2 | 3.3 |
| 3 | 4.1 | 4.2 | 4.3 | 4.4 |
| 4 | 5.1 | 5.2 | 5.3 | 5.4 |
| 5 | 6.1 | 6.2 | 6.3 | 6.4 |
| 6 | 7.1 | 7.2 | 7.3 | 7.4 |

observed. The arrester current I_{BN8} and an unusually long duration phase current I_{B9} suggest the presence of a flashover from phase C to phase B somewhere between poles 8 and 11 for strokes 1, 2, and possibly 3 of this flash. After stroke 3, no more evidence of flashover is observed in measured currents for strokes 4, 5, or 6. Note that stroke peaks were relatively small compared to other flashes.

Measurement I_{B5} was lost due to an ISOBE malfunction, and V_{CB8} is not reliable due to a coaxial cable problem. Also, due to a failure of the Honeywell tape recorder (Section 3.3.3.8) magnetic tape data are not available.

Peak values and calculated charges of all measured current waveforms available for this flash are given in Tables I.12-I.22 for strokes 1-6. Figure 6.14 shows peak values of currents to ground for strokes 1 through 6. Note that current to ground peaks are larger close to the strike point (in the middle of the line) and relatively small at distant poles. Charges transferred to ground (as a percentage of the total stroke charge) are shown in Figures I.1-I.6, for strokes 1-6. Note that distant poles (1, 2, 17, and 18) seem to transfer a larger percentage of the total charge for larger time windows (this effect is more pronounced at poles 17 and 18).

The ground charge transfer matrix of this flash is given by 6.9:

$$\text{GC}_{18} = \begin{pmatrix} 76 & 78 & 79 \\ 75 & 78 & 80 \\ 75 & 78 & 79 \\ 76 & 78 & 81 \\ 75 & 78 & 80 \\ 74 & 77 & 79 \end{pmatrix} \% \quad (6.9)$$

Note from (6.9) that about 25 % of the charge is lost in the $100\mu\text{s}$ time window for all strokes, and about 20 % of the charge is lost in the 1 ms window.

The power spectrum density values integrated over four different frequency bands for each current measurement are presented in Tables I.13-I.23, for strokes 1 through 6.

6.3.4 Flash FPL0032

The configuration for this event is given in Section C.2.1, page 171. The electrical diagram showing voltage and current measurement locations for this strike is shown in Figure C.6. The instrumentation summary is given in Table C.9, and instrumentation settings in Table C.10.

Data for flash FPL0032 are presented in Mata et al. [2000e] which is divided into eight sections. Section 1 presents plots for all data available for this flash. Strokes 1, 2, 3, 4, 5, 6, and 7 are presented in Sections 2, 3, 4, 5, 6, 7, and 8 respectively. Each section is divided into subsections which contain plots of the waveforms on different time scales. The structure of Mata et al. [2000e] is outlined in Table 6.9.

There was a triggering wire from an earlier launch going over the line and also over the overhead protective mesh on Launch Control when we triggered this flash.

Peak values and calculated charges of all measured current waveforms available

Table 6.9: Section numbers of Mata et al. [2000e] containing waveforms displayed on different time scales for Flash FPL0032.

| Return Stroke Number | Section numbers for different time windows | | | |
|-------------------------|--|------|-------------|------------|
| | 10 ms | 1 ms | 100 μ s | 10 μ s |
| 1 | 2.1 | 2.2 | 2.3 | 2.4 |
| 2 | 3.1 | 3.2 | 3.3 | 3.4 |
| 3 | | 4.1 | 4.2 | 4.3 |
| 4 | 5.1 | 5.2 | 5.3 | 5.4 |
| 5 | 6.1 | 6.2 | 6.3 | 6.4 |
| 6 | 7.1 | 7.2 | 7.3 | 7.4 |
| 7 | | 8.1 | 8.2 | 8.3 |

for this flash are given in Tables I.24-I.30 for strokes 1 through 7. Measurement I_{Li} was lost due to a coaxial cable problem.

6.3.5 Flash FPL0033

The configuration for this event is given in Section C.2.1, page 171. The electrical diagram showing voltage and current measurement locations for this strike is shown in Figure C.6. The instrumentation summary is given in Table C.9, and instrumentation settings in Table C.10.

Data for flash FPL0033 are presented in Mata et al. [2000f] which is divided into two sections. Section 1 presents plots for all data available for this flash. Stroke 1 is presented in Section 2. This section is divided into subsections which contain plots of the waveforms on different time scales. The structure of Mata et al. [2000f] is outlined in Table 6.10.

Peak values and calculated charges of all measured current waveforms available for this flash are given in Table I.31.

This was an unusually large single return stroke (56 kA) flash, for which arresters on the line did not fail. Most of the measurements were saturated on this event, but

Table 6.10: Section numbers of Mata et al. [2000f] containing waveforms displayed on different time scales for Flash FPL0033.

| Return Stroke Number | Section numbers for different time windows | | | |
|-------------------------|--|------|-------------|------------|
| | 10 ms | 1 ms | 100 μ s | 10 μ s |
| 1 | 1 | 2.1 | 2.2 | 2.3 |

still, useful information can be extracted from the data. From video records, a phase C to phase B *flashover is observed* at the strike point. The phase current I_{B9} and the arrester current I_{BN8} indicate the occurrence of a flashover from phase C to phase B (most likely the one observed in video records). Probably, this flashover is the reason why *arresters did not fail* on this flash. From current and voltage waveforms, we calculate the values of energy dissipated by phase C arresters at poles 8 and 11 to be approximately 67 kJ and 58 kJ, respectively.

Measurement I_{Li} was lost due to a coaxial cable problem.

6.3.6 Flash FPL0034

The configuration for this event is given in Section C.2.1, page 171. The electrical diagram showing voltage and current measurement locations for this strike is shown in Figure C.6. The instrumentation summary is given in Table C.9, and instrumentation settings in Table C.10.

Data for flash FPL0034 are presented in Mata et al. [2000g] which is divided into six sections. Section 1 presents plots for all data available for this flash. Strokes 1, 2, 3, 4, and 5 are presented in Sections 2, 3, 4, 5, and 6, respectively. Each section is divided into subsections which contain plots of the waveforms on different time scales. The structure of Mata et al. [2000g] is outlined in Table 6.11.

Phase C arrester at pole 8 burned presumably before stroke 1 of this flash (may be at the end of the ICC, as observed from video records). Arrester current I_{BN8}

Table 6.11: Section numbers of Mata et al. [2000g] containing waveforms displayed on different time scales for Flash FPL0034.

| Return Stroke Number | Section numbers for different time windows | | | |
|----------------------|--|------|-------------|------------|
| | 10 ms | 1 ms | 100 μ s | 10 μ s |
| 1 | 2.1 | 2.2 | 2.3 | 2.4 |
| 2 | 3.1 | 3.2 | 3.3 | 3.4 |
| 3 | 4.1 | 4.2 | 4.3 | 4.4 |
| 4 | 5.1 | 5.2 | 5.3 | 5.4 |
| 5 | 6.1 | 6.2 | 6.3 | 6.4 |

and phase current I_{B9} suggest the occurrence of a flashover from phase C to phase B somewhere between poles 8 and 11, for strokes 1, and possibly 2 and 5, of this flash. This flashover is not observed in video records.

Measurement I_{B5} was lost due to an ISOBE malfunction, and I_{Li} was lost due to a coaxial cable problem.

Peak values and calculated charges of all measured current waveforms available for this flash are given in Tables I.32-I.40 for strokes 1-5. Figure 6.15 shows peak values for strokes 1 through 5 of currents to ground.

Charges transferred to ground (as a percentage of the total stroke charge) are shown in Figures I.7-I.11, for strokes 1-5. Note how distant poles (1, 2, 17, and 18) seem to transfer a large percentage of the total charge for larger time windows (this effect is more pronounced at poles 17 and 18).

The ground charge transfer matrix (see the beginning of this chapter) of this flash is given by 6.10:

$$\text{GC}_{S4} = \begin{pmatrix} 73 & 74 & 74 \\ 72 & 73 & 74 \\ 72 & 73 & 74 \\ 71 & 71 & 72 \\ 70 & 70 & 71 \end{pmatrix} \% \quad (6.10)$$

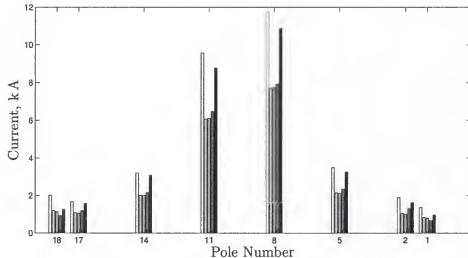


Figure 6.15: Measured peak current to ground for strokes 1 through 5 (in ascending order from left to right) of flash FPL0034 (See Tables I.32, I.34, I.36, I.38, and I.40). Lightning strike point is between poles 9 and 10.

Note from (6.10) that from 25 to 30 % of the charge is lost in all 5 strokes.

6.3.7 Flash FPL0036

The configuration for this event is given in Section C.2.1, page 171. The electrical diagram showing voltage and current measurement locations for this strike is shown in Figure C.6. The instrumentation summary is given in Table C.9, and instrumentation settings in Table C.10.

This is the only flash for which data (only for the first return stroke) are presented and compared to model predictions (Section 6.3.8). Data corresponding to the first stroke of this flash are presented at the end of this section. All data for this flash are presented in Mata et al. [2000j]. Incident current, currents to ground, neutral currents, and phase C arresters and phase currents are shown in Figure 6.18. Additionally, currents to ground, neutral currents, and phase C arresters and phase currents for stroke 1 are shown in Figure 6.18.

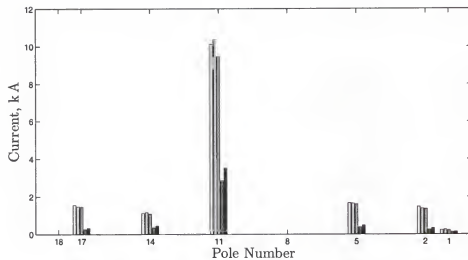


Figure 6.16: Measured peak current through arresters for strokes 1 through 5 (in ascending order from left to right) of flash FPL0036 (See Tables I.42, I.44, I.46, I.48, and I.50). Lightning strike point is between poles 9 and 10.

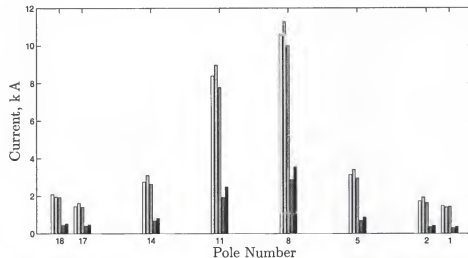


Figure 6.17: Measured peak current to ground for strokes 1 through 5 (in ascending order from left to right) of flash FPL0036 (See Tables I.42, I.44, I.46, I.48, and I.50). Lightning strike point is between poles 9 and 10.

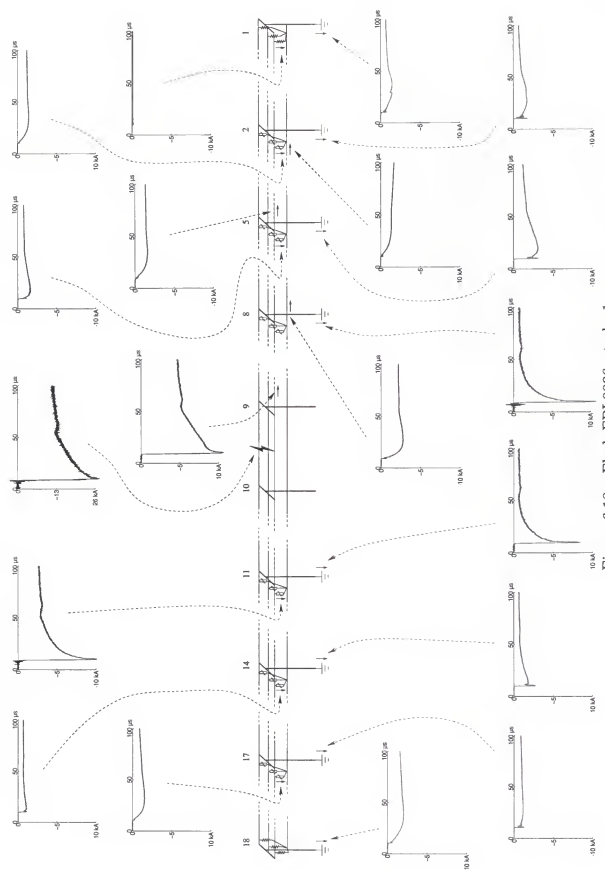


Figure 6.18: Flash FPL0036, stroke 1.

Phase C arrester at pole 8 burned after stroke 5 (last recorded stroke with the total number of strokes being at least 8). Burning of the phase C arrester at pole 8 is observed in video records. There is no indication in the measured current waveforms of a flashover between phases. Phase current I_{B9} appears as a sharp pulse, saturated at -1.5 kA (saturation level) for less than 1 μ s, and the arrester current I_{BN8} also shows a maximum peak of about -1.5 kA for the first three strokes of this flash. Glowing is observed (from video records) at several points in the middle of the line (close to the strike point) but no arcs between phases are observed during this event (at least in the video cameras' fields of view). This is the only flash for which the responses of the line to return strokes were measured without any triggering wires being involved or arrester failure during the ICC. Unfortunately, several measurements were lost due to ISOBES, coaxial cables, and/or oscilloscopes malfunction. Also, current to ground I_{G1} shows a discontinuity near its maximum for the first three return strokes, which was later associated with arcing from the measuring circuit to an underground cable (not used in the experiments presented here) whose termination hangs at pole 1. These arcs are observed in video records. After this event, the terminal of the cable was moved as far away as possible from pole 1. Because of the shape of the waveform of I_{G1} and its magnitude (relative to other currents to ground), it is believed that this arcing does not affect much the calculations of charges.

Current I_{Li} was lost due to a coaxial cable problem, currents I_{Mi} , I_{AN8} , and voltage V_{AN8} are not available for either the second or the third stroke of this flash due to an oscilloscope malfunction, and current I_{CN8} was lost due to an ISOBE failure.

Peak values and calculated charges of all measured current waveforms available for this flash are given in Tables I.42-I.50 for strokes 1-5. Figures 6.16 and 6.17 show peak values for strokes 1 through 5 of arrester currents and currents to ground, respectively. Note that terminating resistor current I_{CN1} is also shown in Figure 6.16.

Transferred charge through phase C arresters at different poles and terminating

resistor at pole 1 for stroke 1 are shown in Figures 6.19 and 6.20, respectively. Note that the distribution of charges are different for the two cases. Most of the stroke flash is transferred through the arresters closest to the strike point, whereas charges transferred to ground are distributed along different grounds. The distribution of charges to ground seems to have the same pattern regardless of the stroke peak current and/or charge, whereas the distribution of charges through arresters depends on the stroke peak current and/or charge. For instance, the distribution of charges through arresters for stroke 1 (27 kA) and 4 (7.7 kA) are shown in Figures 6.19 and 6.21, respectively. Note that for smaller strokes (stroke 4), at later times, charge transferred through the terminating resistor increases significantly, whereas the ratio of charges transferred through arresters seems to remain constant.

The ground charge transfer matrix (see the beginning of this chapter) of this flash is given by 6.11:

$$\mathbf{GC}_{36} = \begin{pmatrix} 68 & 57 & 56 \\ 68 & 58 & 55 \\ 68 & 58 & 57 \\ 71 & 74 & 76 \\ 73 & 74 & 74 \end{pmatrix} \% \quad (6.11)$$

Note from (6.11) and Table 6.5 that there seems to be more charge lost for larger than for smaller strokes. This may be indicative of flashovers to ground, so that some current bypassed current measuring instruments.

The power spectrum density values integrated over four different frequency bands for each current measurement are presented in Tables I.43-I.51, for strokes 1 through 5.

6.3.8 Flash FPL0036, Data and EMTP Modeling

EMTP modeling of this four-conductor distribution line has been performed (Chapter 5) for the first stroke of flash FPL0036.

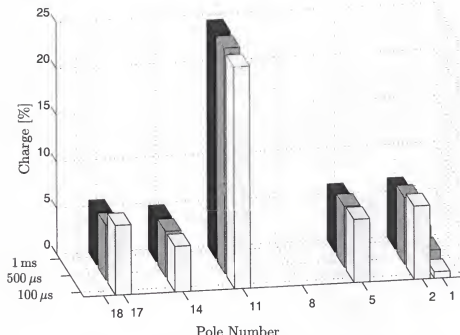


Figure 6.19: Percentage of total charge transferred through phase C arresters at different poles and terminating resistor at pole 1, calculated at three different instants of time ($100\ \mu s$, $500\ \mu s$, and $1\ ms$ from the beginning of the return stroke), for stroke 1 of flash FPL0036 (See Table I.42). Lightning strike point is between poles 9 and 10.

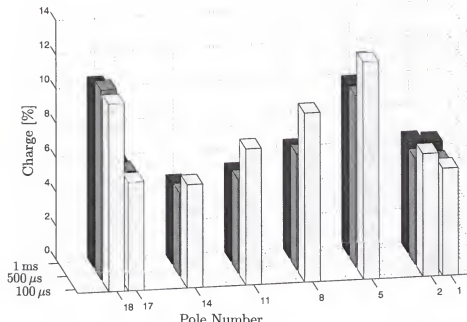


Figure 6.20: Percentage of total charge transferred to ground at different poles, calculated at three different instants of time ($100\ \mu s$, $500\ \mu s$, and $1\ ms$ from the beginning of the return stroke), for stroke 1 of flash FPL0036 (See Table I.42). Lightning strike point is between poles 9 and 10.

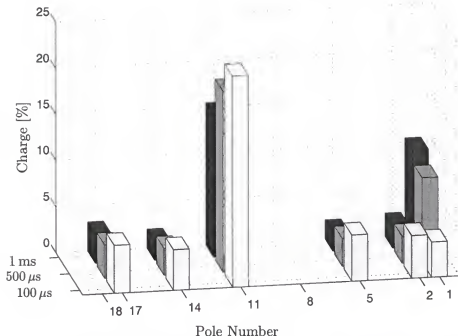


Figure 6.21: Percentage of total charge transferred through phase C arresters at different poles and terminating resistor at pole 1, calculated at three different instants of time ($100 \mu\text{s}$, $500 \mu\text{s}$, and 1 ms from the beginning of the return stroke), for stroke 4 of flash FPL0036 (See Table I.48). Lightning strike point is between poles 9 and 10.

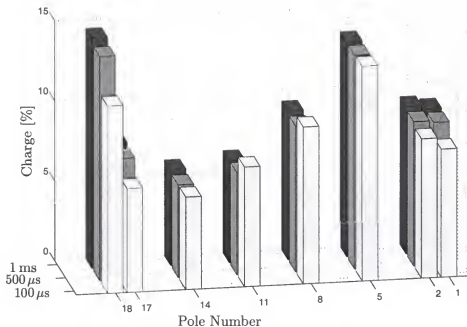


Figure 6.22: Percentage of total charge transferred to ground at different poles, calculated at three different instants of time ($100 \mu\text{s}$, $500 \mu\text{s}$, and 1 ms from the beginning of the return stroke), for stroke 4 of flash FPL0036 (See Table I.48). Lightning strike point is between poles 9 and 10.

Two different cases are considered:

Case 1. Model with measured grounding resistances (see Table 3.1), 40.7, 46.8, 27.7, 51.6, 54.9, 46.4, 37.1, and 22.1 Ω , for poles 1, 2, 5, 8, 11, 14, 17, and 18, respectively.

Case 2. Model with adjusted values of grounding resistances, 49.9, 43.9, 28.3, 34.8, 45.6, 46.7, 34.8, and 18.8 Ω , for poles 1, 2, 5, 8, 11, 14, 17, and 18, respectively. These adjusted values were found with the optimization algorithm explained in Section 6.1. To compare measured and model-predicted currents for this case, the source current used in the model was the measured incident current of stroke 1 (Section 5.1) multiplied by a factor of 0.68, obtained from (6.11). The implication in using the scaling factor for the incident current is that (a) the model is valid, (b) currents to ground are measured accurately, and (c) the incident current is overestimated by about 32%.

The minimization criterion used for *Case 2* is given by (6.12):

$$\min_{Ri} \left[\sum_i \frac{\int_0^{100\mu s} (I_{Gim} - I_{Gic})^2 dt}{\int_0^{100\mu s} I_{Gim} dt} \right] \quad (6.12)$$

where Ri are the grounding resistances used in the model, i takes the values of 1, 2, 5, 8, 11, 14, 17, and 18, I_{Gim} is the measured current at pole i , and I_{Gic} is the model-predicted current waveform at pole i . By integrating the square of the difference between the two current waveforms (I_{Gim} and I_{Gic}) we minimize the difference between the two currents at any instant of time in the time window of interest, instead of the difference between the areas of these two currents. This situation is illustrated in Figure 6.23, from which it is clear that we minimize $\int |I_{Gim} - I_{Gic}|$ which is equivalent to $A_1 + A_2$. By dividing the integral of the square of the difference by the total measured charge transferred to ground at that pole, we normalize each term of the sum in (6.12), assigning all of them the same weight. This means that the difference between the currents at different poles will have the same weight regardless of the magnitude of charges transferred to ground.

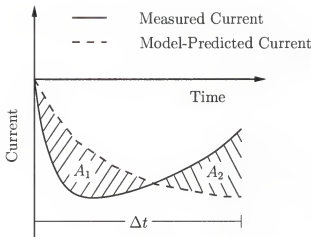


Figure 6.23: Illustration of possible compensation on current waveforms when running the optimization algorithm.

Current to ground at pole 1 is shown in Figure 6.24. Model-predicted waveforms resemble the measured waveform for the two cases; even the fine structure at the beginning of the measured current is reproduced. Case 2 seems to be the best match in this case. Note the relatively fast variation in the measured current to ground waveform near its negative peak. This variation (a dip) was associated with an arc that occurred between an underground cable that was hanging at pole 1 and the downlead connecting the neutral and grounding rod at the pole. The arc occurred above the shunt measuring this current, and therefore, some current bypassed the current sensor. It is believed that a sufficiently high voltage was induced in the underground cable that the arc was produced.

Current to ground at pole 2 is shown in Figure 6.25. Here we also observe a dip near the measured current negative peak. This feature of the waveform was associated with the arcing that took place at pole 1, as explained before. Although model-predicted current waveforms for cases 1 and 2 resemble the measured current to ground at this pole, case 2 provides a better match. Current to ground at pole 5

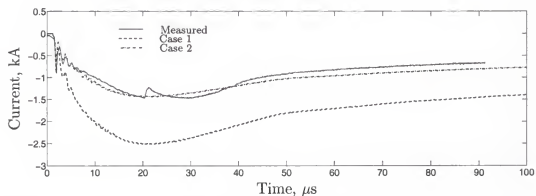


Figure 6.24: Current to ground at pole 1 (I_{G1}) versus time displayed on a $100\text{-}\mu\text{s}$ scale, for stroke 1 of flash FPL0036.

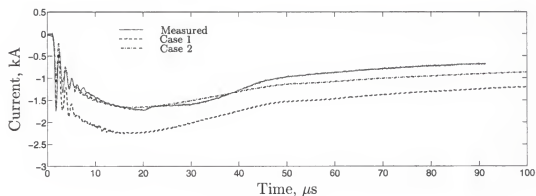


Figure 6.25: Current to ground at pole 2 (I_{G2}) versus time displayed on a $100\text{-}\mu\text{s}$ scale, for stroke 1 of flash FPL0036.

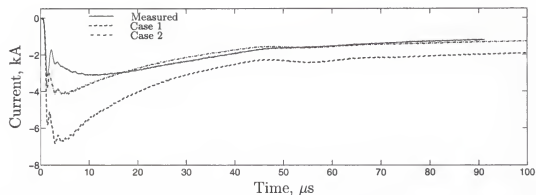


Figure 6.26: Current to ground at pole 5 (I_{G5}) versus time displayed on a $100\text{-}\mu\text{s}$ scale, for stroke 1 of flash FPL0036.

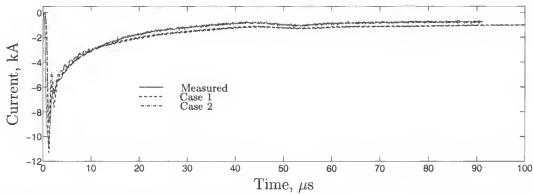


Figure 6.27: Current to ground at pole 8 (I_{G8}) versus time displayed on a $100\text{-}\mu\text{s}$ scale, for stroke 1 of flash FPL0036.

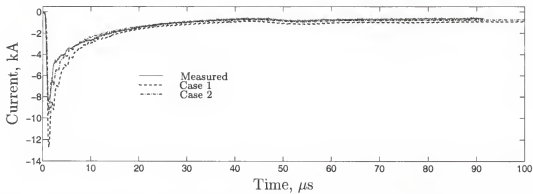


Figure 6.28: Current to ground at pole 11 (I_{G11}) versus time displayed on a $100\text{-}\mu\text{s}$ scale, for stroke 1 of flash FPL0036.

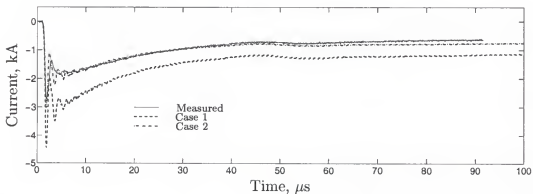


Figure 6.29: Current to ground at pole 14 (I_{G14}) versus time displayed on a $100\text{-}\mu\text{s}$ scale, for stroke 1 of flash FPL0036.

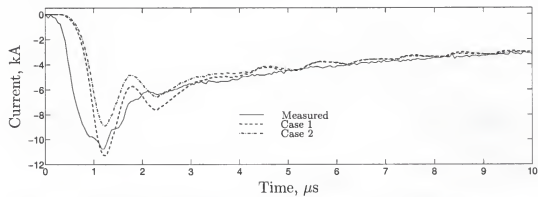


Figure 6.30: Current to ground at pole 8 (I_{G8}) versus time displayed on a 10- μs scale, for stroke 1 of flash FPL0036.

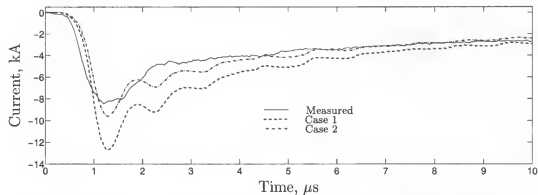


Figure 6.31: Current to ground at pole 11 (I_{G11}) versus time displayed on a 10- μs scale, for stroke 1 of flash FPL0036.

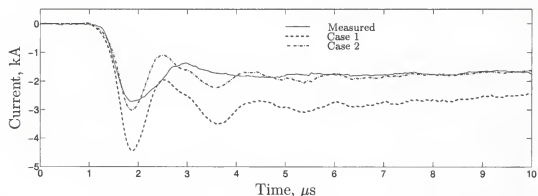


Figure 6.32: Current to ground at pole 14 (I_{G14}) versus time displayed on a 10- μs scale, for stroke 1 of flash FPL0036.

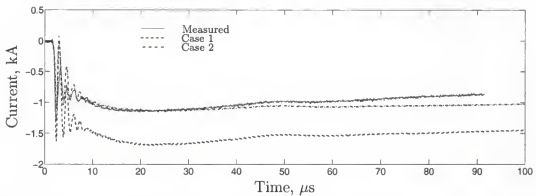


Figure 6.33: Current to ground at pole 17 (I_{G17}) versus time displayed on a $100\text{-}\mu\text{s}$ scale, for stroke 1 of flash FPL0036.

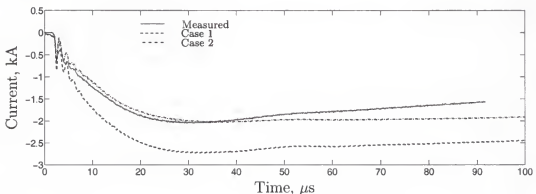


Figure 6.34: Current to ground at pole 18 (I_{G18}) versus time displayed on a $100\text{-}\mu\text{s}$ scale, for stroke 1 of flash FPL0036.

is shown in Figure 6.26. In this case, model-predicted waveforms show a poor match to the measurement for the first $15\text{ }\mu\text{s}$, while a good match is seen at later times. Current measurements indicate that most of the charge is transferred to ground at poles 5 and 8. Current to ground at pole 8 is shown in Figures 6.27 and 6.30 on 100 and $10\text{ }\mu\text{s}$ time scales, respectively. The measured current is well reproduced by the model. Here, case 2 also provides a better match than case 1. Current to ground at pole 11 is shown in Figures 6.28 and 6.31 on 100 and $10\text{ }\mu\text{s}$ time scales, respectively. This current waveform is also well reproduced by the model for both cases considered. Note however that the peak value and the overall waveform is better reproduced in

case 2. Current to ground at pole 14 is shown in Figures 6.29 and 6.32 on 100 and 10 μ s time scales, respectively. Note that the second current peak which occurs at

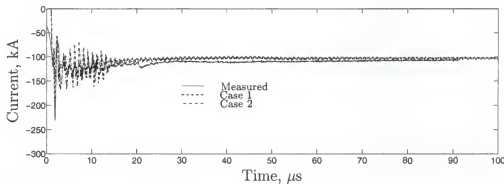


Figure 6.35: Terminating resistor current at pole 1 (I_{CN1}) versus time displayed on a 100- μ s scale, for stroke 1 of flash FPL0036.

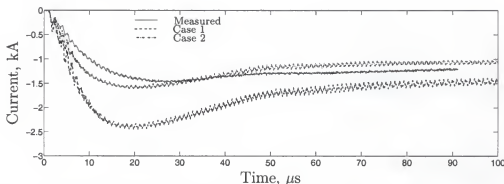


Figure 6.36: Phase C arrester current at pole 2 (I_{CN2}) versus time displayed on a 100- μ s scale, for stroke 1 of flash FPL0036.

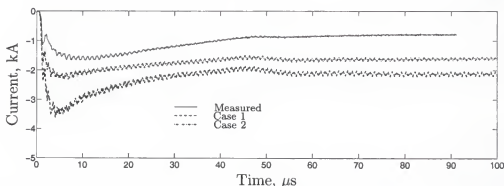


Figure 6.37: Phase C arrester current at pole 5 (I_{CN5}) versus time displayed on a 100- μ s scale, for stroke 1 of flash FPL0036.

about $4\mu s$ in the measured current waveform is reproduced in both cases, but case 1 predicts a fairly large second current peak, not seen in the measured waveform. Again, case 2 provides a better match than case 1. Current to ground at pole 17 is shown in Figure 6.33. Note that the large oscillations during the first $10\mu s$ are reproduced fairly well in both cases, with case 2 yielding a better match. Current to ground at pole 18 is shown in Figure 6.34. Note that the small oscillations in the first $5\mu s$ of the current waveform are well reproduced by the model. Note also that the oscillations in this current to ground are less pronounced than oscillations seen at pole 17, this latter pole having a larger low-frequency, low-current grounding resistance. Overall, currents to ground are very well reproduced by the model, case 2 providing a better match for all of them. Fine structure of measured currents to ground is also well reproduced by model-predicted waveforms. Terminating resistor current at pole 1 is shown in Figure 6.35. Note that the oscillations seen in the measured current during the first $15\mu s$ are damped at later times, this behavior being reproduced by the model. Phase C arrester current at pole 2 is shown in Figure 6.36. Note that the oscillations damped at later times in the measured current waveform are not damped in the model-predicted waveform. Note also that this pole has a relatively low grounding resistance, and yet the current through the arrester at this pole is not much different from the current through phase C arrester at pole 17, which has a larger grounding resistance and, additionally, is farther away from the strike point. From Table I.42 we see that the charge transferred to ground at pole 5 is almost twice the arrester transferred charge at that pole, whereas at all other poles, charges transferred to ground are about the same or less than charges transferred through corresponding arresters. Phase C arrester current at pole 11 is shown in Figure 6.38. Note that the model-predicted waveforms show very large oscillations not seen in the measured current. These oscillations are not present when a slower current source is used. When a crude lumped "corona" model is implemented (a

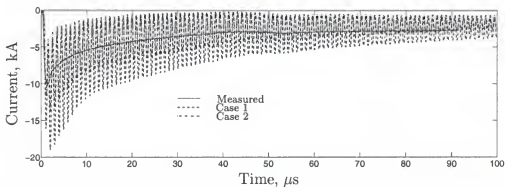


Figure 6.38: Phase C arrester current at pole 11 (I_{CN11}) versus time displayed on a 100- μs scale, for stroke 1 of flash FPL0036.

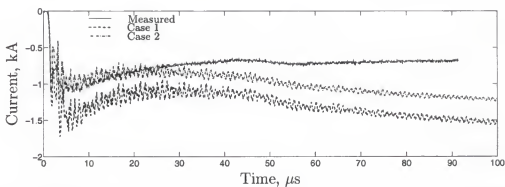


Figure 6.39: Phase C arrester current at pole 14 (I_{CN14}) versus time displayed on a 100- μs scale, for stroke 1 of flash FPL0036.

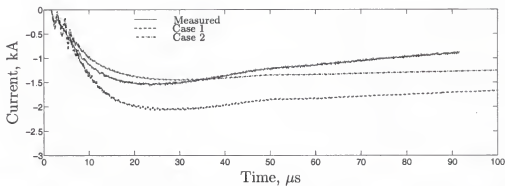


Figure 6.40: Phase C arrester current at pole 17 (I_{CN17}) versus time displayed on a 100- μs scale, for stroke 1 of flash FPL0036.

shunt resistor in parallel with a capacitor to ground at the strike point) and/or the characteristic impedance (500-2000 Ω) of the lightning channel is taken into account

(a shunt resistor to ground), oscillations in model-predicted currents in the middle of the line are damped and model-predicted currents through arresters at poles 8 and 11 resemble measured current waveforms. It seems that certain higher frequency components of the incident current excite some modes of propagation on the line making the line section from the strike point to the first arrester station resonate at these higher frequencies. These oscillations are not seen in model-predicted current to ground waveforms; the oscillations are only present in model-predicted waveforms for the struck phase, neutral, and arresters closest to the strike point. Phase C arrester current at pole 14 is shown in Figure 6.39. This is the worst model-predicted arrester current. The measured arrester current decays after it reaches its peak, whereas in the model-predicted waveform the current initially decays after the peak and after about $30\mu s$ increases again. Phase C arrester current at pole 17 is shown in Figure 6.40. This model-predicted current waveform shows very good agreement with the measured current. Overall, model-predicted waveforms show good agreement with measured currents, with case 2 providing a better match than case 1. It is worth noting that the model lacks such voltage limiting effects such as corona. Also, oscillations are rapidly damped when a parallel combination of capacitor and resistor (a crude lumped model of corona) or the characteristic impedance of the lightning channel (500 - 2000Ω) is connected in parallel with the source (between the strike point and ground).

The distribution of arrester currents is a complex function of the grounding resistances at the different poles and their distance from the strike point. The following observations can be made: 1) arrester current seems to be primarily determined by the distance from the strike point, while the grounding resistance at the arrester station does not seem to have much effect on arrester current. The arresters located closest to the strike point always allowed more current to flow from the struck phase to neutral than more distant arresters, 2) the charge transferred from neutral to ground is

primarily determined by the low-frequency, low-current grounding resistance, while the distance from the strike point does not seem to have much effect on the charge transferred; the lower the grounding resistances the more charge is transferred to ground.

6.3.8.1 Energy dissipated by arrester during a multiple stroke flash

Phase C arrester at pole 11 is the only arrester for which simultaneously recorded voltage and current waveforms for the first 5 strokes in flash FPL0036 are available. From the current and voltage measurement we can estimate the energy dissipated by this arrester for the first 5 strokes of this flash. Flash FPL0036 contained more than 5 strokes, and the arrester failed during one of the strokes after stroke 5.

Table 6.12: Calculated dissipated arrester energy by the phase C arrester at pole 11 for the five strokes of flash FPL0036. Also shown are the arrester transferred charge and peak current. Value in parenthesis indicate the time window of integration.

| Parameter | Stroke 1 | Stroke 2 | Stroke 3 | Stroke 4 | Stroke 5 |
|--------------|----------------|----------------|----------------|-----------------|-----------------|
| Energy [kJ] | 29.8 | 29.5 | 18.7 | 2.7 | 3.1 |
| Charge [C] | 0.84 (4 ms) | 0.82 (4 ms) | 0.45 (4 ms) | 0.036 (2 ms) | 0.061 (2 ms) |
| max I [kA] | 10.0 | 10.2 | 9.3 | 2.7 | 3.4 |

In Figures 6.41a and 6.41b the linear regressions lines, given by (6.13) and (6.14), respectively, are shown. The energy dissipated by the arrester is slightly better correlated with the charge transferred through the arrester than with the peak current. Note that at the end of stroke 5 of this flash, this arrester had already dissipated approximately 84 kJ (the maximum withstand energy of this arrester is about 72 kJ, see Section 6.3.9.1).

$$E(C) = 34 \times C + 1.6 \text{ [kJ]; } \rho = 0.998 \quad (6.13)$$

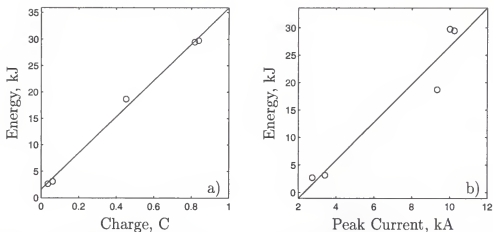


Figure 6.41: Correlation between the arrester's dissipated energy and: a) the arrester transferred charge, and b) the arrester peak current.

$$E(\max I) = 0.0035 \times (\max I) - 8 \text{ [kJ]; } \rho = 0.966 \quad (6.14)$$

where E is the energy in kJ, C is the charge in coulombs, $\max I$ is the current peak, and ρ is the linear correlation coefficient. This arrester failed only after stroke 5, even though the cumulative dissipated energy for the first five strokes exceeded the maximum withstand energy of the arrester. It is important to note that, the cumulative dissipated energy of about 84 kJ does not account for the energy dissipated during the initial stage of the flash. Furthermore, there might have been continuing currents and M components between the strokes that did not trigger the digitizers. Note also that the arrester might have been cooled to some extent during interstroke intervals.

The phase C arrester at pole 8 failed after stroke 5 because it dissipated more energy than the phase C arrester at pole 11. The tape recorder needs to be repaired before we can determine whether current data for strokes of order 6 and higher for this flash were recorded.

6.3.9 Flash FPL0037

The configuration for this event is given in Section C.2.2, page 172. The electrical diagram showing voltage and current measurement locations for this strike is shown in Figure C.7. The instrumentation summary is given in Table C.11, and instrumentation settings in Table C.12.

Data for flash FPL0037 are presented in Mata et al. [2000h] which is divided into four sections. Section 1 presents plots for all data available for this flash. Strokes 1 and 2 are presented in Sections 2 and 3, respectively. Each section is divided into subsections which contain plots of the waveforms on different time scales. The structure of Mata et al. [2000h] is outlined in Table 6.13. Section 4 presents long duration records successfully acquired for this flash.

Table 6.13: Section numbers of Mata et al. [2000h] containing waveforms displayed on different time scales for Flash FPL0037.

| Return Stroke Number | Section numbers for different time windows | | | |
|----------------------|--|------|-------------|------------|
| | 10 ms | 1 ms | 100 μ s | 10 μ s |
| 1 | 2.1 | 2.2 | 2.3 | 2.4 |
| 2 | 3.1 | 3.2 | 3.3 | 3.4 |

Phase C arrester at pole 8 burned during the ICC of this flash (see Section 6.3.9.1). Also, a phase C to phase B flashover was optically observed at the strike point (pole 9). Current measurements I_{B9} and I_{BN8} suggest the presence of such flashover for stroke 1, which was the second largest return stroke of the season (48 kA). Current measurements do not contain an indication of a flashover during stroke 2 (21 kA).

Measurement I_{G1} was lost due to an ISOBE malfunction. The ground charge transfer matrix is not presented for this event, since the ISOBE 3000 measuring I_{G1} failed when this flash occurred.

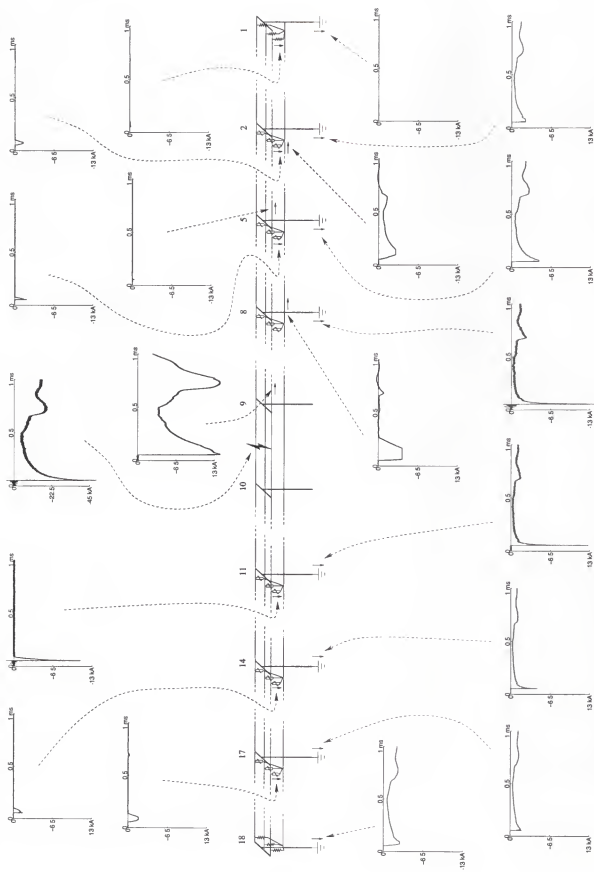


Figure 6.42: Flash FPL0037, stroke 1, displayed on a 1-ms scale (some current waveforms are saturated, see Table 1-52).

Peak values and calculated charges of all measured current waveforms available for this flash are found in Tables I.52 and I.54 for strokes 1 and 2, respectively. The power spectrum density values integrated over four different frequency bands for each current measurement are presented in Tables I.53 and I.55, for strokes 1 and 2 respectively.

Incident current, currents to ground, neutral, and phase C arresters and phase currents for stroke 1 of this flash are presented in Figure 6.42 on a 1-ms scale. This particular flash is of interest because of the large M component that follows the stroke. Also, phase C arrester at pole 17 was the only arrester that operated on this M component (see Figure 6.42).

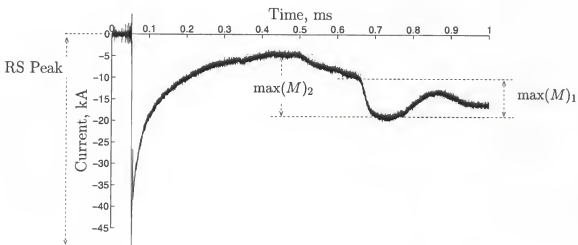


Figure 6.43: Measurement of return-stroke peak current, RS peak, and two measurements of M-component current, $\max(M)_1$ and $\max(M)_2$. The current waveform was recorded at the launcher (at the channel base).

The measured and calculated (Section 6.3.8) grounding conductances at each pole of the horizontal distribution line are shown in Figure 6.44 as a percentage of the total (the combination of all grounding conductances) measured and calculated grounding conductances, respectively. Note that Figure 6.44 is very similar to those that show

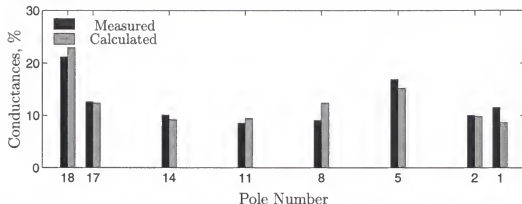


Figure 6.44: Measured and calculated conductances in percent of the total conductance of the grounding system.

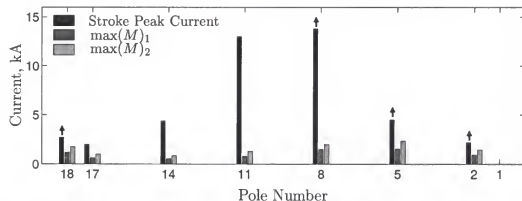


Figure 6.45: Measured stroke peak current, M component peak current $\max(M)_1$, and M component peak current $\max(M)_2$ for flash FPL0037 (See Figure 6.43). Arrows indicate saturated current waveforms (See Table I.52). Lightning strike point was at Pole 9, phase C.

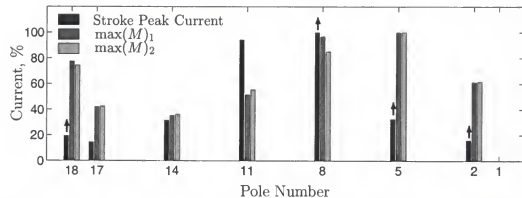


Figure 6.46: Measured stroke peak current, M component peak current $\max(M)_1$, and M component peak current $\max(M)_2$ for flash FPL0037 in percent of their respective maximums at the channel base (See Figure 6.43). Arrows indicate saturated current waveforms (See Table I.52). Lightning strike point was at Pole 9, phase C.

the charge transferred to ground (see for instance Figure I.15, page 375). Figure 6.45 shows the peak current comparison of stroke 1 and the M component that follows this return stroke at each ground rod. Measurements of the return stroke peak current and two measurements of the M-component peak current $\max(M)_1$ and $\max(M)_2$, are illustrated in Figure 6.43. Note from Figures 6.45 and 6.46 that the distribution of return-stroke peak current among the ground rods appears to be symmetric with respect to the strike point (in this case the strike point was located at pole 9), whereas the distribution of M component peak current is similar to the distribution of the grounding conductances shown in Figure 6.44. Apparently, the lower frequency components of the stroke current flow to ground according to the distribution of the grounding conductances (or resistances) along the line, and the higher frequency components of the stroke current, which are also those with largest amplitudes, flow to ground primarily near the strike point, regardless of grounding resistances.

6.3.9.1 Energy dissipated by arrester during initial-stage current

The arrester installed at pole 8 on phase C of the cross arm configuration repeatedly failed during the 2000 experiments (see Section 6.3.10). All arresters on the line survived only one flash (single-stroke flash FPL0033, Section 6.3.5), during which flashovers were observed on the line. Arrester voltage and low-level current (see Table C.12 for instrumentation settings) measured during the ICC of Flash FPL0037 allowed us to study the responses of arresters to the ICC. From the voltage and current waveforms we calculate the instantaneous power ($P(t) = v(t) * i(t)$) and integrated it over time to obtain the energy. These are the first ever simultaneously-recorded arrester low-level current and voltage waveforms from which we can compute the energy dissipated in the arrester.

The measured low-level incident current, arrester current at pole 11, arrester voltage and current at pole 8, and the calculated energy as a function of time are shown

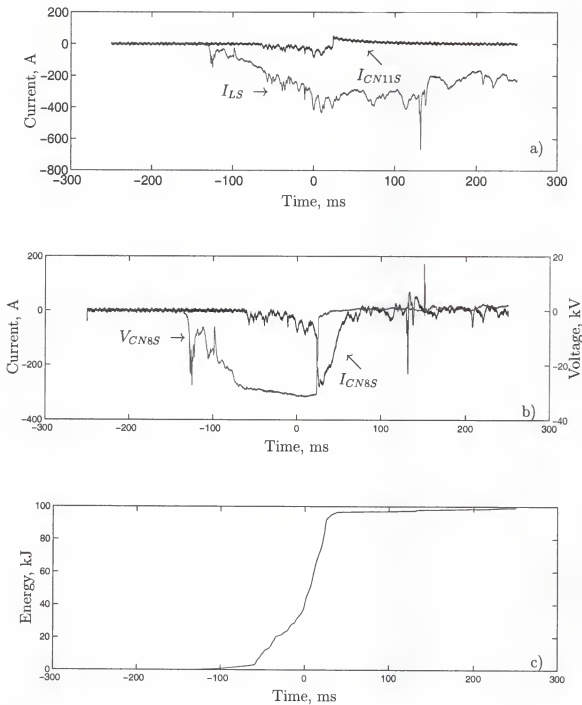


Figure 6.47: a) Incident lightning channel current and current through arrester at pole 11 (I_{LS} and I_{CN11S} , respectively), b) measured arrester voltage and current at pole 8 (V_{CN8S} and I_{CN8S}), c) computed energy for the arrester at pole 8 which failed during flash FPL0037.

in Figure 6.47. When overlapping arrester current at pole 11 and arrester current at pole 8, the latter seems to be slightly larger than the former. Higher resolved currents would reveal the difference between them, but due to dynamic range of equipment, and 8-bit resolution of digital oscilloscopes, the comparison cannot be done reliably. Figure 6.47c shows that the energy dissipated by the arrester had reached about 90 kJ before the arrester failed (the collapse of the discharge voltage across the arrester in Figure 6.47b is the instant at which the arrester fails, at about 25 ms). This value of failure-causing energy seems to be consistent with the maximum dissipation energy for MOV arresters given by Greenwood [1991], which is on the order of 4 kJ/kV of kV rating (Greenwood [1991]). Since the arresters used in these experiments have a voltage rating of 18 kV, the expected withstand energy is about 72 kJ. The voltage across the arrester remained clamped at about 30 kV while there was detectable current through the device (see Table 3.3, page 33). Note the voltage response of the MOV (Figure 6.47b) to the initial ICC pulse at about -120 ms (Figure 6.47a) even when there is no detectable current flowing through the arrester. From Figure 6.47b we see how the failed arrester takes all the current right after it fails, saving other arresters connected in parallel to it. Note also that the ICC (a few hundred of amperes) was rather typical of either the initial stage in rocket-triggered lightning or of long continuing current following return strokes in both triggered and natural lightning. As noted in Section 2.1.1.1 continuing current occurs in about half of all natural flashes to ground. Shorter-duration continuing currents probably occur in most, if not all, natural cloud-to-ground flashes.

6.3.10 Summary of the 2000 Experiments

We believe that arresters failed more frequently in the 2000 experiments than they did in the 1999 experiments because of the use of high-energy terminating resistors in 2000 that did not fail. Also, no other device failures occurred anywhere on the

line in 2000, that could divert current from the struck phase conductor to adjacent conductors and/or to neutral, reducing the stress on the arresters.

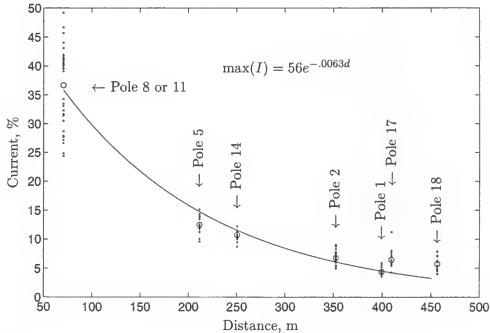


Figure 6.48: Measured peak current to ground in percent of the total lightning peak current as a function of distance from the strike point. Dots represent measured peak current to ground for all strokes triggered in 2000 with no severe saturation, circles indicate mean values, and the solid line is the exponential function that fits the mean values.

An important finding in this study is that the distribution of peak currents to ground is more or less symmetrical with respect to the strike point (see Figure 6.14) and appears to be strongly dependent on the distance from the strike point, regardless of the low-frequency, low-current grounding resistances (see Figure 6.48), whereas the charges transferred to ground are distributed according to the low-frequency, low-current grounding resistances (see Figure 6.13). The distribution of arrester currents is a complex function of grounding resistances at different poles and the distance from the strike point. The following observations were made: 1) arrester current

is primarily determined by the distance from the strike point, while the grounding resistance at the arrester station does not appear to have much effect on arrester current. The arresters located closest to the strike point always allowed more current to flow from the struck phase to neutral than more distant arresters, 2) the charge transferred from neutral to ground is primarily determined by the low-frequency, low-current grounding resistance, while the distance from the strike point does not seem to have much effect on the charge transferred; the lower the grounding resistances the more charge is transferred to ground.

We observed a 20 to 30 % discrepancy between the total charge injected into the system, and the total charge transferred to ground (represented by the ground charge transfer matrix), the injected charge being larger than the charge transferred to ground. This difference might be the result of the limited resolution of the measuring systems, calibration errors (overestimation of the incident current and/or underestimation of currents to ground), and appreciable capacitive and resistive leakage currents. Note that in 1999, the injected charge was observed to be smaller than the charge transferred to ground, apparently due to calibration errors.

The model predicts oscillations in the current waveforms between the strike point and the nearby arrester stations clearly seen in the model-predicted arrester currents at poles 8 and 11 (Figure 6.38). These oscillations are not seen in measurements. When a crude lumped "corona" model is implemented (a shunt resistor in parallel with a capacitor at the strike point) and/or the characteristic impedance ($500\text{-}2000\ \Omega$) of the lightning channel is taken into account, oscillations in model-predicted currents in the middle of the line are damped and the model-predicted currents through arresters at poles 8 and 11 resemble measured current waveforms. Therefore, it is believed that corona on line conductors and other elements of the system near the strike point may contribute (although not known to what degree) to the difference between total charge injected into the system and the total charge transferred to ground, observed in 2000.

In Florida, where the ground flash density is about 10 flashes per square kilometer per year, distribution lines on 7-m and 10-m poles are expected to be struck by lightning on average from 0.075 to 0.60 times/km/year and 0.093 to 0.87 times/km/year, respectively (Bazelyan et al. 1978). A kilometer of the horizontal-configuration distribution line we tested has about 20 arresters, therefore, we should expect to have about 0.33-2.6 % of all installed arresters fail each year if 90 % of the flashes destroy each one arrester. A mile of the vertical-configuration distribution line has about 12 arresters, therefore, we should expect to have about 0.65-5.9 % of all installed arresters fail each year if 90 % of the flashes destroy each one arrester. These percentages are not much dissimilar from the 0.14 - 1.4 % arrester failure rate per year reported by Barker et al. [1998] for power lines on 20-m poles, but considerably higher than the industry cited arrester failure rates which are usually in the range of 0.01 to 0.1 % per year. If the rate we observe is applicable to typical lines, essentially every lightning strike will destroy an arrester near the strike point.

Table 6.14: Summary of the 2000 experiments.

| Flash ID | Section | Observations |
|----------|---------|--|
| FPL0011 | 6.3.1 | Trailing wires over the two lines. Phase C arrester at pole 8 failed on the second return stroke. |
| FPL0014 | 6.3.2 | Arcing across the failed arrester from the previous flash. A three-phase and a two-phase flashovers close to the strike point were observed. |
| FPL0018 | 6.3.3 | Phase C arrester at pole 8 failed during the ICC. Possible flashover from phase C to phase B. |
| FPL0025 | - | Phase C arrester at pole 8 failed during the ICC. |
| FPL0032 | 6.3.4 | Trailing wires over the lines. No arrester failure. |
| FPL0033 | 6.3.5 | Single stroke flash. Flashover at the strike point is observed. No arrester failure. |
| FPL0034 | 6.3.6 | Phase C arrester at pole 8 failed before stroke 1. Possible flashover from phase C to phase B. |
| FPL0036 | 6.3.7 | Phase C arrester at pole 8 failed after stroke 5. At this point we cannot determine whether there was a flashover or not. |
| FPL0037 | 6.3.9 | Phase C arrester at pole 8 failed during the ICC. Flashover between phase C and B at the strike point. |

CHAPTER 7 SUMMARY

7.1 1996 Experiments

Three versions of EMTP models that differ in their level in complexity of representation of the line, ground leads, and grounding rods are compared for the 1996 experiments in Section 6.1. Although each reproduces fairly well the overall measured waveforms, the fine structure of the measured waveforms is better reproduced by the most complex model. In the modeling, measured dc grounding resistances were adjusted (within 50 % of measured values) in order to reproduce better the measured currents to ground. The adjusted values of dc ground resistances were obtained by minimizing the area between the measured and calculated current-to-ground waveforms, in which ATP is run from MATLAB, and the ground resistances are changed, until an optimization criterion is satisfied. The minimization variables are the dc ground resistances, and the variable to be minimized is the sum of the areas between the measured and model-predicted currents to ground. Initial spikes at the beginning of the arrester voltage waveforms were found by modeling to be attributable to magnetic coupling of the current flowing through the arrester to the voltage measurement circuit. This finding led to the design and implementation of a novel *magnetic-flux-compensated voltage divider* that reduces this magnetic coupling. This device is still under study.

7.2 1999 Experiments

Seven flashes, each containing one or more return strokes, were triggered to phases C and B at the center of the line, and voltages and currents were measured with submicrosecond time resolution at various locations on the line, in addition to the measurement of the incident lightning current. For the seven flashes, 3 to phase C and 4 to phase B, at least 4 flashes produced flashovers, although nylon phase-wire separators, triggering wire from a previous rocket launch, the hard-wire connection from the rocket launcher to phase B, and parts of measurement systems may have been involved in individual cases. During the experiments, one arrester and several line terminators were destroyed, and at least two 1.41 MV voltage dividers at the line center were damaged. It is believed that only one arrester failed in these experiments since the weak points of the line were the terminating resistors. When the terminating resistors were removed from the line (configuration FPL-B-99, section C.1.2), one arrester failed on the first trigger (Flash UF-9911). Also, when terminating resistors were connected in parallel with terminating inductors (in an attempt to protect the terminating resistors from the low-frequency continuing current), the arresters operated normally (flashes UF-9916 and UF-9917).

7.3 2000 Experiments

During the 2000 experiments, the horizontal distribution line was subjected to a total of ten flashes, eight of which contained return strokes. One of these flashes was triggered with a failed arrester on the line (Section 6.3.2). Two arresters failed after the first stroke of two flashes (one of them with triggering wires involved, see Section 6.3.1 and the other without triggering wires involved, see Section 6.3.7), three arresters failed during the ICC of three different flashes (Sections 6.3.3, 6.3.6, and 6.3.9), one arrester failed during a flash without return strokes (FPL0025, Ta-

ble 6.4), and two flashes did not destroy any arresters (one of them with triggering wires involved, see Section 6.3.4, and the other without triggering wires but with visible arcing on the line, see Section 6.3.5).

The vertical configured distribution line was subjected to two flashes, one of which contained return strokes. One arrester failed during the first flash (flash FPL0039, Table 6.4), and the second flash, without return strokes, was triggered with the failed arrester on the line. Data from the magnetic tape (presently not accessible) may tell us at what stage of the flash it failed.

In every triggered flash to the lines either arresters failed or flashovers were observed, or both. It follows that if the *distribution lines tested* behave like *distribution lines* in service, the power distribution system is extremely vulnerable to direct lightning strikes, and distribution arresters do not have the capability of providing protection against direct strikes. It is still questionable how well the responses of the tested distribution line sections reproduce those of real distribution lines, the main difference being the length and any equipment connected to the lines that may affect their responses, such as transformers, underground cables, capacitor banks, and motors. In an operating distribution system, components other than arresters could be damaged as a result of direct lightning strikes to the line. In our experiment, at least one arrester failed in seven out of eight cases that the line was subjected to flashes containing return strokes (we do not count cases for which failed arresters were already on the line, or triggering wires across the line may have served to protect the arresters), which indicates that arrester failures should be expected to occur in about 90% of the cases when a similarly-protected distribution line is directly struck by lightning, and at least momentary service interruptions (due to either arrester failure or flashover on the line) should be expected in 100% of the cases. Both arrester failure and flashover on an acutal distribution line will require a circuit breaker to operate. In Florida, where the ground flash density is about 10 flashes per square kilometer

per year, distribution lines on 7-m and 10-m poles are expected to be struck by lightning on average from 0.075 to 0.60 times/km/year and 0.093 to 0.87 times/km/year, respectively (Bazelyan et al. 1978). A kilometer of the horizontal-configuration distribution line we tested has about 20 arresters, therefore, we should expect to have about 0.33-2.6 % of all installed arresters fail each year if 90 % of the flashes destroy each one arrester. A mile of the vertical-configuration distribution line has about 12 arresters, therefore, we should expect to have about 0.65-5.9 % of all installed arresters fail each year if 90 % of the flashes destroy each one arrester. These percentages are not much dissimilar from the 0.14 - 1.4 % arrester failure rate per year reported by Barker et al. [1998] for power lines on 20-m poles, but considerably higher than the industry cited arrester failure rates which are usually in the range of 0.01 to 0.1 % per year. If the rate we observe is applicable to typical lines, essentially every lightning strike will destroy an arrester near the strike point.

Arresters in the 2000 experiments failed either during the initial-stage current or during the following strokes of the flash. Section 6.3.9.1 shows how the energy withstand capability of the arrester was exceeded during the initial stage of that flash, this initial-stage current (a few hundreds of amperes) being typical of either the initial-stage current in rocket-triggered lightning or of long continuing current following return strokes in both triggered and natural lightning. Additionally, Section 6.3.8.1 shows how the total arrester dissipated energy associated with multiple strokes may exceed the arrester energy withstand capability. Thus, arresters may fail (Section 6.3.8.1) as a result of cumulative effect of multiple strokes (it is important to note that the value of cumulative dissipated energy for this flash does not account for the energy dissipated during the initial stage and possibly during continuing currents and M components occurring between the strokes, which did not trigger the digitizers). Arrester failures usually occur when arresters are not capable of absorbing the energy imparted by the lightning event (Andoh et al. 2000). Our experiments

demonstrate that, under direct lightning strike conditions, such failures may well occur more frequently than it is thought. It is possible that MOV arresters are incapable of preventing service interruptions under direct lightning strike conditions, although some authors believe that lightning-related interruptions on transmission lines can be totally avoided by using surge arresters (Tarasiewicz et al. 2000).

We observed that currents at different points in the system have different wave-shapes complicating the study of the division of lightning current among multiple available paths in the system. It might be more appropriate to analyze the division of charge instead. The distribution of charge is different from the distribution of peak current. For instance, from considering peak currents to ground (Figure 7.1), ground rods at Poles 8 and 11 are the preferred paths for the current flow to ground, whereas from the analysis of charges transferred to ground (Figures 7.2, 7.3, and 7.4), ground rods at Poles 5 and 18 are the preferred paths. Poles 5 and 8 have the lowest measured low-frequency, low-current grounding resistances.

There is a linear relationship between the peak current to ground and the total lightning peak current (Figure 7.1). Also, a linear relationship is observed between the stroke charge and charges transferred to ground (Figures 7.2, 7.3, and 7.4).

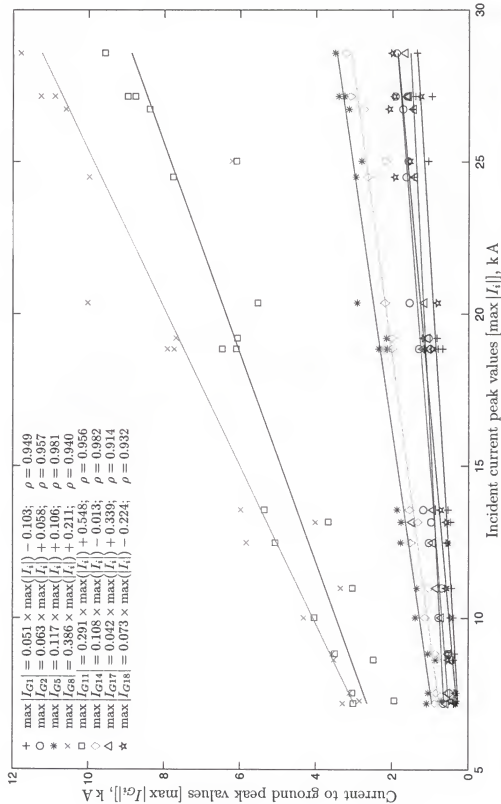


Figure 7.1: Measured peak current to ground versus measured incident peak current for the 2000 experiment.

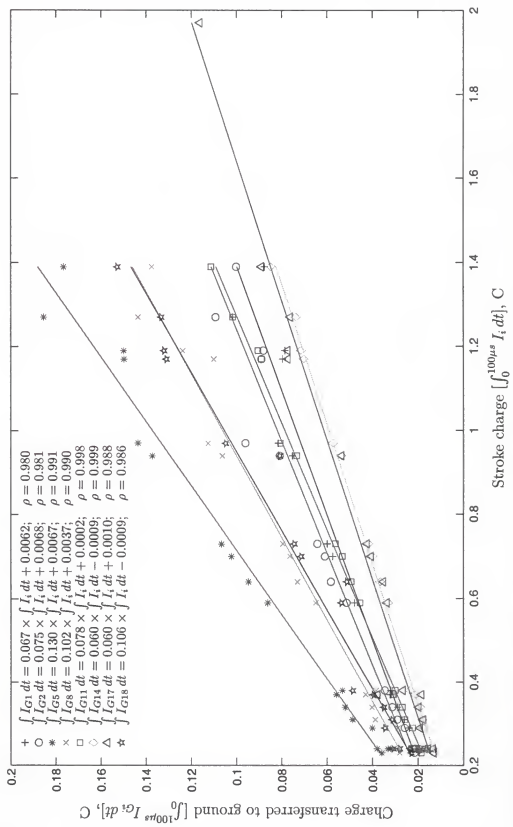


Figure 7.2: Calculated charge transferred to ground at different poles versus calculated stroke charge, on a $100\mu s$ window, for the 2000 experiment.

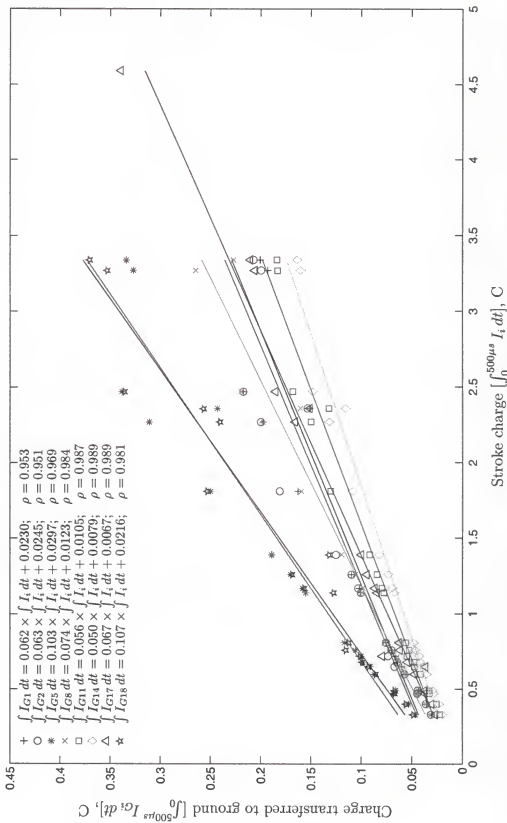


Figure 7.3: Calculated charge transferred to ground at different poles versus calculated stroke charge, on a 500 μ s window, for the 2000 experiment.

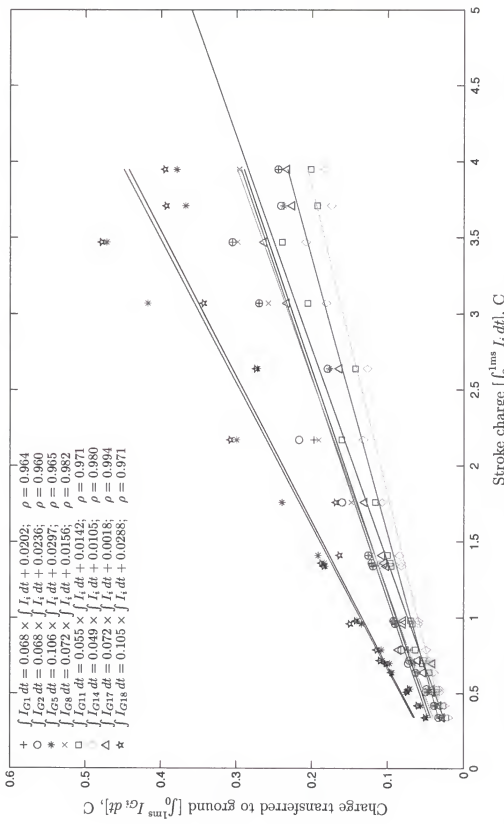


Figure 7.4: Calculated charge transferred to ground at different poles versus calculated stroke charge, on a 1 ms window, for the 2000 experiment.

CHAPTER 8

RECOMMENDATIONS FOR FUTURE RESEARCH

We recommend modifying the existing test distribution lines by adding transformers with dummy loads, for instance, to provide a more "realistic" path to ground for the low frequency components of the lightning current. Preferably, tests on a operating distribution line should be performed to check if the test distribution line sections built at the ICLRT behave like operating distribution lines. If the test distribution line sections built at the ICLRT behave like operating distribution lines, new distribution line designs with better lightning protection than current distribution lines should be designed, built, and tested.

A new high voltage divider should be design, tested, and implemented, to measure phase-to-neutral voltages close to the strike point. With some voltage waveforms near the strike point, the development of a more complete model, in which corona, lightning channel characteristic impedance, and possibly electromagnetic coupling between the lightning channel and line conductors, would be more feasible.

Overall, the experimental setup and data acquisition system was improved significantly from 1999 to 2000. The following recommendations are made to improve even more the 2000 experimental setup and data acquisition system:

1. Design a high voltage divider capable of measuring about 10 MV to measure phase-to-neutral voltages at the middle of the line.
2. Test and calibrate voltage dividers and current viewing resistors in a high voltage laboratory prior to and after their installation and use in the experiments.

3. Use a high resolution deep memory digital oscilloscope (12 bits, 16 Mbytes) to record currents through arresters and currents to ground. This will allow a more complete frequency analysis, since the frequency resolution in the frequency domain analysis is determined by the time window under study. For instance, a time window of 100 ms would mean a frequency resolution of 10 Hz.
4. Design and implement a smart triggering circuit to turn on and off the video cameras remotely when needed. Video cameras were turned on and left recording at the beginning of the storm. When storms last for long periods of time, video cameras run out of tape and therefore video records for some events are not available.
5. Design and implement an automated and redundant computer-oscilloscope-interface to minimize data that would be lost in case of oscilloscope-recording failures. For some unknown reason, when some of the LeCroy oscilloscopes trigger, they do not always store the data from memory to the hard drive. If this is the case, when the oscilloscopes are re-armed to acquire another event, data in the memory not recorded to the hard drive are lost.
6. Use a more resistant and stable fiber optic transmitter and receiver pair to dedicate more time to the experiments and less time constantly checking and replacing ISOBES. Several measurements were lost due to ISOBE failures. These devices are not designed to be operated outdoors, and are very sensitive to weather conditions.

APPENDIX A
MEASURING STATIONS ON POWER DISTRIBUTION LINES (DRAWINGS)

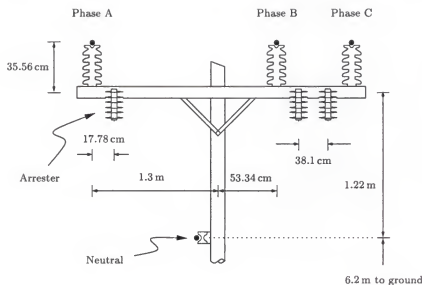


Figure A.1: Conductor's layout and clearance distances of the distribution line with horizontal phase conductor arrangement.

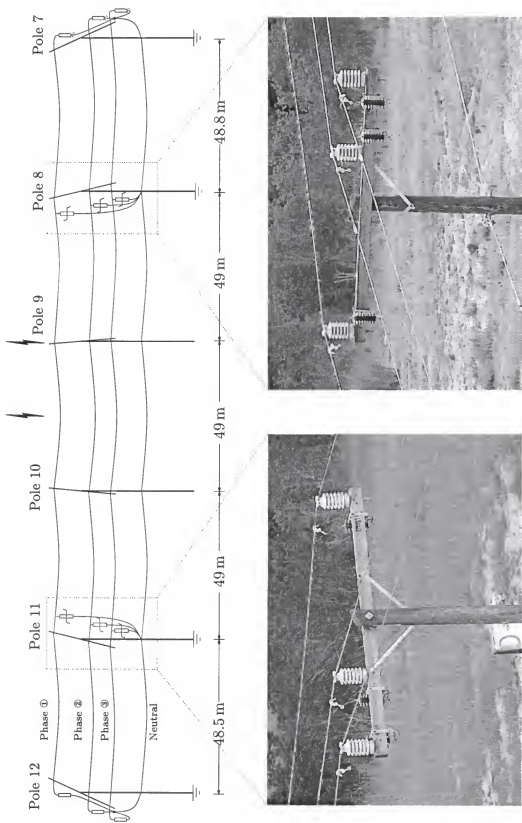


Figure A.2: Distribution line with horizontal configuration, distance between poles and location of arresters.

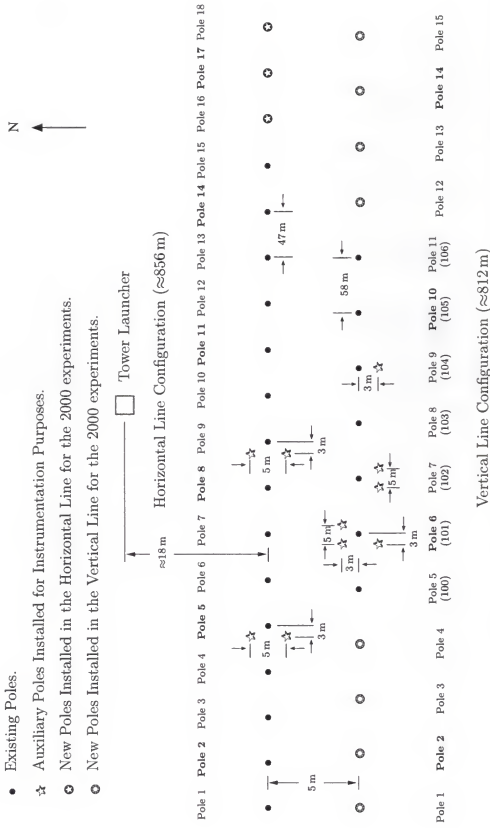


Figure A.3: Horizontal and vertical line changes from 1999 to 2000 (bold-pole labels represent arrester poles). Distance between poles on the horizontal line are about 47 m on average, except for distances from Pole 12 to 13, 13 to 14, and 14 to 15 of the horizontal line which are 61 m, 72 m, and 65 m, respectively. Distance between poles on the vertical line are about 58 m on average.

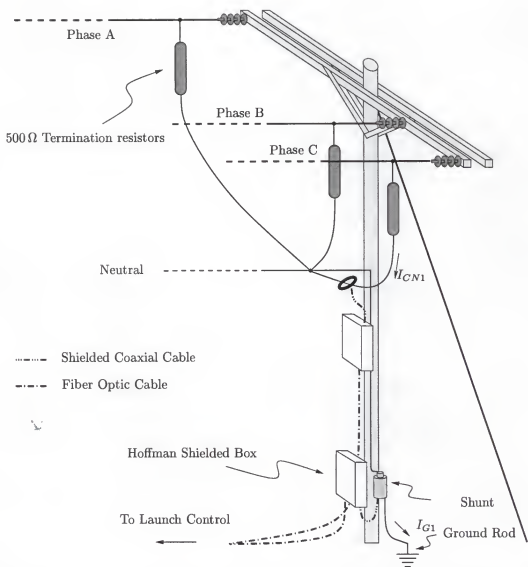


Figure A.4: Diagram of connections at Pole 1 of the horizontal configuration distribution line, summer 2000.

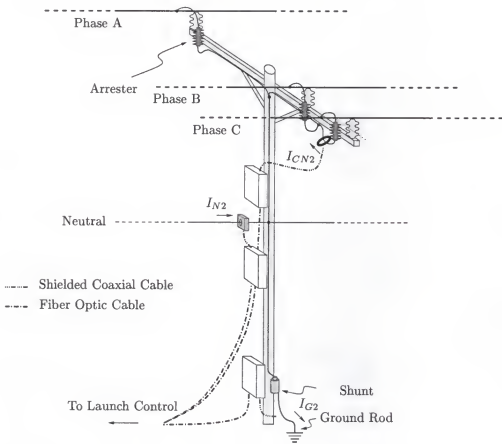


Figure A.5: Diagram of connections at Pole 2 of the horizontal configuration distribution line, summer 2000.

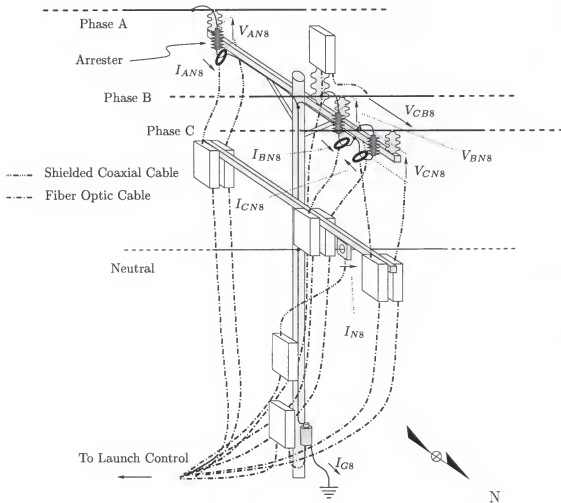


Figure A.6: Diagram of connections at Pole 8 of the horizontal configuration distribution line, summer 2000.

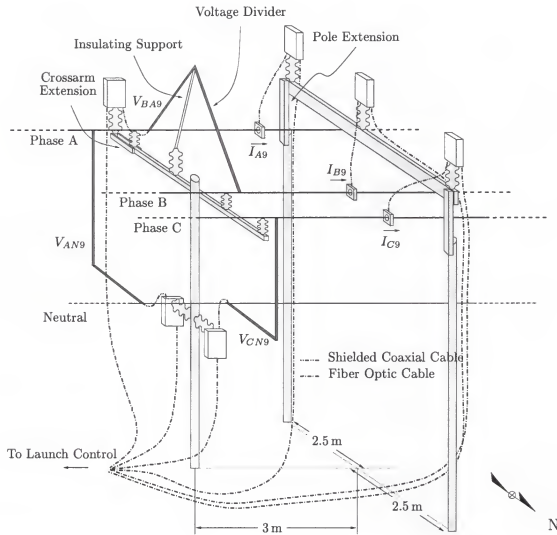


Figure A.7: Diagram of connections at Pole 9 of the horizontal configuration distribution line, summer 2000.

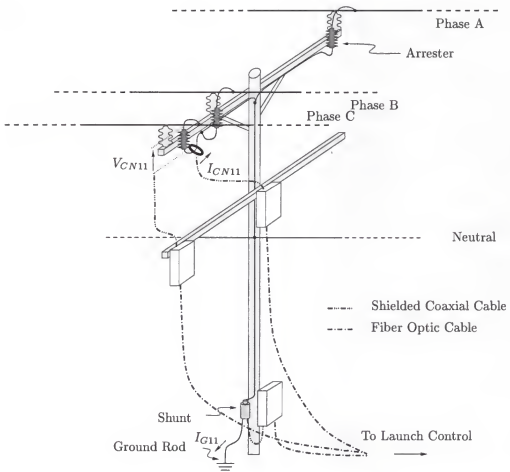


Figure A.8: Diagram of connections at Pole 11 of the horizontal configuration distribution line, summer 2000.

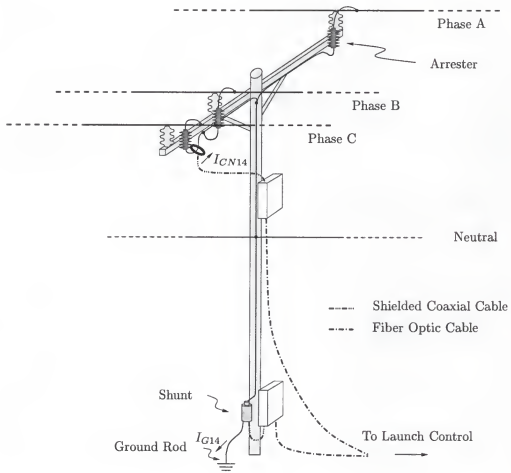


Figure A.9: Diagram of connections at Pole 14 of the horizontal configuration distribution line, summer 2000.

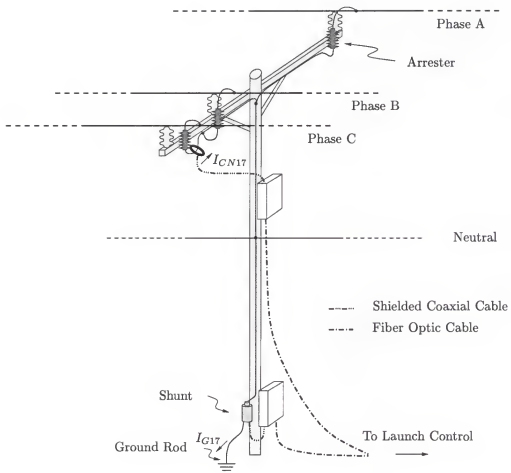


Figure A.10: Diagram of connections at Pole 17 of the horizontal configuration distribution line, summer 2000.

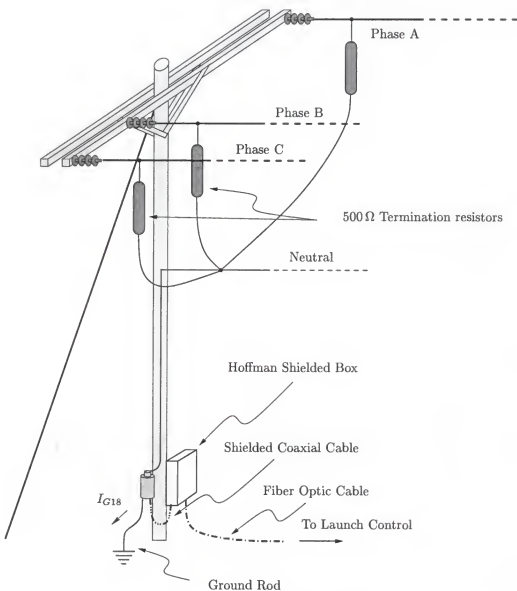


Figure A.11: Diagram of connections at Pole 18 of the horizontal configuration distribution line, summer 2000.

APPENDIX B SENSORS

B.1 Voltage Dividers

The voltage divider (also known as potential divider) is a device used to allow the measurement of a small fraction of the total voltage waveform, that fraction falling within the range of the recording device. This device usually consists of two impedances in series, the high and the low voltage arms. There exist many types of voltage dividers, including the resistive voltage divider, capacitive voltage divider, and mixed voltage divider.¹ Each of these voltage dividers has its area of application (Khalifa [1990]). The most widely used method to measured high voltage pulses is the *impulse voltage divider* (Creed [1989]).

B.1.1 Resistive Voltage Dividers

The simplest voltage divider consists of resistors connected in series, as shown in Figure B.1. To improve the upper frequency response of this device, the high voltage resistor ($R_{HV} = \sum_{i=1}^n R_i$) is built with two long wires counterwound on an insulator (minimizing the overall inductance of the high voltage resistor). Also, the low voltage resistor is shielded from the electric field by placing it in a metal box. The transfer function of this divider (neglecting parasitic capacitances and lead inductances) is

¹A mixed divider has both, resistors and capacitors connected in series or parallel (Creed [1989]).

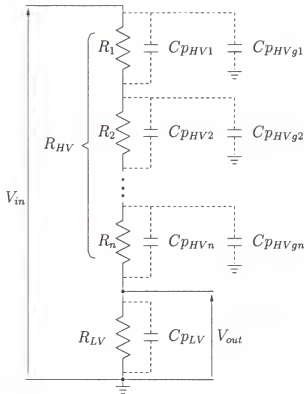


Figure B.1: High frequency circuit diagram of a resistive voltage divider

given by:

$$\frac{V_{out}}{V_{in}} = \frac{R_{LV}}{(R_{LV} + R_{HV})} \quad (\text{B.1})$$

The presence of parasitic capacitances ($C_{p_{HV_i}}$, $C_{p_{HVgi}}$ and $C_{p_{LV}}$) and lead inductances (not shown in Figure B.1) in this divider makes the transfer function (B.1) frequency dependent. At high frequencies, the distributed parasitic capacitance ($C_{p_{HV_i}}$ and $C_{p_{HVgi}}$) on the high voltage resistor (R_{HV}), the parasitic capacitance ($C_{p_{LV}}$) on the low voltage resistor (R_{LV}), and the inductance of the high and low voltage resistors limit the upper frequency response of this device. These parameters are not easy to determine, so the voltage dividers need to be tested to determine their frequency response. For voltage dividers with high attenuation, this is a difficult task because of the need for a very high voltage, high frequency source to produce measurable, realistic output signals above threshold.

B.1.2 Mixed Dividers

To avoid problems generated by parasitic capacitances (as explained in section B.1.1), a combination of resistors and capacitors can be used, as shown in Figure B.2 (R_x and R_c can be added since they are connected in series, and considered as a single resistor). The dotted square on the left side of Figure B.2 represents the

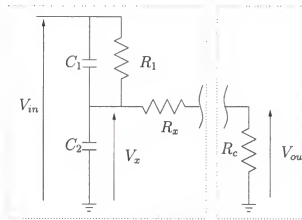


Figure B.2: Capacitive-Compensated Voltage Divider

actual divider, while the dotted square on the right side represents the characteristic impedance of a coaxial cable terminated in a 50Ω load (R_c). The 50Ω characteristic impedance of a coaxial cable needs to be taken into account when choosing the value of R_x . The idea of the capacitive-compensated voltage divider is to minimize the effects of parasitic capacitances (Section B.1.1). If C_1 and C_2 are considerably larger than the parasitic capacitances (usually few pF) across resistors R_1 and R_x , the parasitics will not have much effect on the divider frequency response, improving the upper frequency response of the device. The voltage V_x in Figure B.2 is given by:

$$\frac{V_x}{V_{in}} = \frac{(R_x + R_c)(R_1 C_1 S + 1)}{R_1 R_1 C_2 S + R_1 + R_1(R_x + R_c)C_2 S + (R_x + R_c)} \quad (B.2)$$

and V_{out} is given in terms of V_x as:

$$\frac{V_{out}}{V_x} = \frac{R_c}{R_x + R_c} \quad (\text{B.3})$$

If we consider the case in which $R_1C_1 = (R_x + R_c)C_2$, and combine (B.2) and (B.3), we obtain a transfer function which is not frequency dependent:

$$\frac{V_{out}}{V_{in}} = \frac{R_c}{(R_1 + R_x + R_c)} \quad (\text{B.4})$$

The inductance of the high voltage arm limits the response of these mixed dividers (see Mata et al. [1999b]).

B.2 Anti-Aliasing Filters

The circuit diagram of the anti-aliasing filters used on the experiments of summer of 1999 is shown in Figure B.3. The frequency response of this filter is shown in Figure B.4. Each filter was tested² and its frequency response measured. These results are given in Table B.1. Each filter was assigned to a specific ISOBE as follows:

| ISOBE | \iff | Filter # | ISOBE | \iff | Filter # |
|--------|--------|----------|--------|--------|----------|
| 1 | \iff | 18 | 2 | \iff | 21 |
| 6 | \iff | 14 | 7 | \iff | 25 |
| 9 | \iff | 07 | 10 | \iff | 22 |
| 11 | \iff | 20 | 12 | \iff | 08 |
| 13 | \iff | 04 | 14 | \iff | 17 |
| 16 | \iff | 13 | 17 | \iff | 19 |
| 18 | \iff | 02 | 19 | \iff | 10 |
| 20 | \iff | 01 | 21 | \iff | 24 |
| 22 | \iff | 05 | 3000R1 | \iff | 11 |
| 3000R2 | \iff | 06 | 3000R3 | \iff | 16 |
| 3000R4 | \iff | 15 | 3000R5 | \iff | 12 |
| 3000R6 | \iff | 09 | 3000R7 | \iff | 23 |
| 3000R8 | \iff | 03 | | | |

²The test consisted of a signal generator with an output impedance of 50Ω feeding the filter with a load of 50Ω connected to the output of the filters. The magnitude of the voltage at the output of the filters was measured as the frequency of the signal generator was increased from 300kHz to 15MHz .

³The value in parenthesis indicates the commercially available values used to achieve the desired value.

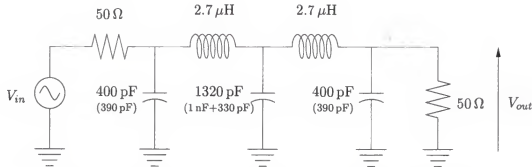
Figure B.3: Circuit diagram of the 5 MHz anti-aliasing filters.³

Table B.1: Measured frequency response of the anti-aliasing filters in volts for a 2-V input signal.

| Filter | Frequency | | | | | | | | | |
|--------|-----------|-------|-------|-------|-------|-------|-------|--------|--------|--|
| | 300 kHz | 1 MHz | 3 MHz | 4 MHz | 5 MHz | 6 MHz | 7 MHz | 10 MHz | 15 MHz | |
| # 1 | 1.0 | 1.0 | 0.934 | 0.850 | 0.617 | 0.340 | 0.175 | 0.0287 | 0.0030 | |
| # 2 | 1.0 | 1.0 | 0.940 | 0.852 | 0.609 | 0.330 | 0.165 | 0.0271 | 0.0033 | |
| # 3 | 1.0 | 1.0 | 0.934 | 0.846 | 0.620 | 0.337 | 0.176 | 0.0293 | 0.0032 | |
| # 4 | 1.0 | 1.0 | 0.936 | 0.856 | 0.645 | 0.373 | 0.195 | 0.0326 | 0.0040 | |
| # 5 | 1.0 | 1.0 | 0.930 | 0.846 | 0.606 | 0.328 | 0.168 | 0.0280 | 0.0031 | |
| # 6 | 1.0 | 1.0 | 0.930 | 0.846 | 0.617 | 0.340 | 0.176 | 0.0290 | 0.0032 | |
| # 7 | 1.0 | 1.0 | 0.930 | 0.862 | 0.637 | 0.353 | 0.181 | 0.0296 | 0.0031 | |
| # 8 | 0.992 | 0.996 | 0.912 | 0.824 | 0.595 | 0.330 | 0.171 | 0.0284 | 0.0003 | |
| # 9 | 0.992 | 0.990 | 0.912 | 0.828 | 0.609 | 0.350 | 0.180 | 0.0308 | 0.0002 | |
| # 10 | 0.992 | 0.990 | 0.912 | 0.820 | 0.593 | 0.330 | 0.167 | 0.0286 | 0.0004 | |
| # 11 | 0.992 | 0.990 | 0.914 | 0.820 | 0.598 | 0.335 | 0.168 | 0.0288 | 0.0004 | |
| # 12 | 0.992 | 0.990 | 0.912 | 0.828 | 0.609 | 0.341 | 0.173 | 0.0296 | 0.0010 | |
| # 13 | 0.992 | 0.990 | 0.908 | 0.834 | 0.620 | 0.345 | 0.176 | 0.0298 | 0.0005 | |
| # 14 | 0.992 | 0.990 | 0.908 | 0.830 | 0.618 | 0.347 | 0.180 | 0.0310 | 0.0003 | |
| # 15 | 0.992 | 0.990 | 0.908 | 0.830 | 0.609 | 0.338 | 0.172 | 0.0296 | 0.0007 | |
| # 16 | 0.992 | 0.990 | 0.908 | 0.820 | 0.596 | 0.327 | 0.167 | 0.0285 | 0.0008 | |
| # 17 | 0.992 | 0.990 | 0.908 | 0.820 | 0.601 | 0.332 | 0.170 | 0.0288 | 0.0010 | |
| # 18 | 0.992 | 0.990 | 0.906 | 0.820 | 0.606 | 0.338 | 0.172 | 0.0300 | 0.0004 | |
| # 19 | 0.992 | 0.990 | 0.906 | 0.820 | 0.604 | 0.330 | 0.168 | 0.0285 | 0.0004 | |
| # 20 | 0.992 | 0.990 | 0.906 | 0.818 | 0.604 | 0.328 | 0.168 | 0.0282 | 0.0010 | |
| # 21 | 1.006 | 1.006 | 0.934 | 0.864 | 0.696 | 0.435 | 0.230 | 0.0398 | 0.0046 | |
| # 22 | 1.006 | 1.006 | 0.928 | 0.864 | 0.685 | 0.412 | 0.213 | 0.0362 | 0.0045 | |
| # 23 | 1.006 | 1.006 | 0.936 | 0.874 | 0.714 | 0.445 | 0.234 | 0.0410 | 0.0051 | |
| # 24 | 1.006 | 1.006 | 0.928 | 0.862 | 0.706 | 0.448 | 0.240 | 0.0492 | 0.0051 | |
| # 25 | 1.006 | 1.002 | 0.936 | 0.878 | 0.708 | 0.437 | 0.225 | 0.0378 | 0.0040 | |

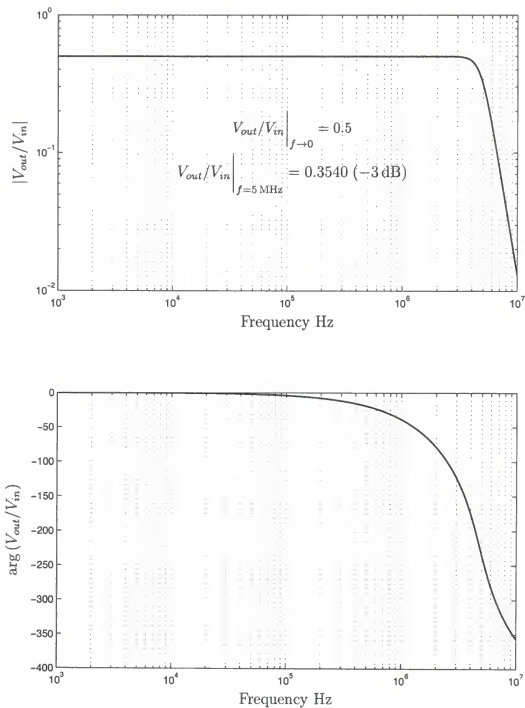


Figure B.4: Theoretical frequency response of the 5 MHz anti-aliasing filters.

APPENDIX C CONFIGURATIONS AND INSTRUMENTATION SETTINGS

C.1 1999 Configurations

In 1999, the test distribution line was subjected to direct lightning strikes under four different configurations.

C.1.1 Configuration FPL-A-99

The circuit diagram for this configuration is shown in Figure C.1. A total of 17 measurement locations were installed on the distribution line (See Table C.1). Single-impulse 6.2 kJ rated 433Ω termination resistors assembled by UF were installed on each phase at each termination pole. These resistors were composed of 13 sections (connected in series) of six $200\text{ k}\Omega$, 80 J, Ohmite single-impulse resistors connected in parallel.

The down-lead from the tower was connected to the phase C conductor at the mid-point between poles 9 and 10. A total of three nylon cords were used to keep the separation of the conductors close to nominal since the tension of the down-lead from the tower launcher pulled the connected conductor apart from the others. Two nylon cords were used between phases C and B, each cord being approximately at a distance of 2 m on each side from the strike point. A third nylon cord was used between phase B and A at a distance of 2 m on the east side of the striking point.

C.1.2 Configuration FPL-B-99

This configuration is illustrated in Figure C.2. A total of 14 measurement instruments were installed on the line (See Table C.2). The down-lead from the tower was connected to the phase C conductor at the mid-point between poles 9 and 10, as in configuration FPL-A-99. No termination impedances were installed on the line, so for this particular event, the line was left open-circuited.

C.1.3 Configuration FPL-C-99

The circuit diagram for this configuration is shown in Figure C.3. A total of 24 measurement instruments were installed on the distribution line (See Table C.3). The down-lead from the tower was connected to the phase B conductor at the mid-point between poles 9 and 10. A total of three nylon cords were used to keep the tension off the phase B conductor. A nylon cord was used between the downlead from the tower launcher and the neutral of the horizontal configuration distribution line. The down-lead from the tower launcher was connected (from bellow) to phase B with an angle of 45°. Two additional nylon cords were connected between Phase B and Phase A each being approximately 2 m on each side from the strike point. 25 kJ, 500 Ω resistors were connected on each phase at the termination poles in parallel to 16 mH inductors. The 25 kJ, 500 Ω termination resistors are wirewound resistors manufactured by Power Technologies, Inc. (PTI). The 16 mH inductors were manufactured by UF and their purpose was to protect the terminating resistors from the continuing current by providing a preferred path to ground for the low-frequency low-level currents.

C.1.4 Configuration FPL-D-99

This configuration was the same as configuration FPL-C with the difference that voltage measuring instruments at the middle of the line were removed. The circuit

diagram for this configuration is shown in Figure C.4. A total of 21 measurement locations were installed on the distribution line (See Table C.4).

C.2 2000 Configurations

In 2000, the horizontal distribution line configuration was exposed to triggered lightning under three different configurations.

C.2.1 Configuration FPL-A-00

This configuration is illustrated in Figure C.6. The down-lead from the tower was connected to phase C of the horizontal configuration (mid-point between poles 9 and 10). A nylon cord (attached to phase A of the vertical configuration line) pulled the down-lead from the tower to keep the tension off phase C of the horizontal configuration. Ohio Brass PDV 100 18-kV MOV arresters were installed at poles 8 and 11, and Cooper UltraSIL Housed VariSTAR Heavy Duty 18-kV MOV arresters were installed at poles 2, 5, 14, and 17 (Section 3.2.2). High energy dissipation resistors (manufactured by High Power Technologies) where used as terminating resistors in the line:

- Pole 1:
 - Phase A: single 524Ω , 1.25 MJ enclosed in PVC housing.
 - Phase B: single 510Ω , 1.25 MJ enclosed in PVC housing.
 - Phase C: 1027Ω and 964Ω resistors connected in parallel, 1.75 MJ (each) immersed in oil and enclosed in PVC housing.
- Pole 18:
 - Phase A: single 506Ω , 1.25 MJ enclosed in PVC housing.

- Phase B: single $480\ \Omega$, 1.25 MJ enclosed in PVC housing.
- Phase C: $1051\ \Omega$ and $911\ \Omega$ resistors connected in parallel, 1.75 MJ (each) immersed in oil and enclosed in PVC housing.

C.2.2 Configuration FPL-B-00

Same as configuration FPL-A-00 with the strike point located at phase C, Pole 9.

C.2.3 Configuration FPL-C-00

The down-lead from the tower was connected to phase A of the vertical configuration at pole 8 (mid-point between arrester stations at poles 6 and 10). Ohio Brass PDV 100 18-kV MOV arresters were installed at poles 6 and 10, and Cooper UltraSIL Housed VariSTAR Heavy Duty 18-kV MOV arresters were installed at poles 2, and 14 (Section 3.2.2). The same high energy dissipation resistors used in the previous configurations were used as terminating resistors in the line:

- Pole 1:

- Phase A: $1027\ \Omega$ and $964\ \Omega$ resistors connected in parallel, 1.75 MJ (each) immersed in oil and enclosed in PVC housing.
- Phase B: single $510\ \Omega$, 1.25 MJ enclosed in PVC housing.
- Phase A: single $524\ \Omega$, 1.25 MJ enclosed in PVC housing.

- Pole 15:

- Phase A: $1051\ \Omega$ and $911\ \Omega$ resistors connected in parallel, 1.75 MJ (each) immersed in oil and enclosed in PVC housing.
- Phase B: single $480\ \Omega$, 1.25 MJ enclosed in PVC housing.
- Phase C: single $506\ \Omega$, 1.25 MJ enclosed in PVC housing.

The following is a list of abbreviations and concepts used in the tables in this appendix.

| | | | |
|----|------------------------|------|----------------------|
| LC | LeCroy Scope | P90 | Pro 90 Nicolet Scope |
| MP | Multipro Nicolet Scope | Att. | Attenuation |
| MS | Megashunt | Ch | Channel |
| MT | Magnetic Tape Recorder | | |

Fiber: this is the fiber label of the form XXX-YY, where XXX is the length of the fiber in meters (this is not true for all fibers since some of them have been cut and reterminated), and YY a unique ID.

Ratio: this indicates the ratio of V/V and V/A for voltage and current sensors, respectively.

Range: the range is obtained as follows: $Setting / (Ratio \times 10^{-Att./20})$

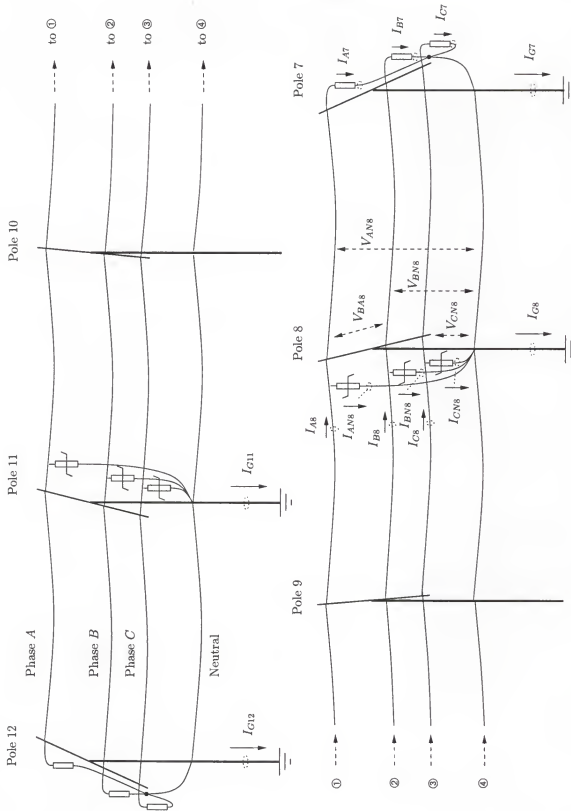


Figure C.1: Locations of measurements for Flash UF-9904, strike to phase C of the horizontal configuration at the middle of the line, between poles 9 and 10.

Table C.1: Instrumentation settings for flash UF-9904; strike to Phase C of the horizontal configuration distribution line, mid-point between poles 9 and 10.

| Location Fig. C.1 | Fiber | Isobe Number | Setting | Delay ^a | Device | Ratio | Att. [dB] | Range | Scope | MT Ch |
|-------------------|--------|--------------|---------|---------------------|--------|---------------------|-----------|---------|---------------|-------|
| I_1^b | 100-01 | 1 | 10 V | 600 ns ^c | MS #5 | 5E - 4 ^c | - | 20 kA | LC Ch-1 | 10 |
| I_{A8} | 220-01 | 7 | 10 V | 1.06 μ s | P3525 | 0.05 | 20 | 2 kA | P90-1 Ch3-1 | - |
| I_{B8} | 220-02 | 3000R-7 | 10 V | 1.18 μ s | P3525 | 0.05 | 20 | 2 kA | P90-1 Ch4-2 | - |
| I_{C8} | 220-06 | 2 | 10 V | 1.12 μ s | P3525 | 0.05 | 34 | 10 kA | MP 1C-2C | 14 |
| V_{CN8} | 220-10 | 21 | 1 V | 1.52 μ s | 120kV | 3.2816E - 5 | 14 | 152 kV | LC Ch-2 MP 3C | 7 |
| V_{BN8} | 220-03 | 3000R-8 | 1 V | 1.145 μ s | 120kV | 3.2816E - 5 | 14 | 152 kV | MP 1A-2A | - |
| V_{AN8} | 220-04 | 10 | 1 V | 1.165 μ s | 120kV | 3.2816E - 5 | 14 | 152 kV | MP 3A | - |
| V_{BA8} | 220-05 | 17 | 10 V | 1.16 μ s | 300kV | 1.0637E - 4 | 6 | 188 kV | P90-2 Ch4-2 | - |
| I_{AN8} | 220-07 | 22 | 10 V | 1.125 μ s | 110A | 0.05 | 14 | 1 kA | P90-2 Ch3-1 | - |
| I_{BN8} | 220-08 | 20 | 10 V | 1.13 μ s | 110A | 0.05 | 14 | 1 kA | MP 1D-2D | - |
| I_{CN8} | 220-09 | 13 | 10 V | 1.125 μ s | 110A | 0.05 | 34 | 10 kA | LC Ch-3 MP 3D | 8 |
| I_{A7} | 350-01 | 3000R-5 | 10 V | 1.775 μ s | 110A | 0.05 | 14 | 1 kA | P90-3 Ch3-1 | - |
| I_{B7} | 350-02 | 3000R-4 | 10 V | 1.78 μ s | 110A | 0.05 | 14 | 1 kA | P90-3 Ch4-2 | - |
| I_{C7} | 420-01 | 3000R-2 | 10 V | 2.2 μ s | 110A | 0.05 | 14 | 1 kA | P90-4 Ch3-1 | - |
| I_{G7} | 550-01 | 3000R-1 | 1 V | 2.805 μ s | MS #1 | 5.09E - 4 | 6 | 3.88 kA | P90-4 Ch4-2 | 11 |
| I_{G8} | 310-01 | 18 | 1 V | 1.605 μ s | MS #2 | 5.17E - 4 | 14 | 9.72 kA | LC Ch-4 | 9 |
| I_{G11} | 298-01 | 12 | 1 V | 1.51 μ s | MS #3 | 5.17E - 4 | 14 | 9.72 kA | MP 1B-2B | 12 |
| I_{G12} | 360-01 | 3000R-3 | 1 V | 1.885 μ s | MS #4 | 5.145E - 4 | 6 | 3.88 kA | MP 3B | 13 |

^a Delays were obtained experimentally

^b Incident current not shown in Figure C.1

^c These values were obtained from manufacturer

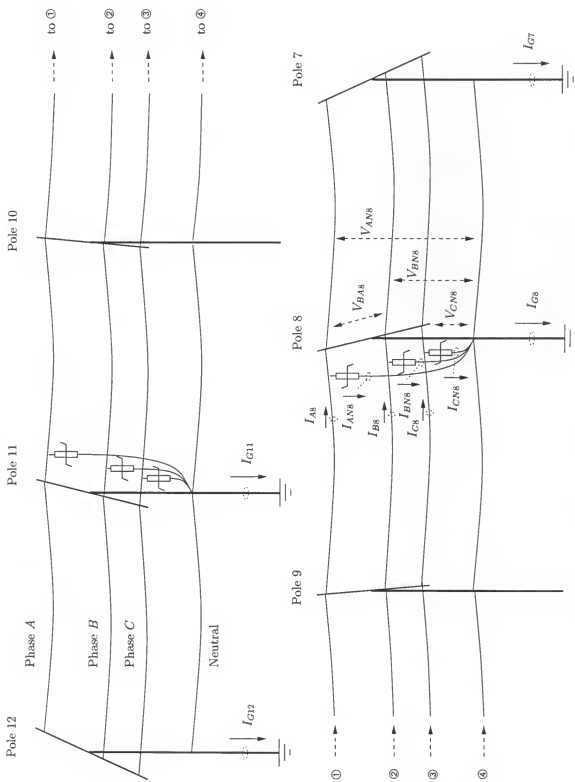


Figure C.2: Locations of measurements for Flashes UF-9911 and UF-9912, strikes to phase C of the horizontal configuration at the middle of the line, between poles 9 and 10.

Table C.2: Instrumentation settings for flashes UF-9911 and UF-9912; strike to Phase C of the horizontal configuration distribution line, mid-point between poles 9 and 10, no termination resistors.

| Location Fig. C.2 | Fiber | Isobee Number | Setting | Delay ^a | Device | Ratio | Att. [dB] | Range | Scope | MT Ch |
|----------------------|--------|------------------|---------|---------------------|--------|---------------------|--------------|---------|---------------|----------|
| I_i^b | 100-01 | 1 | 10 V | 600 ns ^c | MS #5 | 5E - 4 ^c | - | 20 kA | LC Ch-1 | 10 |
| I_{A8} | 220-01 | 7 | 10 V | 1.06 μ s | P3525 | 0.05 | 20 | 2 kA | P90-1 Ch3-1 | - |
| I_{B8} | 220-02 | 3000R-7 | 10 V | 1.18 μ s | P3525 | 0.05 | 20 | 2 kA | P90-1 Ch4-2 | - |
| I_{C8} | 220-06 | 2 | 10 V | 1.12 μ s | P3525 | 0.05 | 34 | 10 kV | MP IC-2C | 14 |
| V_{CN8} | 220-10 | 21 | 1 V | 1.52 μ s | 120kV | 3.2816E - 5 | 14 | 152 kV | LC Ch-2 MP 3C | 7 |
| V_{BN8} | 220-03 | 3000R-8 | 1 V | 1.145 μ s | 120kV | 3.2816E - 5 | 14 | 152 kV | MP 1A-2A | - |
| V_{AN8} | 220-04 | 10 | 1 V | 1.165 μ s | 120kV | 3.2816E - 5 | 14 | 152 kV | MP 3A | - |
| V_{BA8} | 220-05 | 17 | 10 V | 1.16 μ s | 300kV | 1.0637E - 4 | 6 | 188 kV | P90-2 Ch4-2 | - |
| I_{AN8} | 220-07 | 22 | 10 V | 1.125 μ s | 110A | 0.05 | 14 | 1 kA | P90-2 Ch3-1 | - |
| I_{BN8} | 220-08 | 20 | 10 V | 1.13 μ s | 110A | 0.05 | 14 | 1 kA | MP 1D-2D | - |
| I_{CN8} | 220-09 | 13 | 10 V | 1.125 μ s | 110A | 0.05 | 34 | 10 kA | LC Ch-3 MP 3D | 8 |
| I_{G7} | 550-01 | 3000R-1 | 1 V | 2.805 μ s | MS #1 | 5.09E - 4 | 9 | 5.54 kA | P90-4 Ch4-2 | 11 |
| I_{G8} | 310-01 | 18 | 1 V | 1.605 μ s | MS #2 | 5.17E - 4 | 14 | 9.72 kA | LC Ch-4 | 9 |
| I_{G11} | 298-01 | 12 | 1 V | 1.51 μ s | MS #3 | 5.17E - 4 | 14 | 9.72 kA | MP 1B-2B | 12 |
| I_{G12} | 360-01 | 3000R-3 | 1 V | 1.885 μ s | MS #4 | 5.145E - 4 | 9 | 5.54 kA | MP 3B | 13 |

^a Delays were calculated experimentally

^b Incident current not shown in Figure C.2

^c These values were obtained from specs

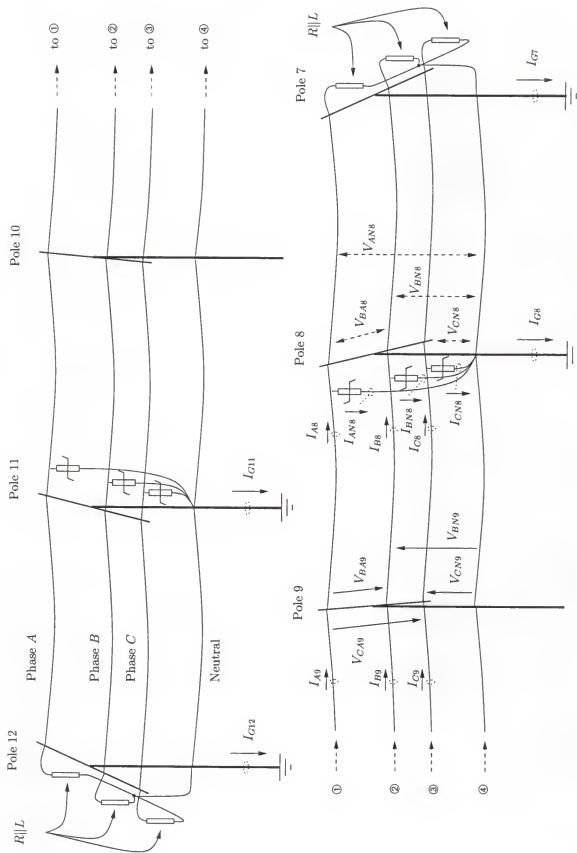


Figure C.3: Locations of measurements for Flashes UF-9914 and UF-9915, strikes to phase B of the horizontal configuration at the middle of the line, between poles 9 and 10.

Table C.3: Instrumentation settings for flashes UF-9914 and UF-9915, strike to Phase *B* of the horizontal configuration distribution line with termination resistors and inductors; mid-point between poles 9 and 10.

| Location Fig. C.3 | Fiber | Isobe | | Device | Ratio | Att. [dB] | Range | Scope | MT Ch |
|-------------------|--------|---------|------|---------------------|----------|---------------------|-------|--------|-----------------|
| | | Number | Set. | | | | | | |
| I_i^o | 100-01 | 1 | 10 V | 600 ns ^c | MS #5 | 5E - 4 ^c | - | 20 kA | LC-1 Ch-1 |
| I_{A7} | 350-01 | 3000R-5 | 10 V | 1.775 μ s | 110A | 0.05 | 6 | 400 A | P90-3 Ch3-1 |
| I_{B7} | 350-02 | 3000R-4 | 10 V | 1.78 μ s | 110A | 0.05 | 14 | 1 kA | P90-3 Ch4-2 |
| I_{C7} | 420-01 | 3000R-2 | 10 V | 2.2 μ s | 110A | 0.05 | 6 | 400 A | P90-4 Ch3-1 |
| I_{A8} | 220-01 | 7 | 10 V | 1.06 μ s | P3525 | 0.05 | 20 | 2 kA | P90-1 Ch3-1 |
| I_{B8} | 220-02 | 3000R-7 | 10 V | 1.18 μ s | P3525 | 0.05 | 34 | 10 kA | MP 1C |
| I_{C8} | 220-06 | 2 | 10 V | 1.12 μ s | P3525 | 0.05 | 20 | 2 kA | P90-1 Ch4-2 |
| I_{AN8} | 220-07 | 22 | 10 V | 1.125 μ s | 110A | 0.05 | 14 | 1 kA | P90-2 Ch3-1 |
| I_{BN8} | 220-08 | 20 | 10 V | 1.13 μ s | 110A | 0.05 | 34 | 10 kA | LC-1 Ch-3 MP 3D |
| I_{CN8} | 220-09 | 13 | 10 V | 1.125 μ s | 110A | 0.05 | 14 | 1 kA | MP 1D |
| V_{AN8} | 220-04 | 10 | 1 V | 1.165 μ s | 120kV | 3.2816E - 5 | 14 | 152 kV | MP 3A |
| V_{BN8} | 220-03 | 3000R-8 | 1 V | 1.145 μ s | 120kV | 3.2816E - 5 | 14 | 152 kV | LC-1 Ch-2 MP 3C |
| V_{CN8} | 220-10 | 21 | 1 V | 1.52 μ s | 120kV | 3.2816E - 5 | 14 | 152 kV | MP 1A |
| V_{B18} | 220-05 | 17 | 10 V | 1.16 μ s | 300kV | 1.0637E - 4 | 6 | 188 kV | P90-2 Ch4-2 |
| I_{A9} | 18-179 | 19 | 10 V | 934 ns | P3525 | 0.05 | 20 | 2 kA | MP 2A |
| I_{B9} | 160-05 | 16 | 10 V | 854 ns | P3525 | 0.05 | 34 | 10 kA | MP 2B |
| I_{C9} | 160-03 | 11 | 10 V | 855 ns | P3525 | 0.05 | 20 | 2 kA | MP 2C |
| V_{B19} | 160-02 | 6 | 10 V | 855 ns | 1.41MV-3 | 2.2634E - 5 | 14 | 2.2 MV | P90-5 Ch3-1 |
| V_{CA9} | 160-04 | 9 | 10 V | 855 ns | 1.41MV-4 | 2.2634E - 5 | 14 | 2.2 MV | MP 2D |
| V_{B19} | 170-02 | 14 | 10 V | 855 ns | 1.41MV-1 | 2.2634E - 5 | 14 | 2.2 MV | LC-2 Ch1 |
| V_{C19} | 170-01 | 3000R-6 | 10 V | 920 ns | 1.41MV-2 | 2.2634E - 5 | 14 | 2.2 MV | P90-5 4-2 |

Table C.3 – continued.

| Location Fig. C.3 | Fiber | Isolate | | Device | Ratio | Att. [dB] | Range ^b | Scope | MT Ch |
|-------------------|--------|---------|------|---------------|-------|------------|--------------------|----------------------------|---------------------------|
| | | Number | Set. | | | | | | |
| I_{G7} | 550-01 | 3000R-1 | 1 V | 2.805 μs | MS #1 | 5.09E - 4 | 9 | 5.54 kA Ch-2 | P90-4 Ch4-2 LC-2 11 |
| I_{G8} | 310-01 | 18 | 1 V | 1.005 μs | MS #2 | 5.17E - 4 | 14 | 9.72 kA LC-1 Ch-4 | 9 |
| I_{G11} | 298-01 | 12 | 1 V | 1.51 μs | MS #3 | 5.17E - 4 | 14 | 9.72 kA MP 1B LC-2 Ch-3 | 12 |
| I_{G12} | 360-01 | 3000R-3 | 1 V | 1.885 μs | MS #4 | 5.145E - 4 | 9 | 5.54 kA MP 3B LC-2 Ch-4 | 13 |

^a Delays were calculated experimentally^b Incident current not shown in Figure C.3^c These values were obtained from specs

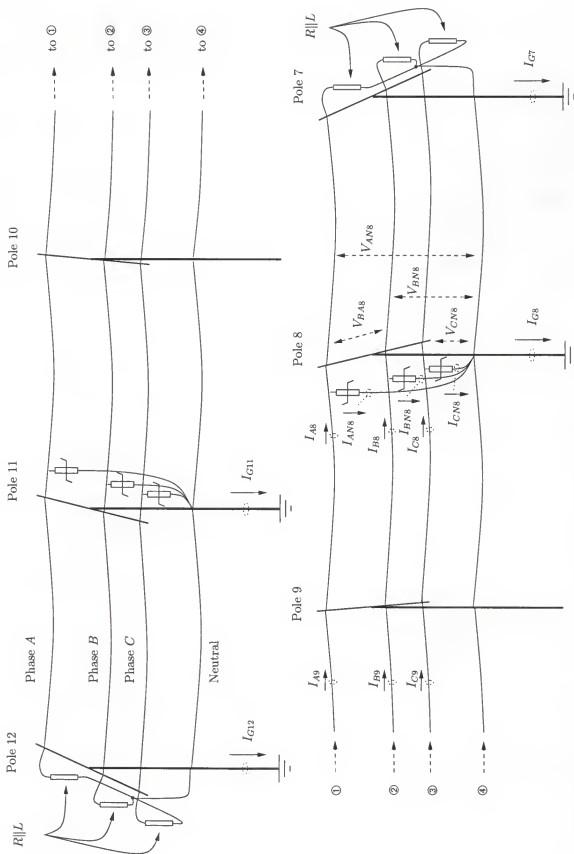


Figure C.4: Locations of measurements for Flashes UF-9916 and UF-9917, strikes to phase B of the horizontal configuration at the middle of the line, between poles 9 and 10.

Table C.4: Instrumentation settings for flashes UF-9916 and UF-9917, strike to Phase B of the horizontal configuration distribution line with termination resistors and inductors; mid-point between poles 9 and 10.

| Location Fig. C.4 | Fiber | Isobe Number | Delay ^a | Device | Ratio | Att. [dB] | Range | Scope | MT Ch |
|-------------------|--------|--------------|--------------------|---------------------|-------|---------------|-------|---------|-----------------------|
| I_1^b | 100-01 | 1 | 10 V | 600 ns ^c | MS #5 | $5E - 4^c$ | — | 20 kA | LC-1 Ch-1 |
| I_{A7} | 350-01 | 3000R-5 | 10 V | 1.775 μ s | 110A | 0.05 | 6 | 400 A | P90-3 Ch3-1 |
| I_{B7} | 350-02 | 3000R-4 | 10 V | 1.78 μ s | 110A | 0.05 | 14 | 1 kA | P90-3 Ch4-2 |
| I_{C7} | 420-01 | 3000R-2 | 10 V | 2.2 μ s | 110A | 0.05 | 6 | 400 A | P90-4 Ch3-1 |
| I_{A8} | 220-01 | 7 | 10 V | 1.06 μ s | P3525 | 0.05 | 20 | 2 kA | P90-1 Ch3-1 |
| I_{B8} | 220-02 | 3000R-7 | 10 V | 1.18 μ s | P3525 | 0.05 | 34 | 10 kA | MP 1C |
| I_{C8} | 220-06 | 2 | 10 V | 1.12 μ s | P3525 | 0.05 | 20 | 2 kA | P90-1 Ch4-2 |
| $I_{A\bar{N}8}$ | 220-07 | 22 | 10 V | 1.125 μ s | 110A | 0.05 | 14 | 1 kA | P90-2 Ch3-1 |
| $I_{B\bar{N}8}$ | 220-08 | 20 | 10 V | 1.13 μ s | 110A | 0.05 | 34 | 10 kA | LC-1 Ch-3 MP 3D |
| $I_{C\bar{N}8}$ | 220-09 | 13 | 10 V | 1.125 μ s | 110A | 0.05 | 14 | 1 kA | MP 1D |
| $V_{A\bar{N}8}$ | 220-04 | 10 | 1 V | 1.165 μ s | 120kV | $3.2816E - 5$ | 14 | 152 kV | MP 3A |
| $V_{B\bar{N}8}$ | 220-03 | 3000R-8 | 1 V | 1.145 μ s | 120kV | $3.2816E - 5$ | 14 | 152 kV | LC-1 Ch-2 MP 3C |
| $V_{C\bar{N}8}$ | 220-10 | 21 | 1 V | 1.52 μ s | 120kV | $3.2816E - 5$ | 14 | 152 kV | MP 1A |
| $V_{B\bar{A}8}$ | 220-05 | 17 | 10 V | 1.16 μ s | 300kV | $1.0637E - 4$ | 6 | 188 kV | P90-2 Ch4-2 |
| I_{A9} | 18-179 | 19 | 10 V | 934 ns | P3525 | 0.05 | 20 | 2 kA | MP 2A |
| I_{B9} | 160-05 | 16 | 10 V | 854 ns | P3525 | 0.05 | 34 | 10 kA | MP 2B |
| I_{C9} | 160-03 | 11 | 10 V | 845 ns | P3525 | 0.05 | 20 | 2 kA | MP 2C |
| I_{G7} | 550-01 | 3000R-1 | 1 V | 2.805 μ s | MS #1 | $5.09E - 4$ | 9 | 5.54 kA | P90-4 Ch4-2 LC-2 Ch-2 |
| I_{G8} | 310-01 | 18 | 1 V | 1.605 μ s | MS #2 | $5.17E - 4$ | 14 | 9.72 kA | LC-1 Ch-4 |
| I_{G11} | 298-01 | 12 | 1 V | 1.51 μ s | MS #3 | $5.17E - 4$ | 14 | 9.72 kA | MP 1B LC-2 Ch-3 |
| I_{G12} | 360-01 | 3000R-3 | 1 V | 1.885 μ s | MS #4 | $5.145E - 4$ | 9 | 5.54 kA | MP 3B LC-2 Ch-4 |

^a Delays were calculated experimentally

^b Incident current not shown in Figure C.3

^c These values were obtained from specs

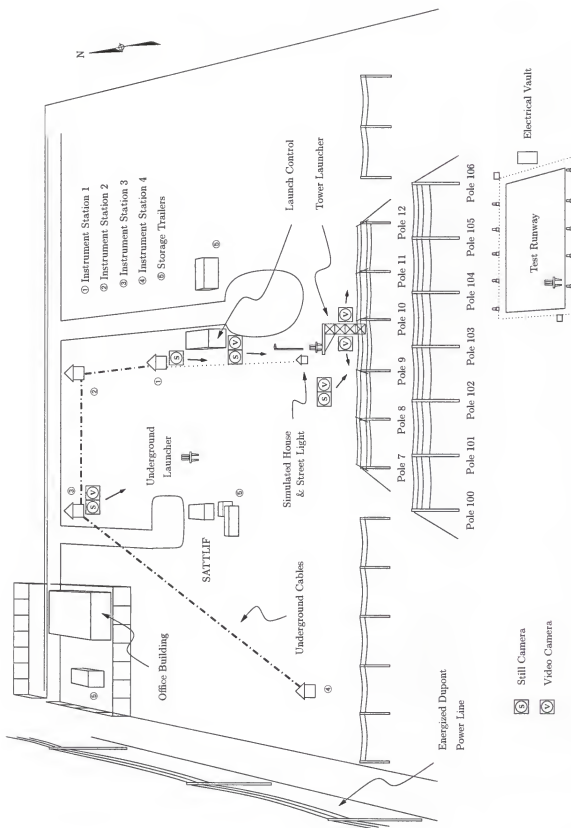


Figure C.5: Still and video camera locations for the summer of 1999 experiments. The directions of the arrows indicate the field of view of the devices (See Table 3.9).

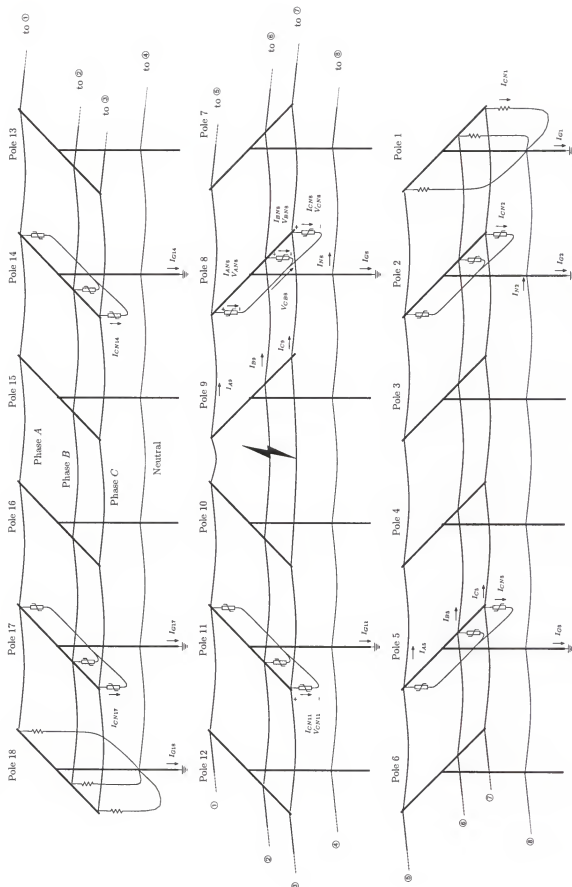


Figure C.6: Locations of measurements for flashes FPL0011 and FPL0014, strike to phase C of the horizontal configuration at the middle of the line, between poles 9 and 10.

Table C.5: Instrumentation summary for flashes FPI0011 and FPI0014, strike to phase C of the horizontal configuration distribution line with high power termination resistors; mid-point between poles 9 and 10 (see also Table C.6)

| Location Fig. C.6 | Fiber | Isoibe | | Delay | Device | Ratio | Att. [dB] | Range | Scope | MT Ch |
|-------------------|--------|---------|-------|---------|---------|-------------|-----------|-----------|-------|-------|
| | | Number | Sett. | | | | | | | |
| I_1 | 100-1 | 1 | 10.0 | 639 ns | MS #9 | $6.165E-04$ | 3 | 22.91 kA | L9Ch4 | 10 |
| I_{M1} | 100-1 | 1 | 10.0 | 639 ns | MS #9 | $6.165E-04$ | 3 | 22.91 kA | L8Ch1 | 11 |
| I_{L6} | 100-02 | 19 | 1.0 | 573 ns | MS #9 | $6.165E-04$ | 3 | 2.29 kA | L7Ch2 | 13 |
| I_{CN1} | 550-03 | 3000R7C | 10.0 | 2.75 us | 110A-1 | $5.000E-02$ | | 200.00 A | L6Ch3 | |
| I_G1 | 550-02 | 3000R1A | 0.1 | 2.75 us | MS #3 | $5.170E-04$ | 17 | 1.37 kA | L1Ch1 | |
| I_{CN2} | 500-02 | 3000R1B | 10.0 | 2.51 us | 110A-4 | $5.000E-02$ | 20 | 2.00 kA | L3Ch1 | |
| I_{N2} | 500-03 | 3000R5C | 10.0 | 2.52 us | 5179-1 | $5.000E-02$ | 20 | 2.00 kA | L6Ch1 | |
| I_{G2} | 500-01 | 3000R2A | 0.1 | 2.52 us | MS #6 | $6.197E-04$ | 19 | 1.44 kA | L1Ch2 | |
| I_{CN5} | 500-04 | 3000R8C | 10.0 | 2.51 us | 6801-1 | $1.250E-02$ | 9 | 2.25 kA | L6Ch4 | |
| I_A5 | 500-05 | 11 | 10.0 | 2.52 us | 5179-2 | $5.000E-02$ | 14 | 1.00 kA | L7Ch1 | |
| I_{B5} | 500-06 | 9 | 10.0 | 2.35 us | 5179-3 | $5.000E-02$ | 14 | 1.00 kA | L8Ch2 | |
| I_{C5} | 500-07 | 3000R3C | 10.0 | 2.51 us | 6801-2 | $1.250E-02$ | 9 | 2.25 kA | L5Ch3 | |
| I_{G5} | 500-00 | 3000R3A | 1.0 | 2.52 us | MS #7 | $6.222E-04$ | 6 | 3.21 kA | L1Ch3 | |
| I_{A8} | 298-01 | 4 | 10.0 | 1.51 us | 110A-2 | $5.000E-02$ | 20 | 2.00 kA | L8Ch3 | |
| I_{BN8} | 310-01 | 3000R1C | 10.0 | 1.60 us | 110A-3 | $5.000E-02$ | 20 | 2.00 kA | L5Ch1 | |
| I_{CN8} | 350-02 | 3000R3B | 10.0 | 1.78 us | 6805-3 | $1.250E-02$ | 20 | 8.00 kA | L3Ch3 | |
| V_{AN8} | 500-12 | 3 | 0.1 | 2.36 us | 175kV-1 | $1.923E-06$ | 3 | 73.45 kV | L8Ch4 | |
| V_{BN8} | 350-01 | 3000R2C | 0.1 | 1.78 us | 175kV-2 | $1.923E-06$ | 3 | 73.45 kV | L5Ch2 | |
| V_{CN8} | 360-01 | 3000R4B | 0.1 | 1.87 us | 175kV-3 | $1.923E-06$ | 3 | 73.45 kV | L3Ch4 | |
| I_{N8} | 400-01 | 3000R6C | 10.0 | 2.02 us | 5179-6 | $5.000E-02$ | 23 | 2.83 kA | L6Ch2 | |
| V_{CB8} | 420-01 | 3000R2B | 0.1 | 2.19 us | 350kV-1 | $5.000E-06$ | 17 | 141.59 kV | L3Ch2 | |
| I_{G8} | 300-01 | 3000R4A | 1.0 | 1.62 us | MS #1 | $5.090E-04$ | 14 | 9.85 kA | L1Ch4 | 9 |

Table C.5 – continued.

| Location Fig. | C.6 | Fiber | Isobe Number | Sett. | Delay | Device | Ratio [dB] | Att. [dB] | Range | Scope | MT Ch |
|---------------|--------|---------|--------------|---------|--------|--------------------------|--------------------|--------------------|--------------------|---------|-------|
| I_{A9} | 220-04 | | 12 | | 10.0 | 1.19 us | $5.179 \cdot 4$ | $5.000 \cdot E-02$ | 14 | 1.00 kA | L9Ch1 |
| I_{B9} | 220-05 | | 16 | | 10.0 | 1.17 us | $5.179 \cdot 5$ | $5.000 \cdot E-02$ | 14 | 1.00 kA | L9Ch2 |
| I_{C9} | 220-08 | 3000R4C | 10.0 | 1.13 us | | | $6.805 \cdot 4$ | $1.250 \cdot E-02$ | 20 | 8.00 kA | L5Ch4 |
| I_{CN11} | 160-05 | 3000R5B | 10.0 | | 874 ns | | $6.805 \cdot 5$ | $1.250 \cdot E-02$ | 20 | 8.00 kA | L4Ch1 |
| V_{GN11} | 220-06 | 3000R6B | 0.1 | 1.14 us | | $175 \text{ kV} \cdot 4$ | $1.923 \cdot E-06$ | 3 | 73.45 kV | L4Ch2 | 14 |
| I_{G11} | 220-07 | 3000R5A | 1.0 | 1.14 us | | MS #2 | $5.170 \cdot E-04$ | 14 | 9.69 kA | L2Ch1 | |
| I_{CN14} | 500-08 | 3000R7B | 10.0 | 2.49 us | | $6.805 \cdot 6$ | $1.250 \cdot E-02$ | 9 | 2.25 kA | L4Ch3 | |
| I_{G14} | 500-09 | 3000R6A | 1.0 | 2.51 us | | MS #8 | $6.200 \cdot E-04$ | 6 | 3.22 kA | L2Ch2 | |
| I_{CN17} | 500-10 | 3000R8B | 10.0 | 2.51 us | | $11.0 \text{ A} \cdot 5$ | $5.000 \cdot E-02$ | 20 | 2.00 kA | L4Ch4 | |
| I_{G17} | 500-11 | 3000R7A | 0.1 | 2.51 us | | MS #5 | $5.000 \cdot E-04$ | 17 | 1.42 kA | L2Ch3 | |
| I_{G18} | 550-04 | 3000R8A | 0.1 | 2.75 us | | MS #4 | $5.140 \cdot E-04$ | 17 | 1.38 kA | L2Ch4 | |

Table C.6: Instrumentation settings for flashes FPL0011 and FPL0014 (see also Table C.5 and Figure C.6).

| ID | Sensitivity per quantization level | Scope Range | | Sampling Rate |
|------------|------------------------------------|-------------|-----------|---------------|
| | | Max. | Min. | |
| I_i | 143.2 A/level | 32.1 kA | -4.6 kA | 25 MHz |
| I_{Mi} | 71.6 A/level | 16.0 kA | -2.3 kA | 25 MHz |
| I_{Li} | 10.7 A/level | 2.4 kA | -0.3 kA | 20 MHz |
| I_{CN1} | 1.2 A/level | 40.0 A | -0.3 kA | 20 MHz |
| I_{G1} | 8.6 A/level | 273.9 A | -1.9 kA | 10 MHz |
| I_{N2} | 12.5 A/level | 400.0 A | -2.8 kA | 20 MHz |
| I_{G2} | 9.0 A/level | 287.6 A | -2.0 kA | 10 MHz |
| I_{CN5} | 14.1 A/level | 450.9 A | -3.2 kA | 20 MHz |
| I_{A5} | 6.3 A/level | 801.9 A | -0.8 kA | 20 MHz |
| I_{B5} | 6.3 A/level | 801.9 A | -0.8 kA | 25 MHz |
| I_{C5} | 14.1 A/level | 450.9 A | -3.2 kA | 20 MHz |
| I_{G5} | 20.0 A/level | 641.3 A | -4.5 kA | 10 MHz |
| I_{AN8} | 12.5 A/level | 400.0 A | -2.8 kA | 25 MHz |
| I_{BN8} | 12.5 A/level | 400.0 A | -2.8 kA | 20 MHz |
| I_{CN8} | 50.0 A/level | 1.6 kA | -11.2 kA | 10 MHz |
| V_{AN8} | 459.1 V/level | 14.7 kV | -102.8 kV | 25 MHz |
| V_{BN8} | 459.1 V/level | 14.7 kV | -102.8 kV | 20 MHz |
| V_{CN8} | 459.1 V/level | 14.7 kV | -102.8 kV | 10 MHz |
| I_{N8} | 17.7 A/level | 565.0 A | -4.0 kA | 20 MHz |
| V_{CB8} | 884.9 V/level | 28.3 kV | -198.2 kV | 10 MHz |
| I_{G8} | 61.5 A/level | 2.0 kA | -13.8 kA | 10 MHz |
| I_{A9} | 6.3 A/level | 801.9 A | -0.8 kA | 25 MHz |
| I_{B9} | 6.3 A/level | 801.9 A | -0.8 kA | 25 MHz |
| I_{C9} | 50.0 A/level | 1.6 kA | -11.2 kA | 20 MHz |
| I_{CN11} | 50.0 A/level | 1.6 kA | -11.2 kA | 20 MHz |
| V_{CN11} | 459.1 V/level | 14.7 kV | -102.8 kV | 20 MHz |
| I_{G11} | 60.6 A/level | 1.9 kA | -13.6 kA | 10 MHz |
| I_{CN14} | 14.1 A/level | 450.9 A | -3.2 kA | 20 MHz |
| I_{G14} | 20.1 A/level | 643.6 A | -4.5 kA | 10 MHz |
| I_{CN17} | 12.5 A/level | 400.0 A | -2.8 kA | 20 MHz |
| I_{G17} | 8.8 A/level | 283.2 A | -2.0 kA | 10 MHz |
| I_{G18} | 8.6 A/level | 275.5 A | -1.9 kA | 10 MHz |

Table C.7: Instrumentation summary for flash FPL0018, strike to phase C of the horizontal configuration distribution line with high power termination resistors; mid-point between poles 9 and 10 (see also Table C.8)

| Location Fig. | C.6 | Fiber | Isobe | | Delay | Device | Ratio | Att. [dB] | Range | Scope | MT Ch |
|---------------|--------|---------|--------|---------|---------|-----------|-------|-----------|-------|-------|-------|
| | | | Number | Sett. | | | | | | | |
| I_4 | 100-1 | 1 | 10.0 | 4.36 us | MS #9 | 6.165E-04 | 3 | 22.91 kA | L9Ch4 | 10 | |
| I_{Mi} | 100-1 | 1 | 10.0 | 4.36 us | MS #9 | 6.165E-04 | 3 | 22.91 kA | L8Ch1 | 11 | |
| I_{Li} | 100-02 | 19 | 1.0 | 4.43 us | MS #9 | 6.165E-04 | 3 | 2.29 kA | L7Ch2 | 13 | |
| I_{CN1} | 550-03 | 3000R7C | 10.0 | 2.25 us | 110A-1 | 5.000E-02 | | 200.00 A | L6Ch3 | | |
| I_G1 | 550-02 | 3000R1A | 0.1 | 2.25 us | MS #3 | 5.170E-04 | 18 | 1.54 kA | L1Ch1 | | |
| I_{CN2} | 500-02 | 3000R1B | 10.0 | 2.49 us | 110A-4 | 5.000E-02 | 20 | 2.00 kA | L3Ch1 | | |
| I_{N2} | 500-03 | 3000R5C | 10.0 | 2.48 us | 5179-1 | 5.000E-02 | 20 | 2.00 kA | L6Ch1 | | |
| I_{G2} | 500-01 | 3000R2A | 0.1 | 2.48 us | MS #6 | 6.197E-04 | 20 | 1.61 kA | L1Ch2 | | |
| I_{CN5} | 500-04 | 3000R8C | 10.0 | 2.49 us | 6801-1 | 1.250E-02 | 9 | 2.25 kA | L6Ch4 | | |
| I_{A5} | 500-05 | 11 | 10.0 | 2.48 us | 5179-2 | 5.000E-02 | 14 | 1.00 kA | L7Ch1 | | |
| I_{B5} | 500-06 | 18 | 10.0 | 2.65 us | 5179-3 | 5.000E-02 | 14 | 1.00 kA | L8Ch2 | | |
| I_{C5} | 500-07 | 3000R3C | 10.0 | 2.49 us | 6801-2 | 1.250E-02 | 9 | 2.25 kA | L5Ch3 | | |
| I_{G5} | 500-00 | 3000R3A | 1.0 | 2.48 us | MS #7 | 6.222E-04 | 6 | 3.21 kA | L1Ch3 | | |
| I_{AN8} | 298-01 | 4 | 10.0 | 3.49 us | 110A-2 | 5.000E-02 | 20 | 2.00 kA | L8Ch3 | | |
| I_{BN8} | 310-01 | 3000R1C | 10.0 | 3.40 us | 110A-3 | 5.000E-02 | 20 | 2.00 kA | L5Ch1 | | |
| I_{CN8} | 350-02 | 3000R3B | 10.0 | 3.22 us | 6805-3 | 1.250E-02 | 20 | 8.00 kA | L3Ch3 | | |
| V_{AN8} | 500-12 | 3 | 0.1 | 2.64 us | 175kV-1 | 1.923E-06 | 3 | 73.45 kV | L8Ch4 | | |
| V_{B8} | 350-01 | 3000R2C | 0.1 | 3.22 us | 175kV-2 | 1.923E-06 | 3 | 73.45 kV | L5Ch2 | | |
| V_{CN8} | 360-01 | 3000R4B | 0.1 | 3.13 us | 175kV-3 | 1.923E-06 | 3 | 73.45 kV | L3Ch4 | | |
| I_{N8} | 400-01 | 3000R6C | 10.0 | 2.98 us | 5179-6 | 5.000E-02 | 23 | 2.83 kA | L6Ch2 | | |
| V_{GB8} | 420-01 | 3000R2B | 0.1 | 2.81 us | 350kV-1 | 5.000E-06 | 17 | 141.59 kV | L3Ch2 | | |
| I_{G8} | 300-01 | 3000R4A | 1.0 | 3.38 us | MS #1 | 5.090E-04 | 14 | 9.85 kA | L1Ch4 | 9 | |

Table C.7 - continued.

| Location Fig. C.6 | Fiber | Isobe | | Delay | Device | Ratio | Att. [dB] | Range | Scope | MT Ch |
|-------------------------|--------|---------|-------|---------|---------|-------------|--------------|----------|-------|----------|
| | | Number | Sett. | | | | | | | |
| I_{A9} | 220-04 | 12 | 10.0 | 3.81 us | 5179-4 | $5.000E-02$ | 14 | 1.00 kA | L9Ch1 | |
| I_{B9} | 220-05 | 16 | 10.0 | 3.83 us | 5179-5 | $5.000E-02$ | 14 | 1.00 kA | L9Ch2 | |
| I_{C9} | 220-08 | 3000R4C | 10.0 | 3.87 us | 6805-4 | $1.250E-02$ | 22 | 10.07 kA | L5Ch4 | |
| I_{CN11} | 160-05 | 3000R5B | 10.0 | 4.13 us | 6805-5 | $1.250E-02$ | 20 | 8.00 kA | L4Ch1 | 12 |
| V_{GN11} | 220-06 | 3000R6B | 0.1 | 3.86 us | 175kV-4 | $1.923E-06$ | 3 | 73.45 kV | L4Ch2 | 14 |
| I_{G11} | 220-07 | 3000R5A | 1.0 | 3.86 us | MS#2 | $5.170E-04$ | 14 | 9.69 kA | L2Ch1 | |
| I_{CN14} | 500-08 | 3000R7B | 10.0 | 2.51 us | 6805-6 | $1.250E-02$ | 9 | 2.25 kA | L4Ch3 | |
| I_{G14} | 500-09 | 3000R6A | 1.0 | 2.49 us | MS#8 | $6.200E-04$ | 6 | 3.22 kA | L2Ch2 | |
| I_{CN17} | 500-10 | 3000R8B | 10.0 | 2.49 us | 110A-5 | $5.000E-02$ | 20 | 2.00 kA | L4Ch4 | |
| I_{G17} | 500-11 | 3000R7A | 0.1 | 2.49 us | MS#5 | $5.000E-04$ | 20 | 2.00 kA | L2Ch3 | |
| I_{G18} | 550-04 | 3000R8A | 0.1 | 2.25 us | MS#4 | $5.140E-04$ | 20 | 1.95 kA | L2Ch4 | |

Table C.8: Instrumentation settings for flash FPL0018 (see also Table C.7 and Figure C.6).

| ID | Sensitivity per quantization level | Scope Range | | Sampling Rate |
|------------|------------------------------------|---------------|---------------|---------------|
| | | Max. | Min. | |
| I_i | 143.2 A/level | 32.1 kA | -4.6 kA | 25 MHz |
| I_{Mi} | 71.6 A/level | 16.0 kA | -2.3 kA | 25 MHz |
| I_{Li} | 12.5 A/level | 2.6 kA | -0.6 kA | 20 MHz |
| I_{CN1} | 1.2 A/level | 40.0 A | -0.3 kA | 20 MHz |
| I_{G1} | 9.6 A/level | 307.3 A | -2.2 kA | 20 MHz |
| I_{CN2} | 15.6 A/level | 1.2 kA | -2.8 kA | 20 MHz |
| I_{N2} | 12.5 A/level | 400.0 A | -2.8 kA | 20 MHz |
| I_{G2} | 10.1 A/level | 322.7 A | -2.3 kA | 20 MHz |
| I_{CN5} | 17.6 A/level | 1.4 kA | -3.2 kA | 20 MHz |
| I_{A5} | 11.7 A/level | 1.5 kA | -1.5 kA | 20 MHz |
| I_{B5} | 11.7 A/level | 1.5 kA | -1.5 kA | 25 MHz |
| I_{C5} | 14.1 A/level | 450.9 A | -3.2 kA | 20 MHz |
| I_{G5} | 20.0 A/level | 641.3 A | -4.5 kA | 20 MHz |
| I_{AN8} | 23.4 A/level | 3.0 kA | -3.0 kA | 25 MHz |
| I_{BN8} | 23.4 A/level | 3.0 kA | -3.0 kA | 20 MHz |
| I_{CN8} | 50.0 A/level | 1.6 kA | -11.2 kA | 20 MHz |
| V_{AN8} | 860.8 V/level | 110.2 kV | -110.2 kV | 25 MHz |
| V_{BN8} | 860.8 V/level | 110.2 kV | -110.2 kV | 20 MHz |
| V_{CN8} | 573.9 V/level | 44.1 kV | -102.8 kV | 20 MHz |
| I_{N8} | 17.7 A/level | 565.0 A | -4.0 kA | 20 MHz |
| V_{CB8} | 1659.2 V/level | 212.4 kV | -212.4 kV | 20 MHz |
| I_{G8} | 61.5 A/level | 2.0 kA | -13.8 kA | 20 MHz |
| I_{A9} | 11.7 A/level | 1.5 kA | -1.5 kA | 25 MHz |
| I_{B9} | 11.7 A/level | 1.5 kA | -1.5 kA | 25 MHz |
| I_{C9} | 62.9 A/level | 2.0 kA | -14.1 kA | 20 MHz |
| V_{AN9} | $NaN\text{V}$ /level | $NaN\text{V}$ | $NaN\text{V}$ | 20 MHz |
| V_{CN9} | $NaN\text{V}$ /level | $NaN\text{V}$ | $NaN\text{V}$ | 20 MHz |
| V_{BA9} | $NaN\text{V}$ /level | $NaN\text{V}$ | $NaN\text{V}$ | 25 MHz |
| I_{CN11} | 62.5 A/level | 4.8 kA | -11.2 kA | 20 MHz |
| V_{CN11} | 573.9 V/level | 44.1 kV | -102.8 kV | 20 MHz |
| I_{G11} | 60.6 A/level | 1.9 kA | -13.6 kA | 20 MHz |
| I_{CN14} | 17.6 A/level | 1.4 kA | -3.2 kA | 20 MHz |
| I_{G14} | 20.1 A/level | 643.6 A | -4.5 kA | 20 MHz |
| I_{CN17} | 15.6 A/level | 1.2 kA | -2.8 kA | 20 MHz |
| I_{G17} | 12.5 A/level | 400.0 A | -2.8 kA | 20 MHz |
| I_{G18} | 12.2 A/level | 389.1 A | -2.7 kA | 20 MHz |

Table C.9: Instrumentation summary for flashes FPL0032, FPL0033, FPL0034, and FPL0036, strike to phase C of the horizontal configuration distribution line with high power termination resistors; mid-point between poles 9 and 10

| Location Fig. | C.6 | Fiber | Isobe | | Delay | Device | Ratio | Att. [dB] | Range | Scope | MT Ch |
|---------------|--------|---------|--------|---------|---------|-----------|-------|-----------|-------|-------|-------|
| | | | Number | Sett. | | | | | | | |
| I_i | 100-1 | 1 | 10.0 | 4.36 us | MS #9 | 6.165E-04 | 9 | 45.72 kA | L9Ch4 | 10 | |
| I_{Mi} | 100-1 | 1 | 10.0 | 4.36 us | MS #9 | 6.165E-04 | 9 | 45.72 kA | L8Ch1 | 11 | |
| I_{Li} | 100-02 | 19 | 1.0 | 4.43 us | MS #9 | 6.165E-04 | 9 | 4.57 kA | L7Ch2 | 13 | |
| I_{CN1} | 550-03 | 3000R7C | 10.0 | 2.25 us | 110A-1 | 5.000E-02 | | 200.00 A | L6Ch3 | | |
| I_G1 | 550-02 | 3000R1A | 0.1 | 2.25 us | MS #3 | 5.170E-04 | 18 | 1.54 kA | L1Ch1 | | |
| I_{CN2} | 500-02 | 3000R1B | 10.0 | 2.49 us | 110A-4 | 5.000E-02 | 20 | 2.00 kA | L3Ch1 | | |
| I_{N2} | 500-03 | 3000R5C | 10.0 | 2.48 us | 5179-1 | 5.000E-02 | 20 | 2.00 kA | L6Ch1 | | |
| I_G2 | 500-01 | 3000R2A | 0.1 | 2.48 us | MS #6 | 6.197E-04 | 20 | 1.61 kA | L1Ch2 | | |
| I_{CN5} | 500-04 | 3000R8C | 10.0 | 2.49 us | 6801-1 | 1.250E-02 | 9 | 2.25 kA | L6Ch4 | | |
| I_{A5} | 500-05 | 11 | 10.0 | 2.48 us | 5179-2 | 5.000E-02 | 14 | 1.00 kA | L7Ch1 | | |
| I_B5 | 500-06 | 18 | 10.0 | 2.65 us | 5179-3 | 5.000E-02 | 14 | 1.00 kA | L8Ch2 | | |
| I_C5 | 500-07 | 3000R3C | 10.0 | 2.49 us | 6801-2 | 1.250E-02 | 9 | 2.25 kA | L5Ch3 | | |
| I_G5 | 500-00 | 3000R3A | 1.0 | 2.48 us | MS #7 | 6.222E-04 | 6 | 3.21 kA | L1Ch3 | | |
| I_{AN8} | 298-01 | 4 | 10.0 | 3.49 us | 110A-2 | 5.000E-02 | 20 | 2.00 kA | L8Ch3 | | |
| I_{BN8} | 310-01 | 3000R1C | 10.0 | 3.40 us | 110A-3 | 5.000E-02 | 20 | 2.00 kA | L5Ch1 | | |
| I_{GN8} | 350-02 | 3000R3B | 10.0 | 3.22 us | 6805-3 | 1.250E-02 | 20 | 8.00 kA | L3Ch3 | | |
| V_{A18} | 500-12 | 3 | 0.1 | 2.64 us | 175kV-1 | 1.923E-06 | 3 | 73.45 kV | L8Ch4 | | |
| V_{BN8} | 350-01 | 3000R2C | 0.1 | 3.22 us | 175kV-2 | 1.923E-06 | 3 | 73.45 kV | L5Ch2 | | |
| V_{CN8} | 360-01 | 3000R4B | 0.1 | 3.13 us | 175kV-3 | 1.923E-06 | 3 | 73.45 kV | L3Ch4 | | |
| I_{N8} | 400-01 | 3000R6C | 10.0 | 2.98 us | 5179-6 | 5.000E-02 | 23 | 2.83 kA | L6Ch2 | | |
| V_{CB8} | 420-01 | 3000R2B | 0.1 | 2.81 us | 350kV-1 | 5.000E-06 | 17 | 141.59 kV | L3Ch2 | | |
| I_{G8} | 300-01 | 3000R4A | 1.0 | 3.38 us | MS #1 | 5.090E-04 | 14 | 9.85 kA | L1Ch4 | 9 | |

Table C.9 – continued.

| Location Fig. C.6 | Fiber | Isolate | | Delay | Device | Ratio | Att. [dB] | Range | Scope | MT Ch |
|-------------------------|--------|---------|-------|---------|---------|-------------|--------------|----------|-------|----------|
| | | Number | Sett. | | | | | | | |
| I_{A9} | 220-04 | 12 | 10.0 | 3.81 us | 5179-4 | $5.000E-02$ | 14 | 1.00 kA | L9Ch1 | |
| I_{B9} | 220-05 | 16 | 10.0 | 3.83 us | 5179-5 | $5.000E-02$ | 14 | 1.00 kA | L9Ch2 | |
| I_{C9} | 220-08 | 3000R4C | 10.0 | 3.87 us | 6805-4 | $1.250E-02$ | 22 | 10.07 kA | L5Ch4 | |
| I_{CN11} | 160-05 | 3000R5B | 10.0 | 4.13 us | 6805-5 | $1.250E-02$ | 20 | 8.00 kA | L4Ch1 | 12 |
| V_{CN11} | 220-06 | 3000R6B | 0.1 | 3.86 us | 175kV-4 | $1.923E-06$ | 3 | 73.45 kV | L4Ch2 | 14 |
| I_{G11} | 220-07 | 3000R5A | 1.0 | 3.86 us | MS #2 | $5.170E-04$ | 14 | 9.69 kA | L2Ch1 | |
| I_{CN14} | 500-08 | 3000R7B | 10.0 | 2.51 us | 6805-6 | $1.250E-02$ | 9 | 2.25 kA | L4Ch3 | |
| I_{G14} | 500-09 | 3000R6A | 1.0 | 2.49 us | MS #8 | $6.200E-04$ | 6 | 3.22 kA | L2Ch2 | |
| I_{CN17} | 500-10 | 3000R8B | 10.0 | 2.49 us | 110A-5 | $5.000E-02$ | 20 | 2.00 kA | L4Ch4 | |
| I_{G17} | 500-11 | 3000R7A | 0.1 | 2.49 us | MS #5 | $5.000E-04$ | 20 | 2.00 kA | L2Ch3 | |
| I_{G18} | 550-04 | 3000R8A | 0.1 | 2.25 us | MS #4 | $5.140E-04$ | 20 | 1.95 kA | L2Ch4 | |
| $I_{Ls,s}$ | 100-02 | 19 | 1.0 | 4.43 us | MS #9 | $6.165E-04$ | 9 | 4.57 kA | L0Ch1 | 13 |
| $I_{CN8,s}$ | 350-02 | 3000R3B | 10.0 | 3.22 us | 6805-3 | $1.250E-02$ | 20 | 8.00 kA | L0Ch2 | |
| $V_{CN8,s}$ | 360-01 | 3000R4B | 0.1 | 3.13 us | 175kV-3 | $1.923E-06$ | 3 | 73.45 kV | L0Ch3 | |
| $I_{CN11,s}$ | 160-05 | 3000R5B | 10.0 | 4.13 us | 6805-5 | $1.250E-02$ | 20 | 8.00 kA | L0Ch4 | 12 |

Table C.10: Instrumentation settings for flashes FPL0032, FPL0033, FPL0034, and FPL0036 (see also Table C.9 and Figure C.6).

| ID | Sensitivity per quantization level | Scope Range | | Sampling Rate |
|------------|------------------------------------|-------------|-----------|---------------|
| | | Max. | Min. | |
| I_i | 285.7 A/level | 64.0 kA | -9.1 kA | 25 MHz |
| I_{Mi} | 85.7 A/level | 19.2 kA | -2.7 kA | 25 MHz |
| I_{Li} | 17.9 A/level | 4.0 kA | -0.6 kA | 20 MHz |
| I_{CN1} | 1.2 A/level | 40.0 A | -0.3 kA | 20 MHz |
| I_{G1} | 9.6 A/level | 307.3 A | -2.2 kA | 20 MHz |
| I_{CN2} | 15.6 A/level | 1.2 kA | -2.8 kA | 20 MHz |
| I_{N2} | 12.5 A/level | 400.0 A | -2.8 kA | 20 MHz |
| I_{G2} | 10.1 A/level | 322.7 A | -2.3 kA | 20 MHz |
| I_{CN5} | 17.6 A/level | 1.4 kA | -3.2 kA | 20 MHz |
| I_{A5} | 11.7 A/level | 1.5 kA | -1.5 kA | 20 MHz |
| I_{B5} | 11.7 A/level | 1.5 kA | -1.5 kA | 25 MHz |
| I_{C5} | 14.1 A/level | 450.9 A | -3.2 kA | 20 MHz |
| I_{G5} | 20.0 A/level | 641.3 A | -4.5 kA | 20 MHz |
| I_{AN8} | 23.4 A/level | 3.0 kA | -3.0 kA | 25 MHz |
| I_{BN8} | 23.4 A/level | 3.0 kA | -3.0 kA | 20 MHz |
| I_{CN8} | 50.0 A/level | 1.6 kA | -11.2 kA | 20 MHz |
| V_{AN8} | 860.8 V/level | 110.2 kV | -110.2 kV | 25 MHz |
| V_{BN8} | 860.8 V/level | 110.2 kV | -110.2 kV | 20 MHz |
| V_{CN8} | 573.9 V/level | 44.1 kV | -102.8 kV | 20 MHz |
| I_{N8} | 17.7 A/level | 565.0 A | -4.0 kA | 20 MHz |
| V_{CB8} | 1659.2 V/level | 212.4 kV | -212.4 kV | 20 MHz |
| I_{G8} | 61.5 A/level | 2.0 kA | -13.8 kA | 20 MHz |
| I_{A9} | 11.7 A/level | 1.5 kA | -1.5 kA | 25 MHz |
| I_{B9} | 11.7 A/level | 1.5 kA | -1.5 kA | 25 MHz |
| I_{C9} | 62.9 A/level | 2.0 kA | -14.1 kA | 20 MHz |
| I_{CN11} | 62.5 A/level | 4.8 kA | -11.2 kA | 20 MHz |
| V_{CN11} | 573.9 V/level | 44.1 kV | -102.8 kV | 20 MHz |
| I_{G11} | 60.6 A/level | 1.9 kA | -13.6 kA | 20 MHz |
| I_{CN14} | 17.6 A/level | 1.4 kA | -3.2 kA | 20 MHz |
| I_{G14} | 20.1 A/level | 643.6 A | -4.5 kA | 20 MHz |
| I_{CN17} | 15.6 A/level | 1.2 kA | -2.8 kA | 20 MHz |
| I_{G17} | 12.5 A/level | 400.0 A | -2.8 kA | 20 MHz |
| I_{G18} | 12.2 A/level | 389.1 A | -2.7 kA | 20 MHz |

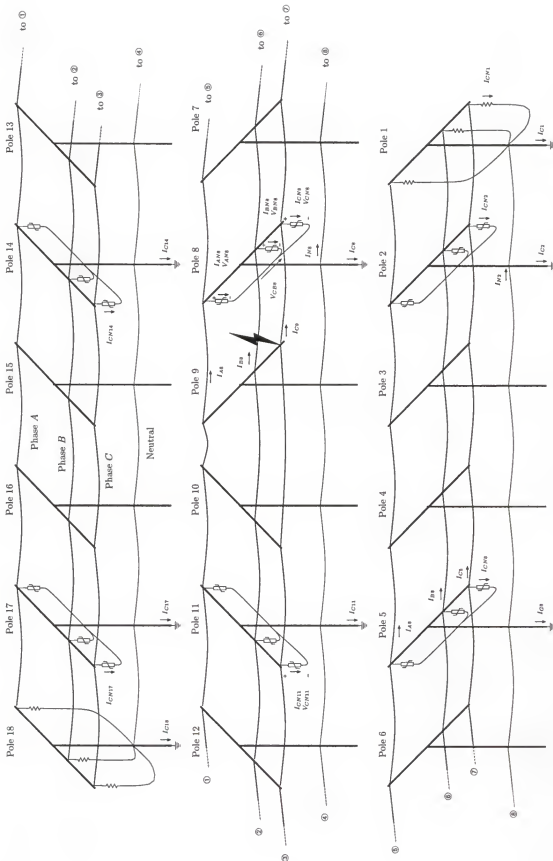


Figure C.7: Locations of measurements for flash FPL0037, strike to phase C of the horizontal configuration at pole 9.

Table C.11: Instrumentation summary for flash FPI0037, strike to phase C of the horizontal configuration distribution line with high power termination resistors; pole 9 (see also Table C.12)

| Location Fig. C.7 | Fiber | Isobe | | Delay | Device | Ratio | Att. [dB] | Range | Scope | MT Ch |
|-------------------|--------|---------|-------|---------|---------|-------------|-----------|-----------|-------|-------|
| | | Number | Sett. | | | | | | | |
| I_i | 100-1 | 1 | 10.0 | 4.36 us | MS #9 | $6.165E-04$ | 9 | 45.72 kA | L9Ch4 | 10 |
| I_{Mi} | 100-1 | 1 | 10.0 | 4.36 us | MS #9 | $6.165E-04$ | 9 | 45.72 kA | L8Ch1 | 11 |
| I_{Li} | 100-02 | 19 | 1.0 | 4.43 us | MS #9 | $6.165E-04$ | 9 | 4.57 kA | L7Ch2 | 13 |
| I_{CN1} | 550-03 | 3000R7C | 10.0 | 2.25 us | 110A-1 | $5.000E-02$ | 200.00 A | L6Ch3 | | |
| I_{G1} | 550-02 | 3000R1A | 0.1 | 2.25 us | MS #3 | $5.170E-04$ | 18 | 1.54 kA | L1Ch1 | |
| I_{CN2} | 500-02 | 3000R1B | 10.0 | 2.49 us | 110A-4 | $5.000E-02$ | 20 | 2.00 kA | L3Ch1 | |
| I_{N2} | 500-03 | 3000R5C | 10.0 | 2.48 us | 5179-1 | $5.000E-02$ | 20 | 2.00 kA | L6Ch1 | |
| I_{G2} | 500-01 | 3000R2A | 0.1 | 2.48 us | MS #6 | $6.197E-04$ | 20 | 1.61 kA | L1Ch2 | |
| I_{CN5} | 500-04 | 3000R8C | 10.0 | 2.49 us | 6801-1 | $1.250E-02$ | 9 | 2.25 kA | L6Ch4 | |
| I_{A5} | 500-05 | 11 | 10.0 | 2.48 us | 5179-2 | $5.000E-02$ | 14 | 1.00 kA | L7Ch1 | |
| I_{B5} | 500-06 | 18 | 10.0 | 2.65 us | 5179-3 | $5.000E-02$ | 14 | 1.00 kA | L8Ch2 | |
| I_{C5} | 500-07 | 3000R3C | 10.0 | 2.49 us | 6801-2 | $1.250E-02$ | 9 | 2.25 kA | L5Ch3 | |
| I_{G5} | 500-00 | 3000R3A | 1.0 | 2.48 us | MS #7 | $6.222E-04$ | 6 | 3.21 kA | L1Ch3 | |
| I_{AN8} | 298-01 | 4 | 10.0 | 3.49 us | 110A-2 | $5.000E-02$ | 20 | 2.00 kA | L8Ch3 | |
| I_{BN8} | 310-01 | 3000R1C | 10.0 | 3.40 us | 110A-3 | $5.000E-02$ | 20 | 2.00 kA | L5Ch1 | |
| I_{CN8} | 350-02 | 3000R3B | 10.0 | 3.22 us | 6805-3 | $1.250E-02$ | 20 | 8.00 kA | L3Ch3 | |
| V_{ANS} | 500-12 | 3 | 0.1 | 2.64 us | 175kV-1 | $1.923E-06$ | 3 | 73.45 kV | L8Ch4 | |
| V_{BN8} | 350-01 | 3000R2C | 0.1 | 3.22 us | 175kV-2 | $1.923E-06$ | 3 | 73.45 kV | L5Ch2 | |
| V_{CN8} | 360-01 | 3000R4B | 0.1 | 3.13 us | 175kV-3 | $1.923E-06$ | 3 | 73.45 kV | L3Ch4 | |
| I_{N8} | 400-01 | 3000R6C | 10.0 | 2.98 us | 5179-6 | $5.000E-02$ | 23 | 2.83 kA | L6Ch2 | |
| V_{CB8} | 420-01 | 3000R2B | 0.1 | 2.81 us | 350kV-1 | $5.000E-06$ | 17 | 141.59 kV | L3Ch2 | |
| I_{G8} | 300-01 | 3000R4A | 1.0 | 3.38 us | MS #1 | $5.090E-04$ | 14 | 9.85 kA | L1Ch4 | 9 |

Table C.11 – continued.

| Location Fig. C.7 | Fiber | Iso-be | | Delay | Device | Ratio | Att. [dB] | Range | Scope | MT Ch |
|----------------------|--------|---------|-------|---------|---------|-----------|--------------|----------|-------|----------|
| | | Number | Sett. | | | | | | | |
| I_{A9} | 220-04 | 12 | 10.0 | 3.81 us | 5179-4 | 5.000E-02 | 14 | 1.00 kA | L9Ch1 | |
| I_{B9} | 220-05 | 16 | 10.0 | 3.83 us | 5179-5 | 5.000E-02 | 14 | 1.00 kA | L9Ch2 | |
| I_{C9} | 220-08 | 3000R4C | 10.0 | 3.87 us | 6805-4 | 1.250E-02 | 22 | 10.07 kA | L5Ch4 | |
| I_{CN11} | 160-05 | 3000R5B | 10.0 | 4.13 us | 6805-5 | 1.250E-02 | 20 | 8.00 kA | L4Ch1 | 12 |
| V_{CN11} | 220-06 | 3000R6B | 0.1 | 3.86 us | 175kV-4 | 1.923E-06 | 3 | 73.45 kV | L4Ch2 | 14 |
| I_{G11} | 220-07 | 3000R5A | 1.0 | 3.86 us | MS #2 | 5.170E-04 | 14 | 9.69 kA | L2Ch1 | |
| I_{GN14} | 500-08 | 3000R7B | 10.0 | 2.51 us | 6805-6 | 1.250E-02 | 9 | 2.25 kA | L4Ch3 | |
| I_{G14} | 500-09 | 3000R6A | 1.0 | 2.49 us | MS #8 | 6.200E-04 | 6 | 3.22 kA | L2Ch2 | |
| I_{CN17} | 500-10 | 3000R8B | 10.0 | 2.49 us | 110A-5 | 5.000E-02 | 20 | 2.00 kA | L4Ch4 | |
| I_{G17} | 500-11 | 3000R7A | 0.1 | 2.49 us | MS #5 | 5.000E-04 | 20 | 2.00 kA | L2Ch3 | |
| I_{G18} | 550-04 | 3000R8A | 0.1 | 2.25 us | MS #4 | 5.140E-04 | 20 | 1.95 kA | L2Ch4 | |
| I_{Lts} | 100-02 | 19 | 1.0 | 4.43 us | MS #9 | 6.165E-04 | 9 | 4.57 kA | L0Ch1 | 13 |
| I_{CN8s} | 350-02 | 3000R3B | 10.0 | 3.22 us | 6805-3 | 1.250E-02 | 20 | 8.00 kA | L0Ch2 | |
| V_{CN8s} | 360-01 | 3000R4B | 0.1 | 3.13 us | 175kV-3 | 1.923E-06 | 3 | 73.45 kV | L0Ch3 | |
| I_{CN11s} | 160-05 | 3000R5B | 10.0 | 4.13 us | 6805-5 | 1.250E-02 | 20 | 8.00 kA | L0Ch4 | 12 |

Table C.12: Instrumentation settings for flash FPL0037 (see also Table C.11 and Figure C.7).

| ID | Sensitivity per quantization level | Scope Range | | Sampling Rate |
|-------------|------------------------------------|-------------|-----------|---------------|
| | | Max. | Min. | |
| I_i | 285.7 A/bit | 64.0 kA | -9.1 kA | 25 MHz |
| I_{Mi} | 85.7 A/bit | 19.2 kA | -2.7 kA | 25 MHz |
| I_{Li} | 17.9 A/bit | 4.0 kA | -0.6 kA | 20 MHz |
| I_{CN1} | 1.2 A/bit | 40.0 A | -0.3 kA | 20 MHz |
| I_{G1} | 9.6 A/bit | 307.3 A | -2.2 kA | 20 MHz |
| I_{CN2} | 15.6 A/bit | 1.2 kA | -2.8 kA | 20 MHz |
| I_{N2} | 12.5 A/bit | 400.0 A | -2.8 kA | 20 MHz |
| I_{G2} | 10.1 A/bit | 322.7 A | -2.3 kA | 20 MHz |
| I_{CN5} | 17.6 A/bit | 1.4 kA | -3.2 kA | 20 MHz |
| I_{A5} | 11.7 A/bit | 1.5 kA | -1.5 kA | 20 MHz |
| I_{B5} | 11.7 A/bit | 1.5 kA | -1.5 kA | 25 MHz |
| I_{C5} | 14.1 A/bit | 450.9 A | -3.2 kA | 20 MHz |
| I_{G5} | 20.0 A/bit | 641.3 A | -4.5 kA | 20 MHz |
| I_{AN8} | 23.4 A/bit | 3.0 kA | -3.0 kA | 25 MHz |
| I_{BN8} | 23.4 A/bit | 3.0 kA | -3.0 kA | 20 MHz |
| I_{CN8} | 50.0 A/bit | 1.6 kA | -11.2 kA | 20 MHz |
| V_{AN8} | 860.8 V/bit | 110.2 kV | -110.2 kV | 25 MHz |
| V_{BN8} | 860.8 V/bit | 110.2 kV | -110.2 kV | 20 MHz |
| V_{CN8} | 573.9 V/bit | 44.1 kV | -102.8 kV | 20 MHz |
| I_{N8} | 17.7 A/bit | 565.0 A | -4.0 kA | 20 MHz |
| V_{CB8} | 1659.2 V/bit | 212.4 kV | -212.4 kV | 20 MHz |
| I_{G8} | 61.5 A/bit | 2.0 kA | -13.8 kA | 20 MHz |
| I_{A9} | 11.7 A/bit | 1.5 kA | -1.5 kA | 25 MHz |
| I_{B9} | 11.7 A/bit | 1.5 kA | -1.5 kA | 25 MHz |
| I_{C9} | 62.9 A/bit | 2.0 kA | -14.1 kA | 20 MHz |
| I_{CN11} | 62.5 A/bit | 4.8 kA | -11.2 kA | 20 MHz |
| V_{CN11} | 573.9 V/bit | 44.1 kV | -102.8 kV | 20 MHz |
| I_{G11} | 60.6 A/bit | 1.9 kA | -13.6 kA | 20 MHz |
| I_{CN14} | 17.6 A/bit | 1.4 kA | -3.2 kA | 20 MHz |
| I_{G14} | 20.1 A/bit | 643.6 A | -4.5 kA | 20 MHz |
| I_{CN17} | 15.6 A/bit | 1.2 kA | -2.8 kA | 20 MHz |
| I_{G17} | 12.5 A/bit | 400.0 A | -2.8 kA | 20 MHz |
| I_{G18} | 12.2 A/bit | 389.1 A | -2.7 kA | 20 MHz |
| I_{Lis} | 4.3 A/bit | 960.0 A | -0.1 kA | 500 kHz |
| I_{CN8s} | 5.0 A/bit | 160.0 A | -1.1 kA | 500 kHz |
| V_{CN8s} | 573.9 V/bit | 44.1 kV | -102.8 kV | 500 kHz |
| I_{CN11s} | 7.5 A/bit | 1.7 kA | -0.2 kA | 500 kHz |

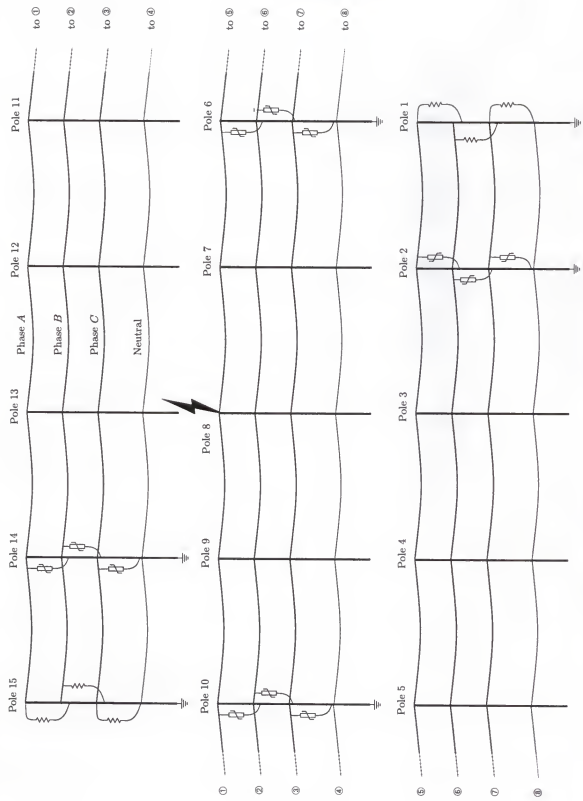


Figure C.8: Flash FPL0039 and FPL0040 to the vertical configuration distribution line, no measurements installed, strike to phase A at pole 8.

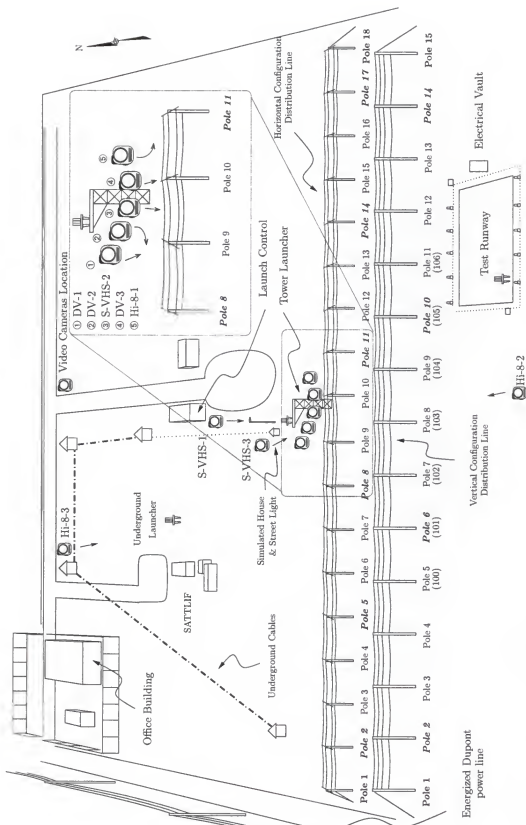


Figure C.9: Video cameras locations for the summer of 2000 experiments for configuration FPL-A-00, Section C.2.1. The directions of the arrows indicate the field of view of the devices (see Table 3.10).

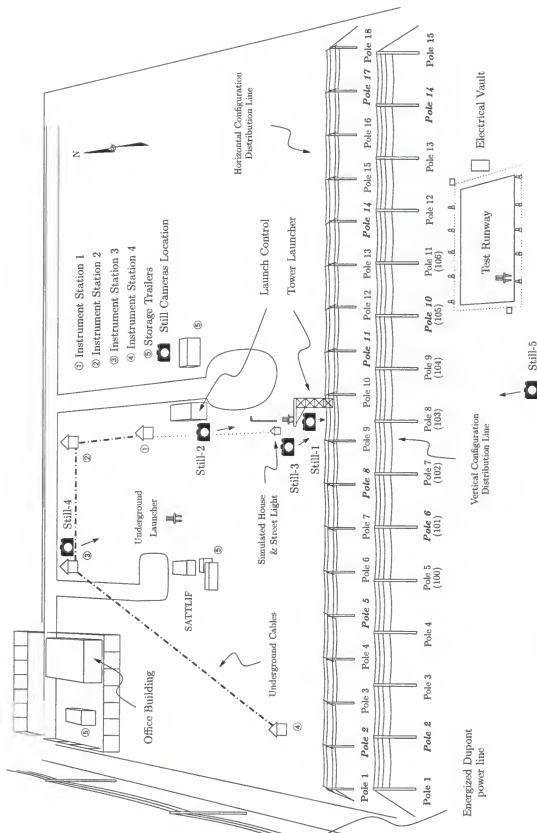


Figure C.10: Still cameras location for the summer of 2000 experiments for configuration FPL-A-00, Section C.2.1. The directions of the arrows indicate the field of view of the devices (see Table 3.10).

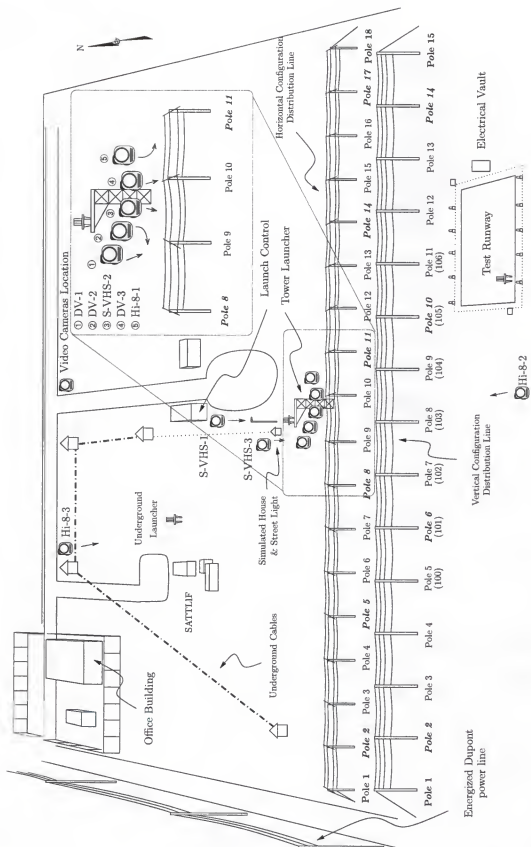


Figure C.11: Video cameras location for the summer of 2000 experiments for configuration FPL-B-00, Section C.2.2. The directions of the arrows indicate the field of view of the devices (see Table 3.11).

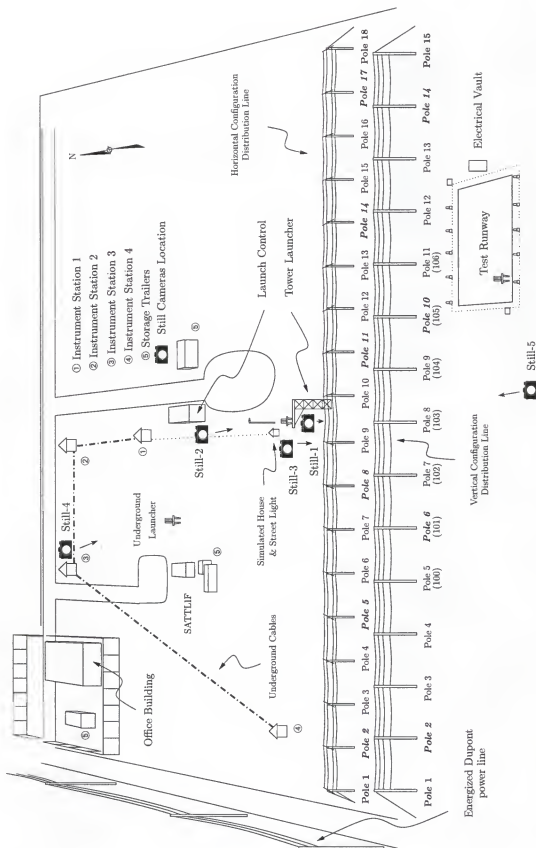


Figure C.12: Still cameras location for the summer of 2000 experiments for configuration FPI-B-00, Section C.2.2. The directions of the arrows indicate the field of view of the devices (see Table 3.11).

APPENDIX D DESCRIPTION OF THE ELECTROMAGNETIC TRANSIENT PROGRAM (EMTP)

The Electromagnetic Transients Program (EMTP) is a time-domain circuit-analyzing program originally developed for modeling power systems (Dommel [1986]). EMTP has its origin at the Bonneville Power Administration (BPA), which led EMTP development for more than a decade. The developments were in the public-domain, and the program was given freely to any interested party. In 1984, a new version of EMTP known by the acronym ATP (Alternative Transient Program) evolved following an attempt of commercialization of the EMTP by the Electric Power Research Institute (EPRI) and the EMTP Development Coordination Group (DCG). EMTP in this study actually refers to the ATP version of EMTP. ATP materials are royalty-free for those who have not participated in "EMTP commerce", but they are not public-domain in nature (Alternative Transient Program (ATP) Rule Book [1987-1998]).

D.1 Lumped and Distributed Elements in EMTP

The EMTP uses the trapezoidal rule¹ to integrate the ordinary differential equations describing the transient behavior of electric elements. Node voltages are used as state variables, therefore it is necessary to express the branch currents as functions of the node voltages. We know examine the equations of the basic elements of the EMTP (i.g., resistor, inductor, capacitor, and lossless transmission line).

¹The trapezoidal rule states that $\int_a^b f(x)dx = \frac{h}{2} \left[f(a) + f(b) + 2 \sum_{k=1}^{n-1} f(x_k) \right] + R_n$, with n an integer (even or odd), $h = (b - a)/n$, $x_k = a + kh$ for $k = 0, 1, 2, \dots, n$, and the remainder term $R_n = -nh^3 f^{(2)}(\xi)/12$ for some ξ such that $a < \xi < b$ (Abramowitz and Stegun 1972; Jeffrey 1995).

D.1.1 Resistor

The equation of the resistor is given by (D.1), and its impedance equivalent network is shown in Figure D.1a.

$$i_{k,m}(t) = \frac{v_k(t) - v_m(t)}{R} \quad (\text{D.1})$$

D.1.2 Inductor

In the case of an inductor we have:

$$v_k(t) - v_m(t) = L \frac{di_{k,m}(t)}{dt} \quad (\text{D.2})$$

which must be integrated from the known state at $t - \Delta t$ to the unknown state t in order to find $i_{k,m}(t)$:

$$i_{k,m}(t) = i_{k,m}(t - \Delta t) + \frac{1}{L} \int_{t-\Delta t}^t (v_k(t) - v_m(t)) dt \quad (\text{D.3})$$

using the integration trapezoidal rule, (D.3) can be rewritten as:

$$i_{k,m}(t) = \frac{\Delta t}{2L} (v_k(t) - v_m(t)) + I_{k,m}(t - \Delta t) \quad (\text{D.4})$$

where the equivalent current source $I_{k,m}$ is known from the past history and given by (D.5). The impedance equivalent network corresponding to (D.4) is shown in Figure D.1b.

$$I_{k,m}(t - \Delta t) = i_{k,m}(t - \Delta t) + \frac{\Delta t}{2L} (v_k(t - \Delta t) - v_m(t - \Delta t)) \quad (\text{D.5})$$

D.1.3 Capacitor

In the case of a capacitor we have the equation:

$$i_{k,m}(t) = \frac{1}{C} \frac{d(v_k(t) - v_m(t))}{dt} \quad (\text{D.6})$$

which must be also integrated from the known state at $t - \Delta t$ to the unknown state t in order to find $v_k(t) - v_m(t)$:

$$v_k(t) - v_m(t) = \frac{1}{C} \int_{t-\Delta t}^t i_{k,m}(t) dt + v_k(t - \Delta t) - v_m(t - \Delta t) \quad (\text{D.7})$$

Equation (D.7) can be integrated one more time, using the trapezoidal rule, to yield:

$$i_{k,m}(t) = \frac{2C}{\Delta t} (v_k(t) - v_m(t)) + I_{k,m}(t - \Delta t) \quad (\text{D.8})$$

where the equivalent current source $I_{k,m}$ is known from the past history and given by (D.9). The impedance equivalent network corresponding to (D.8) is shown in Figure D.1c.

$$I_{k,m}(t - \Delta t) = -i_{k,m}(t - \Delta t) - \frac{2C}{\Delta t} (v_k(t - \Delta t) - v_m(t - \Delta t)) \quad (\text{D.9})$$

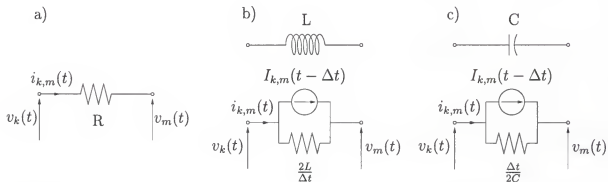


Figure D.1: Equivalent impedance network for: a) resistor; b) inductor; c) capacitor.

D.1.4 Lossless Transmission Line

For a lossless transmission line with inductance L' and capacitance C' per unit length we can write (Sadiku 1992):

$$-\frac{\partial v(x, t)}{\partial x} = L' \frac{\partial i(x, t)}{\partial t} \quad (\text{D.10})$$

$$-\frac{\partial i(x, t)}{\partial x} = C' \frac{\partial v(x, t)}{\partial t} \quad (\text{D.11})$$

The general solution of the system of partial differential equations (PDE) given by (D.10 and D.11) is:

$$i(x, t) = f_1(x - \nu t) + f_2(x + \nu t) \quad (\text{D.12})$$

$$v(x, t) = Z f_1(x - \nu t) - Z f_2(x + \nu t) \quad (\text{D.13})$$

where f_1 and f_2 are arbitrary functions of the variables $(x - \nu t)$ and $(x + \nu t)$, ν is the phase velocity given by (D.14), and Z is the surge impedance given by (D.15).

$$\nu = \frac{1}{\sqrt{L'C'}} \quad (\text{D.14})$$

$$Z = \sqrt{\frac{L'}{C'}} \quad (\text{D.15})$$

If we multiply (D.12) by Z and add it to (D.13) we obtain (D.16), and if we multiply (D.12) by Z and subtract it from (D.13) we obtain (D.17):

$$v(x, t) + Z i(x, t) = 2Z f_1(x - \nu t) \quad (\text{D.16})$$

$$v(x, t) - Z i(x, t) = -2Z f_2(x + \nu t) \quad (\text{D.17})$$

Note that in (D.16) and (D.17), $v(x, t) + Z i(x, t)$ and $v(x, t) - Z i(x, t)$ are constants for the characteristics of the PDE.² But $(x - \nu t)$ is constant to an observer traveling with a forward traveling wave, thus, $v(x, t) + Z i(x, t)$ is also constant to him. Similarly, $(x + \nu t)$ is constant to an observer traveling with a backward traveling wave, thus, $v(x, t) - Z i(x, t)$ is also constant to him. If the travel time for the line is:

$$\tau = \frac{d}{\nu} = d\sqrt{L'C'} \quad (\text{D.18})$$

where d is the line length, then $v(x, t) + Z i(x, t)$ encountered by the observer when he leaves node m at time $t - \tau$ must still be the same when he arrives at node k at time t , that is:

$$v_m(t - \tau) + Z i_{m,k}(t - \tau) = v_k(t) + Z (-i_{k,m}(t)) \quad (\text{D.19})$$

From this equation follows the simple two-port equation for $i_{k,m}(t)$ (see Figure D.2).³

$$i_{k,m} = \frac{1}{Z} v_k(t) + I_k(t - \tau) \quad (\text{D.20})$$

and similarly,

$$i_{m,k} = \frac{1}{Z} v_m(t) + I_m(t - \tau) \quad (\text{D.21})$$

where the current sources I_k and I_m are known from the past history at time $(t - \tau)$:

$$I_k(t - \tau) = -\frac{1}{Z} v_m(t - \tau) - i_{m,k}(t - \tau) \quad (\text{D.22})$$

$$I_m(t - \tau) = -\frac{1}{Z} v_k(t - \tau) - i_{k,m}(t - \tau) \quad (\text{D.23})$$

²The characteristics are those curves on which the solutions of the PDE are constant, in this case $(x - \nu t) = C_1$ and $(x + \nu t) = C_2$ (where C_1 and C_2 are constants) are the characteristics of the PDE given in (D.10) and (D.11), see Berg and McGregor [1966].

³In this derivation, we have used Dommel's convention for the direction of the currents and waves, Dommel [1969].

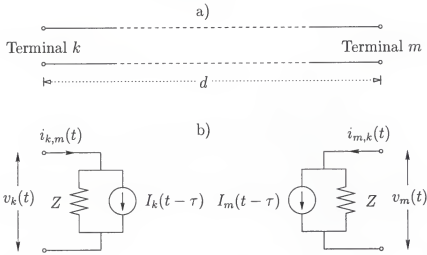


Figure D.2: a) Lossless line of length d ; b) Equivalent impedance network (adapted from Dommel [1969]).

D.2 Rigorous Frequency-Dependent Transmission Line Models

Although the method of characteristics discussed in Section D.1.4 is applicable to lossy lines, the ordinary differential equations it produces are not directly integrable (Branin 1967). For this reason, in the case of lossy lines, a resistance of $R/4$ (where R is the total series resistance of the line) is connected to both ends and $R/2$ in the middle of the line, as shown in Figure D.3. The lumped resistance approximation is valid only if $R \ll Z$, and should therefore not be used if the resistance is high (Dommel 1986).



Figure D.3: Equivalent circuit used for lossy transmission lines.

The frequency dependence of the transmission line parameters is the result of considering the skin effect (Alternative Transient Program (ATP) Rule Book [1987-1998];

Shneerson 1997), and the ground return currents (Carson 1926). Several sophisticated frequency-dependent models of transmission lines are available in the EMTP (Meyer and Dommel 1974; Semlyen and Dabuleanu 1975; Ametani 1976, Hauer 1981; Marti 1982; Noda et al. 1996; Noda 1997; Noda and Ametani 1998), the most rigorous of which are the J. Marti and the Noda models. These last two are described in the sections D.2.1 and D.2.2, respectively.

Budner [1970] proposed one of the first frequency dependent line models in which the concept of weighting functions (highly oscillatory) was used. Snelson [1972] introduced a change of variables to relate currents and voltages in the time domain, in a way that is analogous to Bergeron's interpretation of the simplified wave equations. This idea was further developed by Meyer and Dommel [1974] and resulted in a new set of weighting functions. Carroll and Nozari [1975] presented also a technique similar to the adaptation of Bergeron's method that used simpler weighting functions, therefore more efficient. Marti [1982] introduced a set of improved weighting functions (similar to the work of Carroll and Nozari [1975]) in the frequency domain.

D.2.1 J. Marti Frequency-Dependent Transmission Line Model

In the EMTP, multiphase lines are first decoupled through modal transformation matrices, so that each mode can be studied separately as a single-phase circuit. The phase equations are related to the modal equations as follows (Power System Analysis ATP/EMTP Short Course [1999]):

$$[i_{phase}] = [T_i][i_{modal}] \quad (D.24)$$

$$[v_{phase}] = [T_v][v_{modal}] \quad (D.25)$$

where $[T_i]$ and $[T_v]$ are the current and voltage transformation matrices, respectively. For the transformation to be “power invariant” it is required that:

$$[T_v]^T = [T_i]^{-1} \quad (\text{D.26})$$

now, if we consider the impedance matrix,

$$\begin{aligned} [v_{phase}] &= [Z_{phase}][i_{phase}] \\ [T_v][v_{modal}] &= [Z_{phase}][T_i][i_{modal}] \\ [v_{modal}] &= [T_v]^{-1}[Z_{phase}][T_i][i_{modal}] \\ [v_{modal}] &= [Z_{modal}][i_{modal}] \end{aligned} \quad (\text{D.27})$$

where

$$[Z_{modal}] = [T_v]^{-1}[Z_{phase}][T_i] \quad (\text{D.28})$$

The resulting $[Z_{modal}]$ matrix is symmetric (choosing the right $[T_i]$ and $[T_v]$). Equation (D.27) represents a set of decoupled equations ($[Z_{modal}]$ has nonzero terms only in its main diagonal). The problem is that these modal transformation matrices are frequency dependent. Nevertheless, as concluded by Magnusson [1973] and Wasley and Selvavinayagamoorthy [1974], it seems that it is still possible to obtain a reasonably good approximation under the assumption of constant transformation matrices.⁴

When the frequency dependence of the line parameters and the distributed nature of the losses are taken into account, writing the solutions of the line equations in the time domain becomes almost impossible (Marti 1982). This solution, however, can

⁴In this ATP/EMTP sub-routine, the user needs to specify the frequency at which the transformation matrices will be calculated.

be easily obtained in the frequency domain (Matick 1995):

$$V_k(\omega) = \cosh[\gamma(\omega)l]V_m(\omega) - Z_c(\omega) \sinh[\gamma(\omega)l]I_{m,k}(\omega) \quad (\text{D.29})$$

and

$$I_{k,m}(\omega) = \frac{1}{Z_c(\omega)} \sinh[\gamma(\omega)l]V_m(\omega) - Z_c(\omega) \cosh[\gamma(\omega)l]I_{m,k}(\omega) \quad (\text{D.30})$$

where

$$Z_c(\omega) = \sqrt{\frac{R'(\omega) + j\omega L'(\omega)}{G'(\omega) + j\omega C'(\omega)}} \quad \text{characteristic impedance,} \quad (\text{D.31})$$

$$\gamma(\omega) = \sqrt{(R'(\omega) + j\omega L'(\omega))(G'(\omega) + j\omega C'(\omega))} \quad \text{propagation constant} \quad (\text{D.32})$$

V_k and $I_{k,m}$ are the sending-end voltage and current, V_m and $I_{m,k}$ the receiving-end voltage and currents, R' , L' , G' , and C' are the series resistance, series inductance, shunt conductance, and shunt capacitance per unit length, respectively. The J. Marti model differs from the line with lumped resistances in that the resistance becomes *truly distributed* now.⁵

If we subtract Z_c times (D.30) from (D.29) we obtain the expression as if we traveled with the wave from node m to node k :

$$I_{k,m}(\omega) = \frac{V_k(\omega)}{Z_c(\omega)} - \left(\frac{V_m(\omega)}{Z_c(\omega)} + I_{m,k}(\omega) \right) e^{-\gamma(\omega)l} \quad (\text{D.33})$$

Our goal is to take (D.33) into an expression in the time domain. First with consider the second term on the right of (D.33). Let:

$$I_{m,\text{total}}(\omega) = \left(\frac{V_m(\omega)}{Z_c(\omega)} + I_{m,k}(\omega) \right) \quad (\text{D.34})$$

⁵When dealing with multiphase lines, R' , L' , G' , and C' are matrices, and V_k , $I_{k,m}$, V_m , and $I_{m,k}$ are column matrices.

and let $\gamma(\omega) = \alpha(\omega) + j\beta\omega$, so that we define the propagation factor:

$$A(\omega) = e^{-\gamma(\omega)t} = e^{-\alpha(\omega)t} e^{-j\beta(\omega)t} \quad (\text{D.35})$$

which consists of an attenuation factor $e^{-\alpha(\omega)t}$ as well as a phase shift factor $e^{-j\beta(\omega)t}$. The time domain form of $A(\omega)$ can be seen as a “weighting function” $a(t)$, which acts on the waves propagating on the line. Either end of the line would see this as weighting of history terms. This weighting of history at the other end of the line is done with the convolution integral:

$$I_{k,h} = \int_{\tau_{\min}}^{\tau_{\max}} i_{m,\text{total}}(t-u)a(u) du \quad (\text{D.36})$$

where τ_{\min} is the travel time of the fastest wave, τ_{\max} is the travel time of the slowest wave, and $i_{m,\text{total}}$ is the time domain form of (D.34). Now that we have already taken the second term on the right of (D.33) to the time domain, let’s work with the first term ($V_k(\omega)/Z_c(\omega)$).

As first suggested by Groschupf [1976], and further developed by Marti [1981], a frequency dependent impedance ($Z_c(\omega)$ for instance) can be approximated by a Foster-I $R-C$ network. Then the line seen from node k becomes a simple $R-C$ network in parallel with a current source $I_{k,h}$ (Figure D.4). The implicit integration with linear interpolation on the current (as explained later) can be applied to these capacitances transforming each $R-C$ block into a current source in parallel with an equivalent resistance. In the solution of the equivalent network, the frequency dependent line is simply represented by a constant resistance R_{eq} to ground in parallel with a current source $I_{k,h} + I_{R-C}$.

Marti [1982] showed that it is best to approximate $A(\omega)$ and $Z_c(\omega)$ by rational

⁷Note that $I_{k,h}$ is given by (D.36) and I_{R-C} is given by (D.50).

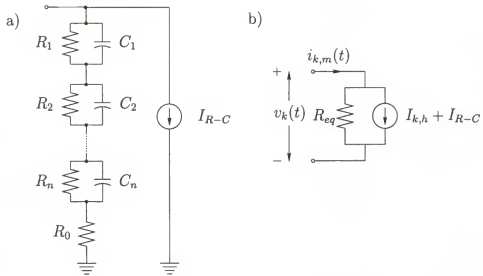


Figure D.4: Frequency dependent line representation seen from line end k ; a) with $R-C$ network; b) with equivalent resistance after applying implicit integration (adapted from Dommel [1986]).⁷

functions in the frequency domain. So, $A(\omega)$ can be approximated as follows:

$$A(\omega) \approx e^{-s\tau_{min}} k \frac{(s+z_1)(s+z_2)\cdots(s+z_n)}{(s+p_1)(s+p_2)\cdots(s+p_m)} \quad (\text{D.37})$$

where $s = j\omega$ and with $n < m$, the rational function part of (D.37) can be expanded into partial fractions,

$$\frac{(s+z_1)(s+z_2)\cdots(s+z_n)}{(s+p_1)(s+p_2)\cdots(s+p_m)} = \frac{k_1}{s+p_1} + \frac{k_2}{s+p_2} + \cdots + \frac{k_m}{s+p_m} \quad (\text{D.38})$$

and then,

$$a(t) \approx \begin{cases} [k_1 e^{-p_1(t-\tau_{min})} + k_2 e^{-p_2(t-\tau_{min})} + \cdots + k_m e^{-p_m(t-\tau_{min})}] & \text{for } t > \tau_{min} \\ 0 & \text{for } t < \tau_{min} \end{cases} \quad (\text{D.39})$$

Similarly, $Z_c(\omega)$ is approximated by a rational function of the form:

$$Z_c(\omega) \approx \frac{(s + z_1)(s + z_2) \cdots (s + z_n)}{(s + p_1)(s + p_2) \cdots (s + p_n)} \quad (\text{D.40})$$

where $s = j\omega$, all poles and zeros are real, negative and simple, and the number of poles is the same as the number of zeros, which can be expressed as:

$$Z_c(\omega) \approx k_0 + \frac{k_1}{s + p_1} + \frac{k_2}{s + p_2} + \cdots + \frac{k_n}{s + p_n} \quad (\text{D.41})$$

and corresponds to the $R - C$ network in Figure D.4a, with:

$$R_0 = k_0 \quad (\text{D.42})$$

$$R_i = \frac{k_i}{p_i}, \quad C_i = \frac{1}{k_i}, \quad \forall i = 1, \dots, n \quad (\text{D.43})$$

For each $R - C$ block we have:

$$i(t) = \frac{v_i(t)}{R_i(t)} + C_i \frac{dv_i(t)}{dt} \quad (\text{D.44})$$

which has the exact solution:

$$v_i(t) = e^{-\frac{\Delta t}{R_i C_i}} v_i(t - \Delta t) + \frac{1}{C_i} \int_{t-\Delta t}^t e^{-\frac{(t-u)}{R_i C_i}} i(u) du \quad (\text{D.45})$$

by using linear interpolation on i , the solution takes the form:

$$v_i(t) = R_{eq-i} i(t) + e_i(t - \Delta t) \quad (\text{D.46})$$

where $e_i(t - \Delta t)$ are known from the preceding time step. After adding all $R - C$

blocks and R_0 we can rewrite (D.46) as,

$$v_l(t) = R_{eq}i(t) + e(t - \Delta t) \quad (\text{D.47})$$

with

$$R_{eq} = R_0 + \sum_{i=1}^n R_{eq-i} \quad \text{and} \quad e = \sum_{i=1}^n e_i \quad (\text{D.48})$$

which can be rewritten as:

$$i(t) = \frac{1}{R_{eq}}v(t) + I_{R-C} \quad (\text{D.49})$$

where

$$I_{R-C} = -\frac{e(t - \Delta t)}{R_{eq}} \quad (\text{D.50})$$

The equivalent resistance R_{eq} enters into matrix $[G]$ in (D.62), whereas the sum of the history terms $i_{R-C} + I_{k,h}$ enters into $[I]$.

D.2.2 Noda Frequency-Dependent Transmission Line Model

Noda et al. [1996] presented a method for *time-domain* transient calculation in which transmission lines and cables are modeled in the time domain rather than in the modal domain. The time domain convolution (presented in section D.2.1) is replaced by an Auto-Regressive Moving Average (ARMA) model (Noda 1997; Noda and Ametani 1998), further improved by an Interpolated ARMA model (IARMA). The new methodology (IARMA) offers two useful features. i) it is no longer necessary to recalculate the ARMA coefficients if the time step is changed from one simulation to another;⁸ ii) it is possible to use different time steps for different parts of the computations in order to more flexibly accommodate to the nature of the respective responses. This new technique eliminates the error produced when assuming constant

⁸In the ARMA presented by Noda et al. [1996], the ARMA coefficients had to be calculated for each different time step used.

transformation matrices, when their frequency dependence is heavy (e.g., large earth-return currents).

Equations (D.29) and (D.30) can be rewritten as:

$$\mathbf{I}_{m,k}(\omega) = \mathbf{Y}_0(\omega)\mathbf{V}_m(\omega) - e^{-j\omega\tau}\mathbf{H}^T(\omega)[\mathbf{Y}_0(\omega)\mathbf{V}_k(\omega) + \mathbf{I}_{k,m}(\omega)] \quad (\text{D.51})$$

$$\mathbf{I}_{k,m}(\omega) = \mathbf{Y}_0(\omega)\mathbf{V}_k(\omega) - e^{-j\omega\tau}\mathbf{H}^T(\omega)[\mathbf{Y}_0(\omega)\mathbf{V}_m(\omega) + \mathbf{I}_{m,k}(\omega)] \quad (\text{D.52})$$

where $\mathbf{H}(\omega) = e^{j\omega\tau}e^{-\Gamma(\omega)t}$ and it is defined as the phase-domain wave-deformation matrix, $\Gamma(\omega)$ the propagation constant matrix, τ the minimum traveling time, and \mathbf{Y}_0 the characteristic admittance matrix. Transforming (D.51) and (D.52) into the time domain, we obtain:

$$\mathbf{i}_{m,k}(t) = \mathbf{y}_0(t) * \mathbf{v}_m(t) - \mathbf{h}^T(t) * [\mathbf{y}_0(t) * \mathbf{v}_k(t - \tau) + \mathbf{i}_{k,m}(t - \tau)] \quad (\text{D.53})$$

$$\mathbf{i}_{k,m}(t) = \mathbf{y}_0(t) * \mathbf{v}_k(t) - \mathbf{h}^T(t) [\mathbf{y}_0(t) * \mathbf{v}_m(t - \tau) + \mathbf{i}_{m,k}(t - \tau)] \quad (\text{D.54})$$

Each ARMA model, which represents the frequency dependence of an element of the wave-deformation matrix or of the characteristic admittance matrix, is defined in the Z -domain as:

$$G(z) = \frac{a_0 + a_1 z^{-1} + \cdots + a_N z^{-n}}{1 + b_1 z^{-1} + \cdots + b_N z^{-n}} \quad (\text{D.55})$$

where a_n, b_n are constants and N is the order. By substituting $z = e^{j\omega\Delta t}$ the frequency response of the above ARMA model (D.55) is obtained. The time domain form of (D.55) follows from the recursive-convolution:

$$y(t) = a_0x(t) + a_1x(t - \Delta t) + \cdots + a_Nx(t - N\Delta t) - b_1y(t - \Delta t) - \cdots - b_Ny(t - N\Delta t) \quad (\text{D.56})$$

From (D.51) and (D.52), we can derive the admittance matrix, which is of the

form:

$$\mathbf{Y}(\omega) = \begin{bmatrix} \mathbf{Y}_0(\omega) \coth(\Gamma(\omega)l) & -\mathbf{Y}_0(\omega) \operatorname{cosech}(\Gamma(\omega)l) \\ -\mathbf{Y}_0(\omega) \operatorname{cosech}(\Gamma(\omega)l) & \mathbf{Y}_0(\omega) \coth(\Gamma(\omega)l) \end{bmatrix} \quad (\text{D.57})$$

The above matrix-hyperbolic functions can be decomposed into matrix-exponential functions as follows:

$$\coth(\Gamma(\omega)l) = [e^{\Gamma(\omega)l} + e^{-\Gamma(\omega)l}] \cdot [e^{\Gamma(\omega)l} - e^{-\Gamma(\omega)l}]^{-1} \quad (\text{D.58})$$

$$\operatorname{cosech}(\Gamma(\omega)l) = 2 [e^{\Gamma(\omega)l} - e^{-\Gamma(\omega)l}] \quad (\text{D.59})$$

The above matrix-exponential functions can be obtained from the phase-domain wave-deformation matrix $\mathbf{H}(\omega)$ as:

$$e^{-\Gamma(\omega)l} = e^{-j\omega\tau} \mathbf{H}(\omega), \quad e^{\Gamma(\omega)l} = [e^{-\Gamma(\omega)l}]^{-1} \quad (\text{D.60})$$

Each element of the phase-domain wave-deformation matrix $\mathbf{H}(\omega)$ and of the characteristic admittance matrix $\mathbf{Y}_0(\omega)$ can be evaluated by the frequency response of the corresponding ARMA model using (D.55). Once $\mathbf{H}(\omega)$ is known, $e^{-\Gamma(\omega)l}$ and $e^{\Gamma(\omega)l}$ are calculated by (D.60), and then $\coth(\Gamma(\omega)l)$ and $\operatorname{cosech}(\Gamma(\omega)l)$ can also be calculated by (D.58) and (D.59), respectively. We found all the unknown in (D.57), so the admittance matrix is now defined.

The modeling of a transmission line (overhead lines and cables) using the NODA SETUP (available as a subroutine in the EMTP) requires the following two steps:⁹

1. Calculation of the frequency-dependent line constants of the transmission line, referred to as “frequency data”. This is done using either the CABLE PARAMETERS or the LINE CONSTANTS supporting subroutines in EMTP (note that CABLE CONSTANTS cannot be used to obtain this response).

⁹Noda [1997] describes how to implement an ARMA model in the EMTP.

2. Fitting the frequency data with IARMA models for the time-domain realization of the frequency dependence. This procedure is performed by an independent fitting program ARMAFIT.

D.3 Type 1 Source

Data can be used as an external source in the EMTP using the Type 1 (user defined) current source. The user has to specify the value of the external source at each time step (Alternative Transient Program (ATP) Rule Book [1987-1998]) and this can be done in three different ways:

- ① By including point-by-point the source data in the datacase,
- ② By using the \$INCLUDE command, or
- ③ By using the \$INSERT command

The technique in ① (where each point represents a punched card) was the first approach to use the Type 1 source. This technique is implemented as follows (using data sorting by card):

| |
|---|
| ————— ① point-by-point ————— |
| <pre>/SOURCE C < n 1><>< Ampl. >< Freq. ><Phase/T0>< A1 >< T1 >< TSTART >< TSTOP > 1SOURCE-1 /PLOT C Next come the data cards for user-defined Type-1 source on node "SOURCE": C-E8.0-> 3.4 .8485282 0.0 -.434314 -.2 -.848528 -.4 -1.56569 3.41 .8500000 0.0 -.430000 -.2 9999</pre> |

The input datacards are terminated with a 9999-card. To avoid the difficulty of providing all these points in the datacase, the technique in ② was provided. In this case, it is allowed to store the data in a separate file as follows:

```
② $INCLUDE _____
/SOURCE
C < n 1><>< Ampl. >< Freq. ><Phase/T0>< A1 >< T1 >< TSTART >< TSTOP >
1SOURCE-1
/PLOT
$INCLUDE, source.txt
```

Here, all the data points of the source are stored in the file `source.txt`, and included in the simulation by the `$INCLUDE` command. Although the technique in ② is obviously better than ①, still presents some problems when the Δt is small and the simulation time is relatively large. The problem is that each data-point of the source is seen by ATP as a **branch card**, therefore for voluminous cases, a burden on LIMCRD¹⁰ cannot be avoided. To overcome this problem, the more recent technique ③ was provided avoiding the burden on LIMCRD. The usage is similar to ②:

```
③ $INSERT _____
/SOURCE
C < n 1><>< Ampl. >< Freq. ><Phase/T0>< A1 >< T1 >< TSTART >< TSTOP >
1SOURCE-1
/PLOT
$INSERT, source.txt
```

D.4 EMTP Algorithm

The combination of elements, for which the state variable equations have been derived previously, is then solved by the equality:

$$\sum_{j=1}^n i_{k,j}(t) = i_k(t) \quad (\text{D.61})$$

¹⁰LIMCRD is a variable of ATP that defines the number of 80-column card images that can be stored in the cache of LUNT10 (see Alternative Transient Program (ATP) Rule Book [1987-1998], Section I-E-1).

where n is the number of branches connected to node k , $i_{k,j}(t)$ are the branch currents flowing away from the node, and $i_k(t)$ is the current injected into the node.

By writing the equations for each node of the network, we obtain a system of equations that can be expressed in matrix form as follows:

$$[G][v(t)] = [i(t)] - [I] \quad (\text{D.62})$$

where $[G]$ is the nodal conductance matrix,¹¹ $[v(t)]$ a column matrix of node voltages at time t , $[i(t)]$ a column matrix of current sources, and $[I]$ a column matrix of past history terms. In (D.62) some of the voltages will be known, so we can reformulate (D.62) by identifying known and unknown voltages. Let A be the subset of unknown voltages, and B the subset of known voltages, then we can write:

$$\begin{bmatrix} [G_{AA}] & [G_{AB}] \\ [G_{BA}] & [G_{BB}] \end{bmatrix} \begin{bmatrix} [v_A(t)] \\ [v_B(t)] \end{bmatrix} = \begin{bmatrix} [i_A(t)] \\ [i_B(t)] \end{bmatrix} - \begin{bmatrix} [I_A] \\ [I_B] \end{bmatrix} \quad (\text{D.63})$$

from which the unknown $[v_A(t)]$ is found by solving:

$$[G_{AA}][v_A(t)] = [I_{total}] - [G_{AB}][v_B(t)] \quad (\text{D.64})$$

where

$$[I_{total}] = [i(t)] - [I] \quad (\text{D.65})$$

Now, (D.64) represents a linear system of equations that needs to be solved for each time step, with a constant coefficient matrix $[G_{AA}]$, provided that Δt does not change.

¹¹ $[G]$ depends on Δt , therefore, $[G]$ remains unchanged for a constant Δt . From here we see why the EMT formulation works with a fixed time step.

APPENDIX E ATP FILES

E.1 Transmission Line Models

The following file (`hor_24m.atp`) represents the J. Marti source file of a 24-m long horizontal distribution line section (Section 5.2).

```
BEGIN NEW DATA CASE
JMARTI SETUP, 1.0,
$ERASE
BRANCH NOD001NOD002NOD003NOD004NOD005NOD006NOD007NOD008
LINE CONSTANTS
METRIC
C   1       2       3       4       5       6       7       8
C 3456789012345678901234567890123456789012345678901234567890
  1 0.50.995437 4      0.74168    -1.3  7.7756  7.4708
  2 0.50.995437 4      0.74168  0.5334  7.7756  7.4708
  3 0.50.995437 4      0.74168    1.3  7.7756  7.4708
  4 0.50.626342 4      0.93472    -0.2   6.2  5.8952
BLANK
  4000      5000          0.024
  4000      60            0.024
  4000      0.01          0.024      11 30   1
BLANK
BLANK
DEFAULT
$PUNCH
BLANK
BEGIN NEW DATA CASE
BLANK
```

The following file (`hor_24m.mod.bak`) is the DBM source derived from the output when running the input DBM file `hor_24m.atp` with ATP.

The following file (`hor_24m_mod.pch`) is the DBM file obtained when running the input DBM file `hor_24m.mod.bak` with ATP.

```
KARD 3 3 38 38 59 59 82 82
KARG 1 5 2 6 3 7 4 8
KBEG 3 9 3 9 3 9 3 9
KEND 8 14 8 14 8 14 8 14
KTEX 1 1 1 1 1 1 1 1
```


| | | |
|------------------------------|--------------------------|--------------------------|
| 1.74371846971240401E+08 | 2.68375000310310960E+08 | 4.68372111611106336E+08 |
| 1.01263238509060848E+09 | 5.45516541066744804E+09 | 5.46062057607812214E+09 |
| 1.98120594835723090E+09 | 1.98318715430559087E+09 | |
| -2NOD003NOD004 | 2. 1.00 | -2 4 |
| 19 3.1794031725508995123E+02 | | |
| 3.15607970730197530E+03 | 1.94879158862814916E+03 | 5.43380752755809226E+03 |
| 6.97682200397618453E+03 | 1.33266408526604682E+04 | 2.12842618698240403E+04 |
| 4.62799607795456250E+04 | 1.64739101976579659E+04 | 1.87023577624849895E+04 |
| 3.70430663930402670E+03 | 8.28077714319918960E+03 | 2.13760279037361443E+03 |
| 5.32895056708368429E+03 | 7.16284611050733201E+03 | 6.57962750093027717E+04 |
| 6.20930940876676977E+04 | 8.27570622254096961E+04 | 2.77385770699778979E+05 |
| 3.65922629665503511E+06 | | |
| 1.99108985490782597E-01 | 4.87886879667485451E-01 | 1.71036703997812434E+00 |
| 4.79759309596061190E+00 | 1.47969805728296055E+01 | 4.399278555533675542E+01 |
| 1.46382068482144206E+02 | 3.19539986078008610E+02 | 5.92815463962570448E+02 |
| 7.28838286797111209E+02 | 1.22567296506384127E+03 | 2.05645600245236301E+03 |
| 4.38195169708782487E+03 | 5.83892379089185124E+03 | 4.54648726306343597E+04 |
| 4.84349240903484315E+04 | 6.34027670323235507E+04 | 2.07623590530591522E+05 |
| 2.73739621033982839E+06 | | |
| 4 8.0050982808653455107E-08 | | |
| 6.18296814734505606E+05 | 5.99617626048557181E+06 | -4.18585249062934935E+08 |
| 3.31773791863241310E+10 | | |
| 1.05819711721886113E+08 | 1.00230537490362525E+09 | 6.14396473493853073E+10 |
| 3.33445431412512207E+10 | | |
| -3NOD005NOD006 | 2. 1.00 | -2 4 |
| 23 3.9002171807055714225E+02 | | |
| 1.60183152548428870E+03 | -8.98855529521741488E+02 | 2.88388481106641530E+03 |
| 8.77445474565119071E+02 | 2.76376542366027206E+03 | 1.37454877951757089E+03 |
| 3.27682153028026187E+03 | 6.94630804064017593E+03 | 1.34126196036662659E+04 |
| 2.33257023199414180E+04 | 2.61956159664300430E+04 | 1.55470397172414432E+04 |
| 1.82715163268674587E+04 | 1.34766907845318801E+04 | 3.45899917906921200E+03 |
| 7.56373727039505229E+03 | 3.93727313755579962E+03 | 4.58531113001884023E+03 |
| 7.81879555569614422E+03 | 1.10428725278386381E+05 | 1.09711469935225803E+05 |
| 2.23868443901593360E+05 | 8.14336827966271248E+06 | |
| 1.96336466802315118E-01 | 3.23841814313557741E-01 | 2.77057292569864999E-01 |
| 4.65553782331707022E-01 | 9.40128952703652598E-01 | 1.40463101636378984E+00 |
| 2.57806523615750427E+00 | 4.80614878812141466E+00 | 1.40959292198398813E+01 |
| 4.14248731444735796E+01 | 1.11825182427167377E+02 | 1.70462082874339671E+02 |
| 2.75846468532180950E+02 | 4.55239892738618515E+02 | 5.62292295239123973E+02 |
| 9.54977207497965765E+02 | 1.61566599804920156E+03 | 3.26352242730790749E+03 |
| 5.35042493696821293E+03 | 7.2754066550656018E+04 | 6.63845507849434362E+04 |
| 1.43286407634684991E+05 | 5.18418912591000646E+06 | |
| 6 8.0028703992187345047E-08 | | |
| 1.23300281651602662E+06 | 3.08863152368968702E+05 | 1.44056246021475829E+06 |
| 1.44620683658332867E+06 | -3.47383127036881089E+08 | 1.51900155280827942E+10 |
| 2.74938232773324430E+08 | 7.13311112102724761E+07 | 3.24369984602372408E+08 |
| 3.53603910246453822E+08 | 6.03028140298551712E+10 | 1.53680678778688927E+10 |
| -4NOD007NOD008 | 2. 1.00 | -2 4 |
| 15 3.8352720722489414129E+02 | | |
| 2.83882218979119762E+03 | 2.10459369419458926E+03 | 4.54555491994203476E+03 |
| 5.94609983519814068E+03 | 1.07359158522041853E+04 | 1.73639930504231634E+04 |
| 2.92600910667632488E+04 | 2.60840718542476825E+04 | -8.21832116589013822E+02 |
| 4.61131778833116823E+03 | 6.03083445885868241E+03 | 3.10129318226044597E+03 |
| 7.09188067249425603E+03 | 1.41869116516879585E+05 | 1.68186931916195480E+06 |

```

2.15875094479622026E-01 5.32028296757342978E-01 1.63535190085242110E+00
4.32660719403835436E+00 1.23406489516505040E+01 3.46060764934525125E+01
9.90279178850874757E+01 2.46972471531934474E+02 3.15141934633042297E+02
4.62260073138035807E+02 7.76473197766807289E+02 1.30924091924136496E+03
2.65396705438153685E+03 4.67415151349192747E+04 5.56963666712381179E+05
       6     8.0045180970380522976E-08
9.33244359427184099E+05 2.27687567160125729E+06 6.04426095844756463E+05
7.40325012354510929E+06 1.98433356841445826E+07 2.04629452051763458E+10
2.18478034546405643E+08 5.17387153160408020E+08 1.39825084705543011E+08
1.69747326045622039E+09 1.11972096231173468E+09 2.12068558816705017E+10
0.51428331 -0.09487501 0.86282714 0.04589618
0.00000000 0.00000000 0.00000000 0.00000000
0.41079736 0.75544939 -0.20267474 0.37013319
0.00000000 0.00000000 0.00000000 0.00000000
0.46933938 -0.64820438 -0.35411723 0.43048047
0.00000000 0.00000000 0.00000000 0.00000000
0.58862446 -0.01122664 -0.29841795 -0.82193767
0.00000000 0.00000000 0.00000000 0.00000000
$EOF User-supplied header cards follow.      26-May-00 08:15:44
ARG,NODO01,NODO03,NODO05,NODO07,NODO02,NODO04,NODO06,NODO08

```

E.2 Arresters Equivalent Circuits

The following file (pdv100_18kV.mod) represents the input DBM file for the Ohio Brass PDV 100, 18 kV rated arrester (Section 3.2.2), using the circuit model proposed by Pinceti and Giannettoni [1999] (Section 5.3).

```

BEGIN NEW DATA CASE --NOSORT--
DATA BASE MODULE
$ERASE
ARG,NODO01,NODO04
DUM,NODO02,NODO03
/BRANCH
C
C
C           -----
C           | Carlos T. Mata |
C           -----
C This file was created on 25-Sep-2000, using the m-file dbm_arrester_create.m
C this arrester model consists of two non-linear sections,
C two inductors, and a resistor
C This is the simplified arrester model presented by Pinceti 1999
C
C The parameters are:
C   Rated Voltage:                                18.00 kV
C   Residual Voltage at 10kA with an 8/20 us waveform: 60.00 kV
C   Residual Voltage at 10kA for fast current surge: 68.00 kV
C
C   1          2          3          4          5          6          7          8
C 34567890123456789012345678901234567890123456789012345678901234567890
C <++++++> Cards punched by support routine on 25-Sep-00 17:32:54 <++++++>
C ZNO FITTER

```



```

3.600000000000000E+04 -1.000000000000000E+02
C Multiplier Exponent V-min
3.5375497595143481E-04 4.6051099956965686E+01 1.1135073155700943E+00
1.2948494800517163E-01 2.4395197598527446E+01 1.3133333333333315E+00
1.6063962621533618E+00 1.7532824224878791E+01 1.443333333333322E+00
9.6795765772248696E+00 1.3352284768216220E+01 1.5366666666666635E+00
9.9409255430853591E+01 8.8711523235028054E+00 1.6816666666666644E+00
9999

$VINTAGE, 1
NOD001NOD002 2.0000000000E-04
NOD002NOD003 6.0000000000E-04
NOD001NOD004 1.0000000000E+06

$VINTAGE, 0
BEGIN NEW DATA CASE
C
$PUNCH
BEGIN NEW DATA CASE
BLANK

```

The following file (`pdv100_18kV_mod.pch`) is the DBM obtained when running the input DBM file `pdv100_18kV.mod` with ATP.

C C NEXP IPHASE ERRRLIM IPRZNO VREF VFLASH
C -1 1 .05 33.600000E+04 0
C C
C C A1 A2 A3 A4 A5 AMIN
C 1.800000E+041.800000E+041.000000E+001.000000E+001.000000E+005.000000E-02
C 2.000000E-034.860000E+04
C 1.000000E+025.844000E+04
C 1.000000E+036.312000E+04
C 3.000000E+036.648000E+04
C 1.000000E+047.170000E+04
C 2.000000E+047.662000E+04
C C Current[A] Voltage[V]
C BLANK card bounds points of the ZnO characteristic
C Rating = 18000.0 V-mult = 1.00000E+00 I-mult = 1.00000E+00 Gapless
92NOD002NOD004 5555.
C V-reference V-flashover
3.600000000000000000E+04 -1.000000000000000000E+02
C Multiplier Exponent V-min
4.4943609061957635E-11 5.8682888861267138E+01 1.4261187973444669E+00
5.1411446202049274E-05 2.9889305311276594E+01 1.623333333333322E+00
6.8276845252587858E-03 2.1182774768718719E+01 1.753333333333312E+00
1.7145476159231318E-01 1.5927757934680342E+01 1.84666666666666656E+00
7.4981403473683930E+00 1.0444092545305748E+01 1.99166666666666638E+00
9999
C <++++++> Cards punched by support routine on 25-Sep-00 17:32:55 <++++++>
C ZNO FITTER
C \$ERASE
C BRANCH NOD003NOD004
C C
C C 1 2 3 4 5 6 7
C C 3456789012345678901234567890123456789012345678901234567890123456789012345678
C C
C C NEXP IPHASE ERRRLIM IPRZNO VREF VFLASH
C -1 1 .05 33.600000E+04 0
C C
C C A1 A2 A3 A4 A5 AMIN
C 1.800000E+041.800000E+041.000000E+001.000000E+001.000000E+005.000000E-02
C 2.000000E-033.738000E+04
C 1.000000E+024.728000E+04
C 1.000000E+035.196000E+04
C 3.000000E+035.532000E+04
C 1.000000E+046.054000E+04
C 2.000000E+046.546000E+04
C C Current[A] Voltage[V]
C BLANK card bounds points of the ZnO characteristic
C Rating = 18000.0 V-mult = 1.00000E+00 I-mult = 1.00000E+00 Gapless
92NOD003NOD004 5555.
C V-reference V-flashover
3.600000000000000000E+04 -1.000000000000000000E+02
C Multiplier Exponent V-min
3.5375497595143481E-04 4.6051099956965686E+01 1.1135073155700943E+00
1.2948494800517163E-01 2.4395197598527446E+01 1.3133333333333315E+00
1.6063962621533618E+00 1.7532824224878791E+01 1.4433333333333322E+00
9.6795765772248696E+00 1.3352284768216220E+01 1.53666666666666635E+00

```

9.9409255430853591E+01 8.8711523235028054E+00 1.681666666666644E+00
9999
$VINTAGE, 1
NOD001NOD002 2.0000000000E-04
NOD002NOD003 6.0000000000E-04
NOD001NOD004 1.0000000000E+06
$VINTAGE, 0
$EOF User-supplied header cards follow. 25-Sep-00 17:32:55
ARG,NOD001,NOD004
DUM,NOD002,NOD003

```

The following file (`ultrasil_18kV.mod`) represents the input DBM file for the Ohio Brass PDV 100, 18 kV rated arrester (Section 3.2.2), using the circuit model proposed by Pinceti and Giannettoni [1999] (Section 5.3).

```

BEGIN NEW DATA CASE --NOSORT--
DATA BASE MODULE
$ERASE
ARG,NOD001,NOD004
DUM,NOD002,NOD003
/BRANCH
C
C -----
C | Carlos T. Mata |
C -----
C This file was created on 25-Sep-2000, using the m-file dbm_arrester_create.m
C this arrester model consists of two non-linear sections,
C two inductors, and a resistor
C This is the simplified arrester model presented by Pinceti 1999
C
C The parameters are:
C   Rated Voltage: 18.00 kV
C   Residual Voltage at 10kA with an 8/20 us waveform: 58.80 kV
C   Residual Voltage at 10kA for fast current surge: 64.90 kV
C
C   1      2      3      4      5      6      7      8
C 34567890123456789012345678901234567890123456789012345678901234567890
C <+++++> Cards punched by support routine on 25-Sep-00 17:32:52 <+++++>
C ZNO FITTER
C $ERASE
C BRANCH NOD002NOD004
C C
C   1      2      3      4      5      6      7
C 34567890123456789012345678901234567890123456789012345678901234567890
C C
C   NEXP    IPHASE    ERRLIM    IPRZNO      VREF      VFLASH
C   -1        1       .05     33.600000E+04        0
C C
C   A1      A2      A3      A4      A5      AMIN
C 1.800000E+041.800000E+041.000000E+001.000000E+001.000000E+005.000000E-02
C 2.000000E-034.762800E+04
C 1.000000E+025.727120E+04
C 1.000000E+036.185760E+04

```



```
C
$PUNCH
BEGIN NEW DATA CASE
BLANK
```

The following file (ultrasil_18kV_mod.pch) is the DBM obtained when running the input DBM file ultrasil_18kV.mod with ATP.

```
KARD 3 3 11 11 20 20 21 21 22 22
KARG 2 -1 2 -2 1 -1 -1 -2 1 2
KBEG 9 3 9 3 3 9 3 9 3 9
KEND 14 8 14 8 8 14 8 14 8 14
KTEX 1 1 1 1 1 1 1 1 1 1
$ERASE
/BRANCH
C
C
-----+
C | Carlos T. Mata |
C -----
C This file was created on 25-Sep-2000, using the m-file dbm_arrester_create.m
C this arrester model consists of two non-linear sections,
C two inductors, and a resistor
C This is the simplified arrester model presented by Pinceti 1999
C
C The parameters are:
C   Rated Voltage: 18.00 kV
C   Residual Voltage at 10kA with an 8/20 us waveform: 58.80 kV
C   Residual Voltage at 10kA for fast current surge: 64.90 kV
C
C      1      2      3      4      5      6      7      8
C 34567890123456789012345678901234567890123456789012345678901234567890
C <++++++> Cards punched by support routine on 25-Sep-00 17:32:52 <++++++>
C ZNO FITTER
C $ERASE
C BRANCH NOD002NOD004
C C
C C      1      2      3      4      5      6      7
C C 34567890123456789012345678901234567890123456789012345678901234567890
C C
C C     NEXP     IPHASE     ERRLLIM     IPRZNO      VREF      VFLASH
C C      -1          1        .05       33.60000E+04         0
C C
C C     A1        A2        A3        A4        A5      AMIN
C C 1.800000E+041.800000E+041.000000E+001.000000E+001.000000E+005.000000E-02
C C 2.000000E-034.762800E+04
C C 1.000000E+025.727120E+04
C C 1.000000E+036.185760E+04
C C 3.000000E+036.515040E+04
C C 1.000000E+047.026600E+04
C C 2.000000E+047.508760E+04
C C Current[A] Voltage[V]
C BLANK card bounds points of the ZnO characteristic
C Rating = 18000.0  V-mult = 1.00000E+00  I-mult = 1.00000E+00  Gapless
```

```

92NOD002NOD004          5555.
C   V-reference           V-flashover
  3.60000000000000E+04 -1.00000000000000E+02
C   Multiplier           Exponent           V-min
  1.4707781496119149E-10 5.8682888861267180E+01 1.3975964213975776E+00
  9.4038636418739102E-05 2.9889305311276292E+01 1.5908666666666655E+00
  1.0474408533101682E-02 2.1182774768719170E+01 1.7182666666666644E+00
  2.3653667804667192E-01 1.5927757934680596E+01 1.8097333333333250E+00
  9.2595363851151831E+00 1.0444092545305573E+01 1.9518333333333291E+00
  9999

C <++++++> Cards punched by support routine on 25-Sep-00 17:32:52 <++++++>
C ZNO FITTER
C $ERASE
C BRANCH NOD003NOD004
C C
C C      1       2       3       4       5       6       7
C C 3456789012345678901234567890123456789012345678901234567890123456789012345678
C C
C C      NEXP     IPHASE    ERRLLIM    IPRZNO      VREF      VFLASH
C C      -1        1        .05       33.600000E+04      0
C C
C C      A1       A2       A3       A4       A5       AMIN
C C 1.800000E+041.800000E+041.000000E+001.000000E+001.000000E+005.000000E-02
C 2.000000E-033.663240E+04
C 1.000000E+024.633440E+04
C 1.000000E+035.092080E+04
C 3.000000E+035.421360E+04
C 1.000000E+045.932920E+04
C 2.000000E+046.415080E+04
C C Current[A] Voltage[V]
C BLANK card bounds points of the ZnO characteristic
C Rating = 18000.0  V-mult = 1.00000E+00  I-mult = 1.00000E+000  Gapless
92NOD003NOD004          5555.
C   V-reference           V-flashover
  3.60000000000000E+04 -1.00000000000000E+02
C   Multiplier           Exponent           V-min
  8.9691527981611947E-04 4.6051099956965686E+01 1.0912371692586924E+00
  2.1196341304458191E-01 2.4395197598527432E+01 1.2870666666666648E+00
  2.2892032698446565E+00 1.7532824224878784E+01 1.4144666666666657E+00
  1.2676760806857976E+01 1.3352284768216181E+01 1.5059333333333309E+00
  1.1892184543214533E+02 8.8711523235028178E+00 1.6480333333333312E+00
  9999

$VINTAGE, 1
  NOD001NOD002          1.5561224490E-04
  NOD002NOD003          4.6683673469E-04
  NOD001NOD004          1.0000000000E+06
$VINTAGE, 0
$EOF User-supplied header cards follow.          25-Sep-00 17:32:53
ARG,NOD001,NOD004
DUM,NOD002,NOD003

```

E.3 Leads Connecting the Neutral to Ground Rods

The following file (`leads_20_6m.mod`) represents the input DBM file for a down-lead of 20 sections (Section 5.4).

```
BEGIN NEW DATA CASE --NOSORT--
DATA BASE MODULE
$ERASE
ARG,NOD001,NOD021
DUM,NOD002,NOD003,NOD004,NOD005,NOD006,NOD007,NOD008,NOD009,NOD010,NOD011
DUM,NOD012,NOD013,NOD014,NOD015,NOD016,NOD017,NOD018,NOD019,NOD020
/BRANCH
$VINTAGE, 1
C
C This file was created on 05-Apr-2000, using the m-file dbm_leads_create.m
C this down lead model consists of:
C    number of sections          = 20
C    length of                   = 6 meters
C    radius of                   = 4.80000e+00 mm
C The formulas to calculate these parameters were taken
C from Bazelyan [1978]
C
C      1      2      3      4      5      6      7      8
C 34567890123456789012345678901234567890123456789012345678901234567890
NOD001NOD002          0.00046792369217
NOD002                  0.00000213904839
NOD002NOD003          0.00046476506816
NOD003                  0.00000215358573
NOD003NOD004          0.00046143087709
NOD004                  0.00000216914704
NOD004NOD005          0.00045790044709
NOD005                  0.00000218587124
NOD005NOD006          0.00045414922567
NOD006                  0.00000220392629
NOD006NOD007          0.00045014774320
NOD007                  0.00000222351758
NOD007NOD008          0.00044586020536
NOD008                  0.00000224489965
NOD008NOD009          0.00044124254290
NOD009                  0.00000226839283
NOD009NOD010          0.00043623964636
NOD010                  0.00000229440728
NOD010NOD011          0.00043078133967
NOD011                  0.00000232347905
NOD011NOD012          0.00042477633215
NOD012                  0.00000235632577
NOD012NOD013          0.00041810279405
NOD013                  0.00000239393621
NOD013NOD014          0.00041059300547
NOD014                  0.00000243772155
NOD014NOD015          0.00040200695485
NOD015                  0.00000248978633
NOD015NOD016          0.00039198370977
```

```

NODO16                               0.00000255345157
NODO16NODO017                         0.00037994346804
NODO17                               0.00000263436933
NODO17NODO18                         0.00036486460235
NODO18                               0.00000274324068
NODO18NODO19                         0.00034467626815
NODO19                               0.00000290391742
NODO19NODO20                         0.00031402673072
NODO20                               0.00000318734465
NODO20NODO21                         0.00024810999340
NODO21                               0.00000403414391

$VINTAGE, 0
BEGIN NEW DATA CASE
C
$PUNCH
BEGIN NEW DATA CASE
BLANK

```

The following file (leads_20_6m_mod.pch) is the DBM obtained when running the input DBM file leads_20_6m.mod with ATP.

```

KARD  4   4   5   6   6   7   8   8   9   10  10  11  12  12  13  14  14  15  16  16  17  18  18  19  20
      20  21  22  22  23  24  24  25  26  26  27  28  28  29  30  30  31  32  32  33  34  34  35  36  36
      37  38  38  39  40  40  41  41  42  42  43
KARG  1   -1  -1  -2  -2  -3  -3  -3  -4  -4  -4  -4  -5  -5  -5  -6  -6  -6  -7  -7  -7  -8  -8  -8
      -9  -9  -9-10-10-10-11-11-11-12-12-12-13-13-13-14-14-14-15-15-15-16-16-17
      -17-17-18-18-18-19-19  2-19  2
KBEG  3   9   3   3   9   3   3   9   3   3   9   3   3   9   3   3   9   3   3   9   3   3   9   3   3
      9   3   3   9   3   3   9   3   3   9   3   3   9   3   3   9   3   3   9   3   3   9   3   3   9
      3   3   9   3   3   9   3   3   9   3   3
KEND  8   14  8   8  14  8   8  14  8   8  14  8   8  14  8   8  14  8   8  14  8   8  14  8   8  14
      14  8   8  14  8   8  14  8   8  14  8   8  14  8   8  14  8   8  14  8   8  14  8   8  14
      8   8  14  8   8  14  8   8  14  8
KTEX  1   1   1   1   1   1   1   1   1   1   1   1   1   1   1   1   1   1   1   1   1   1   1   1   1   1
      1   1   1   1   1   1   1   1   1   1   1   1   1   1   1   1   1   1   1   1   1   1   1   1   1   1
      1   1   1   1   1   1   1   1   1   1
$ERASE
/BRANCH
$VINTAGE, 1
C
C This file was created on 05-Apr-2000, using the m-file dbm_leads_create.m
C this down lead model consists of:
C   number of sections          = 20
C   length of                  = 6 meters
C   radius of                  = 4.80000e+00 mm
C The formulas to calculate these parameters were taken
C from Bazelyan [1978]
C
C           1           2           3           4           5           6           7           8
C 3456789012345678901234567890123456789012345678901234567890123456789012345678901234567890
NODO01NODO02                         0.00046792369217
NODO02                               0.00000213904839
NODO02NODO03                         0.00046476506816

```

| | |
|---|--------------------|
| NOD003 | 0.00000215358573 |
| NOD003NOD004 | 0.00046143087709 |
| NOD004 | 0.00000216914704 |
| NOD004NOD005 | 0.00045790044709 |
| NOD005 | 0.00000218587124 |
| NOD005NOD006 | 0.00045414922567 |
| NOD006 | 0.00000220392629 |
| NOD006NOD007 | 0.00045014774320 |
| NOD007 | 0.00000222351758 |
| NOD007NOD008 | 0.00044586020536 |
| NOD008 | 0.00000224489965 |
| NOD008NOD009 | 0.00044124254290 |
| NOD009 | 0.00000226839283 |
| NOD009NOD010 | 0.00043623964636 |
| NOD010 | 0.00000229440728 |
| NOD010NOD011 | 0.00043078133967 |
| NOD011 | 0.00000232347905 |
| NOD011NOD012 | 0.00042477633215 |
| NOD012 | 0.00000235632577 |
| NOD012NOD013 | 0.00041810279405 |
| NOD013 | 0.00000239393621 |
| NOD013NOD014 | 0.00041059300547 |
| NOD014 | 0.00000243772155 |
| NOD014NOD015 | 0.00040200695485 |
| NOD015 | 0.00000248978633 |
| NOD015NOD016 | 0.00039198370977 |
| NOD016 | 0.00000255345157 |
| NOD016NOD017 | 0.00037994346804 |
| NOD017 | 0.00000263436933 |
| NOD017NOD018 | 0.00036486460235 |
| NOD018 | 0.00000274324068 |
| NOD018NOD019 | 0.00034467626815 |
| NOD019 | 0.00000290391742 |
| NOD019NOD020 | 0.00031402673072 |
| NOD020 | 0.00000318734465 |
| NOD020NOD021 | 0.00024810999340 |
| NOD021 | 0.00000403414391 |
| \$VINTAGE, 0 | |
| \$EOF User-supplied header cards follow. | 05-Apr-00 17:27:24 |
| ARG,NOD001,NOD021 | |
| DUM,NOD002,NOD003,NOD004,NOD005,NOD006,NOD007,NOD008,NOD009,NOD010,NOD011 | |
| DUM,NOD012,NOD013,NOD014,NOD015,NOD016,NOD017,NOD018,NOD019,NOD020 | |

E.4 Ground Rods

The following file (rod_50.mod) represents the input DBM file for a grounding rod of 50 sections (Section 5.5).

```
BEGIN NEW DATA CASE --NOSORT--
DATA BASE MODULE
$ERASE
```


| | | |
|--------------|-----------------|------------------|
| NOD014 | | CAPACITANCE_____ |
| NOD014NOD015 | INDUCTANCE_____ | |
| NOD015 | RESISTANCE_____ | CAPACITANCE_____ |
| | | INDUCTANCE_____ |
| NOD015NOD016 | | |
| NOD016 | RESISTANCE_____ | CAPACITANCE_____ |
| | | INDUCTANCE_____ |
| NOD016NOD017 | | |
| NOD017 | RESISTANCE_____ | CAPACITANCE_____ |
| | | INDUCTANCE_____ |
| NOD017NOD018 | | |
| NOD018 | RESISTANCE_____ | CAPACITANCE_____ |
| | | INDUCTANCE_____ |
| NOD018NOD019 | | |
| NOD019 | RESISTANCE_____ | CAPACITANCE_____ |
| | | INDUCTANCE_____ |
| NOD019NOD020 | | |
| NOD020 | RESISTANCE_____ | CAPACITANCE_____ |
| | | INDUCTANCE_____ |
| NOD020NOD021 | | |
| NOD021 | RESISTANCE_____ | CAPACITANCE_____ |
| | | INDUCTANCE_____ |
| NOD021NOD022 | | |
| NOD022 | RESISTANCE_____ | CAPACITANCE_____ |
| | | INDUCTANCE_____ |
| NOD022NOD023 | | |
| NOD023 | RESISTANCE_____ | CAPACITANCE_____ |
| | | INDUCTANCE_____ |
| NOD023NOD024 | | |
| NOD024 | RESISTANCE_____ | CAPACITANCE_____ |
| | | INDUCTANCE_____ |
| NOD024NOD025 | | |
| NOD025 | RESISTANCE_____ | CAPACITANCE_____ |
| | | INDUCTANCE_____ |
| NOD025NOD026 | | |
| NOD026 | RESISTANCE_____ | CAPACITANCE_____ |
| | | INDUCTANCE_____ |
| NOD026NOD027 | | |
| NOD027 | RESISTANCE_____ | CAPACITANCE_____ |
| | | INDUCTANCE_____ |
| NOD027NOD028 | | |
| NOD028 | RESISTANCE_____ | CAPACITANCE_____ |
| | | INDUCTANCE_____ |
| NOD028NOD029 | | |
| NOD029 | RESISTANCE_____ | CAPACITANCE_____ |
| | | INDUCTANCE_____ |
| NOD029NOD030 | | |
| NOD030 | RESISTANCE_____ | CAPACITANCE_____ |
| | | INDUCTANCE_____ |
| NOD030NOD031 | | |
| NOD031 | RESISTANCE_____ | CAPACITANCE_____ |
| | | INDUCTANCE_____ |
| NOD031NOD032 | | |
| NOD032 | RESISTANCE_____ | CAPACITANCE_____ |

| | | |
|--------------|-----------------|------------------|
| NOD032 | | CAPACITANCE_____ |
| NOD032NOD033 | INDUCTANCE_____ | |
| NOD033 | RESISTANCE_____ | CAPACITANCE_____ |
| | | INDUCTANCE_____ |
| NOD033 | RESISTANCE_____ | CAPACITANCE_____ |
| NOD033NOD034 | INDUCTANCE_____ | |
| NOD034 | RESISTANCE_____ | CAPACITANCE_____ |
| | | INDUCTANCE_____ |
| NOD034 | RESISTANCE_____ | CAPACITANCE_____ |
| NOD034NOD035 | INDUCTANCE_____ | |
| NOD035 | RESISTANCE_____ | CAPACITANCE_____ |
| | | INDUCTANCE_____ |
| NOD035 | RESISTANCE_____ | CAPACITANCE_____ |
| NOD035NOD036 | INDUCTANCE_____ | |
| NOD036 | RESISTANCE_____ | CAPACITANCE_____ |
| | | INDUCTANCE_____ |
| NOD036 | RESISTANCE_____ | CAPACITANCE_____ |
| NOD036NOD037 | INDUCTANCE_____ | |
| NOD037 | RESISTANCE_____ | CAPACITANCE_____ |
| | | INDUCTANCE_____ |
| NOD037 | RESISTANCE_____ | CAPACITANCE_____ |
| NOD037NOD038 | INDUCTANCE_____ | |
| NOD038 | RESISTANCE_____ | CAPACITANCE_____ |
| | | INDUCTANCE_____ |
| NOD038 | RESISTANCE_____ | CAPACITANCE_____ |
| NOD038NOD039 | INDUCTANCE_____ | |
| NOD039 | RESISTANCE_____ | CAPACITANCE_____ |
| | | INDUCTANCE_____ |
| NOD039NOD040 | RESISTANCE_____ | CAPACITANCE_____ |
| NOD040 | | CAPACITANCE_____ |
| | | INDUCTANCE_____ |
| NOD040NOD041 | RESISTANCE_____ | CAPACITANCE_____ |
| NOD041 | | CAPACITANCE_____ |
| | | INDUCTANCE_____ |
| NOD041 | RESISTANCE_____ | CAPACITANCE_____ |
| NOD041NOD042 | INDUCTANCE_____ | |
| NOD042 | RESISTANCE_____ | CAPACITANCE_____ |
| | | INDUCTANCE_____ |
| NOD042 | RESISTANCE_____ | CAPACITANCE_____ |
| NOD042NOD043 | INDUCTANCE_____ | |
| NOD043 | RESISTANCE_____ | CAPACITANCE_____ |
| | | INDUCTANCE_____ |
| NOD043 | RESISTANCE_____ | CAPACITANCE_____ |
| NOD043NOD044 | INDUCTANCE_____ | |
| NOD044 | RESISTANCE_____ | CAPACITANCE_____ |
| | | INDUCTANCE_____ |
| NOD044 | RESISTANCE_____ | CAPACITANCE_____ |
| NOD044NOD045 | INDUCTANCE_____ | |
| NOD045 | RESISTANCE_____ | CAPACITANCE_____ |
| | | INDUCTANCE_____ |
| NOD045 | RESISTANCE_____ | CAPACITANCE_____ |
| NOD045NOD046 | INDUCTANCE_____ | |
| NOD046 | RESISTANCE_____ | CAPACITANCE_____ |
| | | INDUCTANCE_____ |
| NOD046 | RESISTANCE_____ | CAPACITANCE_____ |
| NOD046NOD047 | INDUCTANCE_____ | |
| NOD047 | RESISTANCE_____ | CAPACITANCE_____ |
| | | INDUCTANCE_____ |
| NOD047 | RESISTANCE_____ | CAPACITANCE_____ |
| NOD047NOD048 | INDUCTANCE_____ | |
| NOD048 | RESISTANCE_____ | CAPACITANCE_____ |
| | | INDUCTANCE_____ |
| NOD048 | RESISTANCE_____ | CAPACITANCE_____ |
| NOD048NOD049 | INDUCTANCE_____ | |
| NOD049 | RESISTANCE_____ | CAPACITANCE_____ |
| | | INDUCTANCE_____ |
| NOD049 | RESISTANCE_____ | CAPACITANCE_____ |
| NOD049NOD050 | INDUCTANCE_____ | |
| NOD050 | RESISTANCE_____ | |

| NOD050 | CAPACITANCE_____ |
|---------------------|------------------|
| NOD050NOD051 | INDUCTANCE_____ |
| NOD051 | RESISTANCE_____ |
| NOD051 | CAPACITANCE_____ |
| \$VINTAGE, 0 | |
| BEGIN NEW DATA CASE | |
| C | |
| \$PUNCH | |
| BEGIN NEW DATA CASE | |
| BLANK | |

The following file (`rod_50_mod.pch`) is the DBM obtained when running the input DBM file `rod_50.mod` with ATP.

| | |
|------|---|
| KARD | 4 4 4 5 5 6 6 7 7 8 8 9 9 10 10 10 11 11 12 12 13 13 13 14 |
| | 14 15 15 16 16 16 17 17 18 18 19 19 19 20 20 21 21 22 22 22 23 23 24 24 25 |
| | 25 25 26 26 27 27 28 28 28 29 29 30 30 31 31 31 32 32 33 33 34 34 34 35 35 |
| | 36 36 37 37 37 38 38 39 39 40 40 40 41 41 42 42 43 43 43 44 44 45 45 46 46 |
| | 46 47 47 48 48 49 49 49 50 50 51 51 52 52 52 53 53 54 54 55 55 55 56 56 57 |
| | 57 58 58 58 59 59 60 60 61 61 61 62 62 63 63 64 64 65 65 66 66 67 67 67 |
| | 68 68 69 69 70 70 70 71 71 72 72 73 73 73 74 74 75 75 76 76 76 77 77 78 78 |
| | 79 79 79 80 80 81 81 82 82 82 83 83 84 84 85 85 85 86 86 87 87 88 88 88 89 |
| | 89 90 90 91 91 91 92 92 93 93 94 94 94 95 95 96 96 97 97 97 98 98 99 99 100 |
| | 1001001011011021031031041041051051061061071071081081091091091011010 |
| | 1111111211211211311311411415115116116117117118118119119120120121121 |
| | 121122122123123124124125125126126127127127128128129129130130131131132 |
| | 13213313313313413413513513613613613713713813813913914014014114142142142 |
| | 14314314414414514514614614714714814814914915015015115115125125135135 |
| | 0 |
| KARG | 1 3 -1 2 -1 4 -1 3 -1 -2 2 -2 4 -2 3 -2 -3 2 -3 4 -3 3 -3 -4 2 |
| | -4 4 -4 3 -4 -5 2 -5 4 -5 3 -5 -6 2 -6 4 -6 3 -6 -7 2 -7 4 -7 3 |
| | -7 -8 2 -8 4 -8 3 -8 -9 2 -9 4 -9 3 -9 -10 2 -10 4 -10 3 -10 -11 2 -11 |
| | 4 -11 3 -11 -12 2 -12 4 -12 3 -12 -13 2 -13 4 -13 3 -13 -14 2 -14 4 -14 3 -14 |
| | -15 2 -15 4 -15 3 -15 -16 2 -16 4 -16 3 -16 -17 2 -17 4 -17 3 -17 -18 2 -18 4 |
| | -18 3 -18 -19 2 -19 4 -19 3 -19 -20 2 -20 4 -20 3 -20 -21 2 -21 4 -21 3 -21 -22 |
| | 2 -22 4 -22 3 -22 -23 2 -23 4 -23 3 -23 -24 2 -24 4 -24 3 -24 -25 2 -25 4 -25 |
| | 3 -25 -26 2 -26 4 -26 3 -26 -27 2 -27 4 -27 3 -27 -28 2 -28 4 -28 3 -28 -29 2 |
| | -29 4 -29 3 -29 -30 2 -30 4 -30 3 -30 -31 2 -31 4 -31 3 -31 -32 2 -32 4 -32 3 |
| | 3 -32 -33 2 -33 4 -33 3 -33 -34 2 -34 4 -34 3 -34 -35 2 -35 4 -35 3 -35 -36 2 -36 |
| | 4 -36 3 -36 -37 2 -37 4 -37 3 -37 -38 2 -38 4 -38 3 -38 -39 2 -39 4 -39 3 -39 |
| | -40 2 -40 4 -40 3 -40 -41 2 -41 4 -41 3 -41 -42 2 -42 4 -42 3 -42 -43 2 -43 4 |
| | -43 3 -43 -44 2 -44 4 -44 3 -44 -45 2 -45 4 -45 3 -45 -46 2 -46 4 -46 3 -46 -47 |
| | 2 -47 4 -47 3 -47 -48 2 -48 4 -48 3 -48 -49 2 -49 4 -49 3 -49 -50 2 -50 4 -50 |
| KBEG | 3 43 9 27 3 59 9 43 3 9 27 3 59 9 43 3 9 27 3 59 9 43 3 9 27 3 59 9 43 |
| | 3 59 9 43 3 9 27 3 59 9 43 3 9 27 3 59 9 43 3 9 27 3 59 9 43 3 9 27 3 59 9 43 |
| | 3 9 27 3 59 9 43 3 9 27 3 59 9 43 3 9 27 3 59 9 43 3 9 27 3 59 9 43 3 9 27 3 |
| | 59 9 43 3 9 27 3 59 9 43 3 9 27 3 59 9 43 3 9 27 3 59 9 43 3 9 27 3 59 9 43 3 |
| | 9 27 3 59 9 43 3 9 27 3 59 9 43 3 9 27 3 59 9 43 3 9 27 3 59 9 43 3 9 27 3 59 |
| | 9 43 3 9 27 3 59 9 43 3 9 27 3 59 9 43 3 9 27 3 59 9 43 3 9 27 3 59 9 43 3 9 |
| | 27 3 59 9 43 3 9 27 3 59 9 43 3 9 27 3 59 9 43 3 9 27 3 59 9 43 3 9 27 3 59 9 |
| | 43 3 9 27 3 59 9 43 3 9 27 3 59 9 43 3 9 27 3 59 9 43 3 9 27 3 59 9 43 3 9 27 |
| | 3 59 9 43 3 9 27 3 59 9 43 3 9 27 3 59 9 43 3 9 27 3 59 9 43 3 9 27 3 59 9 43 |
| | 3 9 27 3 59 9 43 3 9 27 3 59 9 43 3 9 27 3 59 9 43 3 9 27 3 59 9 43 3 9 27 3 |

```

59 9 43 3 9 27 3 59 9 43 3 9 27 3 59 9 43 3 9 27 3 59 9 43 3
9 27 3 59 9 43 3 9 27 3 59 9 43 3 9 27 3 59 9 43 3 9 27 3 59
9 43 3 9 27 3 59 9 43 3 9 27 3 59 9 43 3 9 27 3 59 9 43 3 9
27 3 59 9 43 3 9 27 3 59 9 43 3 9 27 3 59 9 43 3 9 27 3 59 9
KEND 8 58 14 42 8 74 14 58 8 14 42 8 74 14 58 8 14 42 8 74 14 58 8
74 14 58 8 14 42 8 74 14 58 8 14 42 8 74 14 58 8 14 42 8 74 14 58
8 14 42 8 74 14 58 8 14 42 8 74 14 58 8 14 42 8 74 14 58 8 14 42 8
74 14 58 8 14 42 8 74 14 58 8 14 42 8 74 14 58 8 14 42 8 74 14 58
14 42 8 74 14 58 8 14 42 8 74 14 58 8 14 42 8 74 14 58 8 14 42 8 74
14 58 8 14 42 8 74 14 58 8 14 42 8 74 14 58 8 14 42 8 74 14 58 8 14
42 8 74 14 58 8 14 42 8 74 14 58 8 14 42 8 74 14 58 8 14 42 8 74 14
58 8 14 42 8 74 14 58 8 14 42 8 74 14 58 8 14 42 8 74 14 58 8 14 42
8 74 14 58 8 14 42 8 74 14 58 8 14 42 8 74 14 58 8 14 42 8 74 14 58
8 14 42 8 74 14 58 8 14 42 8 74 14 58 8 14 42 8 74 14 58 8 14 42 8
74 14 58 8 14 42 8 74 14 58 8 14 42 8 74 14 58 8 14 42 8 74 14 58 8
14 42 8 74 14 58 8 14 42 8 74 14 58 8 14 42 8 74 14 58 8 14 42 8 74
14 58 8 14 42 8 74 14 58 8 14 42 8 74 14 58 8 14 42 8 74 14 58 8 14
42 8 74 14 58 8 14 42 8 74 14 58 8 14 42 8 74 14 58 8 14 42 8 74 14
KTEX 1 0 1 0 1 0 1 0 1 0 1 0 1 0 1 0 1 0 1 0 1 0 1 0 1 0 1 0 1 0 1 0
1 0 1 0 1 0 1 0 1 0 1 0 1 0 1 0 1 0 1 0 1 0 1 0 1 0 1 0 1 0 1 0 1
1 0 1 0 1 0 1 0 1 0 1 0 1 0 1 0 1 0 1 0 1 0 1 0 1 0 1 0 1 0 1 0 1
0 1 0 1 1 0 1 0 1 0 1 0 1 0 1 0 1 0 1 0 1 0 1 0 1 0 1 0 1 0 1 0 1
1 0 1 0 1 0 1 1 0 1 0 1 0 1 0 1 0 1 0 1 0 1 0 1 0 1 0 1 0 1 0 1 0
1 0 1 1 0 1 0 1 0 1 0 1 0 1 0 1 0 1 0 1 0 1 0 1 0 1 0 1 0 1 0 1 0
0 1 0 1 0 1 0 1 0 1 0 1 0 1 0 1 0 1 0 1 0 1 0 1 0 1 0 1 0 1 0 1 0
0 1 1 0 1 0 1 0 1 0 1 0 1 0 1 0 1 0 1 0 1 0 1 0 1 0 1 0 1 0 1 0 1
1 0 1 0 1 0 1 0 1 0 1 0 1 0 1 0 1 0 1 0 1 0 1 0 1 0 1 0 1 0 1 0 1
1 1 0 1 0 1 0 1 0 1 0 1 0 1 0 1 0 1 0 1 0 1 0 1 0 1 0 1 0 1 0 1 0
0 1 0 1 1 0 1 0 1 0 1 0 1 0 1 0 1 0 1 0 1 0 1 0 1 0 1 0 1 0 1 0 1
1 0 1 0 1 0 1 0 1 0 1 0 1 0 1 0 1 0 1 0 1 0 1 0 1 0 1 0 1 0 1 0 1
0 1 0 1 0 1 0 1 0 1 0 1 0 1 0 1 0 1 0 1 0 1 0 1 0 1 0 1 0 1 0 1 0
$ERASE
/BRANCH
$VINTAGE, 1
C
C This file was created on 02-May-2000, using the m-file dbm_grndrod_create.m
C this ground rod model consists of:
C      number of sections = 50
C
C      1          2          3          4          5          6          7          8
C 34567890123456789012345678901234567890123456789012345678901234567890
NOD001 NOD002          INDUCTANCE_____
NOD002 NOD002          RESISTANCE_____
NOD002          CAPACITANCE_____
NOD002 NOD003          INDUCTANCE_____
NOD003 NOD003          RESISTANCE_____
NOD003          CAPACITANCE_____
NOD003 NOD004          INDUCTANCE_____
NOD004 NOD004          RESISTANCE_____
NOD004          CAPACITANCE_____
NOD004 NOD005          INDUCTANCE_____
NOD005 NOD005          RESISTANCE_____
NOD005          CAPACITANCE_____

```

| | |
|--------------|------------------|
| NOD005NOD006 | INDUCTANCE_____ |
| NOD006 | RESISTANCE_____ |
| NOD006 | CAPACITANCE_____ |
| NOD006NOD007 | INDUCTANCE_____ |
| NOD007 | RESISTANCE_____ |
| NOD007 | CAPACITANCE_____ |
| NOD007NOD008 | INDUCTANCE_____ |
| NOD008 | RESISTANCE_____ |
| NOD008 | CAPACITANCE_____ |
| NOD008NOD009 | INDUCTANCE_____ |
| NOD009 | RESISTANCE_____ |
| NOD009 | CAPACITANCE_____ |
| NOD009NOD010 | INDUCTANCE_____ |
| NOD010 | RESISTANCE_____ |
| NOD010 | CAPACITANCE_____ |
| NOD010NOD011 | INDUCTANCE_____ |
| NOD011 | RESISTANCE_____ |
| NOD011 | CAPACITANCE_____ |
| NOD011NOD012 | INDUCTANCE_____ |
| NOD012 | RESISTANCE_____ |
| NOD012 | CAPACITANCE_____ |
| NOD012NOD013 | INDUCTANCE_____ |
| NOD013 | RESISTANCE_____ |
| NOD013 | CAPACITANCE_____ |
| NOD013NOD014 | INDUCTANCE_____ |
| NOD014 | RESISTANCE_____ |
| NOD014 | CAPACITANCE_____ |
| NOD014NOD015 | INDUCTANCE_____ |
| NOD015 | RESISTANCE_____ |
| NOD015 | CAPACITANCE_____ |
| NOD015NOD016 | INDUCTANCE_____ |
| NOD016 | RESISTANCE_____ |
| NOD016 | CAPACITANCE_____ |
| NOD016NOD017 | INDUCTANCE_____ |
| NOD017 | RESISTANCE_____ |
| NOD017 | CAPACITANCE_____ |
| NOD017NOD018 | INDUCTANCE_____ |
| NOD018 | RESISTANCE_____ |
| NOD018 | CAPACITANCE_____ |
| NOD018NOD019 | INDUCTANCE_____ |
| NOD019 | RESISTANCE_____ |
| NOD019 | CAPACITANCE_____ |
| NOD019NOD020 | INDUCTANCE_____ |
| NOD020 | RESISTANCE_____ |
| NOD020 | CAPACITANCE_____ |
| NOD020NOD021 | INDUCTANCE_____ |
| NOD021 | RESISTANCE_____ |
| NOD021 | CAPACITANCE_____ |
| NOD021NOD022 | INDUCTANCE_____ |
| NOD022 | RESISTANCE_____ |
| NOD022 | CAPACITANCE_____ |
| NOD022NOD023 | INDUCTANCE_____ |
| NOD023 | RESISTANCE_____ |
| NOD023 | CAPACITANCE_____ |

| | | |
|--------|--------|------------------|
| NOD023 | NOD024 | INDUCTANCE_____ |
| NOD024 | NOD024 | RESISTANCE_____ |
| | | CAPACITANCE_____ |
| NOD024 | NOD025 | INDUCTANCE_____ |
| NOD025 | NOD025 | RESISTANCE_____ |
| | | CAPACITANCE_____ |
| NOD025 | NOD026 | INDUCTANCE_____ |
| NOD026 | NOD026 | RESISTANCE_____ |
| | | CAPACITANCE_____ |
| NOD026 | NOD027 | INDUCTANCE_____ |
| NOD027 | NOD027 | RESISTANCE_____ |
| | | CAPACITANCE_____ |
| NOD027 | NOD028 | INDUCTANCE_____ |
| NOD028 | NOD028 | RESISTANCE_____ |
| | | CAPACITANCE_____ |
| NOD028 | NOD029 | INDUCTANCE_____ |
| NOD029 | NOD029 | RESISTANCE_____ |
| | | CAPACITANCE_____ |
| NOD029 | NOD030 | INDUCTANCE_____ |
| NOD030 | NOD030 | RESISTANCE_____ |
| | | CAPACITANCE_____ |
| NOD030 | NOD031 | INDUCTANCE_____ |
| NOD031 | NOD031 | RESISTANCE_____ |
| | | CAPACITANCE_____ |
| NOD031 | NOD032 | INDUCTANCE_____ |
| NOD032 | NOD032 | RESISTANCE_____ |
| | | CAPACITANCE_____ |
| NOD032 | NOD033 | INDUCTANCE_____ |
| NOD033 | NOD033 | RESISTANCE_____ |
| | | CAPACITANCE_____ |
| NOD033 | NOD034 | INDUCTANCE_____ |
| NOD034 | NOD034 | RESISTANCE_____ |
| | | CAPACITANCE_____ |
| NOD034 | NOD035 | INDUCTANCE_____ |
| NOD035 | NOD035 | RESISTANCE_____ |
| | | CAPACITANCE_____ |
| NOD035 | NOD036 | INDUCTANCE_____ |
| NOD036 | NOD036 | RESISTANCE_____ |
| | | CAPACITANCE_____ |
| NOD036 | NOD037 | INDUCTANCE_____ |
| NOD037 | NOD037 | RESISTANCE_____ |
| | | CAPACITANCE_____ |
| NOD037 | NOD038 | INDUCTANCE_____ |
| NOD038 | NOD038 | RESISTANCE_____ |
| | | CAPACITANCE_____ |
| NOD038 | NOD039 | INDUCTANCE_____ |
| NOD039 | NOD039 | RESISTANCE_____ |
| | | CAPACITANCE_____ |
| NOD039 | NOD040 | INDUCTANCE_____ |
| NOD040 | NOD040 | RESISTANCE_____ |
| | | CAPACITANCE_____ |
| NOD040 | NOD041 | INDUCTANCE_____ |
| NOD041 | NOD041 | RESISTANCE_____ |
| | | CAPACITANCE_____ |

| | |
|--|--------------------|
| NOD041NOD042 | INDUCTANCE_____ |
| NOD042 | RESISTANCE_____ |
| NOD042 | CAPACITANCE_____ |
| NOD042NOD043 | INDUCTANCE_____ |
| NOD043 | RESISTANCE_____ |
| NOD043 | CAPACITANCE_____ |
| NOD043NOD044 | INDUCTANCE_____ |
| NOD044 | RESISTANCE_____ |
| NOD044 | CAPACITANCE_____ |
| NOD044NOD045 | INDUCTANCE_____ |
| NOD045 | RESISTANCE_____ |
| NOD045 | CAPACITANCE_____ |
| NOD045NOD046 | INDUCTANCE_____ |
| NOD046 | RESISTANCE_____ |
| NOD046 | CAPACITANCE_____ |
| NOD046NOD047 | INDUCTANCE_____ |
| NOD047 | RESISTANCE_____ |
| NOD047 | CAPACITANCE_____ |
| NOD047NOD048 | INDUCTANCE_____ |
| NOD048 | RESISTANCE_____ |
| NOD048 | CAPACITANCE_____ |
| NOD048NOD049 | INDUCTANCE_____ |
| NOD049 | RESISTANCE_____ |
| NOD049 | CAPACITANCE_____ |
| NOD049NOD050 | INDUCTANCE_____ |
| NOD050 | RESISTANCE_____ |
| NOD050 | CAPACITANCE_____ |
| NOD050NOD051 | INDUCTANCE_____ |
| NOD051 | RESISTANCE_____ |
| NOD051 | CAPACITANCE_____ |
| \$VINTAGE, 0 | |
| \$EOF User-supplied header cards follow. | 01-May-00 22:35:19 |
| ARG,NOD001,RESISTANCE_____,INDUCTANCE_____,CAPACITANCE_____- | |
| NUM,RESISTANCE_____,INDUCTANCE_____,CAPACITANCE_____- | |
| DUM,NOD002,NOD003,NOD004,NOD005,NOD006,NOD007,NOD008,NOD009,NOD010,NOD011 | |
| DUM,NOD012,NOD013,NOD014,NOD015,NOD016,NOD017,NOD018,NOD019,NOD020,NOD021,NOD022 | |
| DUM,NOD023,NOD024,NOD025,NOD026,NOD027,NOD028,NOD029,NOD030,NOD031,NOD032,NOD033 | |
| DUM,NOD034,NOD035,NOD036,NOD037,NOD038,NOD039,NOD040,NOD041,NOD042,NOD043,NOD044 | |
| DUM,NOD045,NOD046,NOD047,NOD048,NOD049,NOD050,NOD051 | |

APPENDIX F FREQUENCY RESPONSE OF GROUND RODS

In this appendix we show the computed magnitude of the impedance ($|Z(j\omega)| = |V(j\omega)/I(j\omega)|$) of the grounding rod as a function of frequency, using the model presented in Section 5.5, for different low-frequency, low-current resistances, relative permittivity, and rod lengths. The resistance values are 10, 100, and 1000Ω , relative permittivity, ϵ_r , values 1 and 10, and rod length values 24.1 and 2.4 m. As seen from Figures F.1 to F.12, in a 10 MHz frequency range, the magnitude of the grounding impedance varies as much as two orders in magnitude above and/or below the low-frequency, low-current resistance, depending on the length of the rod and the relative permittivity of the soil.

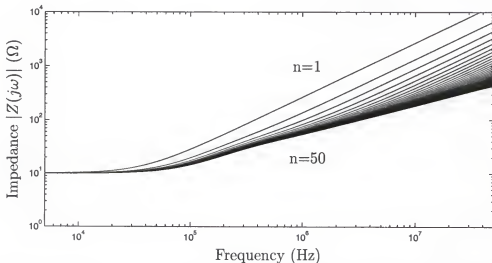


Figure F.1: Frequency response of a vertically driven ground electrode of 24.4 m, with $\epsilon_r = 1$, and a low-frequency low-current resistance of 10Ω for different number of $R - L - C$ sections n (see Figure 5.8).

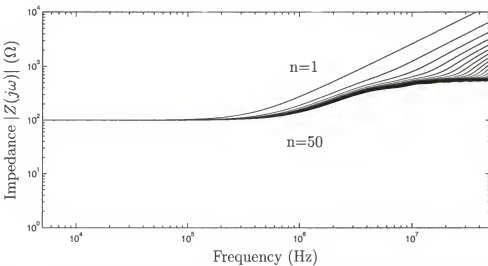


Figure F.2: Frequency response of a vertically driven ground electrode of 24.4 m, with $\epsilon_r = 1$, and a low-frequency low-current resistance of 100Ω for different number of $R - L - C$ sections n (see Figure 5.8).

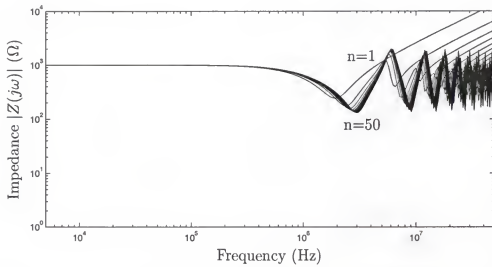


Figure F.3: Frequency response of a vertically driven ground electrode of 24.4 m, with $\epsilon_r = 1$, and a low-frequency low-current resistance of 1000Ω for different number of $R - L - C$ sections n (see Figure 5.8).

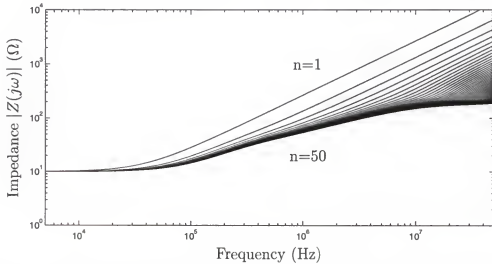


Figure F.4: Frequency response of a vertically driven ground electrode of 24.4 m, with $\epsilon_r = 10$, and a low-frequency low-current resistance of 10Ω for different number of $R - L - C$ sections n (see Figure 5.8).

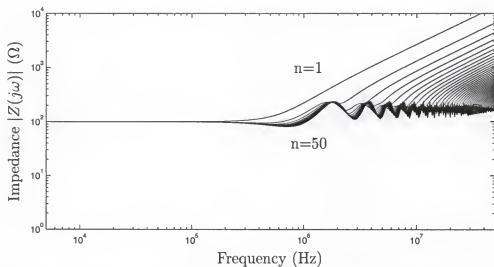


Figure F.5: Frequency response of a vertically driven ground electrode of 24.4 m, with $\epsilon_r = 10$, and a low-frequency low-current resistance of 100Ω for different number of $R - L - C$ sections n (see Figure 5.8).

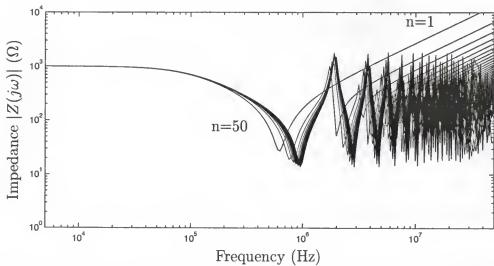


Figure F.6: Frequency response of a vertically driven ground electrode of 24.4 m, with $\epsilon_r = 10$, and a low-frequency low-current resistance of 1000Ω for different number of $R - L - C$ sections n (see Figure 5.8).

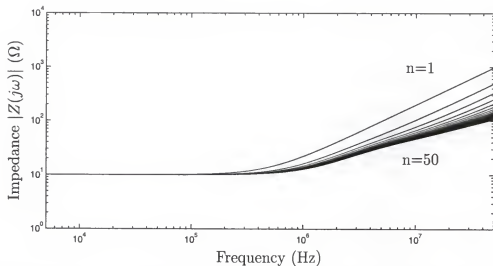


Figure F.7: Frequency response of a vertically driven ground electrode of 2.4 m, with $\epsilon_r = 1$, and a low-frequency low-current resistance of 10Ω for different number of $R - L - C$ sections n (see Figure 5.8).

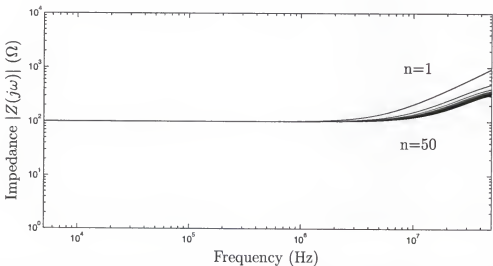


Figure F.8: Frequency response of a vertically driven ground electrode of 2.4 m, with $\epsilon_r = 1$, and a low-frequency low-current resistance of 100Ω for different number of $R - L - C$ sections n (see Figure 5.8).

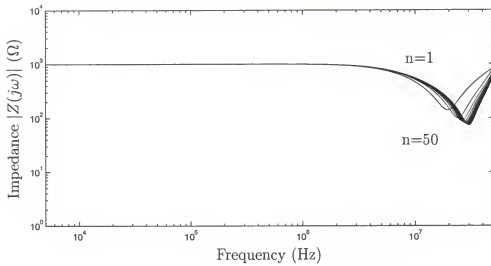


Figure F.9: Frequency response of a vertically driven ground electrode of 2.4 m, with $\epsilon_r = 1$, and a low-frequency low-current resistance of 1000Ω for different number of $R - L - C$ sections n (see Figure 5.8).

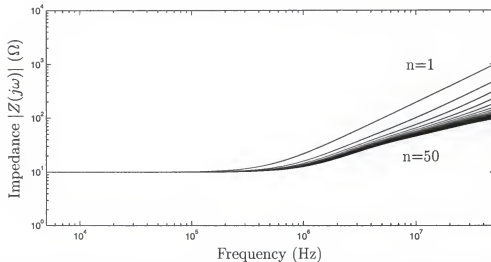


Figure F.10: Frequency response of a vertically driven ground electrode of 2.4 m, with $\epsilon_r = 10$, and a low-frequency low-current resistance of 10Ω for different number of $R - L - C$ sections n (see Figure 5.8).

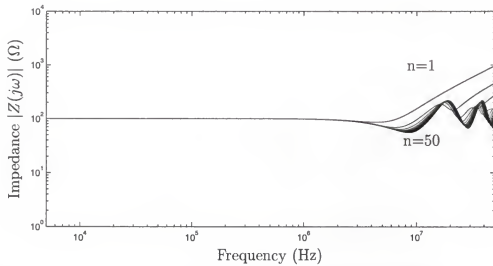


Figure F.11: Frequency response of a vertically driven ground electrode of 2.4 m, with $\epsilon_r = 10$, and a low-frequency low-current resistance of 100Ω for different number of $R - L - C$ sections n (see Figure 5.8).

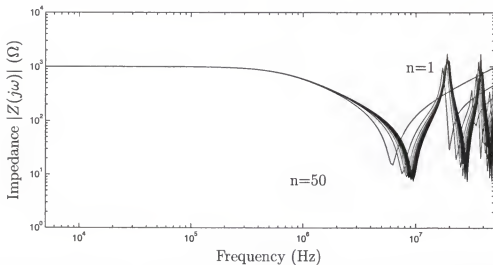


Figure F.12: Frequency response of a vertically driven ground electrode of 2.4 m, with $\epsilon_r = 10$, and a low-frequency low-current resistance of 1000Ω for different number of $R - L - C$ sections n (see Figure 5.8).

APPENDIX G WAVEFORMS ARITHMETIC

To add, subtract, or multiply recorded waveforms, it was necessary to represent them on a common time scale by compensating for delays of the Fiber Optic Links (see Appendix C). As an example, suppose we want to sum two measured waveforms (as seen in Figure G.1) *Waveform 1* and *Waveform 2*. Because of Fiber Optic time delays, and possible different sampling frequencies, sampling times of the two waveforms do not necessarily coincide ($t_{\Delta} \neq t_{\square}$, $t_{\Delta} + \Delta t \neq t_{\square} + \Delta t$, $\dots t_{\Delta} + n\Delta t \neq t_{\square} + n\Delta t$). The sampling points of *Waveform 1* are represented by the blank triangles and the sampling points of *Waveform 2* are represented by the blank boxes. Therefore, we re-sample the waveforms at a common discrete time vector (t_c , $t_c + \Delta t$, $\dots t_c + n\Delta t$) by performing a linear interpolation at every time step in the two waveforms to be processed. The re-sampled points of *Waveform 1* and *Waveform 2* are represented by the blank circles. Once the two waveforms have been re-sampled at a common discrete time vector, *any waveform operations* can be performed. The re-sampled points that result from the addition of the two waveforms are represented by the black-filled circles.

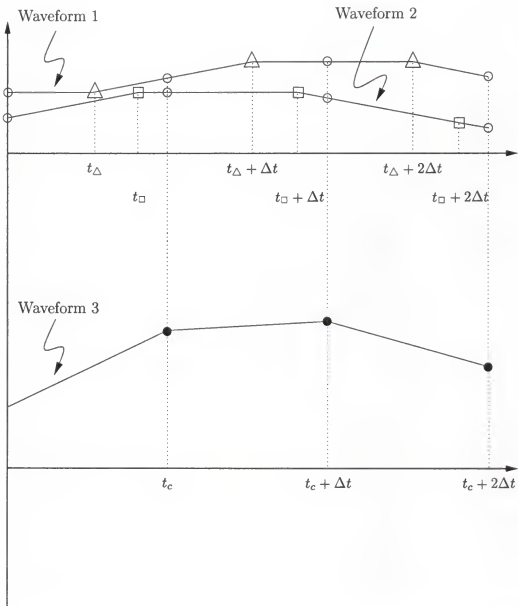


Figure G.1: Re-sampling and interpolating digitally recorded data to sum or subtract waveforms.

APPENDIX H 1999 AND 2000 DATA PRESENTATION

In this appendix we show all waveforms for flash UF-9916 acquired during the 1999 experiments and incident current, currents to ground, neutral, and phase C arresters and phase currents for each stroke of all flashes acquired during the 2000 experiments on a $100\text{-}\mu\text{s}$ scale. The automated data acquisition system implemented in the 2000 experiments by the author of this manuscript allowed us to present the complete 2000 data in this format.

Data for flash UF-9916 is presented, as an example, since neither arrester failures nor flashovers were observed (see Section 6.2). The strike point was located at the mid-point between poles 9 and 10 (see Section C.1.3).

These waveforms are shown on pages 254 to 278. The peak current (shown in Figure H.1) was about -7 kA , having a rise-time of about $2\text{ }\mu\text{s}$. Phase currents arriving at Pole 9 are shown in Figures H.2, H.3, and H.4 on 1 ms, $200\text{ }\mu\text{s}$, and $50\text{ }\mu\text{s}$ time scales, respectively. Phase currents arriving at Pole 8 are shown in Figures H.5, H.6, and H.7 on 1 ms, $200\text{ }\mu\text{s}$, and $50\text{ }\mu\text{s}$ time scales, respectively. Phase A arrester current and voltage at Pole 8 are shown in Figures H.8, H.9, and H.10 on 1 ms, $200\text{ }\mu\text{s}$, and $50\text{ }\mu\text{s}$ time scales, respectively. Phase B arrester current and voltage at Pole 8 are shown in Figures H.11, H.12, and H.13 on 1 ms, $200\text{ }\mu\text{s}$, and $50\text{ }\mu\text{s}$ time scales, respectively. Phase C arrester current and voltage at Pole 8 are shown in Figures H.14, H.15, and H.16 on 1 ms, $200\text{ }\mu\text{s}$, and $50\text{ }\mu\text{s}$ time scales, respectively. Phase to phase voltage at pole 8 is shown in Figure H.17 on different time scales. Phase currents at Pole 7 (currents through the terminating resistors) are shown in Figures H.18, H.19, and

H.20 on 1 ms, 200 μ s, and 50 μ s time scales, respectively. Currents to ground at poles 7, 8, 11, and 12 are shown in Figures H.21, H.22, and H.23, on 1 ms, 200 μ s, and 50 μ s time scales, respectively. Figure H.24 shows the comparison of the sum of currents to ground and the total lightning current. Note that the sum of currents to ground are larger than the incident current. This could be due to the fact that in 1999 no end-to-end calibration factors were experimentally obtained for current sensors. The comparison of computed difference between measured voltages (V_{BN8} and V_{AN8}) and measured voltage [V_{BAS}] is shown in Figure H.25, and their difference was attributed to the nonlinear behavior of the resistors used on the voltage dividers in the 1999 experiments when exposed to high voltages.

Data for strokes 1-5 of flash FPL0011 are shown in Figures H.26-H.30. Data for strokes 1-3 of flash FPL0014 are shown in Figures H.31-H.33. Data for strokes 1-6 of flash FPL0018 are shown in Figures H.34-H.39. Data for strokes 1-7 of flash FPL0032 are shown in Figures H.40-H.46. Data for stroke 1 of flash FPL0033 is shown in Figure H.47. Data for strokes 1-4 of flash FPL0034 are shown in Figures H.48-H.51. Data for strokes 1-5 of flash FPL0036 are shown in Figures H.52-H.55. Data for strokes 1-2 of flash FPL0037 are shown in Figures H.56-H.57.

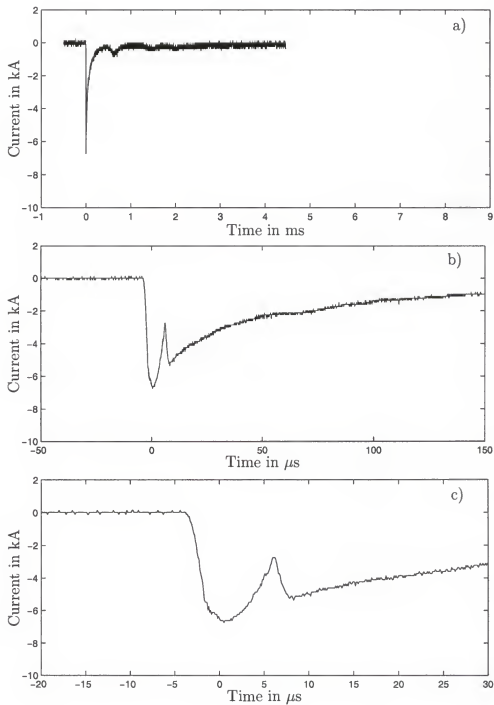


Figure H.1: Total lightning current $[I_i]$ for the first return stroke of flash UF-9916, displayed on three different time scales. a) 10 ms; b) 200 μ s; c) 50 μ s.

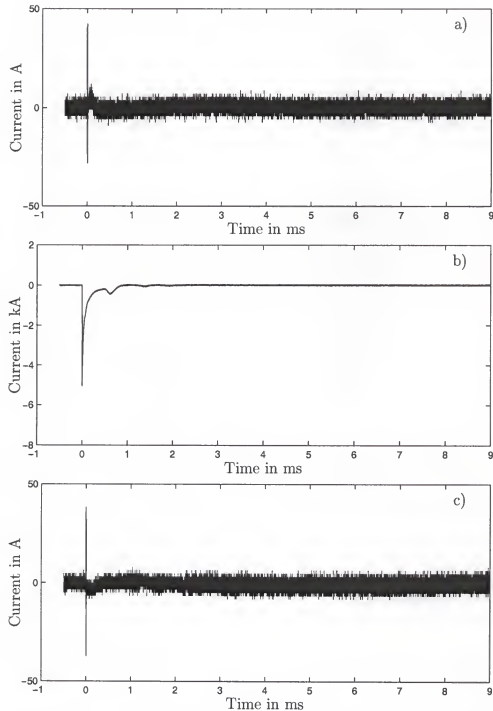


Figure H.2: Phase current versus time waveforms at Pole 9 for the first return stroke of flash UF-9916, displayed on a 10 ms scale. a) Phase A current $[I_{A9}]$; b) Phase B current $[I_{B9}]$; c) Phase C current $[I_{C9}]$.

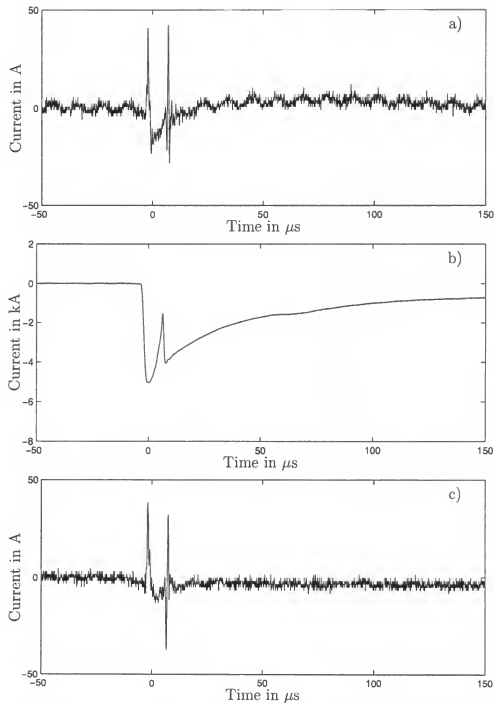


Figure H.3: Phase current versus time waveforms at Pole 9 for the first return stroke of flash UF-9916, displayed on a $200 \mu\text{s}$ scale. a) Phase A current [I_{A9}]; b) Phase B current [I_{B9}]; c) Phase C current [I_{C9}].

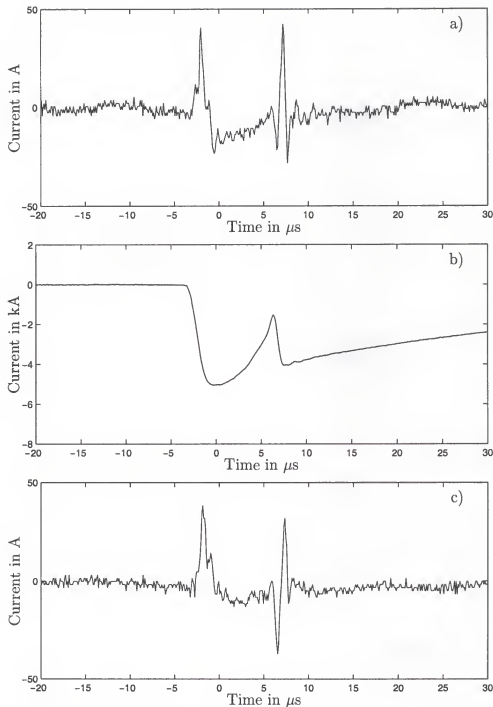


Figure H.4: Phase current versus time waveforms at Pole 9 for the first return stroke of flash UF-9916, displayed on a $50 \mu\text{s}$ scale. a) Phase A current [I_{A9}]; b) Phase B current [I_{B9}]; c) Phase C current [I_{C9}].

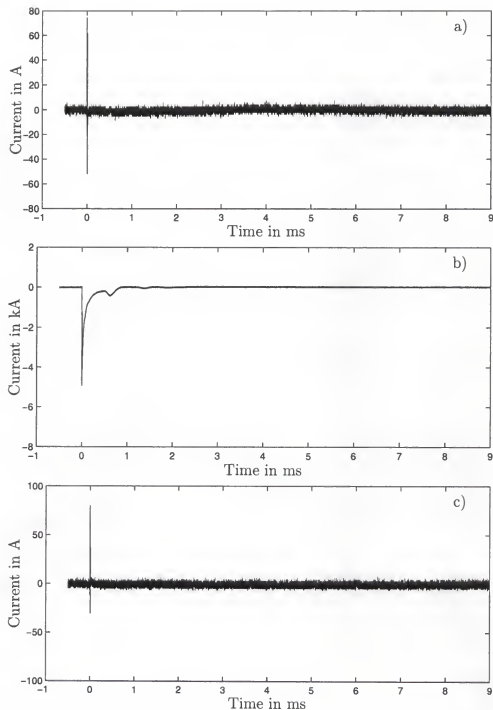


Figure H.5: Phase current versus time waveforms at Pole 8 for the first return stroke of flash UF-9916, displayed on a 10 ms scale. a) Phase A current [I_{A8}]; b) Phase B current [I_{B8}]; c) Phase C current [I_{C8}].

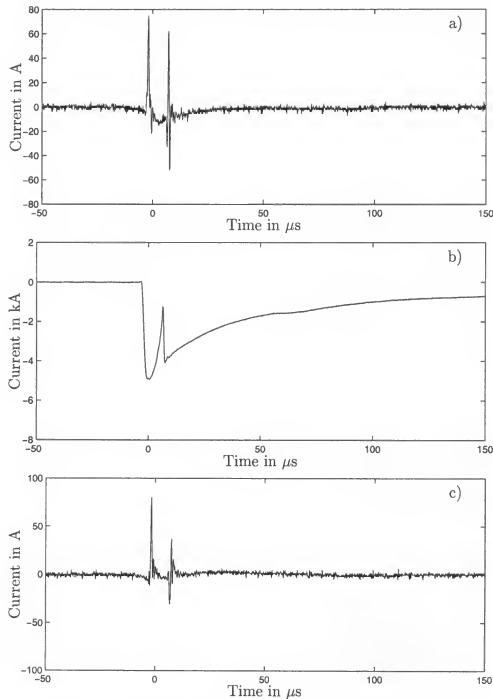


Figure H.6: Phase current versus time waveforms at Pole 8 for the first return stroke of flash UF-9916, displayed on a $200 \mu\text{s}$ scale. a) Phase A current [I_{A8}]; b) Phase B current [I_{B8}]; c) Phase C current [I_{C8}].

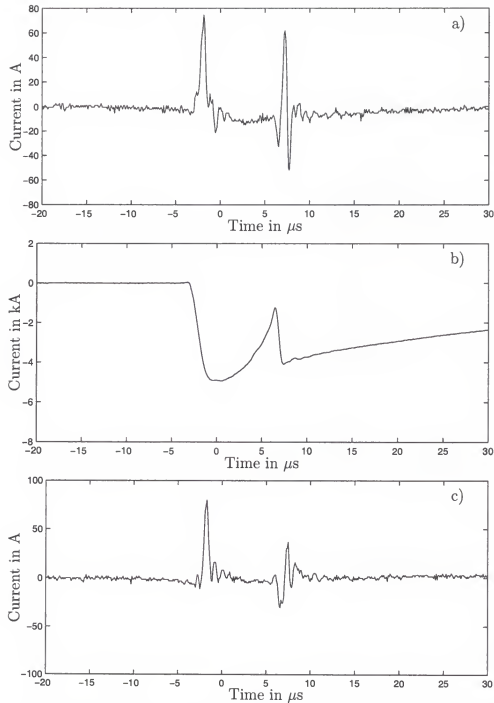


Figure H.7: Phase current versus time waveforms at Pole 8 for the first return stroke of flash UF-9916, displayed on a 50 μ s scale. a) Phase A current [I_{A8}]; b) Phase B current [I_{B8}]; c) Phase C current [I_{C8}].

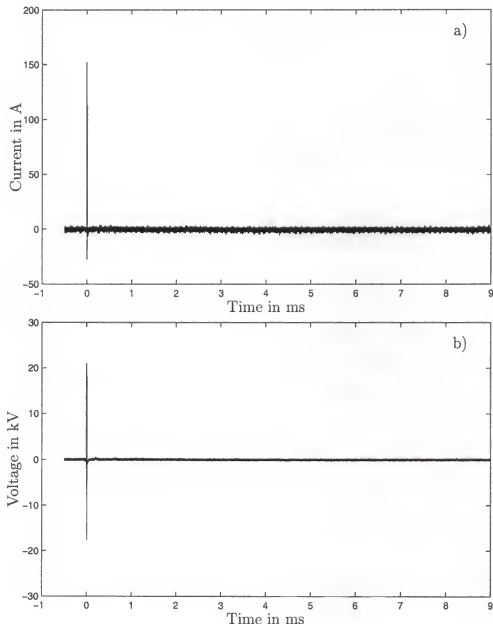


Figure H.8: Phase A arrester at Pole 8 current and voltage versus time waveforms for the first return stroke of flash UF-9916, displayed on a 10 ms scale. a) Current through the arrester [I_{A8}]; b) Voltage across the arrester [V_{A8}];

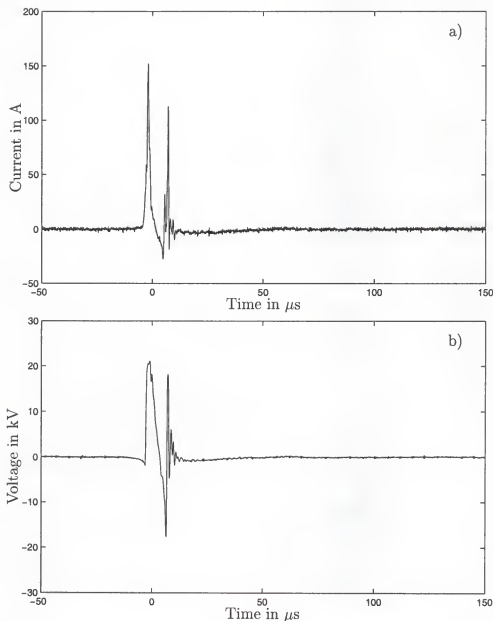


Figure H.9: Phase A arrester at Pole 8 current and voltage versus time waveforms for the first return stroke of flash UF-9916, displayed on a $200 \mu\text{s}$ scale. a) Current through the arrester [I_{A8}]; b) Voltage across the arrester [V_{A8}];

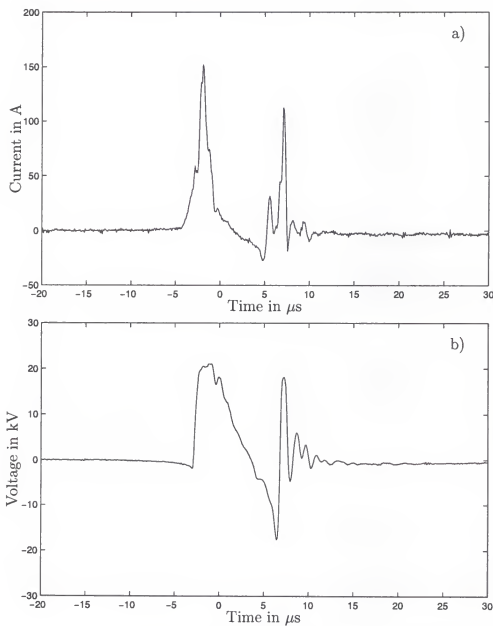


Figure H.10: Phase A arrester at Pole 8 current and voltage versus time waveforms for the first return stroke of flash UF-9916, displayed on a $50\mu\text{s}$ scale. a) Current through the arrester [I_{ANS}]; b) Voltage across the arrester [V_{ANS}];

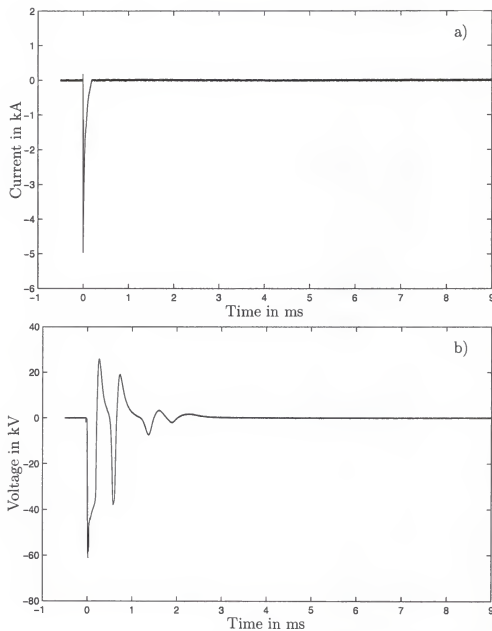


Figure H.11: Phase B arrester at Pole 8 current and voltage versus time waveforms for the first return stroke of flash UF-9916, displayed on a 10 ms scale. a) Current through the arrester [I_{BN8}]; b) Voltage across the arrester [V_{BN8}];

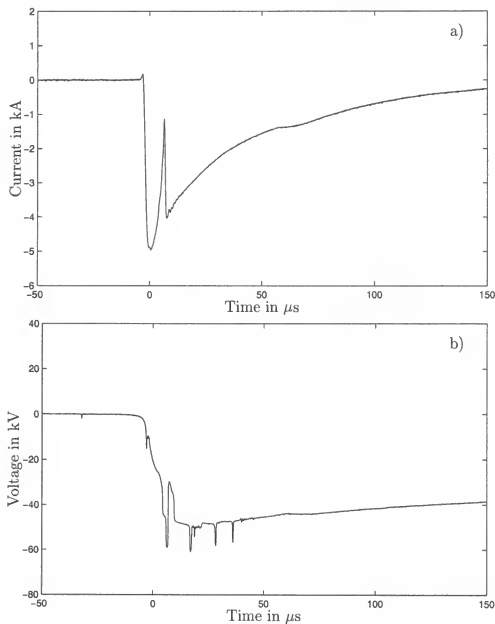


Figure H.12: Phase B arrester at Pole 8 current and voltage versus time waveforms for the first return stroke of flash UF-9916, displayed on a $200 \mu\text{s}$ scale. a) Current through the arrester [I_{BNS}]; b) Voltage across the arrester [V_{BNS}];

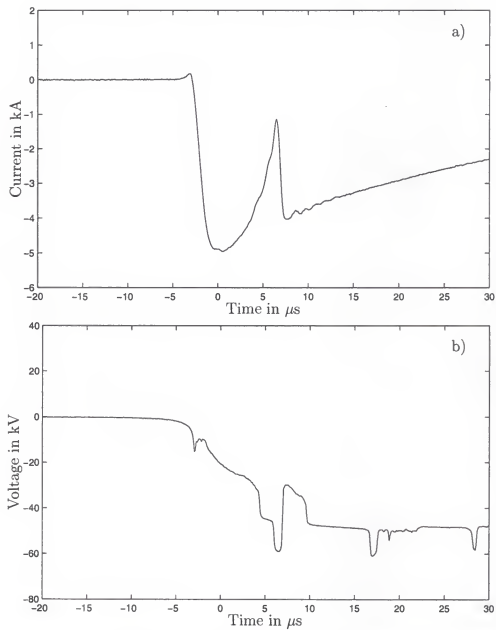


Figure H.13: Phase B arrester at Pole 8 current and voltage versus time waveforms for the first return stroke of flash UF-9916, displayed on a $50\ \mu\text{s}$ scale. a) Current through the arrester [I_{BN8}]; b) Voltage across the arrester [V_{BN8}];

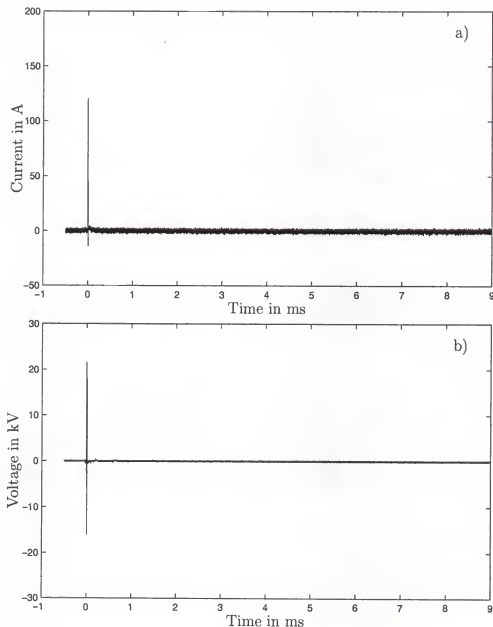


Figure H.14: Phase C arrester at Pole 8 current and voltage versus time waveforms for the first return stroke of flash UF-9916, displayed on a 10 ms scale. a) Current through the arrester [I_{CNS}]; b) Voltage across the arrester [V_{CNS}];

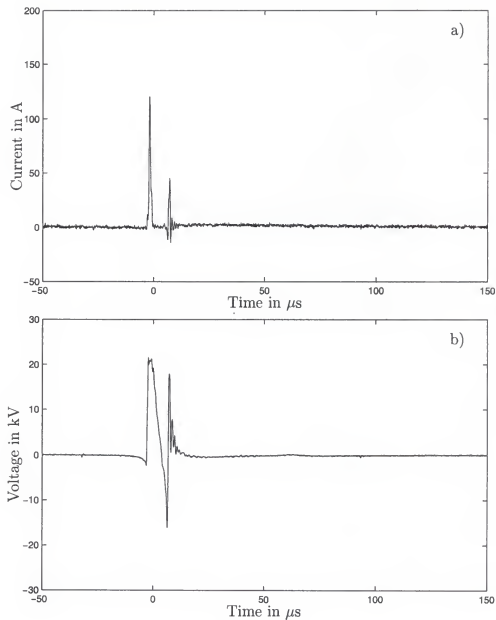


Figure H.15: Phase C arrester at Pole 8 current and voltage versus time waveforms for the first return stroke of flash UF-9916, displayed on a $200 \mu\text{s}$ scale. a) Current through the arrester [I_{CNS}]; b) Voltage across the arrester [V_{CNS}];

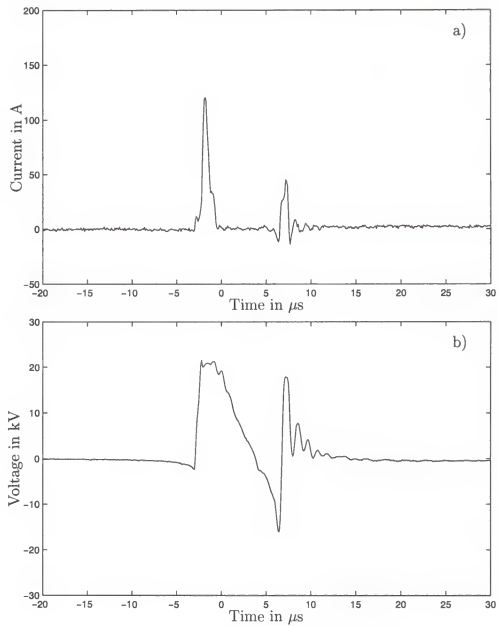


Figure H.16: Phase C arrester at Pole 8 current and voltage versus time waveforms for the first return stroke of flash UF-9916, displayed on a $50\mu\text{s}$ scale. a) Current through the arrester [I_{CNS}]; b) Voltage across the arrester [V_{CNS}];

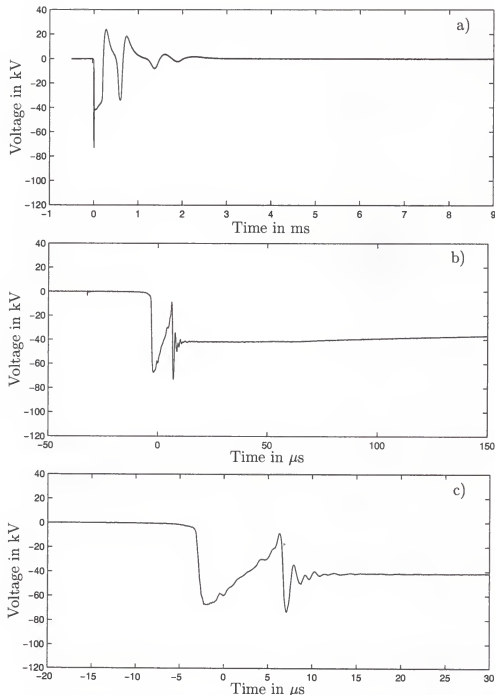


Figure H.17: Phase to phase voltage versus time waveform at Pole 8 [V_{BA8}] for the first return stroke of Flash UF-9916, displayed on different time windows. a) 10 ms; b) 200 μ s; c) 50 μ s.

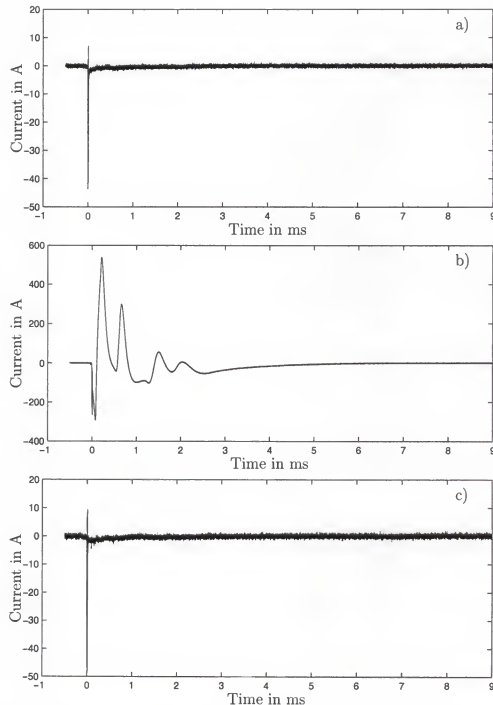


Figure H.18: Phase current versus time waveforms at Pole 7 for the first return stroke of flash UF-9916, displayed on a 10 ms scale. a) Phase A current [I_{A7}]; b) Phase B current [I_{B7}]; c) Phase C current [I_{C7}].

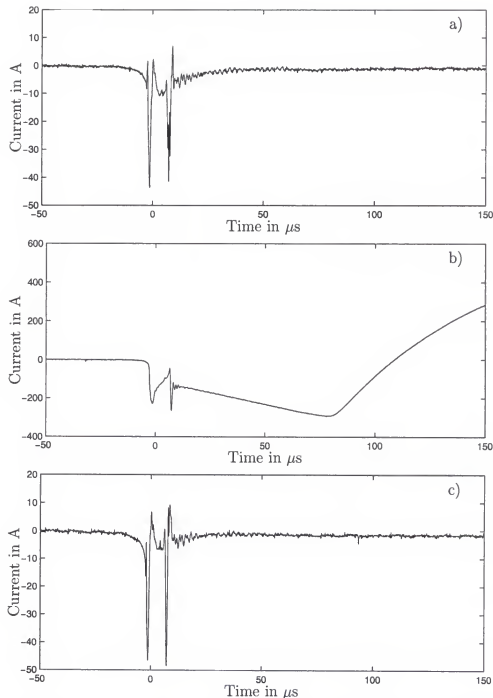


Figure H.19: Phase current versus time waveforms at Pole 7 for the first return stroke of flash UF-9916, displayed on a $200 \mu\text{s}$ scale. a) Phase A current [I_{A7}]; b) Phase B current [I_{B7}]; c) Phase C current [I_{C7}].

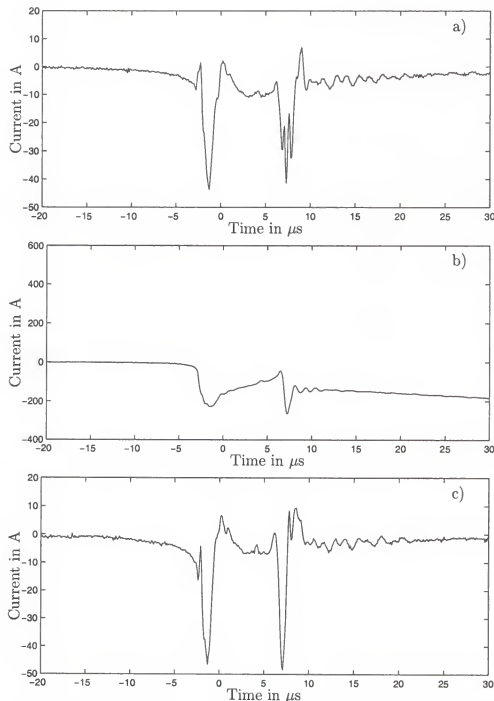


Figure H.20: Phase current versus time waveforms at Pole 7 for the first return stroke of flash UF-9916, displayed on a $50\ \mu$ s scale. a) Phase A current [I_{A7}]; b) Phase B current [I_{B7}]; c) Phase C current [I_{C7}].

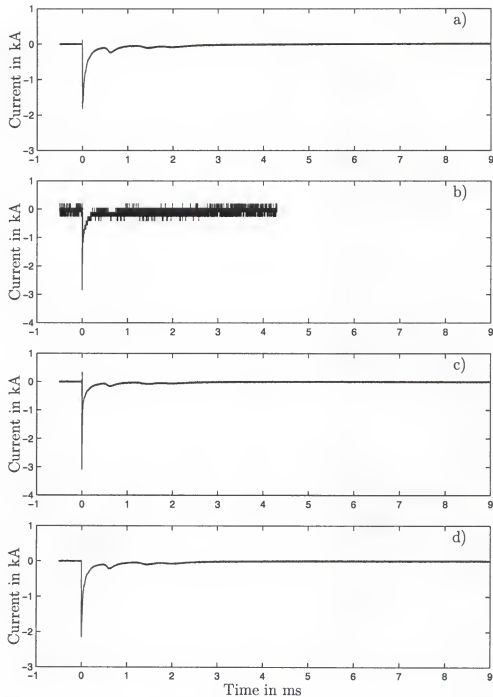


Figure H.21: Currents to ground versus time waveforms at Poles 7, 8, 11, and 12 for the first return stroke of Flash UF-9916, displayed on a 10 ms scale. a) Current to ground at pole 7 [I_{G7}]; b) Current to ground at pole 8 [I_{G8}]; c) Current to ground at pole 11 [I_{G11}]; d) Current to ground at pole 12 [I_{G12}].

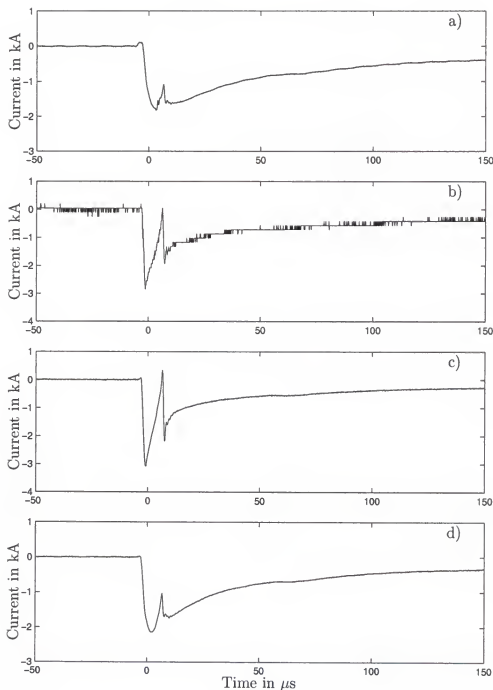


Figure H.22: Currents to ground versus time waveforms at Poles 7, 8, 11, and 12 for the first return stroke of Flash UF-9916, displayed on a $200 \mu s$ scale. a) Current to ground at pole 7 [I_{G7}]; b) Current to ground at pole 8 [I_{G8}]; c) Current to ground at pole 11 [I_{G11}]; d) Current to ground at pole 12 [I_{G12}].

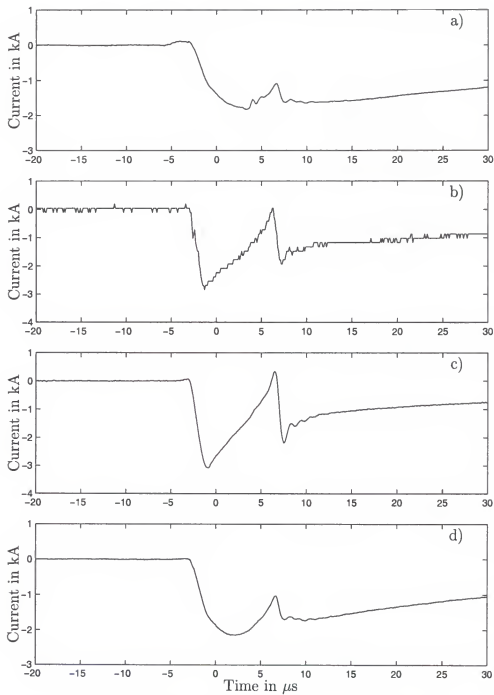


Figure H.23: Currents to ground versus time waveforms at Poles 7, 8, 11, and 12 for the first return stroke of Flash UF-9916, displayed on a $50\ \mu$ s scale. a) Current to ground at pole 7 [I_{G7}]; b) Current to ground at pole 8 [I_{G8}]; c) Current to ground at pole 11 [I_{G11}]; d) Current to ground at pole 12 [I_{G12}].

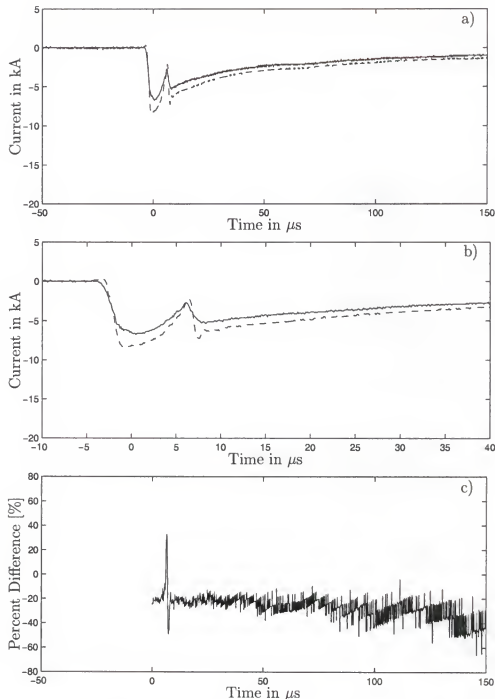


Figure H.24: Comparison of the sum of currents to ground ($\sum I_G = I_{G7} + I_{G8} + I_{G11} + I_{G12}$) and the total lightning current [I_i] for the first return stroke of Flash UF-9916, displayed on $200\mu\text{s}$ and $50\mu\text{s}$. The dashed line is the sum of currents to ground ($\sum I_G$) and the solid line is the lightning channel current. a) $200\mu\text{s}$; b) $50\mu\text{s}$; c) Percent difference between currents to ground and lightning channel current calculated as follows: $\Delta I\% = [(I_i(t) - \sum I_G)/I_i(t)] * 100$.

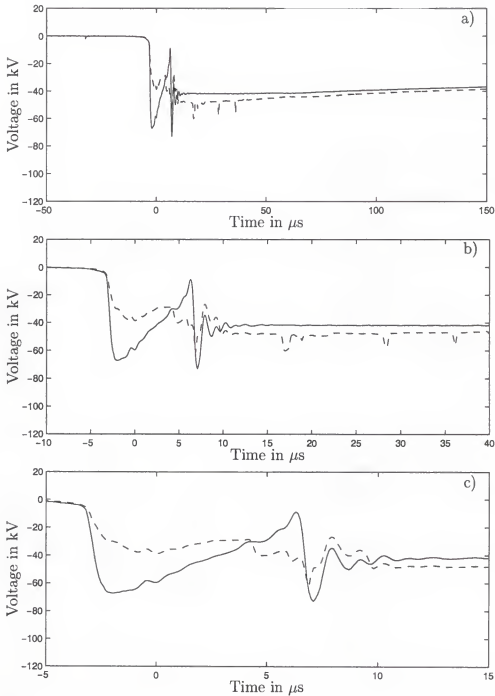


Figure H.25: Comparison of computed difference between measured voltages (V_{BN8} and V_{AN8}) and measured voltage $[V_{BA8}]$ for the first return stroke of Flash UF-9916, displayed in different time windows. The dashed line is the calculated voltage ($V_{BN8} - V_{AN8}$) that was obtained by subtracting the measurements of $[V_{BN8}]$ and $[V_{AN8}]$. a) $200\ \mu s$. b) $50\ \mu s$. c) $20\ \mu s$.

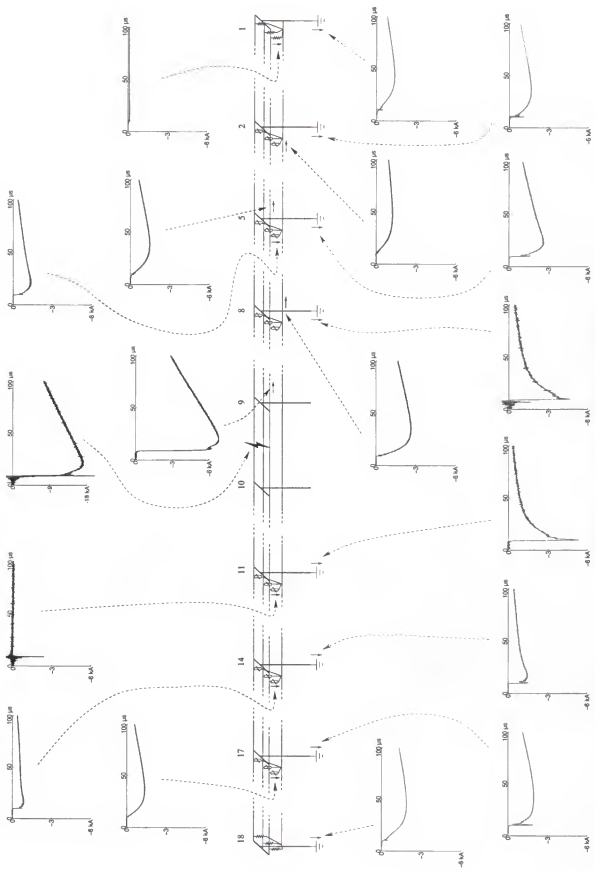


Figure H.26: Flash FPL0011, stroke 1.

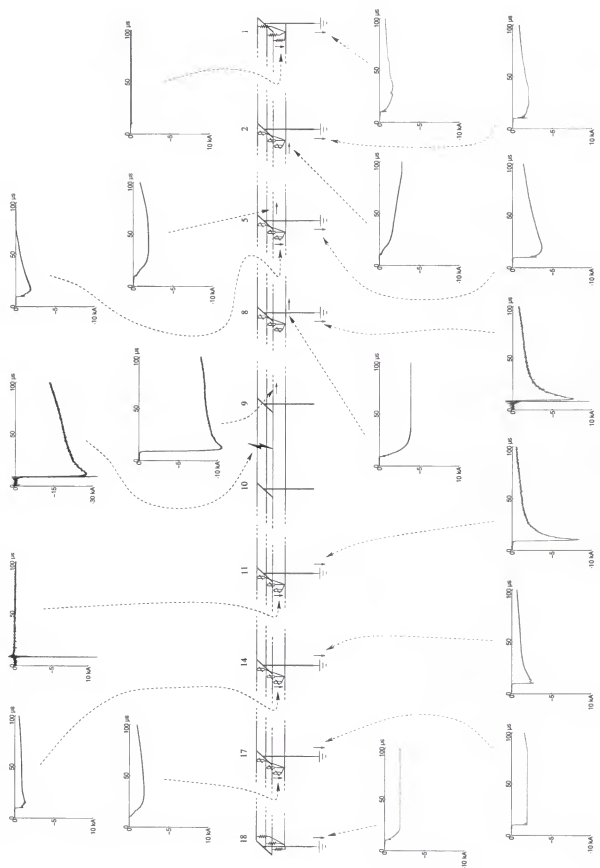


Figure H.27. Flash FPL0011, stroke 2.

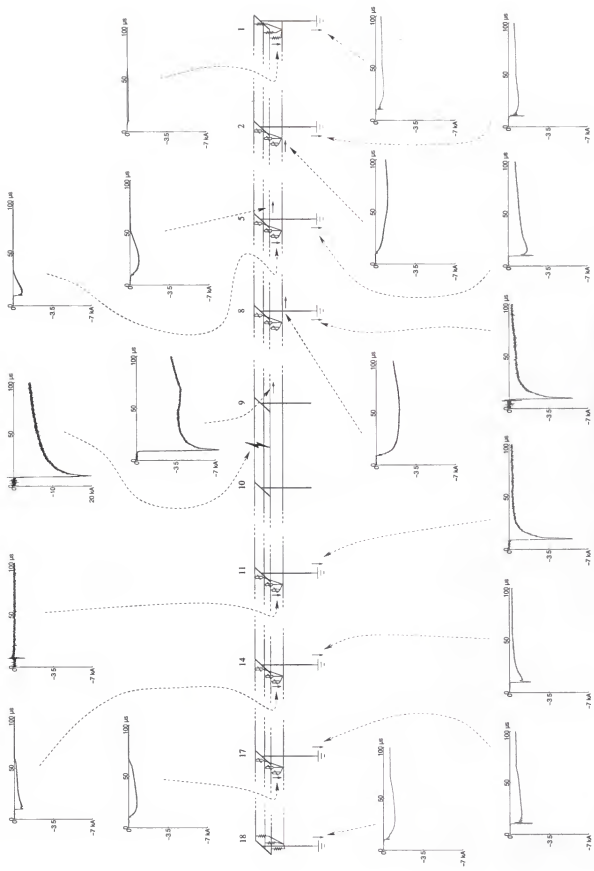


Figure H.28: Flash FPL0011, stroke 3.

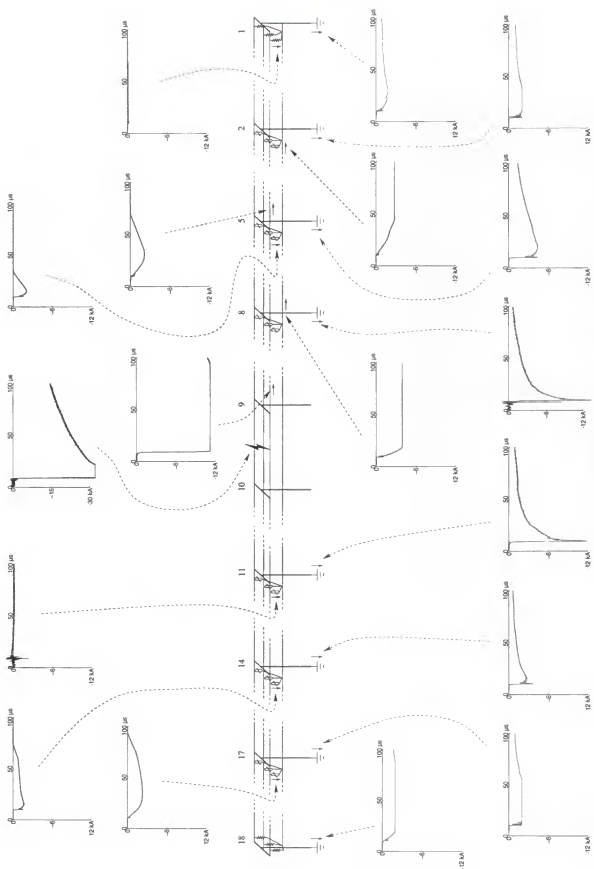


Figure H.29: Flash FPL0011, stroke 4.

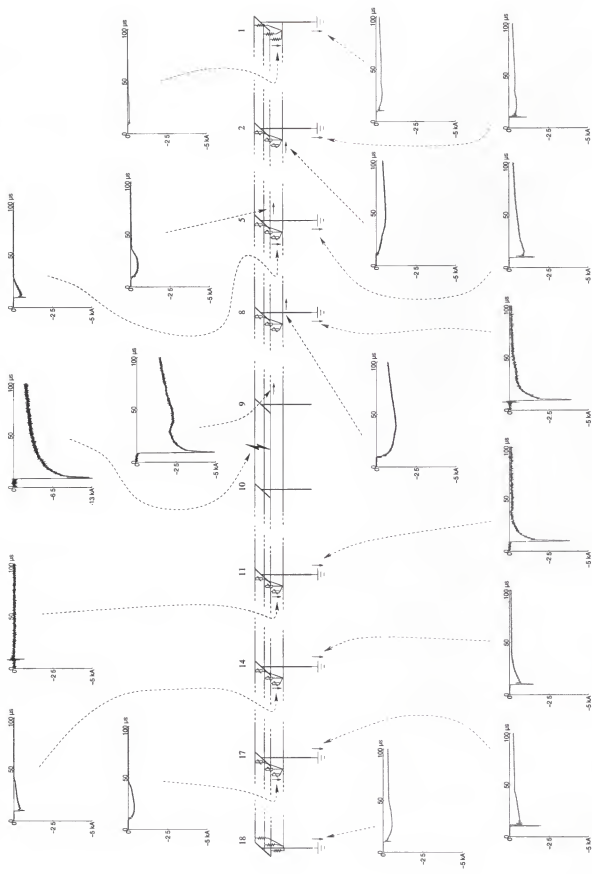


Figure H.30: Flash FPL0011, stroke 5.

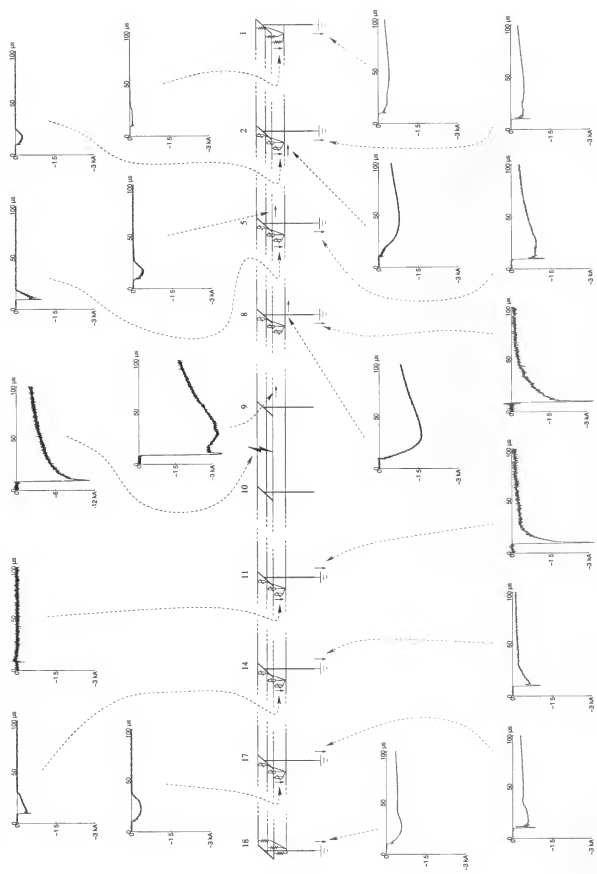


Figure H.31: Flash FPL0014, stroke 1.

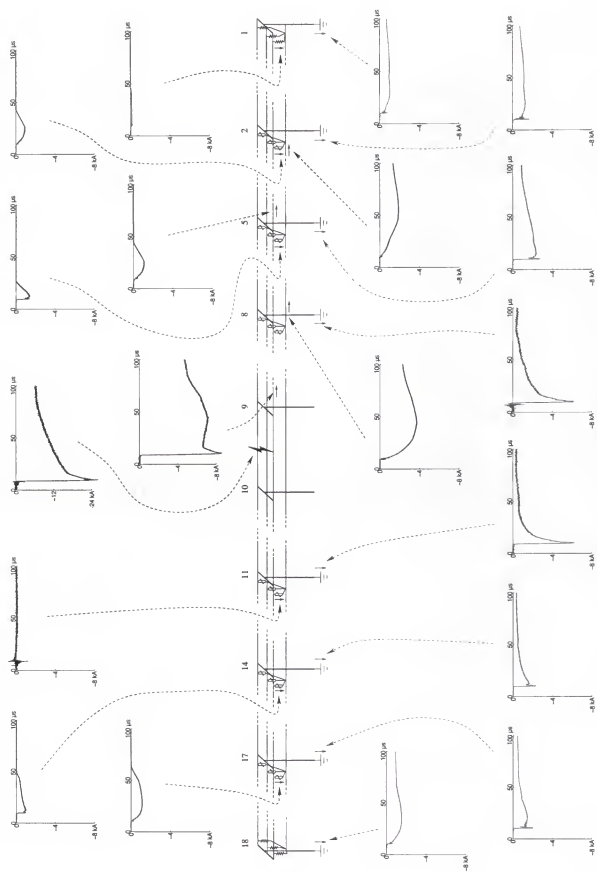


Figure H.32. Flash FPL0014, stroke 2.

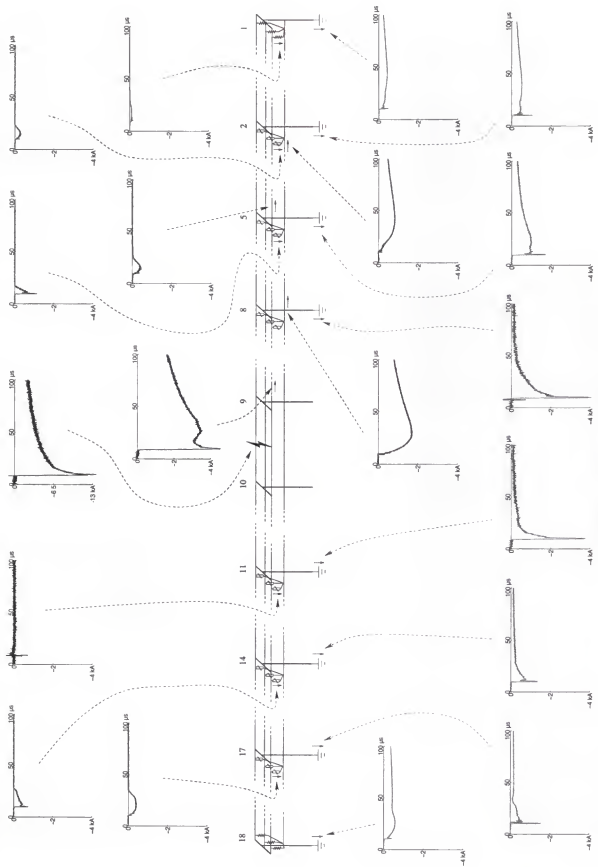


Figure H.33: Flash FPL0014, stroke 3.

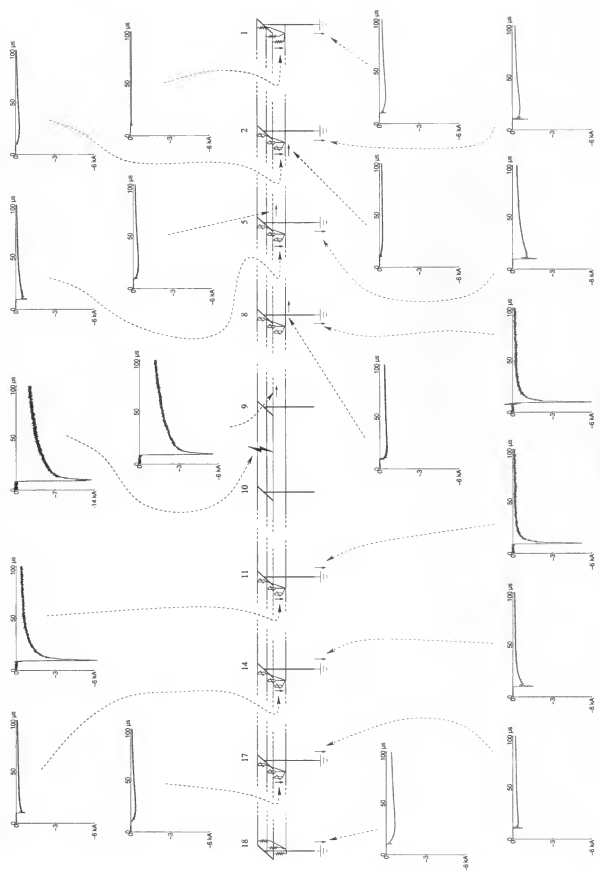


Figure H.34: Flash FPL0018, stroke 1.

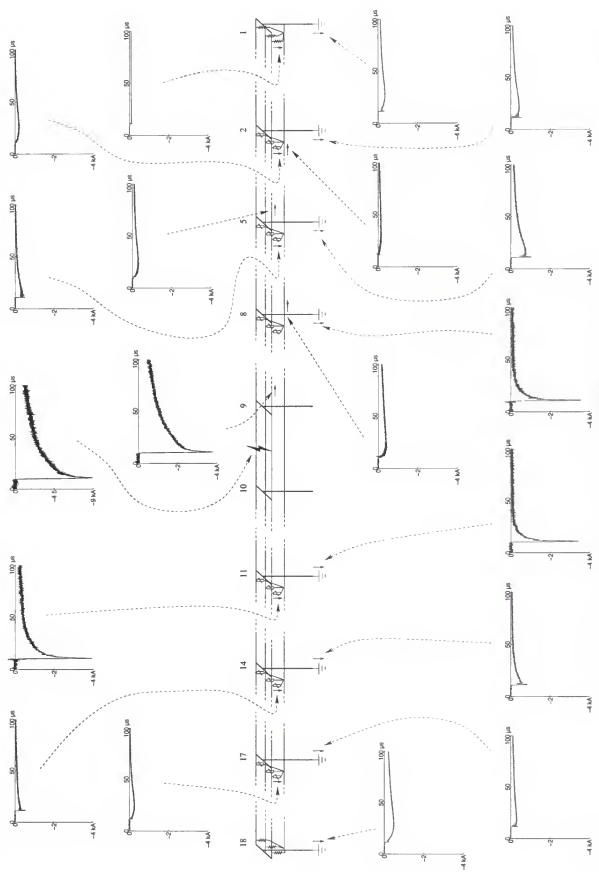


Figure H.35. Flash FPL0018, stroke 2.

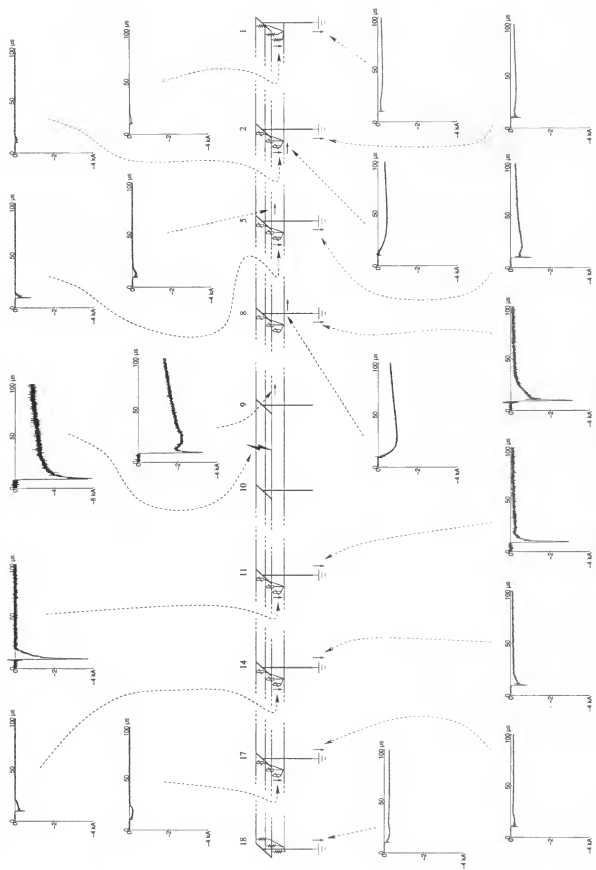


Figure H.36: Flash FPL0018, stroke 3.

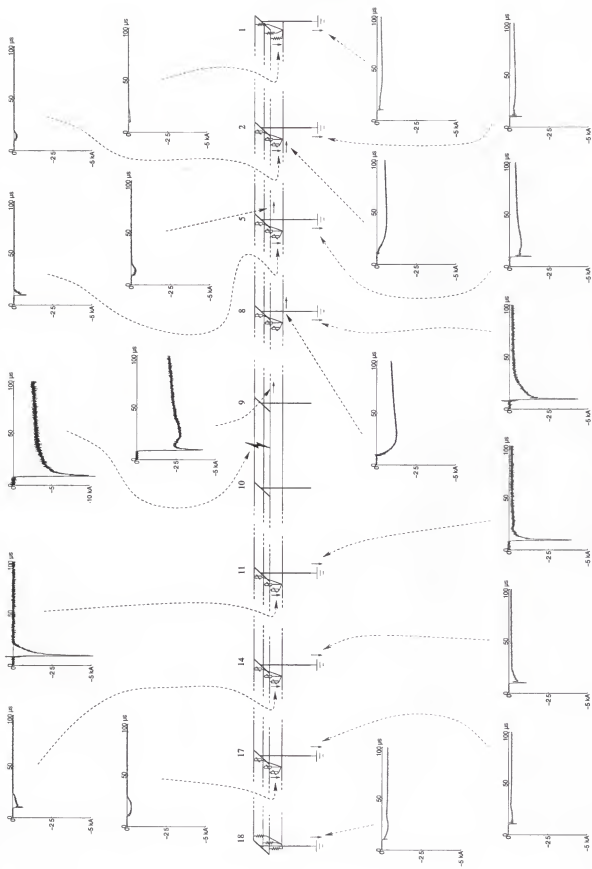


Figure H.37: Flash FPL0018, stroke 4.

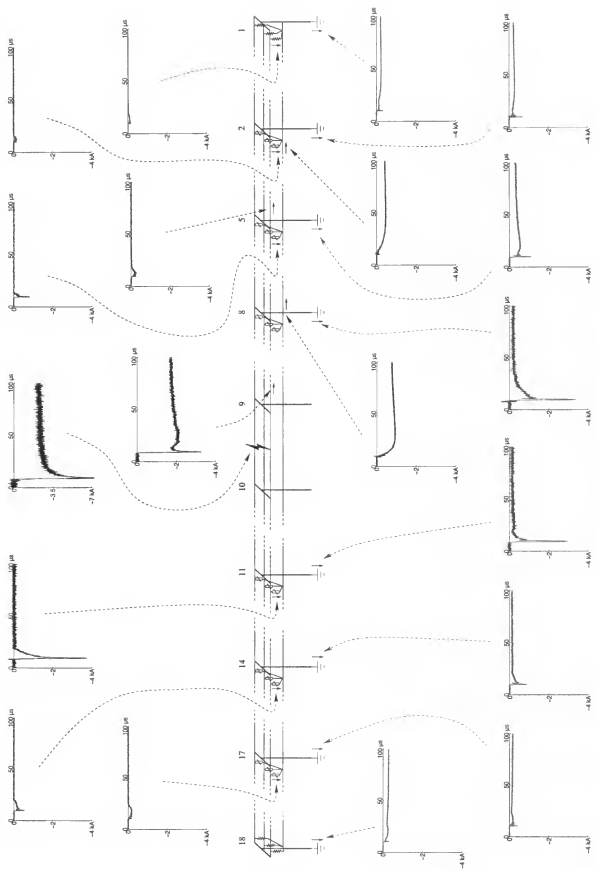


Figure H.38: Flash FPL0018, stroke 5.

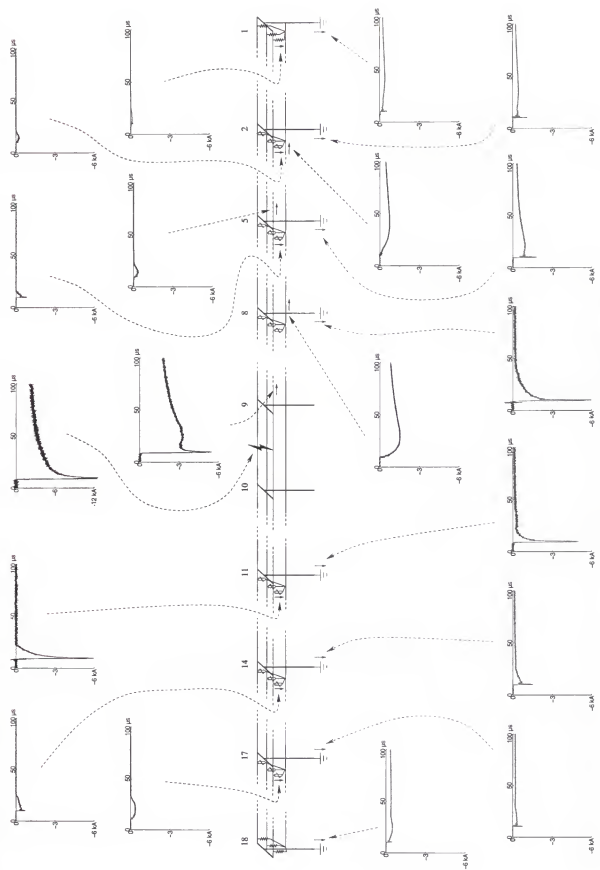


Figure H.39: Flash FPL0018, stroke 6.

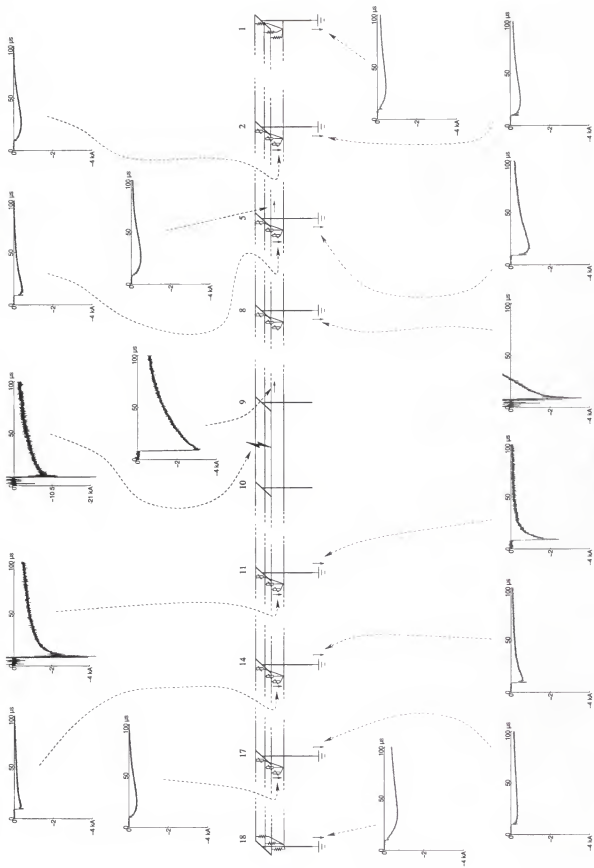


Figure H.40: Flash FPL0032, stroke 1.

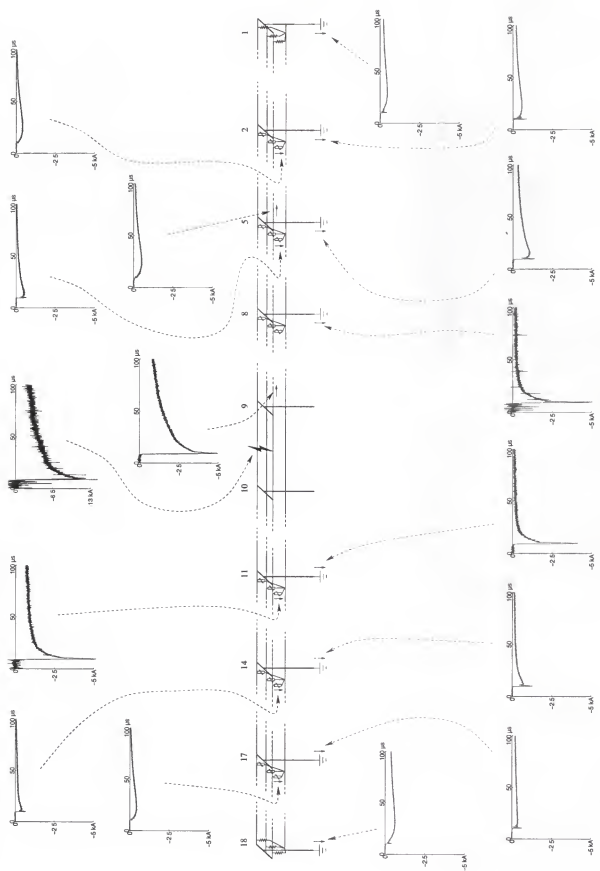


Figure H.41: Flash FPL0032, stroke 2.

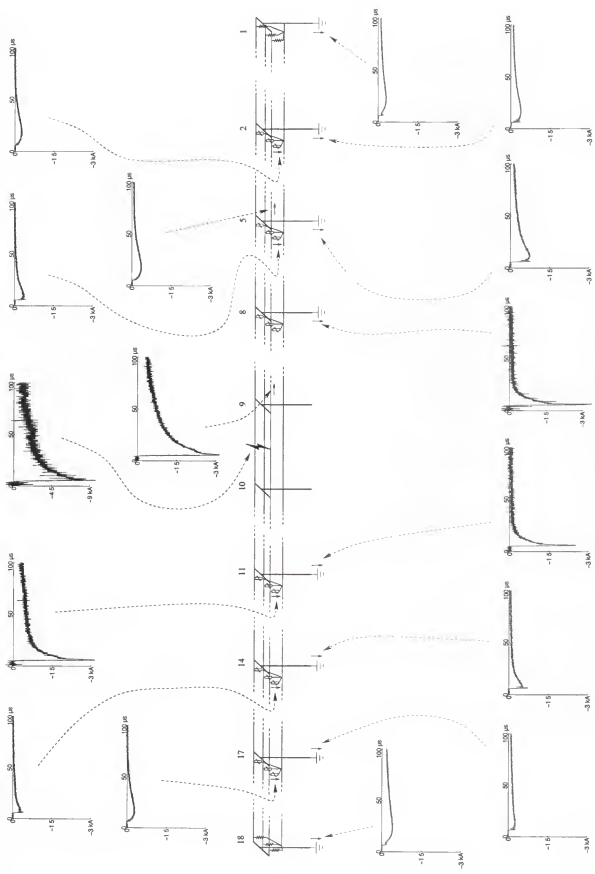


Figure H.42: Flash FPL032, stroke 3.

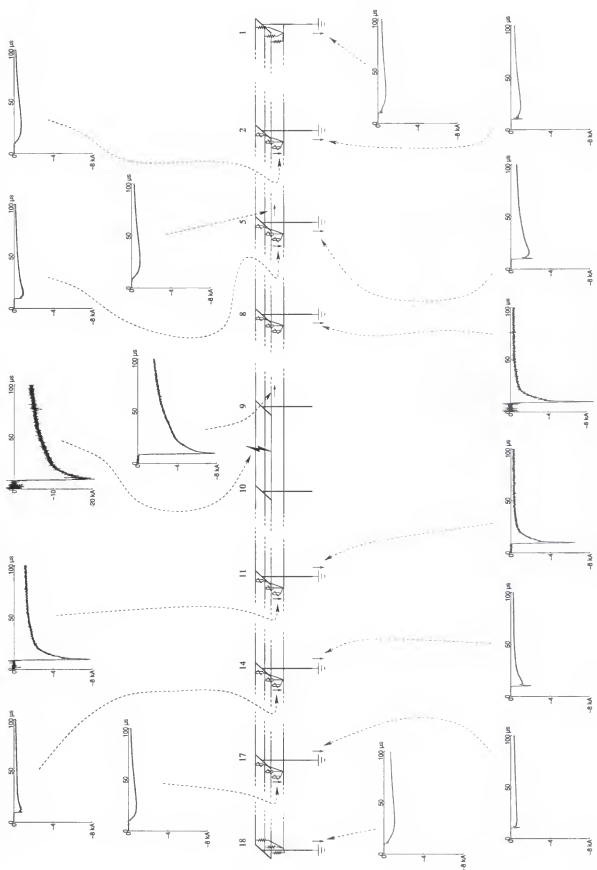


Figure H.43: Flash FPL0032, stroke 4.

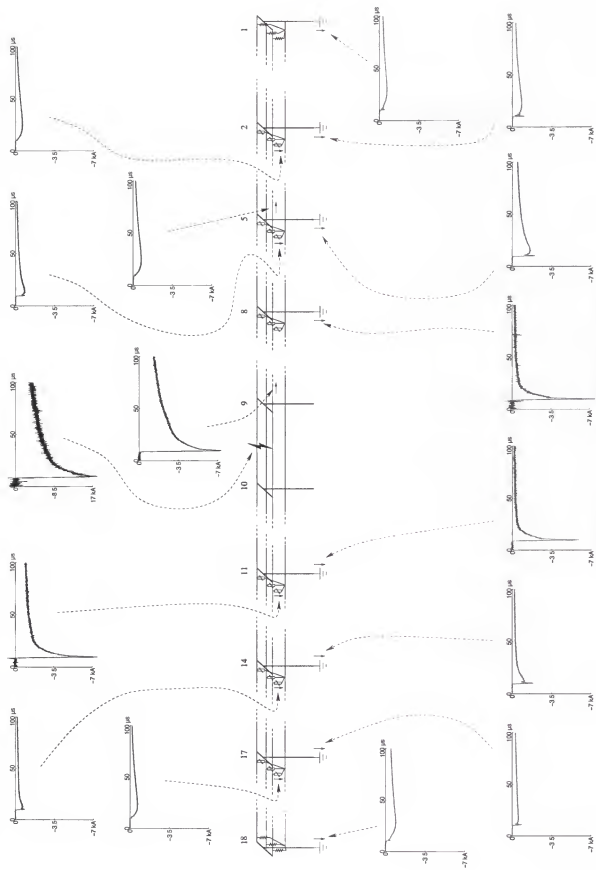


Figure H.44: Flash FPL0032, stroke 5.

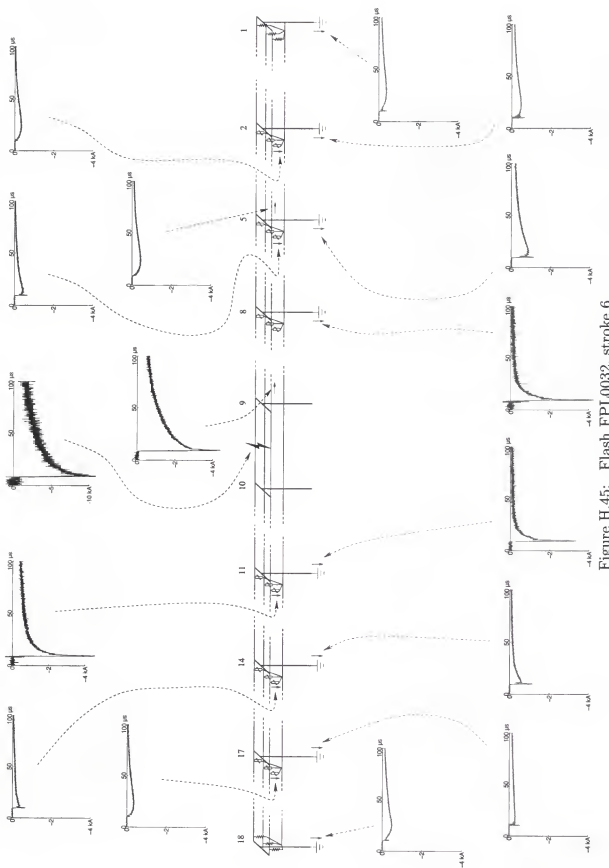


Figure H.45: Flash FPL0032, stroke 6.

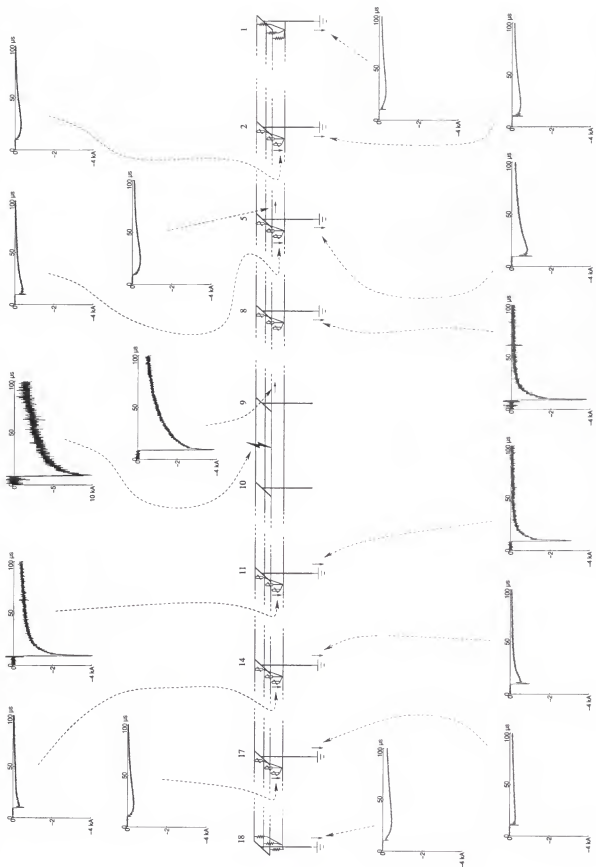


Figure H.46: Flash FPL0032, stroke 7.

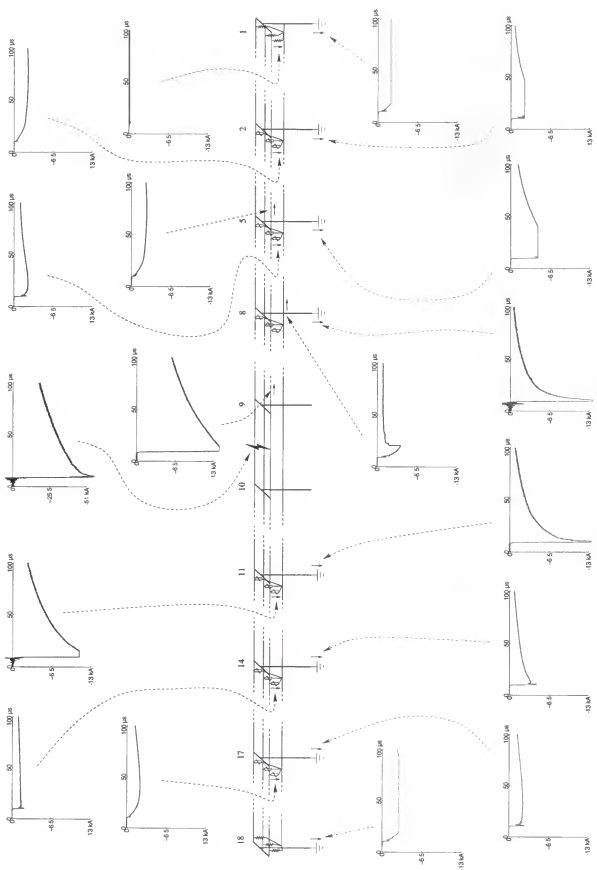


Figure H.47: Flash FPL0033, stroke 1.

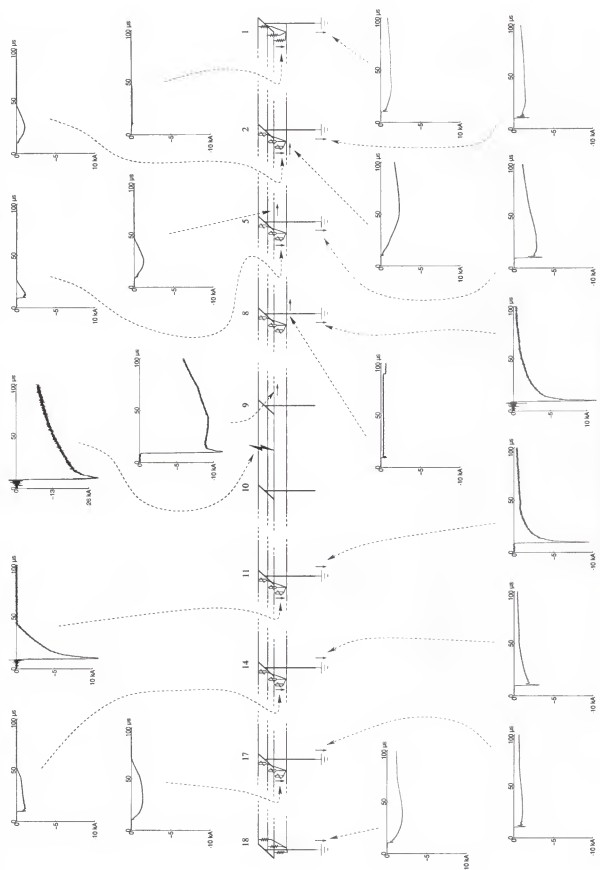


Figure H.48: Flash FPL0034, stroke 1.

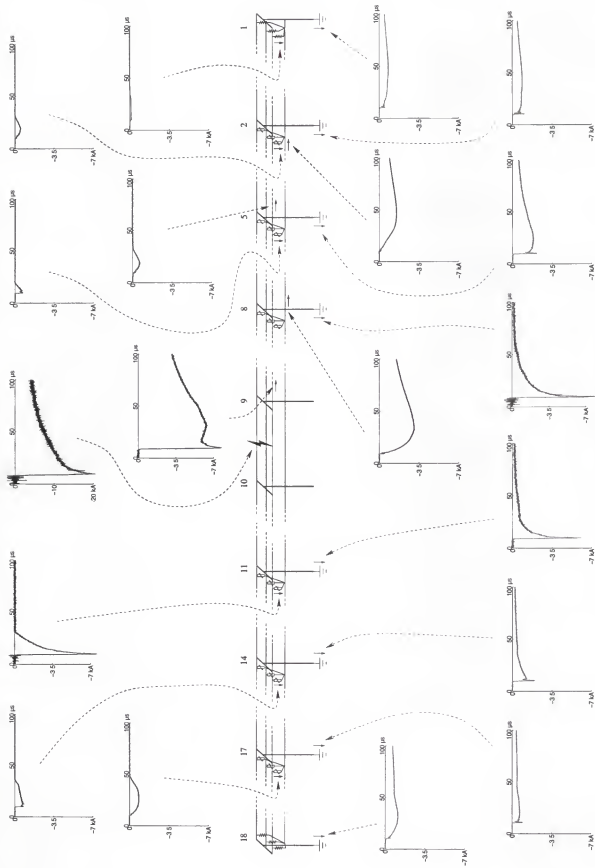


Figure H.49: Flash FPL0034, stroke 2.

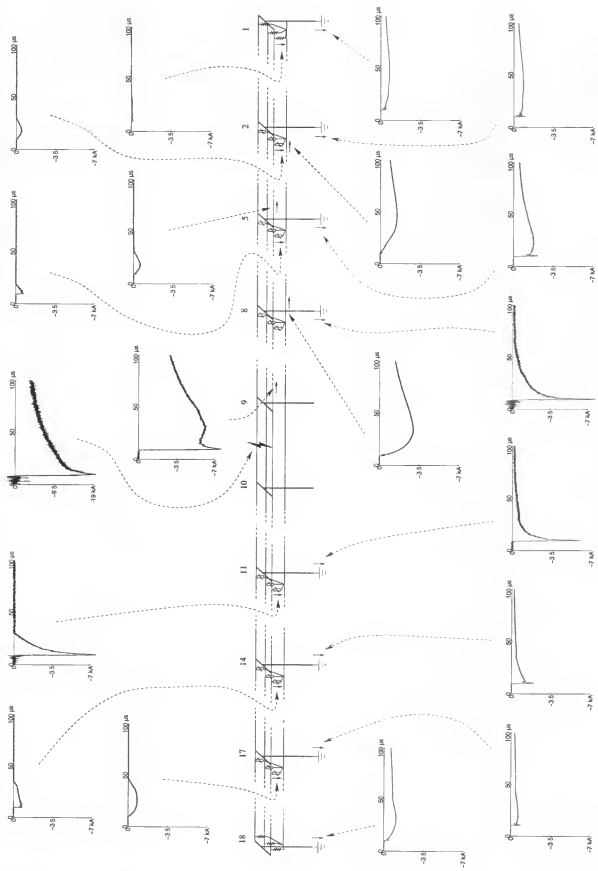


Figure H.50: Flash FPI0034, stroke 3.

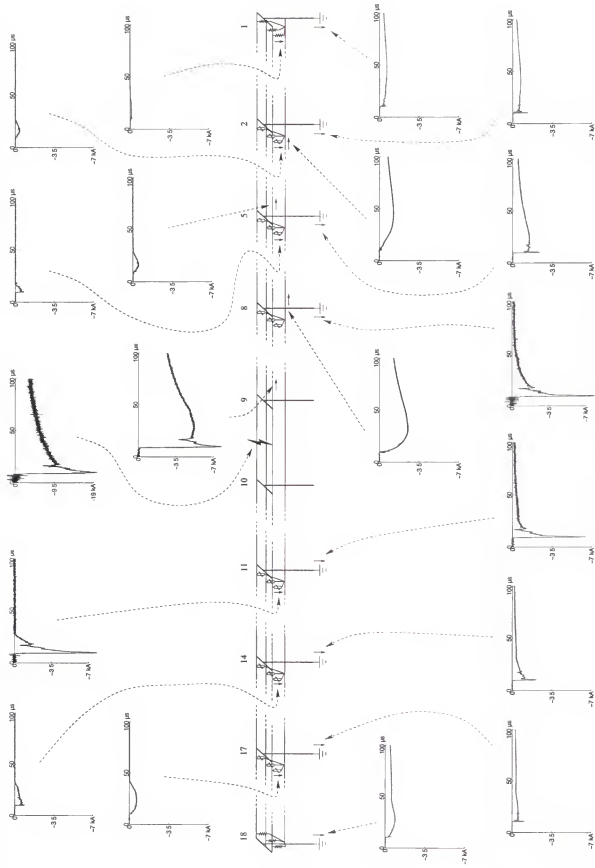


Figure H.51: Flash FPL0034, stroke 4.

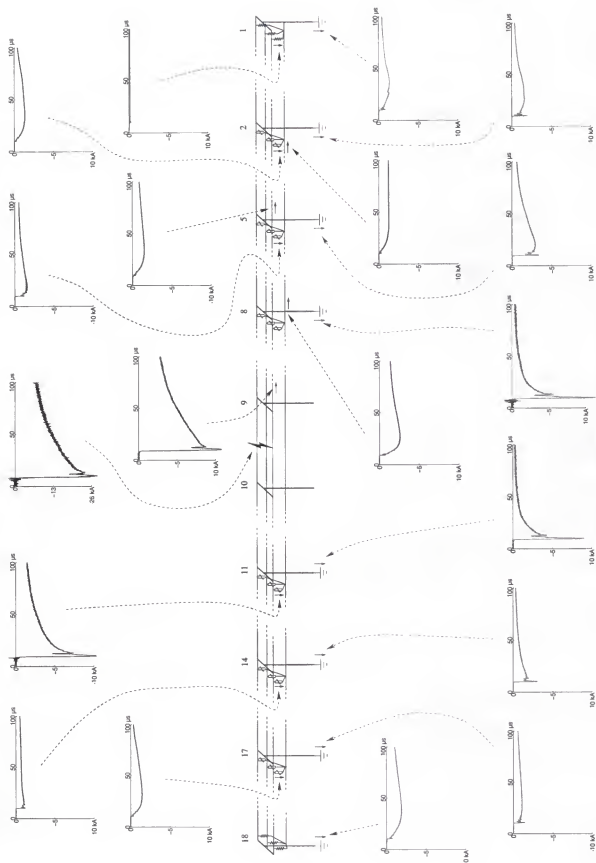


Figure H.52: Flash FPL0036, stroke 2.

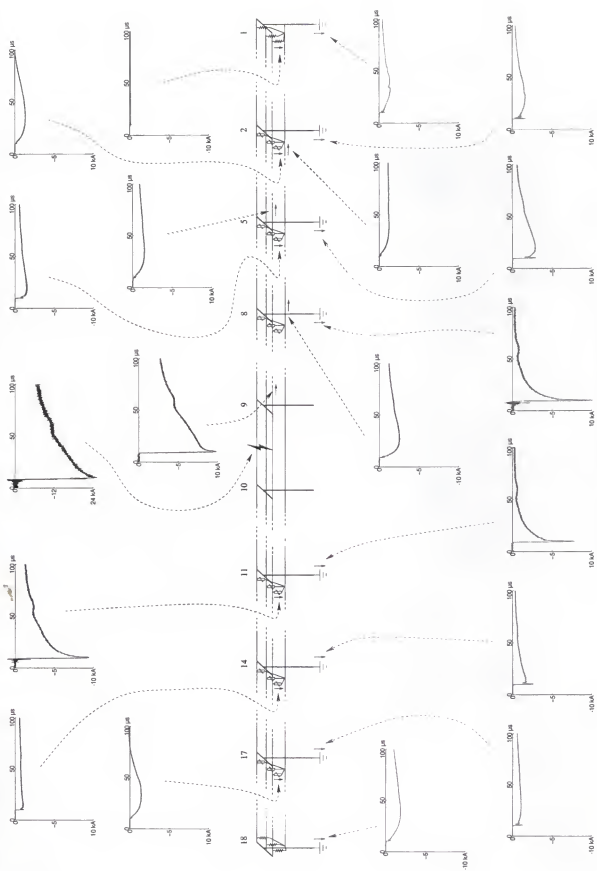


Figure H.53: Flash FPL0036, stroke 3.

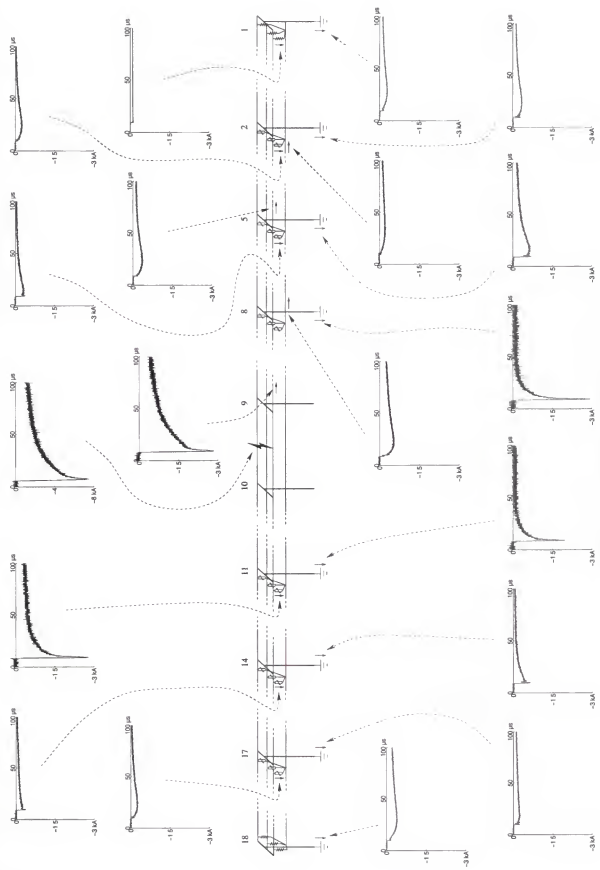


Figure H.54: Flash FPL0036, stroke 4.

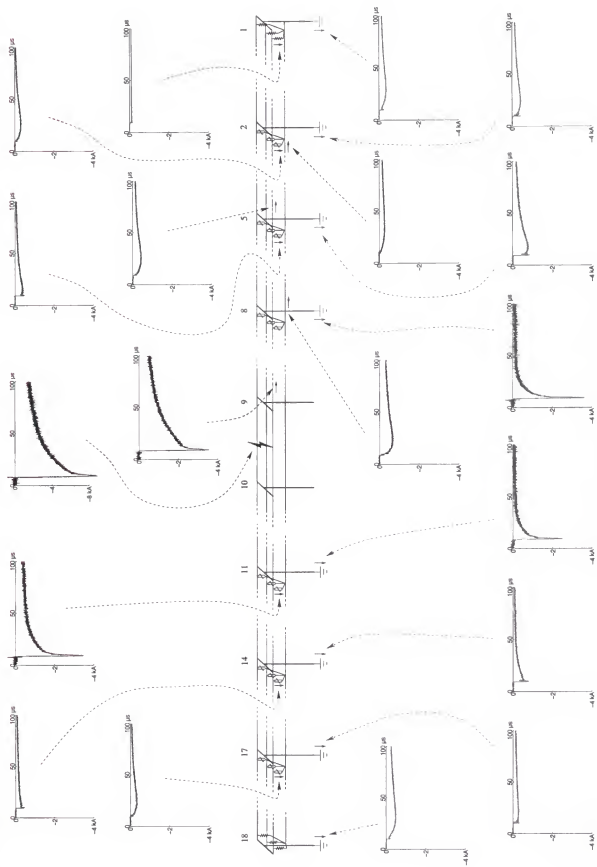


Figure H.55: Flash FPL0036, stroke 5.

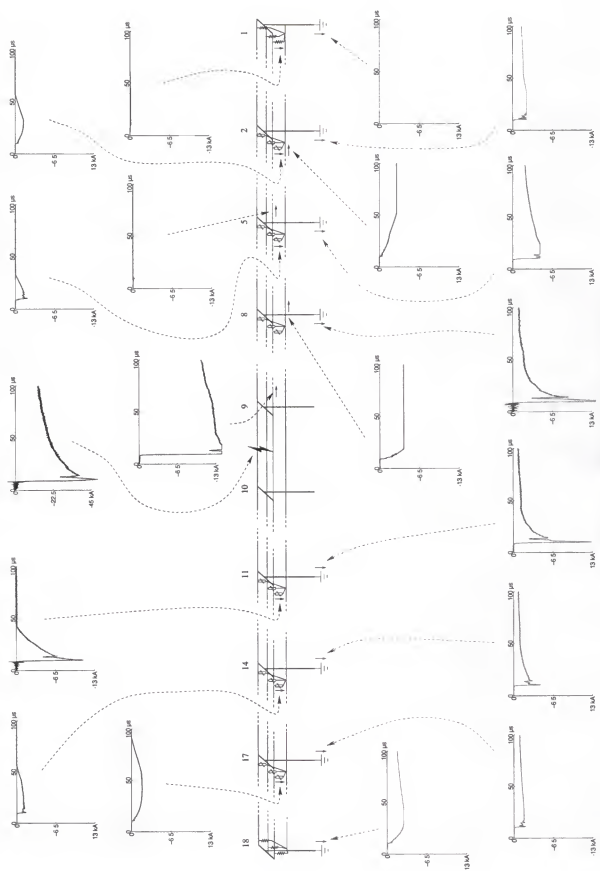


Figure H.56: Flash FPL0037, stroke 1.

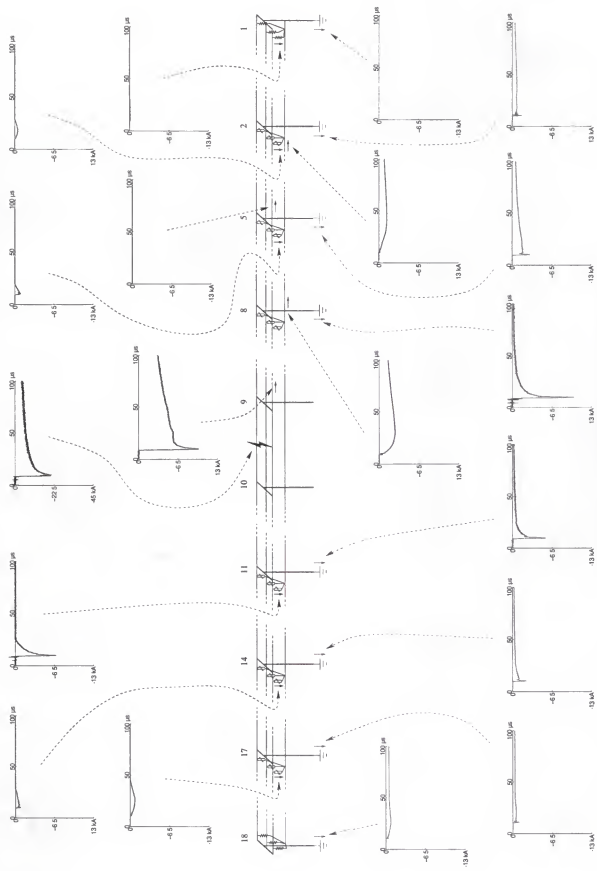


Figure H.57. Flash FPL0037, stroke 2.

APPENDIX I CHARACTERISTICS OF CURRENT WAVEFORMS FOR THE 2000 EXPERIMENTS

In this appendix we present, in tabular form, the various characteristics of measured current waveforms for every return stroke of each flash triggered in the 2000 experiments. Frequency domain analysis tables and 3-D bar plots (Figures I.1, I.2, I.3, I.4, I.5, I.6, I.7, I.8, I.9, I.10, I.11, I.12, I.13, I.14, I.15, and I.16), showing the charge transferred to ground at different points on the line, are additionally presented for flashes FPL0014, FPL0018, FPL0034, FPL0036, and FPL0037, in which no triggering wires were involved (trailing wires going over the transmission line at the time of a trigger).

The time domain tables (Tables I.1, I.2, I.3, I.4, I.5, I.6, I.8, I.10, I.12, I.14, I.16, I.18, I.20, I.22, I.24, I.25, I.26, I.27, I.28, I.29, I.30, I.31, I.32, I.34, I.36, I.38, I.40, I.42, I.44, I.46, I.48, I.50, I.52, and I.54) contain information on the peak current and charge transferred (calculated from current waveforms) in three different time windows ($100\mu s$, $500\mu s$, and 1 ms). The frequency domain tables (Tables I.7, I.9, I.11, I.13, I.15, I.17, I.19, I.21, I.23, I.33, I.35, I.37, I.39, I.41, I.43, I.45, I.47, I.49, I.51, I.53, and I.55) give the power spectrum density (Embree and Danieli 1999) integrated over a frequency band (a measure of the power of the signal in that frequency band) in percentage of the power spectrum density integrated over the bandwidth of the measurement (see Section 6.3).

Table I.1: Peak current and charge transferred at different points in the system calculated at three different instants of time ($100\ \mu s$, $500\ \mu s$, and $1\ ms$) for stroke 1 of flash FPL0011.

| ID | Peak [kA] | Charge calculated in different time windows | | | | | | Saturation | |
|------------|--------------|---|-------|-------------|-------|--------|-------|------------|--|
| | | 100 μs | | 500 μs | | 1 ms | | | |
| | | [C] | % | [C] | % | [C] | % | | |
| I_t | -17.04 | -1.17 | 100.0 | -2.50 | 100.0 | -2.88 | 100.0 | Slight | |
| I_{Mi} | <-15.97 | <-1.16 | >99.0 | <-2.47 | >98.6 | <-2.82 | >98.2 | Severe | |
| I_{Li} | <-1.20 | <-0.11 | >9.5 | <-0.57 | >22.9 | <-0.83 | >28.9 | Severe | |
| I_{CN1} | -0.16 | -0.01 | 0.8 | -0.04 | 1.7 | -0.07 | 2.6 | - | |
| I_{G1} | -1.40 | -0.10 | 8.4 | -0.22 | 9.0 | -0.26 | 9.1 | Slight | |
| I_{CN2} | - | - | - | - | - | - | - | - | |
| I_{N2} | -1.25 | -0.09 | 7.8 | -0.27 | 10.9 | -0.31 | 10.7 | - | |
| I_{G2} | -1.66 | -0.12 | 10.0 | -0.25 | 10.0 | -0.29 | 10.1 | Slight | |
| I_{CN5} | -1.46 | -0.08 | 6.6 | -0.11 | 4.2 | -0.11 | 3.7 | - | |
| I_{A5} | -0.24 | -0.00 | 0.1 | -0.00 | 0.0 | -0.00 | 0.0 | - | |
| I_{B5} | - | - | - | - | - | - | - | - | |
| I_{C5} | -1.47 | -0.10 | 8.5 | -0.16 | 6.5 | -0.20 | 6.9 | - | |
| I_{G5} | -2.76 | -0.17 | 14.2 | -0.34 | 13.7 | -0.39 | 13.7 | - | |
| I_{AN8} | -2.76 | -0.17 | 14.2 | -0.34 | 13.7 | -0.39 | 13.7 | - | |
| I_{BN8} | -0.07 | 0.00 | 0.1 | 0.00 | 0.0 | -0.00 | 0.0 | - | |
| I_{CNS} | -0.07 | 0.00 | 0.1 | 0.00 | 0.0 | -0.00 | 0.0 | - | |
| I_{N8} | -2.67 | -0.20 | 16.9 | -0.54 | 21.7 | -0.63 | 21.8 | - | |
| I_{G8} | -2.67 | -0.20 | 16.9 | -0.54 | 21.7 | -0.63 | 21.8 | - | |
| I_{A9} | -0.18 | -0.00 | 0.0 | 0.00 | 0.0 | 0.00 | 0.0 | - | |
| I_{B9} | -0.43 | 0.00 | 0.0 | 0.00 | 0.0 | 0.00 | 0.0 | - | |
| I_{C9} | -6.87 | -0.46 | 39.6 | -0.94 | 37.7 | -1.11 | 38.8 | - | |
| I_{CN11} | - | - | - | - | - | - | - | - | |
| I_{G11} | -5.10 | -0.10 | 8.6 | -0.18 | 7.4 | -0.21 | 7.3 | - | |
| I_{CN14} | -0.90 | -0.05 | 4.6 | -0.09 | 3.6 | -0.09 | 3.1 | - | |
| I_{G14} | -1.48 | -0.07 | 6.4 | -0.15 | 6.1 | -0.18 | 6.1 | - | |
| I_{CN17} | -1.40 | -0.09 | 7.8 | -0.13 | 5.2 | -0.13 | 4.6 | - | |
| I_{G17} | <-1.96 | <-0.15 | >12.5 | <-0.29 | >11.4 | <-0.31 | >10.9 | Severe | |
| I_{G18} | <-1.90 | <-0.14 | >12.0 | <-0.35 | >14.2 | <-0.42 | >14.5 | Severe | |

Table I.2: Peak current and charge transferred at different points in the system calculated at three different instants of time ($100\ \mu s$, $500\ \mu s$, and $1\ ms$) for stroke 2 of flash FPL0011.

| ID | Peak [kA] | Charge calculated in different time windows | | | | | | Saturation | |
|------------|--------------|---|--------|-------------|--------|--------|--------|------------|--|
| | | 100 μs | | 500 μs | | 1 ms | | | |
| | | [C] | % | [C] | % | [C] | % | | |
| I_i | <-27.71 | <-1.74 | >100.0 | <-3.94 | >100.0 | <-6.24 | >100.0 | Severe | |
| I_{Mi} | <-15.97 | <-1.44 | >82.6 | <-3.62 | >91.9 | <-5.90 | >94.4 | Severe | |
| I_{Li} | <-1.20 | <-0.11 | >6.4 | <-0.57 | >14.5 | <-1.13 | >18.0 | Severe | |
| I_{CN1} | -0.23 | -0.01 | 0.6 | -0.03 | 0.8 | -0.04 | 0.6 | Slight | |
| I_{G1} | -1.69 | -0.10 | 5.9 | -0.22 | 5.6 | -0.35 | 5.7 | Slight | |
| I_{CN2} | - | - | - | - | - | - | - | - | |
| I_{N2} | <-2.80 | <-0.18 | >10.2 | <-0.99 | >25.2 | <-1.33 | >21.3 | Severe | |
| I_{G2} | <-2.01 | <-0.13 | >7.6 | <-0.28 | >7.0 | <-0.43 | >7.0 | Severe | |
| I_{CN5} | -2.02 | -0.06 | 3.3 | -0.06 | 1.5 | -0.06 | 0.9 | - | |
| I_{A5} | -0.57 | -0.00 | 0.2 | -0.00 | 0.1 | -0.00 | 0.1 | - | |
| I_{B5} | - | - | - | - | - | - | - | - | |
| I_{C5} | -1.96 | -0.14 | 8.1 | -0.17 | 4.4 | -0.18 | 2.8 | - | |
| I_{G5} | -3.83 | -0.22 | 12.8 | -0.40 | 10.2 | -0.61 | 9.8 | Slight | |
| I_{AN8} | -3.83 | -0.22 | 12.8 | -0.40 | 10.2 | -0.61 | 9.8 | Slight | |
| I_{BN8} | -1.12 | -0.00 | 0.1 | -0.00 | 0.1 | -0.00 | 0.1 | - | |
| I_{CN8} | -1.12 | -0.00 | 0.1 | -0.00 | 0.1 | -0.00 | 0.1 | - | |
| I_{N8} | <-3.96 | <-0.34 | >19.3 | <-0.85 | >21.7 | <-0.85 | >13.6 | Severe | |
| I_{G8} | -7.74 | -0.19 | 10.7 | -0.27 | 7.0 | -0.39 | 6.3 | - | |
| I_{A9} | -0.36 | -0.00 | 0.1 | -0.00 | 0.0 | -0.00 | 0.0 | - | |
| I_{B9} | <-0.80 | <-0.01 | >0.7 | <-0.02 | >0.5 | <-0.02 | >0.4 | Severe | |
| I_{C9} | -10.54 | -0.79 | 45.4 | -2.41 | 61.2 | -4.16 | 66.5 | Slight | |
| I_{CN11} | - | - | - | - | - | - | - | - | |
| I_{G11} | -8.32 | -0.15 | 8.3 | -0.22 | 5.7 | -0.33 | 5.3 | - | |
| I_{CN14} | -1.42 | -0.08 | 4.4 | -0.09 | 2.2 | -0.09 | 1.4 | - | |
| I_{G14} | -2.70 | -0.11 | 6.1 | -0.19 | 4.8 | -0.28 | 4.5 | - | |
| I_{CN17} | -1.90 | -0.13 | 7.5 | -0.16 | 4.0 | -0.16 | 2.5 | - | |
| I_{G17} | <-1.98 | <-0.17 | >10.0 | <-0.31 | >8.0 | <-0.47 | >7.5 | Severe | |
| I_{G18} | <-1.93 | <-0.17 | >9.5 | <-0.40 | >10.2 | <-0.63 | >10.2 | Severe | |

Table I.3: Peak current and charge transferred at different points in the system calculated at three different instants of time ($100\ \mu s$, $500\ \mu s$, and $1\ ms$) for stroke 3 of flash FPL0011.

| ID | Peak [kA] | Charge calculated in different time windows | | | | | | Saturation | |
|------------|--------------|---|-------|--------------|-------|--------|-------|------------|--|
| | | $100\ \mu s$ | | $500\ \mu s$ | | 1 ms | | | |
| | | [C] | % | [C] | % | [C] | % | | |
| I_i | -19.33 | -0.62 | 100.0 | -1.72 | 100.0 | -3.02 | 100.0 | - | |
| I_{M1} | <-15.97 | <-0.62 | >99.1 | <-1.69 | >98.2 | <-2.96 | >97.9 | Severe | |
| I_{L4} | <-1.20 | <-0.11 | >17.8 | <-0.57 | >33.3 | <-1.15 | >38.0 | Severe | |
| I_{CN1} | -0.19 | -0.00 | 0.8 | -0.01 | 0.4 | -0.01 | 0.3 | - | |
| I_{G1} | -0.73 | -0.05 | 8.2 | -0.15 | 8.8 | -0.27 | 8.9 | - | |
| I_{CN2} | - | - | - | - | - | - | - | - | |
| I_{N2} | -1.08 | -0.08 | 12.1 | -0.26 | 15.3 | -0.47 | 15.7 | - | |
| I_{G2} | -1.32 | -0.06 | 9.8 | -0.17 | 10.0 | -0.30 | 10.0 | - | |
| I_{CN5} | -0.92 | -0.01 | 1.8 | -0.01 | 0.7 | -0.01 | 0.4 | - | |
| I_{A5} | -0.34 | -0.00 | 0.1 | -0.00 | 0.0 | -0.00 | 0.0 | - | |
| I_{B5} | - | - | - | - | - | - | - | - | |
| I_{C5} | -0.79 | -0.02 | 3.6 | -0.03 | 1.5 | -0.03 | 1.0 | - | |
| I_{G5} | -2.25 | -0.09 | 14.6 | -0.24 | 13.9 | -0.41 | 13.7 | - | |
| I_{AN8} | -2.25 | -0.09 | 14.6 | -0.24 | 13.9 | -0.41 | 13.7 | - | |
| I_{BN8} | -2.25 | -0.09 | 14.6 | -0.24 | 13.9 | -0.41 | 13.7 | - | |
| I_{CN8} | -6.62 | -0.31 | 50.2 | -1.10 | 64.2 | -2.04 | 67.4 | - | |
| I_{N8} | -2.07 | -0.16 | 26.2 | -0.49 | 28.8 | -0.51 | 16.7 | - | |
| I_{G8} | -5.65 | -0.07 | 11.4 | -0.16 | 9.2 | -0.26 | 8.6 | - | |
| I_{A9} | -0.15 | 0.00 | 0.0 | 0.00 | 0.0 | 0.00 | 0.0 | - | |
| I_{B9} | <-0.78 | <0.00 | >0.0 | <0.00 | >0.0 | <0.00 | >0.0 | Severe | |
| I_{C9} | -7.27 | -0.35 | 56.3 | -1.16 | 67.6 | -2.12 | 70.1 | - | |
| I_{CN11} | - | - | - | - | - | - | - | - | |
| I_{G11} | -5.48 | -0.05 | 8.2 | -0.13 | 7.3 | -0.22 | 7.2 | - | |
| I_{CN14} | -0.78 | -0.02 | 2.5 | -0.02 | 0.9 | -0.02 | 0.5 | - | |
| I_{G14} | -1.81 | -0.04 | 5.8 | -0.10 | 5.8 | -0.18 | 5.9 | - | |
| I_{CN17} | -0.76 | -0.03 | 4.5 | -0.03 | 1.6 | -0.03 | 1.0 | - | |
| I_{G17} | <-1.98 | <-0.07 | >10.8 | <-0.19 | >10.9 | <-0.33 | >10.8 | Severe | |
| I_{G18} | -1.03 | -0.07 | 10.9 | -0.22 | 13.0 | -0.42 | 13.8 | - | |

Table I.4: Peak current and charge transferred at different points in the system calculated at three different instants of time ($100\ \mu s$, $500\ \mu s$, and $1\ ms$) for stroke 4 of flash FPL0011.

| ID | Peak [kA] | Charge calculated in different time windows | | | | | | Saturation | |
|------------|--------------|---|--------|--------------|--------|--------|--------|------------|--|
| | | $100\ \mu s$ | | $500\ \mu s$ | | 1 ms | | | |
| | | [C] | % | [C] | % | [C] | % | | |
| I_i | <-31.93 | <-2.08 | >100.0 | <-4.41 | >100.0 | <-5.76 | >100.0 | Severe | |
| I_{M1} | <-15.97 | <-1.46 | >70.5 | <-3.78 | >85.7 | <-5.10 | >88.5 | Severe | |
| I_{L1} | <-1.20 | <-0.11 | >5.4 | <-0.57 | >13.0 | <-1.15 | >19.9 | Severe | |
| I_{CN1} | <-0.27 | <-0.01 | >0.4 | <-0.01 | >0.2 | <-0.01 | >0.1 | Severe | |
| I_{G1} | <-1.84 | <-0.11 | >5.4 | <-0.25 | >5.7 | <-0.34 | >5.9 | Severe | |
| I_{CN2} | - | - | - | - | - | - | - | - | |
| I_{N2} | <-2.80 | <-0.21 | >10.2 | <-0.62 | >14.0 | <-0.62 | >10.7 | Severe | |
| I_{G2} | <-2.01 | <-0.14 | >6.7 | <-0.29 | >6.5 | <-0.38 | >6.7 | Severe | |
| I_{CN5} | -2.17 | -0.03 | 1.4 | -0.03 | 0.7 | -0.03 | 0.5 | - | |
| I_{A5} | -0.73 | -0.01 | 0.3 | -0.01 | 0.2 | -0.01 | 0.1 | - | |
| I_{B5} | - | - | - | - | - | - | - | - | |
| I_{C5} | -2.14 | -0.08 | 3.7 | -0.08 | 1.8 | -0.08 | 1.4 | - | |
| I_{G5} | <-4.49 | <-0.26 | >12.4 | <-0.43 | >9.7 | <-0.55 | >9.5 | Severe | |
| I_{AN8} | <-4.49 | <-0.26 | >12.4 | <-0.43 | >9.7 | <-0.55 | >9.5 | Severe | |
| I_{BN8} | <-4.49 | <-0.26 | >12.4 | <-0.43 | >9.7 | <-0.55 | >9.5 | Severe | |
| I_{CN8} | <-11.20 | <-0.98 | >47.0 | <-2.74 | >62.1 | <-3.72 | >64.6 | Severe | |
| I_{N8} | <-3.96 | <-0.35 | >16.7 | <-0.53 | >12.0 | <-0.52 | >9.0 | Severe | |
| I_{G8} | <-12.83 | <-0.22 | >10.7 | <-0.29 | >6.7 | <-0.36 | >6.2 | Severe | |
| I_{A9} | -0.20 | 0.01 | 0.7 | 0.01 | 0.3 | 0.01 | 0.2 | - | |
| I_{B9} | <-0.80 | <0.00 | >0.1 | <0.00 | >0.0 | <0.00 | >0.0 | Severe | |
| I_{C9} | <-11.20 | <-1.02 | >49.1 | <-2.81 | >63.7 | <-3.80 | >65.9 | Severe | |
| I_{CN11} | - | - | - | - | - | - | - | - | |
| I_{G11} | -11.71 | -0.20 | 9.8 | -0.29 | 6.6 | -0.35 | 6.1 | Slight | |
| I_{CN14} | -1.76 | -0.06 | 3.0 | -0.06 | 1.4 | -0.06 | 1.0 | - | |
| I_{G14} | -3.54 | -0.11 | 5.5 | -0.20 | 4.5 | -0.25 | 4.3 | Slight | |
| I_{CN17} | -2.32 | -0.13 | 6.2 | -0.13 | 2.9 | -0.13 | 2.3 | Slight | |
| I_{G17} | <-1.98 | <-0.15 | >7.0 | <-0.26 | >5.9 | <-0.33 | >5.8 | Severe | |
| I_{G18} | <-1.93 | <-0.17 | >8.0 | <-0.41 | >9.4 | <-0.54 | >9.4 | Severe | |

Table I.5: Peak current and charge transferred at different points in the system calculated at three different instants of time (100 μ s, 500 μ s, and 1 ms) for stroke 5 of flash FPL0011.

| ID | Peak [kA] | Charge calculated in different time windows | | | | | | Saturation | |
|------------|--------------|---|-------|-------------|-------|--------|-------|------------|--|
| | | 100 μ s | | 500 μ s | | 1 ms | | | |
| | | [C] | % | [C] | % | [C] | % | | |
| I_i | -12.49 | -0.33 | 100.0 | -0.66 | 100.0 | -0.88 | 100.0 | - | |
| I_{Mi} | -12.42 | -0.32 | 100.0 | -0.64 | 100.0 | -0.86 | 100.0 | - | |
| I_{Li} | <-1.20 | <-0.11 | >34.7 | <-0.35 | >55.2 | <-0.53 | >61.4 | Severe | |
| I_{CN1} | -0.17 | -0.00 | 1.2 | -0.01 | 0.9 | -0.01 | 0.9 | - | |
| I_{G1} | -0.50 | -0.03 | 8.5 | -0.06 | 8.9 | -0.08 | 8.9 | - | |
| I_{CN2} | - | - | - | - | - | - | - | - | |
| I_{N2} | -0.60 | -0.04 | 12.9 | -0.09 | 14.6 | -0.12 | 14.4 | - | |
| I_{G2} | -1.04 | -0.03 | 10.2 | -0.06 | 10.0 | -0.09 | 10.0 | - | |
| I_{CN5} | -0.83 | -0.01 | 1.7 | -0.01 | 0.9 | -0.01 | 0.7 | - | |
| I_{A5} | -0.26 | -0.00 | 0.0 | -0.00 | 0.1 | -0.00 | 0.1 | - | |
| I_{B5} | - | - | - | - | - | - | - | - | |
| I_{C5} | -0.46 | -0.01 | 3.4 | -0.01 | 2.2 | -0.02 | 2.1 | - | |
| I_{G5} | -1.68 | -0.05 | 14.9 | -0.09 | 13.7 | -0.12 | 13.7 | - | |
| I_{AN8} | -1.68 | -0.05 | 14.9 | -0.09 | 13.7 | -0.12 | 13.7 | - | |
| I_{BN8} | -0.03 | 0.00 | 0.1 | -0.00 | 0.1 | -0.00 | 0.2 | - | |
| I_{CN8} | -4.85 | -0.17 | 52.8 | -0.38 | 59.4 | -0.51 | 59.7 | - | |
| I_{N8} | -1.23 | -0.09 | 27.4 | -0.18 | 28.6 | -0.24 | 28.4 | - | |
| I_{G8} | -3.95 | -0.04 | 11.3 | -0.06 | 8.7 | -0.07 | 8.4 | - | |
| I_{A9} | -0.14 | 0.00 | 0.0 | 0.00 | 0.1 | 0.00 | 0.0 | - | |
| I_{B9} | -0.40 | 0.00 | 0.0 | 0.00 | 0.1 | 0.00 | 0.0 | - | |
| I_{C9} | -4.87 | -0.19 | 58.9 | -0.41 | 63.9 | -0.54 | 63.6 | - | |
| I_{CN11} | - | - | - | - | - | - | - | - | |
| I_{G11} | -3.71 | -0.03 | 8.1 | -0.05 | 7.2 | -0.06 | 7.3 | - | |
| I_{CN14} | -0.69 | -0.01 | 2.0 | -0.01 | 0.9 | -0.00 | 0.5 | - | |
| I_{G14} | -1.44 | -0.02 | 5.8 | -0.04 | 5.9 | -0.05 | 6.1 | - | |
| I_{CN17} | -0.41 | -0.01 | 3.0 | -0.01 | 1.5 | -0.01 | 1.1 | - | |
| I_{G17} | <-1.89 | <-0.03 | >10.5 | <-0.07 | >10.5 | <-0.09 | >10.3 | Severe | |
| I_{G18} | -0.57 | -0.03 | 10.9 | -0.09 | 13.7 | -0.12 | 13.9 | - | |

Table I.6: Peak current and charge transferred at different points in the system calculated at three different instants of time ($100\ \mu\text{s}$, $500\ \mu\text{s}$, and $1\ \text{ms}$) for stroke 1 of flash FPL0014.

| ID | Peak [kA] | Charge calculated in different time windows | | | | | | Saturation | |
|------------|--------------|---|-------|-------------------|-------|--------|-------|------------|--|
| | | 100 μs | | 500 μs | | 1 ms | | | |
| | | [C] | % | [C] | % | [C] | % | | |
| I_i | -10.99 | -0.37 | 100.0 | -0.72 | 100.0 | -0.79 | 100.0 | - | |
| I_{Mi} | -11.08 | -0.36 | 100.0 | -0.71 | 100.0 | -0.77 | 100.0 | - | |
| I_{Li} | <-1.20 | <-0.11 | >30.6 | <-0.39 | >54.4 | <-0.44 | >57.4 | Severe | |
| I_{CN1} | -0.15 | -0.00 | 0.6 | -0.00 | 0.4 | -0.00 | 0.6 | - | |
| I_{G1} | -0.44 | -0.03 | 8.6 | -0.06 | 9.2 | -0.07 | 9.2 | - | |
| I_{CN2} | -0.24 | -0.00 | 0.7 | -0.00 | 0.4 | -0.00 | 0.3 | - | |
| I_{N2} | -0.79 | -0.05 | 14.7 | -0.12 | 16.5 | -0.13 | 16.3 | - | |
| I_{G2} | -0.70 | -0.04 | 10.3 | -0.07 | 10.2 | -0.08 | 10.3 | - | |
| I_{CN5} | -1.00 | -0.00 | 1.0 | -0.00 | 0.5 | -0.00 | 0.4 | - | |
| I_{A5} | -0.17 | 0.00 | 0.0 | -0.00 | 0.0 | -0.00 | 0.0 | - | |
| I_{B5} | - | - | - | - | - | - | - | - | |
| I_{C5} | -0.39 | -0.00 | 1.4 | -0.01 | 0.8 | -0.01 | 1.0 | - | |
| I_{G5} | -1.35 | -0.05 | 15.1 | -0.10 | 13.9 | -0.11 | 13.7 | - | |
| I_{AN8} | -1.35 | -0.05 | 15.1 | -0.10 | 13.9 | -0.11 | 13.7 | - | |
| I_{BN8} | -0.52 | -0.00 | 0.1 | -0.00 | 0.0 | -0.00 | 0.2 | - | |
| I_{CN8} | -0.09 | 0.00 | 0.2 | 0.00 | 0.1 | 0.00 | 0.1 | - | |
| I_{N8} | -1.62 | -0.11 | 30.1 | -0.22 | 31.2 | -0.24 | 31.0 | - | |
| I_{G8} | -3.35 | -0.04 | 11.6 | -0.06 | 8.9 | -0.07 | 9.0 | - | |
| I_{A9} | -0.15 | -0.00 | 0.0 | -0.00 | 0.1 | -0.00 | 0.2 | - | |
| I_{B9} | -0.59 | -0.00 | 0.6 | -0.00 | 0.4 | -0.00 | 0.5 | - | |
| I_{C9} | -3.66 | -0.23 | 64.2 | -0.49 | 69.2 | -0.53 | 68.3 | - | |
| I_{CN11} | - | - | - | - | - | - | - | - | |
| I_{G11} | -3.04 | -0.03 | 8.4 | -0.05 | 7.6 | -0.06 | 8.0 | - | |
| I_{CN14} | -0.52 | -0.00 | 1.3 | -0.00 | 0.7 | -0.00 | 0.5 | - | |
| I_{G14} | -1.04 | -0.02 | 5.7 | -0.04 | 5.9 | -0.05 | 6.2 | - | |
| I_{CN17} | -0.38 | -0.01 | 1.9 | -0.01 | 1.0 | -0.01 | 0.9 | - | |
| I_{G17} | -0.85 | -0.04 | 10.2 | -0.08 | 11.0 | -0.08 | 10.8 | - | |
| I_{G18} | -0.59 | -0.04 | 10.7 | -0.10 | 14.1 | -0.11 | 14.5 | - | |

Table I.7: Power spectrum density of measured current waveforms integrated over four different frequency ranges as a percentage of its power spectrum density integrated over the bandwidth of the measurement for stroke 1 of flash FPL0014.

| ID | Δf_1 | Δf_2 | Δf_3 | Δf_4 |
|------------|--------------|--------------|--------------|--------------|
| I_i | 79.75 | 6.51 | 0.93 | 0.33 |
| I_{Mi} | 79.78 | 6.79 | 0.94 | 0.08 |
| I_{Li} | - | - | - | - |
| I_{CN1} | 50.36 | 44.01 | 1.51 | 0.42 |
| I_{G1} | 85.74 | 1.59 | 0.10 | 0.05 |
| I_{CN2} | 20.42 | 66.76 | 6.15 | 5.32 |
| I_{N2} | 85.42 | 2.36 | 0.03 | 0.05 |
| I_{G2} | 85.14 | 2.29 | 0.26 | 0.06 |
| I_{CN5} | 12.04 | 68.94 | 14.13 | 3.87 |
| I_{A5} | 5.01 | 17.38 | 33.55 | 39.59 |
| I_{B5} | - | - | - | - |
| I_{C5} | 32.55 | 59.24 | 2.09 | 3.86 |
| I_{G5} | 81.67 | 6.13 | 0.57 | 0.12 |
| I_{AN8} | 3.83 | 7.79 | 32.80 | 44.91 |
| I_{BN8} | 4.48 | 7.53 | 28.37 | 55.06 |
| I_{CN8} | 2.71 | 9.38 | 44.86 | 42.98 |
| I_{N8} | 84.71 | 3.06 | 0.02 | 0.03 |
| I_{G8} | 57.91 | 25.59 | 7.98 | 1.89 |
| I_{A9} | 9.84 | 3.27 | 21.53 | 51.53 |
| I_{B9} | 26.78 | 40.92 | 21.11 | 7.60 |
| I_{C9} | 84.20 | 2.67 | 0.23 | 0.05 |
| I_{CN11} | - | - | - | - |
| I_{G11} | 51.71 | 25.38 | 12.43 | 3.16 |
| I_{CN14} | 30.43 | 56.77 | 5.70 | 4.75 |
| I_{G14} | 72.15 | 12.83 | 2.78 | 0.73 |
| I_{CN17} | 40.14 | 54.31 | 1.02 | 2.12 |
| I_{G17} | 82.70 | 3.53 | 0.51 | 0.06 |
| I_{G18} | 83.84 | 2.27 | 0.05 | 0.03 |

$100 \text{ Hz} \leq \Delta f_1 < 10 \text{ kHz}$; $10 \text{ kHz} \leq \Delta f_2 < 100 \text{ kHz}$

$100 \text{ kHz} \leq \Delta f_3 < 1 \text{ MHz}$; $1 \text{ MHz} \leq \Delta f_4 < 5 \text{ MHz}$

Table I.8: Peak current and charge transferred at different points in the system calculated at three different instants of time ($100\ \mu\text{s}$, $500\ \mu\text{s}$, and $1\ \text{ms}$) for stroke 2 of flash FPL0014.

| ID | Peak [kA] | Charge calculated in different time windows | | | | | | Saturation |
|------------|--------------|---|-------|-------------------|-------|--------|-------|------------|
| | | 100 μs | | 500 μs | | 1 ms | | |
| | | [C] | % | [C] | % | [C] | % | |
| I_i | -25.02 | -0.97 | 100.0 | -1.81 | 100.0 | -2.17 | 100.0 | Slight |
| I_{Li} | <-1.20 | <-0.11 | >11.5 | <-0.52 | >28.8 | <-0.80 | >36.6 | Severe |
| I_{CN1} | -0.21 | -0.00 | 0.4 | -0.00 | 0.2 | -0.01 | 0.2 | Slight |
| I_{G1} | -1.06 | -0.08 | 8.4 | -0.16 | 9.0 | -0.20 | 9.1 | - |
| I_{CN2} | -0.89 | -0.02 | 2.0 | -0.02 | 1.1 | -0.02 | 0.9 | - |
| I_{N2} | -1.91 | -0.13 | 13.4 | -0.29 | 15.9 | -0.35 | 16.1 | - |
| I_{G2} | -1.59 | -0.10 | 9.9 | -0.18 | 10.0 | -0.22 | 10.0 | Slight |
| I_{CN5} | -1.50 | -0.01 | 1.5 | -0.01 | 0.8 | -0.01 | 0.7 | - |
| I_{A5} | -0.37 | -0.00 | 0.1 | -0.00 | 0.1 | -0.00 | 0.1 | - |
| I_{C5} | -1.08 | -0.02 | 2.4 | -0.02 | 1.4 | -0.03 | 1.3 | - |
| I_{G5} | -2.81 | -0.14 | 14.8 | -0.25 | 13.8 | -0.30 | 13.8 | - |
| I_{BN8} | -2.81 | -0.14 | 14.8 | -0.25 | 13.8 | -0.30 | 13.8 | - |
| I_{CN8} | -0.22 | 0.00 | 0.1 | 0.00 | 0.1 | 0.00 | 0.1 | - |
| I_{N8} | -3.73 | -0.27 | 27.7 | -0.55 | 30.2 | -0.66 | 30.3 | Slight |
| I_{C8} | -6.22 | -0.11 | 11.6 | -0.16 | 8.8 | -0.19 | 8.8 | - |
| I_{A9} | -0.21 | 0.00 | 0.0 | -0.00 | 0.0 | -0.00 | 0.1 | - |
| I_{B9} | <-0.80 | <-0.00 | >0.0 | <-0.00 | >0.1 | <-0.00 | >0.1 | Severe |
| I_{C9} | -8.60 | -0.57 | 59.2 | -1.20 | 66.5 | -1.46 | 67.2 | Slight |
| I_{CN11} | - | - | - | - | - | - | - | - |
| I_{G11} | -6.10 | -0.08 | 8.3 | -0.13 | 7.2 | -0.16 | 7.4 | - |
| I_{CN14} | -0.99 | -0.02 | 2.2 | -0.02 | 1.2 | -0.02 | 0.9 | - |
| I_{G14} | -2.18 | -0.06 | 5.9 | -0.11 | 6.0 | -0.13 | 6.1 | - |
| I_{CN17} | -1.16 | -0.04 | 4.3 | -0.04 | 2.3 | -0.04 | 2.0 | - |
| I_{G17} | <-1.98 | <-0.07 | >7.4 | <-0.15 | >8.2 | <-0.18 | >8.3 | Severe |
| I_{G18} | -1.55 | -0.10 | 10.8 | -0.25 | 14.0 | -0.31 | 14.2 | Slight |

Table I.9: Power spectrum density of measured current waveforms integrated over four different frequency ranges as a percentage of its power spectrum density integrated over the bandwidth of the measurement for stroke 2 of flash FPL0014.

| ID | Δf_1 | Δf_2 | Δf_3 | Δf_4 |
|------------|--------------|--------------|--------------|--------------|
| I_i | 80.64 | 6.20 | 0.71 | 0.05 |
| I_{Li} | - | - | - | - |
| I_{CN1} | 61.84 | 34.10 | 1.02 | 0.23 |
| I_{G1} | 85.76 | 1.54 | 0.04 | 0.01 |
| I_{CN2} | 44.97 | 51.88 | 0.23 | 0.21 |
| I_{N2} | 86.15 | 1.53 | 0.01 | 0.01 |
| I_{G2} | 85.21 | 2.13 | 0.18 | 0.02 |
| I_{CN5} | 24.60 | 70.13 | 3.21 | 0.45 |
| I_{A5} | 14.23 | 62.29 | 15.90 | 6.61 |
| I_{C5} | 49.01 | 47.85 | 0.12 | 0.24 |
| I_{G5} | 82.87 | 5.04 | 0.28 | 0.02 |
| I_{BN8} | 1.71 | 6.75 | 79.24 | 11.09 |
| I_{CN8} | 7.62 | 8.77 | 42.76 | 40.56 |
| I_{N8} | 85.61 | 1.97 | 0.01 | 0.01 |
| I_{G8} | 65.33 | 21.89 | 4.35 | 0.36 |
| I_{A9} | 8.01 | 16.27 | 40.03 | 29.30 |
| I_{B9} | - | - | - | - |
| I_{C9} | 84.67 | 1.99 | 0.19 | 0.01 |
| I_{CN11} | - | - | - | - |
| I_{G11} | 55.35 | 29.13 | 7.06 | 0.55 |
| I_{CN14} | 56.75 | 37.65 | 1.43 | 0.44 |
| I_{G14} | 74.95 | 11.81 | 1.38 | 0.12 |
| I_{CN17} | 68.10 | 27.29 | 0.05 | 0.09 |
| I_{G17} | - | - | - | - |
| I_{G18} | 83.86 | 2.80 | 0.02 | 0.01 |

$100 \text{ Hz} \leq \Delta f_1 < 10 \text{ kHz}$; $10 \text{ kHz} \leq \Delta f_2 < 100 \text{ kHz}$

$100 \text{ kHz} \leq \Delta f_3 < 1 \text{ MHz}$; $1 \text{ MHz} \leq \Delta f_4 < 5 \text{ MHz}$

Table I.10: Peak current and charge transferred at different points in the system calculated at three different instants of time (100 μ s, 500 μ s, and 1 ms) for stroke 3 of flash_FPL0014.

| ID | Peak [kA] | Charge calculated in different time windows | | | | | | Saturation | |
|------------|--------------|---|-------|-------------|-------|--------|-------|------------|--|
| | | 100 μ s | | 500 μ s | | 1 ms | | | |
| | | [C] | % | [C] | % | [C] | % | | |
| I_i | -13.17 | -0.37 | 100.0 | -0.65 | 100.0 | -0.70 | 100.0 | - | |
| I_{M1} | -13.37 | -0.36 | 100.0 | -0.63 | 100.0 | -0.68 | 100.0 | - | |
| I_{L4} | <-1.20 | <-0.11 | >30.8 | <-0.36 | >56.8 | <-0.42 | >62.4 | Severe | |
| I_{CN1} | -0.17 | -0.00 | 0.5 | -0.00 | 0.4 | -0.00 | 0.5 | - | |
| I_{G1} | -0.47 | -0.03 | 8.7 | -0.06 | 9.2 | -0.06 | 9.2 | - | |
| I_{CN2} | -0.26 | -0.00 | 0.7 | -0.00 | 0.4 | -0.00 | 0.3 | - | |
| I_{N2} | -0.82 | -0.06 | 15.3 | -0.10 | 16.5 | -0.11 | 16.4 | - | |
| I_{G2} | -0.98 | -0.04 | 10.3 | -0.06 | 10.3 | -0.07 | 10.4 | - | |
| I_{CN5} | -1.18 | -0.00 | 0.9 | -0.00 | 0.5 | -0.00 | 0.4 | - | |
| I_{A5} | -0.23 | -0.00 | 0.0 | -0.00 | 0.1 | -0.00 | 0.1 | - | |
| I_{B5} | - | - | - | - | - | - | - | - | |
| I_{C5} | -0.44 | -0.00 | 1.3 | -0.01 | 1.0 | -0.01 | 1.4 | - | |
| I_{G5} | -1.77 | -0.05 | 15.1 | -0.09 | 14.0 | -0.09 | 13.9 | - | |
| I_{AN8} | -1.77 | -0.05 | 15.1 | -0.09 | 14.0 | -0.09 | 13.9 | - | |
| I_{BN8} | -1.68 | -0.14 | 37.5 | -0.34 | 53.9 | -0.36 | 52.9 | - | |
| I_{CN8} | -0.15 | -0.00 | 0.0 | 0.00 | 0.0 | 0.00 | 0.0 | - | |
| I_{N8} | -1.70 | -0.11 | 30.9 | -0.20 | 31.2 | -0.21 | 30.7 | - | |
| I_{G8} | -4.02 | -0.04 | 11.6 | -0.06 | 9.0 | -0.06 | 9.3 | - | |
| I_{A9} | -0.20 | 0.00 | 0.0 | -0.00 | 0.0 | -0.00 | 0.2 | - | |
| I_{B9} | -0.47 | -0.00 | 0.0 | -0.00 | 0.2 | -0.00 | 0.5 | - | |
| I_{C9} | -4.84 | -0.24 | 65.5 | -0.44 | 69.3 | -0.46 | 68.1 | - | |
| I_{CN11} | - | - | - | - | - | - | - | - | |
| I_{G11} | -3.67 | -0.03 | 8.3 | -0.05 | 7.3 | -0.05 | 7.7 | - | |
| I_{CN14} | -0.72 | -0.00 | 1.3 | -0.00 | 0.7 | -0.00 | 0.6 | - | |
| I_{G14} | -1.33 | -0.02 | 5.7 | -0.04 | 6.0 | -0.04 | 6.2 | - | |
| I_{CN17} | -0.42 | -0.01 | 1.9 | -0.01 | 1.1 | -0.01 | 1.0 | - | |
| I_{G17} | -1.48 | -0.02 | 5.0 | -0.04 | 5.6 | -0.04 | 5.8 | Slight | |
| I_{G18} | -0.59 | -0.04 | 10.7 | -0.09 | 14.3 | -0.10 | 14.7 | - | |

Table I.11: Power spectrum density of measured current waveforms integrated over four different frequency ranges as a percentage of its power spectrum density integrated over the bandwidth of the measurement for stroke 3 of flash FPL0014.

| ID | Δf_1 | Δf_2 | Δf_3 | Δf_4 |
|------------|--------------|--------------|--------------|--------------|
| I_i | 78.11 | 8.00 | 1.48 | 0.38 |
| I_{Mi} | 77.85 | 8.67 | 1.56 | 0.12 |
| I_{Li} | - | - | - | - |
| I_{CN1} | 41.87 | 53.03 | 2.05 | 0.56 |
| I_{G1} | 85.88 | 1.87 | 0.16 | 0.06 |
| I_{CN2} | 17.05 | 69.76 | 6.12 | 5.93 |
| I_{N2} | 85.44 | 2.83 | 0.03 | 0.05 |
| I_{G2} | 84.98 | 2.60 | 0.52 | 0.08 |
| I_{CN5} | 9.81 | 62.77 | 21.49 | 4.96 |
| I_{A5} | 5.24 | 30.21 | 33.36 | 28.26 |
| I_{B5} | - | - | - | - |
| I_{C5} | 28.85 | 62.30 | 2.05 | 4.31 |
| I_{G5} | 80.36 | 7.51 | 0.93 | 0.14 |
| I_{AN8} | 8.28 | 15.24 | 34.02 | 34.62 |
| I_{BN8} | 85.21 | 0.94 | 0.08 | 0.01 |
| I_{CN8} | 2.64 | 10.03 | 44.36 | 42.85 |
| I_{N8} | 84.46 | 3.77 | 0.03 | 0.03 |
| I_{G8} | 50.45 | 30.47 | 11.32 | 1.98 |
| I_{A9} | 7.46 | 3.00 | 25.52 | 51.31 |
| I_{B9} | 14.43 | 8.18 | 44.34 | 25.51 |
| I_{C9} | 83.44 | 3.68 | 0.44 | 0.05 |
| I_{CN11} | 3.22 | 5.36 | 23.25 | 61.45 |
| I_{G11} | 43.22 | 30.28 | 17.56 | 3.03 |
| I_{CN14} | 26.24 | 58.31 | 9.08 | 4.39 |
| I_{G14} | 68.93 | 14.92 | 4.56 | 0.81 |
| I_{CN17} | 36.89 | 57.80 | 1.07 | 2.01 |
| I_{G17} | 72.35 | 10.26 | 4.88 | 0.50 |
| I_{G18} | 84.11 | 2.32 | 0.07 | 0.03 |

$100 \text{ Hz} \leq \Delta f_1 < 10 \text{ kHz}$; $10 \text{ kHz} \leq \Delta f_2 < 100 \text{ kHz}$

$100 \text{ kHz} \leq \Delta f_3 < 1 \text{ MHz}$; $1 \text{ MHz} \leq \Delta f_4 < 5 \text{ MHz}$

Table I.12: Peak current and charge transferred at different points in the system calculated at three different instants of time ($100\ \mu s$, $500\ \mu s$, and $1\ ms$) for stroke 1 of flash FPL0018.

| ID | Peak [kA] | Charge calculated in different time windows | | | | | | Saturation | |
|------------|--------------|---|-------|--------------|-------|--------|-------|------------|--|
| | | $100\ \mu s$ | | $500\ \mu s$ | | 1 ms | | | |
| | | [C] | % | [C] | % | [C] | % | | |
| I_i | -13.57 | -0.38 | 100.0 | -0.76 | 100.0 | -0.96 | 100.0 | - | |
| I_{Mi} | -13.96 | -0.37 | 100.0 | -0.74 | 100.0 | -0.93 | 100.0 | - | |
| I_{Li} | <-1.31 | <-0.12 | >32.6 | <-0.41 | >54.9 | <-0.57 | >61.4 | Severe | |
| I_{CN1} | -0.17 | -0.01 | 2.3 | -0.04 | 5.3 | -0.07 | 7.9 | - | |
| I_{G1} | -0.54 | -0.03 | 8.4 | -0.07 | 9.2 | -0.09 | 9.4 | - | |
| I_{CN2} | -0.31 | -0.02 | 4.2 | -0.02 | 2.7 | -0.02 | 2.1 | - | |
| I_{N2} | -0.27 | -0.02 | 4.7 | -0.02 | 3.1 | 0.01 | 0.6 | - | |
| I_{G2} | -1.19 | -0.03 | 9.1 | -0.07 | 9.2 | -0.09 | 9.4 | - | |
| I_{CN5} | -0.88 | -0.02 | 5.1 | -0.02 | 3.2 | -0.02 | 2.5 | - | |
| I_{A5} | -0.25 | -0.00 | 0.1 | -0.00 | 0.0 | -0.00 | 0.0 | - | |
| I_{B5} | - | - | - | - | - | - | - | - | |
| I_{C5} | -0.43 | -0.02 | 6.6 | -0.06 | 8.2 | -0.10 | 10.4 | - | |
| I_{G5} | -1.87 | -0.05 | 14.0 | -0.10 | 13.9 | -0.13 | 14.0 | - | |
| I_{AN8} | -0.12 | 0.00 | 0.2 | 0.00 | 0.1 | 0.00 | 0.1 | - | |
| I_{BN8} | <-3.00 | <-0.05 | >13.6 | <-0.09 | >12.2 | <-0.09 | >10.1 | Severe | |
| I_{CN8} | -0.51 | 0.00 | 0.0 | -0.00 | 0.1 | -0.00 | 0.3 | - | |
| I_{N8} | -0.60 | -0.04 | 11.0 | -0.09 | 12.0 | -0.09 | 9.2 | - | |
| I_{G8} | -5.98 | -0.04 | 10.1 | -0.07 | 9.0 | -0.08 | 9.0 | - | |
| I_{A9} | -0.20 | -0.00 | 0.0 | -0.00 | 0.0 | -0.00 | 0.1 | - | |
| I_{B9} | -0.56 | 0.04 | 10.4 | 0.11 | 15.0 | 0.15 | 15.7 | - | |
| I_{C9} | -5.60 | -0.17 | 46.1 | -0.37 | 49.7 | -0.47 | 50.3 | - | |
| I_{CN11} | -6.26 | -0.08 | 20.9 | -0.14 | 18.8 | -0.15 | 16.1 | - | |
| I_{G11} | -5.36 | -0.03 | 7.9 | -0.05 | 6.9 | -0.07 | 7.0 | - | |
| I_{CN14} | -0.69 | -0.02 | 4.6 | -0.02 | 3.1 | -0.02 | 2.5 | - | |
| I_{G14} | -1.55 | -0.02 | 6.2 | -0.05 | 6.1 | -0.06 | 6.2 | - | |
| I_{CN17} | -0.40 | -0.02 | 5.3 | -0.03 | 3.4 | -0.03 | 2.8 | - | |
| I_{G17} | -0.93 | -0.03 | 7.0 | -0.06 | 8.1 | -0.08 | 8.3 | - | |
| I_{G18} | -0.74 | -0.05 | 12.8 | -0.11 | 15.2 | -0.14 | 15.6 | - | |

Table I.13: Power spectrum density of measured current waveforms integrated over four different frequency ranges as a percentage of its power spectrum density integrated over the bandwidth of the measurement for stroke 1 of flash FPL0018.

| ID | Δf_1 | Δf_2 | Δf_3 | Δf_4 |
|------------|--------------|--------------|--------------|--------------|
| I_i | 78.83 | 6.67 | 1.49 | 0.38 |
| I_{Mi} | 78.73 | 7.03 | 1.55 | 0.12 |
| I_{Li} | - | - | - | - |
| I_{CN1} | 83.76 | 0.32 | 0.04 | 0.01 |
| I_{G1} | 83.47 | 3.47 | 0.15 | 0.10 |
| I_{CN2} | 80.81 | 8.16 | 0.53 | 1.21 |
| I_{N2} | 84.68 | 1.44 | 0.22 | 0.38 |
| I_{G2} | 81.56 | 5.03 | 0.84 | 0.15 |
| I_{CN5} | 73.05 | 14.28 | 2.45 | 1.12 |
| I_{A5} | 1.59 | 10.43 | 31.63 | 56.29 |
| I_{B5} | - | - | - | - |
| I_{C5} | 82.98 | 3.03 | 0.13 | 0.24 |
| I_{G5} | 79.59 | 6.83 | 1.03 | 0.19 |
| I_{AN8} | 1.78 | 4.52 | 30.67 | 62.70 |
| I_{BN8} | - | - | - | - |
| I_{CN8} | 3.11 | 3.88 | 23.93 | 68.68 |
| I_{N8} | 84.10 | 2.12 | 0.18 | 0.20 |
| I_{G8} | 42.54 | 26.23 | 21.88 | 2.74 |
| I_{A9} | 1.93 | 2.94 | 23.72 | 71.01 |
| I_{B9} | 84.58 | 0.86 | 0.23 | 0.12 |
| I_{C9} | 80.75 | 4.84 | 1.11 | 0.15 |
| I_{CN11} | 64.69 | 16.70 | 7.50 | 1.03 |
| I_{G11} | 35.26 | 29.82 | 26.19 | 3.21 |
| I_{CN14} | 77.97 | 7.67 | 2.29 | 1.54 |
| I_{G14} | 71.34 | 12.44 | 3.99 | 0.85 |
| I_{CN17} | 81.20 | 8.07 | 0.38 | 0.79 |
| I_{G17} | 82.63 | 3.12 | 0.56 | 0.26 |
| I_{G18} | 84.32 | 2.24 | 0.05 | 0.06 |

$100 \text{ Hz} \leq \Delta f_1 < 10 \text{ kHz}$; $10 \text{ kHz} \leq \Delta f_2 < 100 \text{ kHz}$
 $100 \text{ kHz} \leq \Delta f_3 < 1 \text{ MHz}$; $1 \text{ MHz} \leq \Delta f_4 < 10 \text{ MHz}$

Table I.14: Peak current and charge transferred at different points in the system calculated at three different instants of time (100 μ s, 500 μ s, and 1 ms) for stroke 2 of flash FPL0018.

| ID | Peak [kA] | Charge calculated in different time windows | | | | | | Saturation | |
|------------|--------------|---|-------|-------------|-------|--------|-------|------------|--|
| | | 100 μ s | | 500 μ s | | 1 ms | | | |
| | | [C] | % | [C] | % | [C] | % | | |
| I_i | -8.84 | -0.24 | 100.0 | -0.33 | 100.0 | -0.34 | 100.0 | - | |
| I_{M1} | -9.08 | -0.23 | 100.0 | -0.32 | 100.0 | -0.33 | 100.0 | - | |
| I_{L1} | <-1.31 | <-0.11 | >48.6 | <-0.19 | >58.2 | <-0.20 | >60.0 | Severe | |
| I_{CN1} | -0.13 | -0.01 | 3.3 | -0.02 | 6.4 | -0.02 | 6.4 | - | |
| I_{G1} | -0.36 | -0.02 | 8.6 | -0.03 | 9.2 | -0.03 | 9.3 | - | |
| I_{CN2} | -0.23 | -0.01 | 3.5 | -0.01 | 2.5 | -0.01 | 2.4 | - | |
| I_{N2} | -0.20 | -0.01 | 4.1 | -0.00 | 0.8 | -0.00 | 0.1 | - | |
| I_{G2} | -0.53 | -0.02 | 9.1 | -0.03 | 9.4 | -0.03 | 9.7 | - | |
| I_{CN5} | -0.49 | -0.01 | 4.5 | -0.01 | 3.2 | -0.01 | 3.0 | - | |
| I_{A5} | -0.12 | -0.00 | 0.0 | -0.00 | 0.1 | -0.00 | 0.2 | - | |
| I_{B5} | - | - | - | - | - | - | - | - | |
| I_{C5} | -0.34 | -0.02 | 7.0 | -0.03 | 9.6 | -0.03 | 9.8 | - | |
| I_{G5} | -1.06 | -0.03 | 13.8 | -0.05 | 14.1 | -0.05 | 14.5 | - | |
| I_{AN8} | -0.09 | -0.00 | 0.0 | -0.00 | 0.0 | -0.00 | 0.1 | - | |
| I_{BN8} | <-2.87 | <-0.03 | >13.1 | <-0.03 | >10.8 | <-0.03 | >10.4 | Severe | |
| I_{CN8} | -0.40 | 0.00 | 0.9 | 0.03 | 8.1 | 0.06 | 17.7 | - | |
| I_{N8} | -0.46 | -0.03 | 11.1 | -0.03 | 9.3 | -0.03 | 8.7 | - | |
| I_{G8} | -3.57 | -0.02 | 9.7 | -0.03 | 9.4 | -0.03 | 9.9 | - | |
| I_{A9} | -0.17 | -0.00 | 0.1 | -0.00 | 0.1 | -0.00 | 0.2 | - | |
| I_{B9} | -0.05 | 0.02 | 10.4 | 0.04 | 12.7 | 0.04 | 12.6 | - | |
| I_{C9} | -3.76 | -0.10 | 44.6 | -0.15 | 45.9 | -0.14 | 42.4 | - | |
| I_{CN11} | -3.95 | -0.05 | 22.3 | -0.06 | 19.0 | -0.06 | 18.0 | - | |
| I_{G11} | -3.50 | -0.02 | 7.5 | -0.02 | 6.8 | -0.02 | 6.8 | - | |
| I_{CN14} | -0.52 | -0.01 | 3.8 | -0.01 | 2.8 | -0.01 | 2.6 | - | |
| I_{G14} | -0.88 | -0.01 | 6.0 | -0.02 | 6.0 | -0.02 | 6.0 | - | |
| I_{CN17} | -0.26 | -0.01 | 4.3 | -0.01 | 3.3 | -0.01 | 3.2 | - | |
| I_{G17} | -0.52 | -0.02 | 7.1 | -0.03 | 8.1 | -0.03 | 8.3 | - | |
| I_{G18} | -0.55 | -0.03 | 12.9 | -0.05 | 14.8 | -0.05 | 15.0 | - | |

Table I.15: Power spectrum density of measured current waveforms integrated over four different frequency ranges as a percentage of its power spectrum density integrated over the bandwidth of the measurement for stroke 2 of flash FPL0018.

| ID | Δf_1 | Δf_2 | Δf_3 | Δf_4 |
|------------|--------------|--------------|--------------|--------------|
| I_i | 74.74 | 12.06 | 2.00 | 1.15 |
| I_{Mi} | 75.23 | 12.55 | 1.92 | 0.24 |
| I_{Li} | - | - | - | - |
| I_{CN1} | 84.47 | 1.39 | 0.11 | 0.03 |
| I_{G1} | 82.17 | 6.73 | 0.24 | 0.26 |
| I_{CN2} | 73.26 | 15.30 | 1.40 | 3.89 |
| I_{N2} | 85.40 | 3.09 | 0.82 | 1.91 |
| I_{G2} | 79.38 | 9.68 | 0.60 | 0.34 |
| I_{CN5} | 66.05 | 21.73 | 3.18 | 3.00 |
| I_{A5} | 1.01 | 4.32 | 28.56 | 66.01 |
| I_{B5} | - | - | - | - |
| I_{C5} | 80.58 | 6.73 | 0.37 | 0.88 |
| I_{G5} | 76.08 | 12.35 | 1.24 | 0.55 |
| I_{AN8} | 1.04 | 2.82 | 21.75 | 74.26 |
| I_{BN8} | - | - | - | - |
| I_{CN8} | 74.72 | 0.50 | 2.54 | 8.00 |
| I_{N8} | 84.20 | 4.16 | 0.44 | 0.71 |
| I_{G8} | 32.46 | 34.68 | 22.21 | 6.62 |
| I_{A9} | 1.30 | 2.40 | 21.13 | 74.95 |
| I_{B9} | 84.48 | 2.72 | 0.30 | 0.55 |
| I_{C9} | 76.73 | 10.54 | 1.82 | 0.57 |
| I_{CN11} | 61.51 | 20.59 | 7.60 | 2.27 |
| I_{G11} | 25.08 | 37.55 | 26.24 | 8.38 |
| I_{CN14} | 68.93 | 14.38 | 4.87 | 4.79 |
| I_{G14} | 62.31 | 22.54 | 4.61 | 2.56 |
| I_{CN17} | 73.54 | 16.48 | 1.06 | 2.50 |
| I_{G17} | 81.10 | 6.35 | 0.62 | 0.61 |
| I_{G18} | 83.80 | 4.68 | 0.10 | 0.18 |

$100 \text{ Hz} \leq \Delta f_1 < 10 \text{ kHz}$; $10 \text{ kHz} \leq \Delta f_2 < 100 \text{ kHz}$

$100 \text{ kHz} \leq \Delta f_3 < 1 \text{ MHz}$; $1 \text{ MHz} \leq \Delta f_4 < 10 \text{ MHz}$

Table I.16: Peak current and charge transferred at different points in the system calculated at three different instants of time ($100\ \mu s$, $500\ \mu s$, and $1\ ms$) for stroke 3 of flash FPL0018.

| ID | Peak [kA] | Charge calculated in different time windows | | | | | | Saturation | |
|------------|--------------|---|-------|-------------|-------|--------|-------|------------|--|
| | | 100 μs | | 500 μs | | 1 ms | | | |
| | | [C] | % | [C] | % | [C] | % | | |
| I_i | -7.55 | -0.23 | 100.0 | -0.47 | 100.0 | -0.51 | 100.0 | - | |
| I_{Mi} | -7.75 | -0.22 | 100.0 | -0.45 | 100.0 | -0.48 | 100.0 | - | |
| I_{Li} | <-1.31 | <-0.12 | >54.5 | <-0.33 | >71.8 | <-0.36 | >73.9 | Severe | |
| I_{CN1} | -0.15 | -0.00 | 0.5 | -0.00 | 0.3 | -0.00 | 0.6 | - | |
| I_{G1} | -0.31 | -0.02 | 8.4 | -0.04 | 9.3 | -0.05 | 9.4 | - | |
| I_{CN2} | -0.16 | -0.00 | 0.1 | 0.00 | 0.0 | 0.00 | 0.1 | - | |
| I_{N2} | -0.50 | -0.03 | 15.2 | -0.08 | 17.5 | -0.08 | 17.4 | - | |
| I_{G2} | -0.50 | -0.02 | 9.4 | -0.04 | 9.5 | -0.05 | 9.7 | - | |
| I_{CN5} | -0.79 | -0.00 | 0.5 | -0.00 | 0.1 | 0.00 | 0.1 | - | |
| I_{A5} | -0.13 | 0.00 | 0.1 | 0.00 | 0.0 | 0.00 | 0.0 | - | |
| I_{B5} | - | - | - | - | - | - | - | - | |
| I_{C5} | -0.26 | -0.00 | 0.7 | -0.00 | 0.4 | -0.00 | 0.6 | - | |
| I_{G5} | -1.05 | -0.03 | 15.6 | -0.07 | 14.5 | -0.07 | 14.8 | - | |
| I_{AN8} | -0.08 | 0.00 | 0.2 | 0.00 | 0.5 | 0.00 | 0.7 | - | |
| I_{BN8} | -0.23 | 0.00 | 0.1 | 0.00 | 0.2 | 0.00 | 0.1 | - | |
| I_{CN8} | -0.42 | -0.00 | 0.1 | -0.00 | 0.5 | -0.01 | 1.3 | - | |
| I_{N8} | -0.98 | -0.07 | 31.5 | -0.15 | 32.7 | -0.16 | 32.5 | - | |
| I_{G8} | -3.11 | -0.03 | 12.2 | -0.04 | 9.4 | -0.05 | 9.4 | - | |
| I_{A9} | -0.15 | -0.00 | 0.0 | -0.00 | 0.0 | -0.00 | 0.1 | - | |
| I_{B9} | -0.09 | 0.00 | 0.6 | 0.00 | 0.1 | -0.00 | 0.1 | - | |
| I_{C9} | -3.21 | -0.16 | 72.1 | -0.35 | 76.7 | -0.36 | 75.0 | - | |
| I_{CN11} | -3.72 | -0.01 | 4.3 | -0.01 | 2.1 | -0.01 | 1.7 | - | |
| I_{G11} | -3.04 | -0.02 | 8.1 | -0.03 | 6.9 | -0.03 | 7.0 | - | |
| I_{CN14} | -0.49 | -0.00 | 0.8 | -0.00 | 0.4 | -0.00 | 0.3 | - | |
| I_{G14} | -0.85 | -0.01 | 5.7 | -0.03 | 6.0 | -0.03 | 6.2 | - | |
| I_{CN17} | -0.19 | -0.00 | 0.8 | -0.00 | 0.4 | -0.00 | 0.4 | - | |
| I_{G17} | -0.54 | -0.01 | 5.7 | -0.04 | 7.9 | -0.04 | 8.1 | - | |
| I_{G18} | -0.34 | -0.02 | 10.0 | -0.06 | 14.3 | -0.07 | 14.7 | - | |

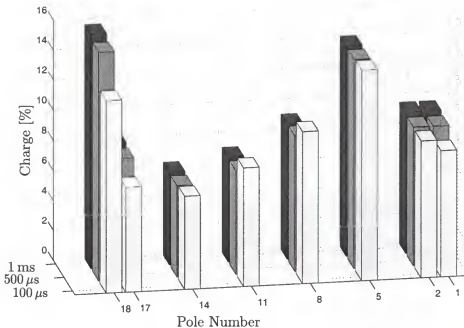


Figure I.1: Percentage of total charge transferred to ground at different poles, calculated at three different instants of time ($100\ \mu s$, $500\ \mu s$, and $1\ ms$ from the beginning of the return stroke), for stroke 1 of flash FPL0018 (See Table I.12). Lightning strike point is between poles 9 and 10.

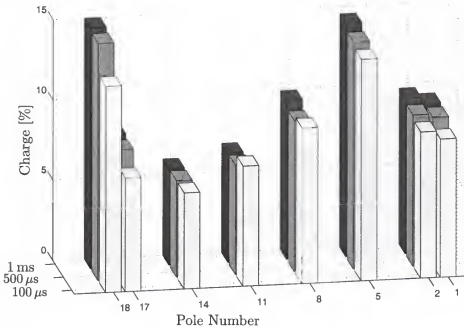


Figure I.2: Percentage of total charge transferred to ground at different poles, calculated at three different instants of time ($100\ \mu s$, $500\ \mu s$, and $1\ ms$ from the beginning of the return stroke), for stroke 2 of flash FPL0018 (See Table I.14). Lightning strike point is between poles 9 and 10.

Table I.17: Power spectrum density of measured current waveforms integrated over four different frequency ranges as a percentage of its power spectrum density integrated over the bandwidth of the measurement for stroke 3 of flash FPL0018.

| ID | Δf_1 | Δf_2 | Δf_3 | Δf_4 |
|------------|--------------|--------------|--------------|--------------|
| I_i | 80.26 | 4.45 | 1.24 | 0.96 |
| I_{Mi} | 80.68 | 4.74 | 1.19 | 0.24 |
| I_{Li} | - | - | - | - |
| I_{CN1} | 38.11 | 52.36 | 4.59 | 1.40 |
| I_{G1} | 85.35 | 1.16 | 0.17 | 0.22 |
| I_{CN2} | 2.92 | 19.33 | 22.86 | 54.71 |
| I_{N2} | 85.40 | 1.58 | 0.06 | 0.12 |
| I_{G2} | 84.65 | 1.88 | 0.41 | 0.27 |
| I_{CN5} | 5.21 | 30.11 | 39.77 | 24.30 |
| I_{A5} | 1.34 | 5.24 | 27.04 | 66.28 |
| I_{B5} | - | - | - | - |
| I_{C5} | 19.12 | 43.82 | 11.41 | 24.39 |
| I_{G5} | 81.81 | 4.44 | 0.83 | 0.43 |
| I_{AN8} | 5.64 | 2.83 | 21.31 | 69.29 |
| I_{BN8} | 2.11 | 2.58 | 23.52 | 71.52 |
| I_{CN8} | 7.56 | 3.13 | 22.25 | 65.75 |
| I_{N8} | 84.72 | 2.24 | 0.04 | 0.07 |
| I_{G8} | 47.38 | 24.49 | 15.06 | 6.21 |
| I_{A9} | 1.18 | 2.19 | 20.79 | 75.63 |
| I_{B9} | 17.25 | 19.93 | 18.40 | 42.94 |
| I_{C9} | 83.63 | 2.38 | 0.38 | 0.16 |
| I_{CN11} | 9.58 | 48.77 | 30.38 | 10.78 |
| I_{G11} | 39.54 | 19.53 | 24.94 | 9.74 |
| I_{CN14} | 12.44 | 43.64 | 20.66 | 22.50 |
| I_{G14} | 73.52 | 7.81 | 3.91 | 2.58 |
| I_{CN17} | 19.42 | 52.32 | 8.37 | 19.00 |
| I_{G17} | 82.84 | 1.63 | 0.62 | 0.71 |
| I_{G18} | 84.50 | 0.93 | 0.10 | 0.19 |

$100 \text{ Hz} \leq \Delta f_1 < 10 \text{ kHz}$; $10 \text{ kHz} \leq \Delta f_2 < 100 \text{ kHz}$

$100 \text{ kHz} \leq \Delta f_3 < 1 \text{ MHz}$; $1 \text{ MHz} \leq \Delta f_4 < 10 \text{ MHz}$

Table I.18: Peak current and charge transferred at different points in the system calculated at three different instants of time ($100\ \mu\text{s}$, $500\ \mu\text{s}$, and $1\ \text{ms}$) for stroke 4 of flash FPL0018.

| ID | Peak [kA] | Charge calculated in different time windows | | | | | | Saturation | |
|------------|--------------|---|-------|-------------------|-------|--------|-------|------------|--|
| | | 100 μs | | 500 μs | | 1 ms | | | |
| | | [C] | % | [C] | % | [C] | % | | |
| I_i | -10.02 | -0.31 | 100.0 | -0.68 | 100.0 | -0.72 | 100.0 | - | |
| I_{Mi} | -10.38 | -0.30 | 100.0 | -0.65 | 100.0 | -0.67 | 100.0 | - | |
| I_{Li} | <-1.31 | <-0.12 | >40.3 | <-0.40 | >61.4 | <-0.44 | >65.4 | Severe | |
| I_{CN1} | -0.14 | -0.00 | 0.5 | -0.00 | 0.3 | -0.00 | 0.5 | - | |
| I_{G1} | -0.41 | -0.03 | 8.4 | -0.06 | 9.4 | -0.06 | 9.7 | - | |
| I_{CN2} | -0.22 | -0.00 | 0.3 | -0.00 | 0.1 | 0.00 | 0.0 | - | |
| I_{N2} | -0.66 | -0.05 | 15.4 | -0.12 | 17.7 | -0.12 | 17.9 | - | |
| I_{G2} | -0.78 | -0.03 | 9.4 | -0.06 | 9.5 | -0.07 | 9.9 | - | |
| I_{CN5} | -0.81 | -0.00 | 0.6 | -0.00 | 0.2 | -0.00 | 0.0 | - | |
| I_{A5} | -0.19 | -0.00 | 0.0 | -0.00 | 0.1 | -0.00 | 0.1 | - | |
| I_{B5} | - | - | - | - | - | - | - | - | |
| I_{C5} | -0.35 | -0.00 | 0.9 | -0.00 | 0.6 | -0.01 | 0.8 | - | |
| I_{G5} | -1.39 | -0.05 | 15.7 | -0.10 | 14.5 | -0.10 | 14.8 | - | |
| I_{AN8} | -0.10 | 0.00 | 0.1 | 0.00 | 0.1 | 0.00 | 0.0 | - | |
| I_{BN8} | -0.23 | 0.00 | 0.1 | 0.00 | 0.1 | 0.00 | 0.2 | - | |
| I_{CN8} | -0.42 | -0.00 | 0.2 | -0.00 | 0.5 | -0.01 | 1.0 | - | |
| I_{N8} | -1.29 | -0.10 | 31.6 | -0.22 | 33.1 | -0.22 | 33.3 | - | |
| I_{G8} | -4.32 | -0.04 | 12.5 | -0.06 | 9.2 | -0.06 | 9.3 | - | |
| I_{A9} | -0.16 | 0.00 | 0.0 | -0.00 | 0.0 | -0.00 | 0.0 | - | |
| I_{B9} | -0.19 | 0.00 | 0.1 | -0.00 | 0.1 | -0.00 | 0.2 | - | |
| I_{C9} | -4.20 | -0.22 | 71.9 | -0.51 | 78.0 | -0.53 | 78.3 | - | |
| I_{CN11} | -4.95 | -0.02 | 5.0 | -0.02 | 2.3 | -0.01 | 2.2 | - | |
| I_{G11} | -4.04 | -0.02 | 8.3 | -0.05 | 7.0 | -0.05 | 7.3 | - | |
| I_{CN14} | -0.64 | -0.00 | 1.0 | -0.00 | 0.4 | -0.00 | 0.3 | - | |
| I_{G14} | -1.14 | -0.02 | 5.8 | -0.04 | 6.1 | -0.04 | 6.3 | - | |
| I_{CN17} | -0.28 | -0.00 | 1.3 | -0.00 | 0.6 | -0.00 | 0.5 | - | |
| I_{G17} | -0.71 | -0.02 | 5.7 | -0.05 | 8.0 | -0.06 | 8.4 | - | |
| I_{G18} | -0.46 | -0.03 | 10.1 | -0.10 | 14.6 | -0.10 | 15.3 | - | |

Table I.19: Power spectrum density of measured current waveforms integrated over four different frequency ranges as a percentage of its power spectrum density integrated over the bandwidth of the measurement for stroke 4 of flash FPL0018.

| ID | Δf_1 | Δf_2 | Δf_3 | Δf_4 |
|------------|--------------|--------------|--------------|--------------|
| I_i | 80.80 | 4.07 | 1.05 | 0.46 |
| I_{Mi} | 80.90 | 4.32 | 1.08 | 0.14 |
| I_{Li} | - | - | - | - |
| I_{CN1} | 40.55 | 50.52 | 3.95 | 0.74 |
| I_{G1} | 85.33 | 1.00 | 0.11 | 0.11 |
| I_{CN2} | 8.30 | 47.90 | 13.21 | 29.97 |
| I_{N2} | 85.31 | 1.32 | 0.03 | 0.06 |
| I_{G2} | 84.69 | 1.44 | 0.48 | 0.14 |
| I_{CN5} | 6.29 | 46.76 | 33.34 | 13.06 |
| I_{A5} | 2.52 | 8.82 | 28.92 | 59.45 |
| I_{B5} | - | - | - | - |
| I_{C5} | 23.70 | 56.15 | 6.02 | 12.04 |
| I_{G5} | 82.21 | 3.84 | 0.66 | 0.20 |
| I_{AN8} | 3.32 | 5.14 | 26.91 | 64.44 |
| I_{BN8} | 1.73 | 2.99 | 26.31 | 68.67 |
| I_{CN8} | 7.10 | 3.88 | 22.46 | 65.23 |
| I_{N8} | 84.72 | 1.83 | 0.03 | 0.04 |
| I_{G8} | 50.51 | 23.85 | 14.56 | 3.28 |
| I_{A9} | 1.39 | 1.87 | 22.78 | 73.73 |
| I_{B9} | 3.41 | 2.96 | 25.27 | 67.73 |
| I_{C9} | 84.03 | 1.72 | 0.31 | 0.08 |
| I_{CN11} | 11.48 | 53.20 | 28.57 | 6.05 |
| I_{G11} | 43.58 | 20.40 | 23.33 | 5.34 |
| I_{CN14} | 17.83 | 53.68 | 15.24 | 12.17 |
| I_{G14} | 74.96 | 7.51 | 3.23 | 1.34 |
| I_{CN17} | 28.59 | 59.93 | 3.26 | 6.74 |
| I_{G17} | 83.21 | 1.52 | 0.46 | 0.35 |
| I_{G18} | 84.47 | 0.89 | 0.06 | 0.09 |

$100 \text{ Hz} \leq \Delta f_1 < 10 \text{ kHz}$; $10 \text{ kHz} \leq \Delta f_2 < 100 \text{ kHz}$

$100 \text{ kHz} \leq \Delta f_3 < 1 \text{ MHz}$; $1 \text{ MHz} \leq \Delta f_4 < 10 \text{ MHz}$

Table I.20: Peak current and charge transferred at different points in the system calculated at three different instants of time ($100\ \mu s$, $500\ \mu s$, and $1\ ms$) for stroke 5 of flash FPL0018.

| ID | Peak [kA] | Charge calculated in different time windows | | | | | | Saturation | |
|------------|--------------|---|-------|-------------|-------|--------|-------|------------|--|
| | | 100 μs | | 500 μs | | 1 ms | | | |
| | | [C] | % | [C] | % | [C] | % | | |
| I_i | -7.20 | -0.24 | 100.0 | -0.60 | 100.0 | -0.64 | 100.0 | - | |
| I_{Mi} | -7.45 | -0.23 | 100.0 | -0.58 | 100.0 | -0.60 | 100.0 | - | |
| I_{Li} | <-1.31 | <-0.12 | >52.4 | <-0.40 | >68.4 | <-0.43 | >70.9 | Severe | |
| I_{CN1} | -0.15 | -0.00 | 0.6 | -0.00 | 0.4 | -0.00 | 0.6 | - | |
| I_{G1} | -0.32 | -0.02 | 8.3 | -0.05 | 9.3 | -0.06 | 9.5 | - | |
| I_{CN2} | -0.16 | -0.00 | 0.2 | -0.00 | 0.0 | 0.00 | 0.0 | - | |
| I_{N2} | -0.50 | -0.04 | 15.3 | -0.10 | 17.7 | -0.11 | 17.8 | - | |
| I_{G2} | -0.65 | -0.02 | 9.4 | -0.05 | 9.5 | -0.06 | 9.8 | - | |
| I_{CN5} | -0.80 | -0.00 | 0.4 | -0.00 | 0.2 | -0.00 | 0.0 | - | |
| I_{A5} | -0.15 | -0.00 | 0.0 | -0.00 | 0.0 | -0.00 | 0.1 | - | |
| I_{B5} | - | - | - | - | - | - | - | - | |
| I_{C5} | -0.29 | -0.00 | 1.0 | -0.00 | 0.6 | -0.00 | 0.8 | - | |
| I_{G5} | -1.09 | -0.04 | 15.8 | -0.08 | 14.5 | -0.09 | 14.7 | - | |
| I_{AN8} | -0.09 | 0.00 | 0.1 | 0.00 | 0.3 | 0.00 | 0.2 | - | |
| I_{BN8} | -0.23 | 0.00 | 0.1 | 0.00 | 0.1 | 0.00 | 0.1 | - | |
| I_{CN8} | -0.44 | -0.00 | 0.2 | -0.00 | 0.6 | -0.01 | 0.9 | - | |
| I_{N8} | -0.96 | -0.07 | 31.9 | -0.19 | 33.1 | -0.20 | 32.9 | - | |
| I_{G8} | -3.29 | -0.03 | 12.7 | -0.05 | 9.4 | -0.06 | 9.7 | - | |
| I_{A9} | -0.14 | 0.00 | 0.1 | 0.00 | 0.0 | -0.00 | 0.0 | - | |
| I_{B9} | -0.12 | 0.00 | 0.1 | -0.00 | 0.0 | -0.00 | 0.1 | - | |
| I_{C9} | -3.18 | -0.17 | 73.4 | -0.45 | 78.4 | -0.47 | 78.5 | - | |
| I_{CN11} | -3.72 | -0.01 | 4.2 | -0.01 | 1.8 | -0.01 | 1.5 | - | |
| I_{G11} | -3.01 | -0.02 | 8.2 | -0.04 | 6.9 | -0.04 | 7.0 | - | |
| I_{CN14} | -0.52 | -0.00 | 0.8 | -0.00 | 0.3 | -0.00 | 0.2 | - | |
| I_{G14} | -0.88 | -0.01 | 5.5 | -0.03 | 5.9 | -0.04 | 6.1 | - | |
| I_{CN17} | -0.20 | -0.00 | 0.7 | -0.00 | 0.3 | -0.00 | 0.3 | - | |
| I_{G17} | -0.58 | -0.01 | 5.6 | -0.05 | 7.9 | -0.05 | 8.3 | - | |
| I_{G18} | -0.35 | -0.02 | 9.8 | -0.08 | 14.3 | -0.09 | 14.9 | - | |

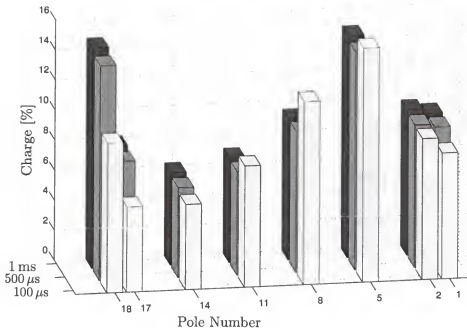


Figure I.3: Percentage of total charge transferred to ground at different poles, calculated at three different instants of time ($100 \mu\text{s}$, $500 \mu\text{s}$, and 1 ms from the beginning of the return stroke), for stroke 3 of flash FPL0018 (See Table I.16). Lightning strike point is between poles 9 and 10.

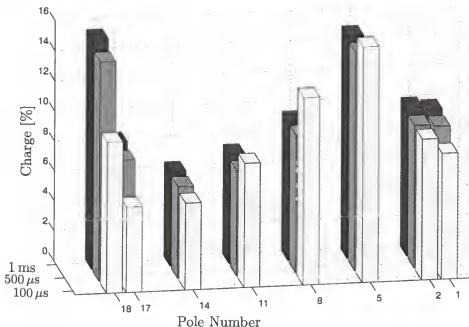


Figure I.4: Percentage of total charge transferred to ground at different poles, calculated at three different instants of time ($100 \mu\text{s}$, $500 \mu\text{s}$, and 1 ms from the beginning of the return stroke), for stroke 4 of flash FPL0018 (See Table I.18). Lightning strike point is between poles 9 and 10.

Table I.21: Power spectrum density of measured current waveforms integrated over four different frequency ranges as a percentage of its power spectrum density integrated over the bandwidth of the measurement for stroke 5 of flash FPL0018.

| ID | Δf_1 | Δf_2 | Δf_3 | Δf_4 |
|------------|--------------|--------------|--------------|--------------|
| I_i | 81.74 | 2.64 | 0.85 | 0.64 |
| I_{Mi} | 82.14 | 2.81 | 0.74 | 0.17 |
| I_{Li} | - | - | - | - |
| I_{CN1} | 43.08 | 45.99 | 4.08 | 1.16 |
| I_{G1} | 85.10 | 0.71 | 0.12 | 0.16 |
| I_{CN2} | 3.78 | 22.51 | 22.88 | 50.53 |
| I_{N2} | 85.17 | 0.92 | 0.04 | 0.08 |
| I_{G2} | 84.57 | 1.09 | 0.42 | 0.20 |
| I_{CN5} | 3.56 | 29.53 | 44.35 | 22.15 |
| I_{A5} | 1.22 | 5.30 | 28.34 | 64.98 |
| I_{B5} | - | - | - | - |
| I_{C5} | 23.42 | 41.72 | 10.73 | 21.23 |
| I_{G5} | 82.65 | 2.72 | 0.63 | 0.32 |
| I_{AN8} | 4.13 | 3.39 | 22.59 | 69.27 |
| I_{BN8} | 1.55 | 2.54 | 24.10 | 71.64 |
| I_{CN8} | 6.23 | 3.89 | 20.89 | 68.00 |
| I_{N8} | 84.70 | 1.35 | 0.03 | 0.05 |
| I_{G8} | 54.12 | 18.71 | 13.00 | 5.02 |
| I_{A9} | 1.86 | 2.34 | 19.13 | 76.30 |
| I_{B9} | 3.49 | 2.53 | 21.25 | 72.09 |
| I_{C9} | 84.10 | 1.26 | 0.25 | 0.11 |
| I_{CN11} | 9.68 | 45.84 | 32.11 | 11.75 |
| I_{G11} | 47.53 | 14.82 | 21.18 | 8.23 |
| I_{CN14} | 10.92 | 43.24 | 21.27 | 23.78 |
| I_{G14} | 76.72 | 4.80 | 3.03 | 1.94 |
| I_{CN17} | 17.56 | 53.43 | 8.72 | 19.56 |
| I_{G17} | 83.50 | 0.85 | 0.44 | 0.46 |
| I_{G18} | 84.61 | 0.45 | 0.07 | 0.12 |

$100 \text{ Hz} \leq \Delta f_1 < 10 \text{ kHz}$; $10 \text{ kHz} \leq \Delta f_2 < 100 \text{ kHz}$

$100 \text{ kHz} \leq \Delta f_3 < 1 \text{ MHz}$; $1 \text{ MHz} \leq \Delta f_4 < 10 \text{ MHz}$

Table I.22: Peak current and charge transferred at different points in the system calculated at three different instants of time ($100\ \mu s$, $500\ \mu s$, and $1\ ms$) for stroke 6 of flash FPL0018.

| ID | Peak [kA] | Charge calculated in different time windows | | | | | | Saturation | |
|------------|--------------|---|-------|-------------|-------|--------|-------|------------|--|
| | | 100 μs | | 500 μs | | 1 ms | | | |
| | | [C] | % | [C] | % | [C] | % | | |
| I_i | -12.49 | -0.34 | 100.0 | -0.81 | 100.0 | -0.98 | 100.0 | - | |
| I_{Mi} | -12.73 | -0.34 | 100.0 | -0.78 | 100.0 | -0.95 | 100.0 | - | |
| I_{Li} | <-1.31 | <-0.12 | >36.0 | <-0.49 | >62.3 | <-0.65 | >68.3 | Severe | |
| I_{CN1} | -0.17 | -0.00 | 0.5 | -0.00 | 0.3 | -0.00 | 0.3 | - | |
| I_{G1} | -0.55 | -0.03 | 8.5 | -0.07 | 9.3 | -0.09 | 9.5 | - | |
| I_{CN2} | -0.27 | -0.00 | 0.4 | -0.00 | 0.1 | -0.00 | 0.0 | - | |
| I_{N2} | -0.77 | -0.05 | 15.2 | -0.14 | 17.3 | -0.17 | 17.4 | - | |
| I_{G2} | -1.04 | -0.03 | 9.2 | -0.07 | 9.3 | -0.09 | 9.4 | - | |
| I_{CN5} | -0.83 | -0.00 | 0.6 | -0.00 | 0.2 | -0.00 | 0.0 | - | |
| I_{A5} | -0.25 | -0.00 | 0.0 | -0.00 | 0.0 | -0.00 | 0.0 | - | |
| I_{B5} | - | - | - | - | - | - | - | - | |
| I_{C5} | -0.41 | -0.00 | 1.0 | -0.00 | 0.6 | -0.01 | 0.6 | - | |
| I_{G5} | -1.78 | -0.05 | 15.3 | -0.11 | 14.4 | -0.14 | 14.3 | - | |
| I_{ANS} | -0.08 | 0.00 | 0.3 | 0.00 | 0.4 | 0.00 | 0.5 | - | |
| I_{BNS} | -0.31 | 0.00 | 0.1 | 0.00 | 0.1 | 0.00 | 0.0 | - | |
| I_{CN8} | -0.52 | -0.00 | 0.2 | -0.00 | 0.4 | -0.01 | 0.7 | - | |
| I_{N8} | -1.56 | -0.10 | 31.0 | -0.25 | 32.4 | -0.31 | 32.2 | - | |
| I_{G8} | -5.83 | -0.04 | 11.8 | -0.07 | 9.5 | -0.09 | 9.5 | - | |
| I_{A9} | -0.15 | 0.00 | 0.1 | 0.00 | 0.1 | 0.00 | 0.0 | - | |
| I_{B9} | -0.54 | 0.00 | 0.0 | -0.00 | 0.1 | -0.00 | 0.1 | - | |
| I_{C9} | -5.43 | -0.23 | 69.2 | -0.60 | 76.1 | -0.73 | 77.0 | - | |
| I_{CN11} | -5.93 | -0.02 | 5.6 | -0.02 | 2.3 | -0.02 | 1.7 | - | |
| I_{G11} | -5.07 | -0.03 | 7.9 | -0.05 | 6.9 | -0.07 | 7.1 | - | |
| I_{CN14} | -0.69 | -0.00 | 1.2 | -0.00 | 0.5 | -0.00 | 0.3 | - | |
| I_{G14} | -1.52 | -0.02 | 5.6 | -0.05 | 5.9 | -0.06 | 6.1 | - | |
| I_{CN17} | -0.39 | -0.01 | 1.7 | -0.01 | 0.7 | -0.01 | 0.6 | - | |
| I_{G17} | -0.94 | -0.02 | 5.8 | -0.06 | 7.7 | -0.08 | 8.1 | - | |
| I_{G18} | -0.56 | -0.03 | 10.3 | -0.11 | 13.9 | -0.14 | 14.5 | - | |

Table I.23: Power spectrum density of measured current waveforms integrated over four different frequency ranges as a percentage of its power spectrum density integrated over the bandwidth of the measurement for stroke 6 of flash FPL0018.

| ID | Δf_1 | Δf_2 | Δf_3 | Δf_4 |
|------------|--------------|--------------|--------------|--------------|
| I_i | 78.98 | 5.85 | 1.37 | 0.41 |
| I_{Mi} | 79.08 | 5.94 | 1.40 | 0.15 |
| I_{Li} | - | - | - | - |
| I_{CN1} | 38.63 | 54.13 | 3.57 | 0.81 |
| I_{G1} | 84.84 | 1.48 | 0.15 | 0.10 |
| I_{CN2} | 11.41 | 56.62 | 9.83 | 21.46 |
| I_{N2} | 84.71 | 1.98 | 0.03 | 0.05 |
| I_{G2} | 83.98 | 2.24 | 0.53 | 0.15 |
| I_{CN5} | 7.82 | 48.51 | 30.46 | 12.63 |
| I_{A5} | 1.95 | 14.79 | 30.01 | 53.21 |
| I_{B5} | - | - | - | - |
| I_{C5} | 24.43 | 60.89 | 4.41 | 8.54 |
| I_{G5} | 80.61 | 5.64 | 0.88 | 0.17 |
| I_{AN8} | 7.15 | 8.80 | 28.50 | 54.58 |
| I_{BN8} | 0.81 | 4.80 | 30.07 | 64.23 |
| I_{CN8} | 10.00 | 3.54 | 20.62 | 64.31 |
| I_{N8} | 83.95 | 2.68 | 0.03 | 0.03 |
| I_{G8} | 44.17 | 29.72 | 17.16 | 2.45 |
| I_{A9} | 2.37 | 2.21 | 22.98 | 72.12 |
| I_{B9} | 2.50 | 5.06 | 46.61 | 45.44 |
| I_{C9} | 82.98 | 2.60 | 0.42 | 0.07 |
| I_{CN11} | 13.06 | 54.93 | 27.26 | 4.06 |
| I_{G11} | 38.34 | 25.49 | 26.23 | 3.69 |
| I_{CN14} | 20.39 | 58.44 | 11.71 | 8.16 |
| I_{G14} | 71.85 | 10.33 | 4.35 | 1.07 |
| I_{CN17} | 33.25 | 59.85 | 1.59 | 3.51 |
| I_{G17} | 82.27 | 2.17 | 0.66 | 0.33 |
| I_{G18} | 83.94 | 1.34 | 0.07 | 0.08 |

$100 \text{ Hz} \leq \Delta f_1 < 10 \text{ kHz}$; $10 \text{ kHz} \leq \Delta f_2 < 100 \text{ kHz}$

$100 \text{ kHz} \leq \Delta f_3 < 1 \text{ MHz}$; $1 \text{ MHz} \leq \Delta f_4 < 10 \text{ MHz}$

Table I.24: Peak current and charge transferred at different points in the system calculated at three different instants of time ($100\ \mu s$, $500\ \mu s$, and $1\ ms$) for stroke 1 of flash FPL0032.

| ID | Peak [kA] | Charge calculated in different time windows | | | | | | Saturation | |
|------------|--------------|---|-------|-------------|-------|--------|-------|------------|--|
| | | 100 μs | | 500 μs | | 1 ms | | | |
| | | [C] | % | [C] | % | [C] | % | | |
| I_i | -10.50 | -0.34 | 100.0 | -0.45 | 100.0 | -0.46 | 100.0 | Slight | |
| I_{M1} | - | - | - | - | - | - | - | - | |
| I_{L1} | <-1.67 | <-0.01 | >1.9 | <-0.03 | >5.7 | <-0.05 | >11.0 | Severe | |
| I_{G1} | -0.47 | -0.03 | 7.9 | -0.04 | 8.9 | -0.04 | 9.1 | - | |
| I_{CN2} | -0.40 | -0.02 | 4.6 | -0.02 | 3.6 | -0.02 | 3.7 | - | |
| I_{G2} | -0.52 | -0.03 | 8.3 | -0.04 | 8.8 | -0.04 | 9.0 | - | |
| I_{CN5} | -0.50 | -0.01 | 3.9 | -0.01 | 2.8 | -0.01 | 2.6 | - | |
| I_{A5} | -0.14 | -0.00 | 0.0 | -0.00 | 0.0 | -0.00 | 0.0 | - | |
| I_{B5} | -0.05 | 0.00 | 0.0 | 0.00 | 0.0 | 0.00 | 0.0 | - | |
| I_{C5} | -0.53 | -0.02 | 7.1 | -0.04 | 9.9 | -0.05 | 11.2 | - | |
| I_{G5} | -0.97 | -0.05 | 13.3 | -0.06 | 13.7 | -0.07 | 14.4 | - | |
| I_{AN8} | -0.07 | 0.00 | 0.2 | 0.00 | 0.2 | 0.00 | 0.2 | - | |
| I_{BN8} | -0.07 | 0.00 | 0.1 | -0.00 | 0.0 | -0.00 | 0.1 | - | |
| I_{CN8} | -3.00 | -0.09 | 25.7 | -0.11 | 24.7 | -0.11 | 23.8 | - | |
| I_{G8} | -3.00 | -0.09 | 25.7 | -0.11 | 24.7 | -0.11 | 23.8 | - | |
| I_{A9} | -0.12 | 0.00 | 0.0 | 0.00 | 0.1 | 0.00 | 0.2 | - | |
| I_{B9} | -0.05 | 0.00 | 0.0 | 0.00 | 0.0 | 0.00 | 0.1 | - | |
| I_{C9} | -3.23 | -0.13 | 37.7 | -0.17 | 38.3 | -0.17 | 37.9 | - | |
| I_{CN11} | -3.43 | -0.09 | 25.0 | -0.11 | 24.7 | -0.11 | 23.6 | - | |
| I_{G11} | -2.54 | -0.03 | 7.5 | -0.03 | 6.7 | -0.03 | 7.1 | - | |
| I_{CN14} | -0.47 | -0.01 | 3.2 | -0.01 | 2.5 | -0.01 | 2.3 | - | |
| I_{G14} | -0.83 | -0.02 | 5.9 | -0.03 | 6.2 | -0.03 | 6.4 | - | |
| I_{CN17} | -0.42 | -0.02 | 5.1 | -0.02 | 3.8 | -0.02 | 3.8 | - | |
| I_{G17} | -0.51 | -0.02 | 6.4 | -0.04 | 7.7 | -0.04 | 8.0 | - | |
| I_{G18} | -0.74 | -0.05 | 13.4 | -0.09 | 19.8 | -0.10 | 21.1 | - | |

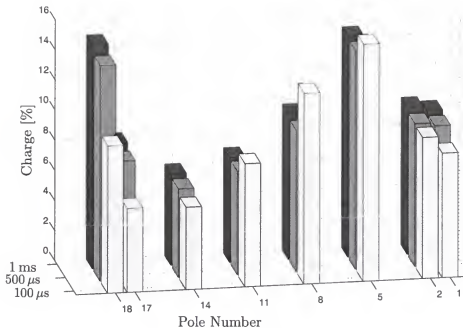


Figure I.5: Percentage of total charge transferred to ground at different poles, calculated at three different instants of time ($100\ \mu s$, $500\ \mu s$, and $1\ ms$ from the beginning of the return stroke), for stroke 5 of flash FPL0018 (See Table I.20). Lightning strike point is between poles 9 and 10.

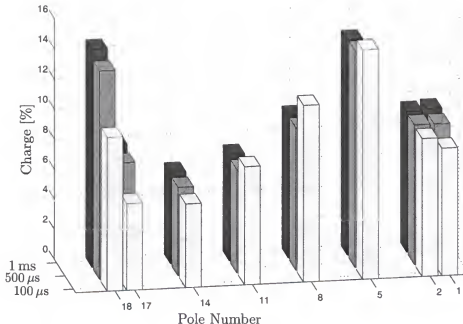


Figure I.6: Percentage of total charge transferred to ground at different poles, calculated at three different instants of time ($100\ \mu s$, $500\ \mu s$, and $1\ ms$ from the beginning of the return stroke), for stroke 6 of flash FPL0018 (See Table I.22). Lightning strike point is between poles 9 and 10.

Table I.25: Peak current and charge transferred at different points in the system calculated at three different instants of time (100 μ s, 500 μ s, and 1 ms) for stroke 2 of flash FPL0032.

| ID | Peak [kA] | Charge calculated in different time windows | | | | | | Saturation | |
|------------|--------------|---|-------|-------------|-------|-------|-------|------------|--|
| | | 100 μ s | | 500 μ s | | 1 ms | | | |
| | | [C] | % | [C] | % | [C] | % | | |
| I_i | -11.00 | -0.39 | 100.0 | -0.73 | 100.0 | -1.03 | 100.0 | - | |
| I_{Mi} | -10.97 | -0.37 | 94.7 | -0.70 | 96.4 | -0.99 | 96.6 | Slight | |
| I_{Li} | - | - | - | - | - | - | - | - | |
| I_{G1} | -0.49 | -0.03 | 7.7 | -0.06 | 8.7 | -0.09 | 8.9 | - | |
| I_{CN2} | -0.42 | -0.02 | 4.8 | -0.02 | 2.7 | -0.02 | 2.2 | - | |
| I_{G2} | -0.84 | -0.03 | 8.4 | -0.06 | 8.6 | -0.09 | 8.8 | - | |
| I_{CN5} | -0.67 | -0.02 | 4.2 | -0.02 | 2.3 | -0.02 | 1.8 | - | |
| I_{A5} | -0.23 | -0.00 | 0.1 | 0.00 | 0.0 | 0.00 | 0.0 | - | |
| I_{B5} | -0.17 | -0.00 | 0.1 | -0.00 | 0.0 | -0.00 | 0.0 | - | |
| I_{C5} | -0.56 | -0.03 | 6.9 | -0.06 | 8.0 | -0.10 | 9.4 | - | |
| I_{G5} | -1.37 | -0.05 | 13.2 | -0.09 | 13.0 | -0.14 | 13.2 | - | |
| I_{AN8} | -0.08 | 0.00 | 0.1 | 0.00 | 0.1 | 0.00 | 0.1 | - | |
| I_{BN8} | -0.08 | 0.00 | 0.0 | -0.00 | 0.0 | -0.00 | 0.1 | - | |
| I_{CN8} | -4.69 | -0.11 | 26.9 | -0.22 | 30.6 | -0.32 | 31.5 | - | |
| I_{G8} | -4.97 | -0.04 | 9.9 | -0.06 | 8.6 | -0.09 | 8.8 | - | |
| I_{A9} | -0.14 | 0.00 | 0.1 | 0.00 | 0.1 | 0.00 | 0.1 | - | |
| I_{B9} | -0.25 | 0.00 | 0.0 | 0.00 | 0.0 | 0.00 | 0.0 | - | |
| I_{C9} | -4.99 | -0.15 | 37.4 | -0.27 | 37.7 | -0.39 | 37.6 | - | |
| I_{CN11} | -5.18 | -0.10 | 24.9 | -0.19 | 26.4 | -0.26 | 25.4 | - | |
| I_{G11} | -4.21 | -0.03 | 7.5 | -0.05 | 6.6 | -0.07 | 6.9 | - | |
| I_{CN14} | -0.66 | -0.01 | 3.5 | -0.02 | 2.2 | -0.02 | 1.8 | - | |
| I_{G14} | -1.31 | -0.02 | 5.9 | -0.04 | 5.8 | -0.06 | 5.9 | - | |
| I_{CN17} | -0.45 | -0.02 | 5.2 | -0.02 | 3.0 | -0.03 | 2.6 | - | |
| I_{G17} | -0.78 | -0.02 | 6.3 | -0.05 | 7.4 | -0.08 | 7.6 | - | |
| I_{G18} | -0.68 | -0.04 | 11.0 | -0.10 | 13.3 | -0.14 | 13.6 | - | |

Table I.26: Peak current and charge transferred at different points in the system calculated at three different instants of time ($100\ \mu\text{s}$, $500\ \mu\text{s}$, and $1\ \text{ms}$) for stroke 3 of flash FPL0032.

| ID | Peak [kA] | Charge calculated in different time windows | | | | | | Saturation | |
|------------|--------------|---|-------|-------------------|-------|-------|-------|------------|--|
| | | 100 μs | | 500 μs | | 1 ms | | | |
| | | [C] | % | [C] | % | [C] | % | | |
| I_i | -7.79 | -0.23 | 100.0 | -0.34 | 100.0 | -0.34 | 100.0 | - | |
| I_{Mi} | -8.10 | -0.22 | 93.9 | -0.33 | 97.6 | -0.34 | 99.8 | Slight | |
| I_{Li} | - | - | - | - | - | - | - | - | |
| I_{G1} | -0.33 | -0.02 | 7.8 | -0.03 | 8.7 | -0.03 | 8.8 | - | |
| I_{CN2} | -0.28 | -0.01 | 3.6 | -0.01 | 2.4 | -0.01 | 2.3 | - | |
| I_{G2} | -0.40 | -0.02 | 8.5 | -0.03 | 8.8 | -0.03 | 8.9 | - | |
| I_{CN5} | -0.44 | -0.01 | 3.4 | -0.01 | 2.2 | -0.01 | 2.1 | - | |
| I_{A5} | -0.11 | 0.00 | 0.0 | 0.00 | 0.1 | 0.00 | 0.1 | - | |
| I_{B5} | -0.02 | 0.00 | 0.1 | 0.00 | 0.1 | 0.00 | 0.1 | - | |
| I_{C5} | -0.39 | -0.02 | 7.1 | -0.04 | 11.6 | -0.04 | 12.0 | - | |
| I_{G5} | -0.77 | -0.03 | 13.0 | -0.04 | 12.9 | -0.04 | 12.9 | - | |
| I_{AN8} | -0.07 | 0.00 | 0.1 | 0.00 | 0.3 | 0.00 | 0.3 | - | |
| I_{BN8} | -0.07 | 0.00 | 0.1 | -0.00 | 0.0 | -0.00 | 0.0 | - | |
| I_{CN8} | -2.92 | -0.07 | 28.3 | -0.11 | 31.6 | -0.11 | 32.8 | - | |
| I_{G8} | -3.17 | -0.02 | 9.6 | -0.03 | 8.8 | -0.03 | 8.9 | - | |
| I_{A9} | -0.06 | 0.00 | 0.0 | 0.00 | 0.2 | 0.00 | 0.2 | - | |
| I_{B9} | -0.04 | 0.00 | 0.0 | 0.00 | 0.1 | 0.00 | 0.1 | - | |
| I_{C9} | -3.21 | -0.08 | 36.6 | -0.12 | 35.9 | -0.12 | 35.5 | - | |
| I_{CN11} | -3.22 | -0.06 | 24.9 | -0.07 | 21.8 | -0.07 | 21.3 | - | |
| I_{G11} | -2.65 | -0.02 | 7.1 | -0.02 | 6.0 | -0.02 | 6.1 | - | |
| I_{CN14} | -0.40 | -0.01 | 2.8 | -0.01 | 1.8 | -0.01 | 1.8 | - | |
| I_{G14} | -0.77 | -0.01 | 5.7 | -0.02 | 5.8 | -0.02 | 5.9 | - | |
| I_{CN17} | -0.30 | -0.01 | 3.9 | -0.01 | 2.6 | -0.01 | 2.5 | - | |
| I_{G17} | -0.43 | -0.01 | 6.3 | -0.03 | 7.5 | -0.03 | 7.5 | - | |
| I_{G18} | -0.47 | -0.03 | 11.2 | -0.05 | 13.4 | -0.05 | 13.5 | - | |

Table I.27: Peak current and charge transferred at different points in the system calculated at three different instants of time ($100\ \mu s$, $500\ \mu s$, and $1\ ms$) for stroke 4 of flash FPL0032.

| ID | Peak [kA] | Charge calculated in different time windows | | | | | | Saturation | |
|------------|--------------|---|-------|-------------|-------|--------|-------|------------|--|
| | | 100 μs | | 500 μs | | 1 ms | | | |
| | | [C] | % | [C] | % | [C] | % | | |
| I_i | -18.29 | -0.68 | 100.0 | -1.29 | 100.0 | -1.91 | 100.0 | - | |
| I_{M1} | <-18.36 | <-0.66 | >97.7 | <-1.25 | >96.9 | <-1.83 | >96.0 | Severe | |
| I_{L1} | - | - | - | - | - | - | - | - | |
| I_{G1} | -0.83 | -0.05 | 7.9 | -0.11 | 8.7 | -0.17 | 8.8 | - | |
| I_{CN2} | -0.76 | -0.04 | 6.1 | -0.05 | 3.9 | -0.06 | 3.3 | - | |
| I_{G2} | -1.20 | -0.06 | 8.7 | -0.11 | 8.8 | -0.17 | 8.8 | - | |
| I_{CN5} | -1.01 | -0.04 | 5.5 | -0.05 | 3.6 | -0.06 | 3.0 | - | |
| I_{A5} | -0.29 | -0.00 | 0.1 | -0.00 | 0.0 | -0.00 | 0.0 | - | |
| I_{B5} | -0.22 | -0.00 | 0.1 | -0.00 | 0.1 | -0.00 | 0.0 | - | |
| I_{C5} | -0.92 | -0.05 | 7.5 | -0.09 | 7.1 | -0.14 | 7.6 | - | |
| I_{G5} | -2.15 | -0.09 | 13.5 | -0.17 | 13.2 | -0.25 | 13.2 | - | |
| I_{AN8} | -0.07 | 0.00 | 0.2 | 0.00 | 0.1 | 0.00 | 0.0 | - | |
| I_{BN8} | -0.31 | 0.00 | 0.1 | 0.00 | 0.0 | -0.00 | 0.0 | - | |
| I_{CN8} | -7.09 | -0.17 | 24.7 | -0.34 | 26.6 | -0.51 | 26.5 | - | |
| I_{G8} | -8.62 | -0.07 | 9.9 | -0.11 | 8.5 | -0.16 | 8.5 | - | |
| I_{A9} | -0.09 | 0.00 | 0.0 | 0.00 | 0.0 | 0.00 | 0.0 | - | |
| I_{B9} | -0.74 | -0.00 | 0.0 | -0.00 | 0.0 | -0.00 | 0.0 | - | |
| I_{C9} | -7.90 | -0.26 | 38.6 | -0.49 | 38.1 | -0.72 | 37.6 | - | |
| I_{CN11} | -7.79 | -0.16 | 24.1 | -0.34 | 26.6 | -0.50 | 26.3 | - | |
| I_{G11} | -6.51 | -0.05 | 7.9 | -0.09 | 6.9 | -0.13 | 6.8 | - | |
| I_{CN14} | -0.85 | -0.03 | 4.3 | -0.04 | 3.2 | -0.05 | 2.8 | - | |
| I_{G14} | -2.08 | -0.04 | 6.0 | -0.08 | 5.9 | -0.11 | 6.0 | - | |
| I_{CN17} | -0.84 | -0.04 | 6.6 | -0.06 | 4.4 | -0.07 | 3.8 | - | |
| I_{G17} | -1.06 | -0.04 | 6.5 | -0.10 | 7.6 | -0.15 | 7.7 | - | |
| I_{G18} | -1.14 | -0.08 | 11.3 | -0.18 | 13.6 | -0.26 | 13.8 | - | |

Table I.28: Peak current and charge transferred at different points in the system calculated at three different instants of time (100 μ s, 500 μ s, and 1 ms) for stroke 5 of flash FPL0032.

| ID | Peak [kA] | Charge calculated in different time windows | | | | | | Saturation |
|------------|--------------|---|-------|-------------|-------|-------|-------|------------|
| | | 100 μ s | | 500 μ s | | 1 ms | | |
| | | [C] | % | [C] | % | [C] | % | |
| I_i | -16.64 | -0.56 | 100.0 | -1.05 | 100.0 | -1.43 | 100.0 | - |
| I_{M1} | -17.12 | -0.55 | 97.8 | -1.03 | 97.8 | -1.39 | 97.0 | Slight |
| I_{Li} | - | - | - | - | - | - | - | - |
| I_{G1} | -0.70 | -0.04 | 8.0 | -0.09 | 8.8 | -0.13 | 8.9 | - |
| I_{CN2} | -0.64 | -0.03 | 6.0 | -0.04 | 3.8 | -0.05 | 3.3 | - |
| I_{G2} | -1.08 | -0.05 | 8.7 | -0.09 | 8.9 | -0.13 | 9.0 | - |
| I_{CN5} | -0.89 | -0.03 | 5.6 | -0.04 | 3.8 | -0.05 | 3.2 | - |
| I_{A5} | -0.28 | -0.00 | 0.1 | -0.00 | 0.0 | -0.00 | 0.0 | - |
| I_{B5} | -0.20 | -0.00 | 0.0 | 0.00 | 0.0 | 0.00 | 0.0 | - |
| I_{C5} | -0.79 | -0.04 | 7.6 | -0.08 | 7.9 | -0.13 | 9.0 | - |
| I_{G5} | -1.98 | -0.08 | 13.5 | -0.14 | 13.3 | -0.19 | 13.3 | - |
| I_{AN8} | -0.08 | 0.00 | 0.2 | 0.00 | 0.1 | 0.00 | 0.0 | - |
| I_{BN8} | -0.07 | 0.00 | 0.1 | 0.00 | 0.1 | 0.00 | 0.0 | - |
| I_{CN8} | -6.54 | -0.14 | 24.6 | -0.28 | 26.5 | -0.37 | 26.0 | - |
| I_{G8} | -7.28 | -0.06 | 9.9 | -0.09 | 8.7 | -0.13 | 8.8 | - |
| I_{A9} | -0.11 | 0.00 | 0.0 | 0.00 | 0.0 | 0.00 | 0.0 | - |
| I_{B9} | -0.47 | -0.00 | 0.0 | 0.00 | 0.0 | -0.00 | 0.0 | - |
| I_{C9} | -7.30 | -0.22 | 38.4 | -0.40 | 38.1 | -0.54 | 37.7 | - |
| I_{CN11} | -7.45 | -0.13 | 24.0 | -0.28 | 26.3 | -0.36 | 25.3 | - |
| I_{G11} | -5.92 | -0.04 | 7.7 | -0.07 | 6.7 | -0.10 | 6.8 | - |
| I_{CN14} | -0.84 | -0.03 | 4.5 | -0.04 | 3.4 | -0.04 | 2.9 | - |
| I_{G14} | -1.89 | -0.03 | 6.0 | -0.06 | 5.9 | -0.09 | 6.0 | - |
| I_{CN17} | -0.69 | -0.04 | 6.4 | -0.05 | 4.4 | -0.05 | 3.8 | - |
| I_{G17} | -0.97 | -0.04 | 6.5 | -0.08 | 7.7 | -0.11 | 7.7 | - |
| I_{G18} | -0.98 | -0.06 | 10.7 | -0.13 | 12.1 | -0.17 | 12.2 | - |

Table I.29: Peak current and charge transferred at different points in the system calculated at three different instants of time ($100\ \mu s$, $500\ \mu s$, and $1\ ms$) for stroke 6 of flash FPL0032.

| ID | Peak [kA] | Charge calculated in different time windows | | | | | | Saturation |
|------------|--------------|---|-------|-------------|-------|-------|-------|------------|
| | | 100 μs | | 500 μs | | 1 ms | | |
| | | [C] | % | [C] | % | [C] | % | |
| I_i | -9.21 | -0.31 | 100.0 | -0.46 | 100.0 | -0.46 | 100.0 | - |
| I_{Mi} | -10.69 | -0.29 | 100.0 | -0.44 | 100.0 | -0.45 | 100.0 | - |
| I_{Li} | - | - | - | - | - | - | - | - |
| I_{G1} | -0.42 | -0.02 | 8.1 | -0.04 | 8.9 | -0.04 | 9.2 | - |
| I_{CN2} | -0.35 | -0.01 | 4.9 | -0.02 | 3.4 | -0.02 | 3.3 | - |
| I_{G2} | -0.65 | -0.03 | 8.8 | -0.04 | 8.9 | -0.04 | 9.0 | - |
| I_{CN5} | -0.67 | -0.01 | 4.9 | -0.01 | 3.3 | -0.01 | 3.0 | - |
| I_{A5} | -0.19 | -0.00 | 0.0 | 0.00 | 0.0 | 0.00 | 0.1 | - |
| I_{B5} | -0.16 | -0.00 | 0.1 | -0.00 | 0.0 | 0.00 | 0.1 | - |
| I_{C5} | -0.48 | -0.02 | 7.8 | -0.05 | 10.7 | -0.05 | 11.9 | - |
| I_{G5} | -1.15 | -0.04 | 13.6 | -0.06 | 13.3 | -0.06 | 13.6 | - |
| I_{AN8} | -0.08 | 0.00 | 0.1 | 0.00 | 0.2 | 0.00 | 0.3 | - |
| I_{BN8} | -0.09 | 0.00 | 0.0 | -0.00 | 0.1 | -0.00 | 0.2 | - |
| I_{CN8} | -4.12 | -0.07 | 25.4 | -0.11 | 24.3 | -0.11 | 24.8 | - |
| I_{G8} | -4.23 | -0.03 | 9.8 | -0.04 | 8.6 | -0.04 | 9.1 | - |
| I_{A9} | -0.12 | 0.00 | 0.0 | 0.00 | 0.2 | 0.00 | 0.2 | - |
| I_{B9} | -0.12 | 0.00 | 0.0 | 0.00 | 0.1 | 0.00 | 0.1 | - |
| I_{C9} | -4.42 | -0.11 | 38.3 | -0.16 | 36.7 | -0.16 | 35.2 | - |
| I_{CN11} | -4.59 | -0.07 | 24.3 | -0.10 | 22.6 | -0.09 | 20.7 | - |
| I_{G11} | -3.41 | -0.02 | 7.5 | -0.03 | 6.5 | -0.03 | 6.7 | - |
| I_{CN14} | -0.64 | -0.01 | 4.2 | -0.01 | 3.0 | -0.01 | 2.8 | - |
| I_{G14} | -1.16 | -0.02 | 5.9 | -0.03 | 6.0 | -0.03 | 6.1 | - |
| I_{CN17} | -0.38 | -0.02 | 5.3 | -0.02 | 3.8 | -0.02 | 3.6 | - |
| I_{G17} | -0.69 | -0.02 | 6.5 | -0.03 | 7.5 | -0.03 | 7.7 | - |
| I_{G18} | -0.54 | -0.02 | 8.4 | -0.02 | 5.1 | -0.02 | 3.9 | - |

Table I.30: Peak current and charge transferred at different points in the system calculated at three different instants of time ($100\ \mu s$, $500\ \mu s$, and $1\ ms$) for stroke 7 of flash FPL0032.

| ID | Peak [kA] | Charge calculated in different time windows | | | | | | Saturation | |
|------------|--------------|---|-------|-------------|-------|-------|-------|------------|--|
| | | 100 μs | | 500 μs | | 1 ms | | | |
| | | [C] | % | [C] | % | [C] | % | | |
| I_i | -8.64 | -0.28 | 100.0 | -0.48 | 100.0 | -0.50 | 100.0 | - | |
| I_{Mi} | -8.94 | -0.27 | 95.4 | -0.45 | 94.7 | -0.48 | 95.7 | Slight | |
| I_{Li} | - | - | - | - | - | - | - | - | |
| I_{G1} | -0.37 | -0.02 | 7.8 | -0.04 | 8.4 | -0.04 | 8.4 | - | |
| I_{CN2} | -0.33 | -0.01 | 4.7 | -0.01 | 3.0 | -0.01 | 2.8 | - | |
| I_{G2} | -0.53 | -0.02 | 8.5 | -0.04 | 8.6 | -0.04 | 8.6 | - | |
| I_{CN5} | -0.60 | -0.01 | 4.7 | -0.01 | 2.9 | -0.01 | 2.5 | - | |
| I_{A5} | -0.18 | -0.00 | 0.1 | -0.00 | 0.0 | 0.00 | 0.0 | - | |
| I_{B5} | -0.12 | -0.00 | 0.0 | 0.00 | 0.0 | 0.00 | 0.1 | - | |
| I_{C5} | -0.45 | -0.02 | 7.5 | -0.05 | 10.2 | -0.06 | 11.3 | - | |
| I_{G5} | -1.04 | -0.04 | 13.0 | -0.06 | 12.7 | -0.06 | 12.9 | - | |
| I_{AN8} | -0.08 | 0.00 | 0.1 | 0.00 | 0.1 | 0.00 | 0.1 | - | |
| I_{BN8} | -0.08 | 0.00 | 0.1 | 0.00 | 0.1 | 0.00 | 0.2 | - | |
| I_{CN8} | -3.67 | -0.07 | 24.1 | -0.11 | 23.0 | -0.11 | 22.4 | - | |
| I_{G8} | -3.78 | -0.03 | 9.4 | -0.04 | 8.1 | -0.04 | 8.4 | - | |
| I_{A9} | -0.12 | 0.00 | 0.1 | 0.00 | 0.2 | 0.00 | 0.2 | - | |
| I_{B9} | -0.08 | 0.00 | 0.0 | 0.00 | 0.1 | 0.00 | 0.1 | - | |
| I_{C9} | -3.92 | -0.10 | 36.5 | -0.17 | 34.6 | -0.16 | 32.2 | - | |
| I_{CN11} | -4.07 | -0.06 | 23.1 | -0.10 | 21.3 | -0.09 | 18.5 | - | |
| I_{G11} | -3.17 | -0.02 | 7.1 | -0.03 | 6.1 | -0.03 | 6.4 | - | |
| I_{CN14} | -0.56 | -0.01 | 4.0 | -0.01 | 2.7 | -0.01 | 2.4 | - | |
| I_{G14} | -1.03 | -0.02 | 5.7 | -0.03 | 5.7 | -0.03 | 5.8 | - | |
| I_{CN17} | -0.34 | -0.01 | 5.0 | -0.02 | 3.2 | -0.02 | 3.0 | - | |
| I_{G17} | -0.62 | -0.02 | 6.3 | -0.03 | 7.2 | -0.04 | 7.4 | - | |
| I_{G18} | -0.52 | -0.03 | 10.5 | -0.05 | 11.4 | -0.06 | 11.1 | - | |

Table I.31: Peak current and charge transferred at different points in the system calculated at three different instants of time ($100\ \mu s$, $500\ \mu s$, and $1\ ms$) for stroke 1 of flash FPL0033.

| ID | Peak [kA] | Charge calculated in different time windows | | | | | | Saturation | |
|------------|--------------|---|-------|-------------|-------|--------|-------|------------|--|
| | | 100 μs | | 500 μs | | 1 ms | | | |
| | | [C] | % | [C] | % | [C] | % | | |
| I_i | -56.00 | -2.79 | 100.0 | -7.06 | 100.0 | -10.16 | 100.0 | Slight | |
| I_{Mi} | <-19.11 | <-1.77 | >63.4 | <-5.99 | >84.9 | <-9.02 | >88.7 | Severe | |
| I_{Li} | - | - | - | - | - | - | - | - | |
| I_{CN1} | <-0.28 | <-0.01 | >0.4 | <-0.05 | >0.7 | <-0.08 | >0.8 | Severe | |
| I_{G1} | <-2.15 | <-0.19 | >6.7 | <-1.00 | >14.2 | <-2.02 | >19.9 | Severe | |
| I_{CN2} | -2.37 | -0.18 | 6.5 | -0.25 | 3.5 | -0.24 | 2.3 | Slight | |
| I_{G2} | <-2.26 | <-0.15 | >5.3 | <-0.28 | >3.9 | <-0.34 | >3.4 | Severe | |
| I_{CN5} | -2.41 | -0.15 | 5.5 | -0.45 | 6.3 | -0.62 | 6.1 | Slight | |
| I_{A5} | -0.92 | -0.01 | 0.3 | -0.01 | 0.1 | -0.01 | 0.1 | - | |
| I_{B5} | -0.38 | -0.00 | 0.0 | -0.00 | 0.0 | -0.00 | 0.0 | - | |
| I_{C5} | -2.56 | -0.20 | 7.2 | -0.68 | 9.6 | -0.89 | 8.8 | Slight | |
| I_{G5} | <-4.49 | <-0.29 | >10.3 | <-0.51 | >7.2 | <-0.58 | >5.7 | Severe | |
| I_{AN8} | -0.08 | 0.01 | 0.4 | 0.01 | 0.2 | 0.01 | 0.1 | - | |
| I_{BN8} | <-3.00 | <-0.05 | >1.9 | <-0.31 | >4.4 | <-0.30 | >3.0 | Severe | |
| I_{CN8} | <-11.20 | <-0.48 | >17.3 | <-0.99 | >14.0 | <-1.39 | >13.7 | Severe | |
| I_{N8} | <-3.87 | <-0.12 | >4.1 | <-0.49 | >7.0 | <-0.87 | >8.6 | Severe | |
| I_{G8} | <-13.79 | <-0.24 | >8.6 | <-0.39 | >5.5 | <-0.42 | >4.2 | Severe | |
| I_{A9} | -0.28 | -0.00 | 0.1 | -0.00 | 0.0 | -0.00 | 0.0 | - | |
| I_{B9} | <-1.50 | <-0.14 | >4.9 | <-0.70 | >9.9 | <-0.79 | >7.8 | Severe | |
| I_{C9} | <-14.10 | <-0.86 | >30.8 | <-2.18 | >30.9 | <-2.99 | >29.4 | Severe | |
| I_{CN11} | <-11.20 | <-0.53 | >18.9 | <-1.01 | >14.2 | <-1.39 | >13.7 | Severe | |
| I_{G11} | <-13.57 | <-0.29 | >10.2 | <-0.42 | >6.0 | <-0.46 | >4.5 | Severe | |
| I_{CN14} | -2.06 | -0.12 | 4.1 | -0.28 | 4.0 | -0.39 | 3.8 | - | |
| I_{G14} | <-4.51 | <-0.16 | >5.6 | <-0.29 | >4.1 | <-0.33 | >3.2 | Severe | |
| I_{CN17} | -2.21 | -0.16 | 5.8 | -0.28 | 3.9 | -0.28 | 2.7 | Slight | |
| I_{G17} | <-2.70 | <-0.17 | >6.2 | <-0.37 | >5.2 | <-0.43 | >4.3 | Severe | |
| I_{G18} | <-2.72 | <-0.23 | >8.3 | <-0.58 | >8.2 | <-0.69 | >6.8 | Severe | |

Table I.32: Peak current and charge transferred at different points in the system calculated at three different instants of time ($100\mu s$, $500\mu s$, and 1 ms) for stroke 1 of flash FPL0034.

| ID | Peak [kA] | Charge calculated in different time windows | | | | | | Saturation | |
|------------|--------------|---|-------|-------------|-------|--------|-------|------------|--|
| | | 100 μs | | 500 μs | | 1 ms | | | |
| | | [C] | % | [C] | % | [C] | % | | |
| I_1 | -28.57 | -1.27 | 100.0 | -2.47 | 100.0 | -3.47 | 100.0 | - | |
| I_{Mi} | <-19.11 | <-1.21 | >95.4 | <-2.36 | >95.7 | <-3.31 | >95.2 | Severe | |
| I_{Li} | - | - | - | - | - | - | - | - | |
| I_{CN1} | -0.23 | -0.00 | 0.3 | -0.00 | 0.2 | -0.01 | 0.2 | Slight | |
| I_{G1} | -1.36 | -0.10 | 8.0 | -0.22 | 8.8 | -0.31 | 8.8 | - | |
| I_{CN2} | -1.07 | -0.02 | 1.8 | -0.02 | 0.9 | -0.02 | 0.7 | - | |
| I_{N2} | -2.36 | -0.16 | 12.7 | -0.38 | 15.5 | -0.54 | 15.7 | Slight | |
| I_{G2} | -1.90 | -0.11 | 8.6 | -0.22 | 8.8 | -0.31 | 8.8 | Slight | |
| I_{CN5} | -1.21 | -0.01 | 0.9 | -0.01 | 0.5 | -0.01 | 0.3 | - | |
| I_{A5} | -0.51 | -0.00 | 0.2 | -0.00 | 0.1 | -0.00 | 0.1 | - | |
| I_{B5} | - | - | - | - | - | - | - | - | |
| I_{CS} | -1.24 | -0.03 | 2.1 | -0.03 | 1.1 | -0.03 | 0.9 | - | |
| I_{G5} | -3.50 | -0.19 | 14.6 | -0.34 | 13.7 | -0.47 | 13.6 | Slight | |
| I_{AN8} | -0.08 | 0.01 | 0.4 | 0.01 | 0.2 | 0.00 | 0.1 | - | |
| I_{BN8} | -2.10 | 0.00 | 0.3 | 0.00 | 0.1 | 0.00 | 0.1 | Slight | |
| I_{CN8} | -0.30 | 0.00 | 0.2 | -0.00 | 0.0 | -0.00 | 0.0 | - | |
| I_{N8} | -0.96 | -0.03 | 2.6 | -0.29 | 11.6 | -0.44 | 12.8 | - | |
| I_{G8} | -11.79 | -0.14 | 11.3 | -0.22 | 8.9 | -0.30 | 8.6 | Slight | |
| I_{A9} | -0.28 | 0.00 | 0.1 | -0.00 | 0.0 | -0.00 | 0.0 | - | |
| I_{B9} | <-1.50 | <0.00 | >0.0 | <-0.00 | >0.0 | <-0.00 | >0.1 | Severe | |
| I_{C9} | -11.31 | -0.75 | 59.1 | -1.66 | 67.3 | -2.38 | 68.6 | Slight | |
| I_{CN11} | <-10.89 | <-0.11 | >8.6 | <-0.11 | >4.3 | <-0.10 | >2.9 | Severe | |
| I_{G11} | -9.57 | -0.10 | 8.0 | -0.17 | 6.8 | -0.24 | 6.9 | - | |
| I_{CN14} | -1.18 | -0.03 | 2.3 | -0.03 | 1.2 | -0.03 | 0.8 | - | |
| I_{G14} | -3.20 | -0.07 | 5.8 | -0.15 | 6.0 | -0.21 | 6.0 | - | |
| I_{CN17} | -1.49 | -0.06 | 4.7 | -0.06 | 2.4 | -0.06 | 1.7 | - | |
| I_{G17} | -1.67 | -0.08 | 6.0 | -0.19 | 7.5 | -0.27 | 7.6 | - | |
| I_{G18} | -2.01 | -0.13 | 10.5 | -0.34 | 13.6 | -0.48 | 13.8 | Slight | |

Table I.33: Power spectrum density of measured current waveforms integrated over four different frequency ranges as a percentage of its power spectrum density integrated over the bandwidth of the measurement for stroke 1 of flash FPL0034.

| ID | Δf_1 | Δf_2 | Δf_3 | Δf_4 |
|------------|--------------|--------------|--------------|--------------|
| I_i | 81.61 | 5.16 | 0.52 | 0.13 |
| I_{Mi} | - | - | - | - |
| I_{Li} | - | - | - | - |
| I_{CN1} | 66.87 | 28.87 | 1.08 | 0.14 |
| I_{G1} | 85.62 | 1.42 | 0.03 | 0.01 |
| I_{CN2} | 48.28 | 48.39 | 0.15 | 0.27 |
| I_{N2} | 86.06 | 1.24 | 0.01 | 0.01 |
| I_{G2} | 85.24 | 1.85 | 0.17 | 0.02 |
| I_{CN5} | 24.00 | 69.84 | 3.51 | 1.01 |
| I_{A5} | 16.86 | 67.05 | 8.76 | 7.02 |
| I_{B5} | 2.85 | 2.30 | 18.26 | 76.17 |
| I_{C5} | 51.69 | 45.15 | 0.15 | 0.24 |
| I_{G5} | 83.57 | 4.12 | 0.27 | 0.02 |
| I_{AN8} | 15.02 | 49.47 | 22.20 | 12.14 |
| I_{BN8} | 4.34 | 22.94 | 65.49 | 6.79 |
| I_{CN8} | 24.57 | 5.18 | 15.77 | 53.50 |
| I_{N8} | 83.79 | 0.44 | 0.05 | 0.02 |
| I_{G8} | 63.77 | 21.18 | 6.83 | 0.35 |
| I_{A9} | 10.27 | 22.97 | 27.26 | 38.07 |
| I_{B9} | - | - | - | - |
| I_{C9} | 84.70 | 1.67 | 0.18 | 0.01 |
| I_{CN11} | - | - | - | - |
| I_{G11} | 59.30 | 23.17 | 8.59 | 0.43 |
| I_{CN14} | 60.60 | 33.96 | 1.15 | 0.34 |
| I_{G14} | 77.02 | 9.23 | 1.49 | 0.11 |
| I_{CN17} | 72.47 | 22.52 | 0.03 | 0.05 |
| I_{G17} | 83.27 | 2.75 | 0.22 | 0.03 |
| I_{G18} | 84.14 | 2.29 | 0.01 | 0.01 |

$100 \text{ Hz} \leq \Delta f_1 < 10 \text{ kHz}$; $10 \text{ kHz} \leq \Delta f_2 < 100 \text{ kHz}$

$100 \text{ kHz} \leq \Delta f_3 < 1 \text{ MHz}$; $1 \text{ MHz} \leq \Delta f_4 < 10 \text{ MHz}$

Table I.34: Peak current and charge transferred at different points in the system calculated at three different instants of time ($100\ \mu s$, $500\ \mu s$, and $1\ ms$) for stroke 2 of flash FPL0034.

| ID | Peak [kA] | Charge calculated in different time windows | | | | | | Saturation | |
|------------|--------------|---|-------|-------------|-------|--------|-------|------------|--|
| | | 100 μs | | 500 μs | | 1 ms | | | |
| | | [C] | % | [C] | % | [C] | % | | |
| I_i | -19.21 | -0.73 | 100.0 | -1.26 | 100.0 | -1.36 | 100.0 | - | |
| I_{Mi} | <-18.99 | <-0.71 | >98.2 | <-1.23 | >97.4 | <-1.34 | >98.2 | Severe | |
| I_{L4} | - | - | - | - | - | - | - | - | |
| I_{CN1} | -0.17 | -0.00 | 0.3 | -0.00 | 0.2 | -0.00 | 0.3 | - | |
| I_{G1} | -0.83 | -0.06 | 8.2 | -0.11 | 8.7 | -0.12 | 8.9 | - | |
| I_{CN2} | -0.51 | -0.01 | 0.9 | -0.01 | 0.5 | -0.01 | 0.5 | - | |
| I_{N2} | -1.52 | -0.10 | 14.1 | -0.20 | 15.7 | -0.21 | 15.7 | - | |
| I_{C2} | -1.05 | -0.06 | 8.8 | -0.11 | 8.7 | -0.12 | 8.9 | - | |
| I_{CN5} | -0.70 | -0.00 | 0.6 | -0.00 | 0.4 | -0.00 | 0.3 | - | |
| I_{A5} | -0.29 | -0.00 | 0.1 | -0.00 | 0.1 | -0.00 | 0.0 | - | |
| I_{B5} | - | - | - | - | - | - | - | - | |
| I_{C5} | -0.67 | -0.01 | 1.2 | -0.01 | 0.7 | -0.01 | 0.7 | - | |
| I_{C5} | -2.15 | -0.11 | 14.6 | -0.17 | 13.5 | -0.18 | 13.5 | - | |
| I_{AN8} | -0.07 | 0.00 | 0.3 | 0.00 | 0.2 | 0.00 | 0.1 | - | |
| I_{BN8} | -0.40 | 0.00 | 0.2 | 0.00 | 0.2 | 0.00 | 0.2 | - | |
| I_{CN8} | -0.20 | -0.00 | 0.0 | -0.01 | 0.5 | -0.01 | 0.9 | - | |
| I_{N8} | -3.12 | -0.21 | 28.9 | -0.37 | 29.6 | -0.40 | 29.3 | Slight | |
| I_{C8} | -7.69 | -0.08 | 10.9 | -0.11 | 8.4 | -0.11 | 8.4 | - | |
| I_{A9} | -0.08 | 0.00 | 0.1 | 0.00 | 0.1 | 0.00 | 0.0 | - | |
| I_{B9} | -0.81 | 0.00 | 0.1 | 0.00 | 0.1 | 0.00 | 0.0 | - | |
| I_{C9} | -7.76 | -0.46 | 62.8 | -0.85 | 67.2 | -0.91 | 66.5 | - | |
| I_{CN11} | -7.59 | -0.05 | 6.7 | -0.05 | 3.8 | -0.05 | 3.5 | - | |
| I_{C11} | -6.07 | -0.06 | 7.7 | -0.08 | 6.7 | -0.10 | 7.1 | - | |
| I_{CN14} | -0.82 | -0.01 | 1.7 | -0.01 | 1.0 | -0.01 | 0.9 | - | |
| I_{C14} | -2.01 | -0.04 | 5.7 | -0.07 | 5.8 | -0.08 | 6.0 | - | |
| I_{CN17} | -0.85 | -0.02 | 3.0 | -0.02 | 1.7 | -0.02 | 1.7 | - | |
| I_{C17} | -1.08 | -0.04 | 5.8 | -0.09 | 7.5 | -0.10 | 7.7 | - | |
| I_{C18} | -1.19 | -0.07 | 10.2 | -0.17 | 13.4 | -0.19 | 13.8 | - | |

Table I.35: Power spectrum density of measured current waveforms integrated over four different frequency ranges as a percentage of its power spectrum density integrated over the bandwidth of the measurement for stroke 2 of flash FPL0034.

| ID | Δf_1 | Δf_2 | Δf_3 | Δf_4 |
|------------|--------------|--------------|--------------|--------------|
| I_i | 79.39 | 7.51 | 0.86 | 0.47 |
| I_{Mi} | - | - | - | - |
| I_{Li} | - | - | - | - |
| I_{CN1} | 49.50 | 47.54 | 1.44 | 0.22 |
| I_{G1} | 86.09 | 1.85 | 0.06 | 0.03 |
| I_{CN2} | 29.41 | 65.23 | 1.07 | 2.50 |
| I_{N2} | 85.80 | 2.57 | 0.01 | 0.01 |
| I_{G2} | 85.54 | 2.50 | 0.21 | 0.04 |
| I_{CN5} | 13.65 | 69.50 | 9.62 | 5.97 |
| I_{A5} | 6.90 | 43.09 | 21.86 | 28.12 |
| I_{B5} | 4.29 | 2.61 | 17.84 | 74.64 |
| I_{C5} | 35.35 | 60.73 | 0.71 | 1.77 |
| I_{G5} | 81.96 | 6.69 | 0.35 | 0.05 |
| I_{AN8} | 7.12 | 32.32 | 25.75 | 34.23 |
| I_{BN8} | 5.88 | 23.54 | 32.19 | 37.78 |
| I_{CN8} | 21.33 | 3.72 | 17.02 | 54.93 |
| I_{N8} | 85.12 | 3.16 | 0.01 | 0.01 |
| I_{G8} | 52.52 | 31.54 | 9.42 | 0.92 |
| I_{A9} | 6.55 | 11.80 | 21.75 | 59.12 |
| I_{B9} | 3.47 | 8.75 | 58.00 | 29.42 |
| I_{C9} | 84.08 | 3.24 | 0.30 | 0.02 |
| I_{CN11} | 25.13 | 59.09 | 13.00 | 1.24 |
| I_{G11} | 52.04 | 28.73 | 10.90 | 1.43 |
| I_{CN14} | 40.67 | 52.42 | 2.94 | 1.43 |
| I_{G14} | 73.28 | 13.21 | 2.18 | 0.30 |
| I_{CN17} | 52.97 | 43.38 | 0.18 | 0.32 |
| I_{G17} | 82.58 | 3.66 | 0.33 | 0.10 |
| I_{G18} | 83.92 | 2.83 | 0.03 | 0.03 |

$100\text{ Hz} \leq \Delta f_1 < 10\text{ kHz}$; $10\text{ kHz} \leq \Delta f_2 < 100\text{ kHz}$

$100\text{ kHz} \leq \Delta f_3 < 1\text{ MHz}$; $1\text{ MHz} \leq \Delta f_4 < 10\text{ MHz}$

Table I.36: Peak current and charge transferred at different points in the system calculated at three different instants of time ($100\ \mu\text{s}$, $500\ \mu\text{s}$, and $1\ \text{ms}$) for stroke 3 of flash FPL0034.

| ID | Peak [kA] | Charge calculated in different time windows | | | | | | Saturation | |
|------------|--------------|---|-------|-------------------|-------|--------|-------|------------|--|
| | | 100 μs | | 500 μs | | 1 ms | | | |
| | | [C] | % | [C] | % | [C] | % | | |
| I_i | -18.86 | -0.70 | 100.0 | -1.17 | 100.0 | -1.34 | 100.0 | - | |
| I_{Mi} | <-19.09 | <-0.68 | >97.5 | <-1.14 | >97.2 | <-1.32 | >98.3 | Severe | |
| I_{Li} | - | - | - | - | - | - | - | - | |
| I_{CN1} | -0.17 | -0.00 | 0.3 | -0.00 | 0.2 | -0.00 | 0.3 | - | |
| I_{G1} | -0.80 | -0.06 | 8.2 | -0.10 | 8.7 | -0.12 | 8.9 | - | |
| I_{CN2} | -0.49 | -0.01 | 0.8 | -0.01 | 0.5 | -0.01 | 0.4 | - | |
| I_{N2} | -1.47 | -0.10 | 14.2 | -0.18 | 15.7 | -0.21 | 15.7 | - | |
| I_{G2} | -1.01 | -0.06 | 8.7 | -0.10 | 8.8 | -0.12 | 8.9 | - | |
| I_{CN5} | -0.71 | -0.00 | 0.6 | -0.00 | 0.4 | -0.00 | 0.3 | - | |
| I_{A5} | -0.29 | -0.00 | 0.1 | -0.00 | 0.1 | -0.00 | 0.1 | - | |
| I_{B5} | - | - | - | - | - | - | - | - | |
| I_{C5} | -0.66 | -0.01 | 1.1 | -0.01 | 0.7 | -0.01 | 0.8 | - | |
| I_{G5} | -2.13 | -0.10 | 14.6 | -0.16 | 13.5 | -0.18 | 13.6 | - | |
| I_{AN8} | -0.08 | 0.00 | 0.3 | 0.00 | 0.1 | 0.00 | 0.0 | - | |
| I_{BN8} | -0.39 | 0.00 | 0.2 | 0.00 | 0.2 | 0.00 | 0.1 | - | |
| I_{CN8} | -0.17 | -0.00 | 0.2 | -0.01 | 0.9 | -0.02 | 1.4 | - | |
| I_{N8} | -3.02 | -0.20 | 28.8 | -0.34 | 29.3 | -0.39 | 28.8 | Slight | |
| I_{G8} | -7.74 | -0.08 | 10.9 | -0.10 | 8.4 | -0.11 | 8.4 | - | |
| I_{A9} | -0.10 | 0.00 | 0.1 | 0.00 | 0.1 | 0.00 | 0.0 | - | |
| I_{B9} | -0.77 | 0.00 | 0.1 | 0.00 | 0.0 | 0.00 | 0.0 | - | |
| I_{C9} | -7.73 | -0.44 | 62.6 | -0.79 | 67.0 | -0.89 | 66.8 | - | |
| I_{CN11} | -7.57 | -0.05 | 6.6 | -0.05 | 4.0 | -0.05 | 3.4 | - | |
| I_{G11} | -6.10 | -0.05 | 7.6 | -0.08 | 6.8 | -0.10 | 7.1 | - | |
| I_{CN14} | -0.78 | -0.01 | 1.7 | -0.01 | 1.0 | -0.01 | 0.9 | - | |
| I_{G14} | -2.01 | -0.04 | 5.7 | -0.07 | 5.9 | -0.08 | 6.1 | - | |
| I_{CN17} | -0.82 | -0.02 | 2.9 | -0.02 | 1.7 | -0.02 | 1.6 | - | |
| I_{G17} | -1.06 | -0.04 | 5.8 | -0.09 | 7.4 | -0.10 | 7.6 | - | |
| I_{G18} | -1.14 | -0.07 | 10.2 | -0.16 | 13.4 | -0.18 | 13.8 | - | |

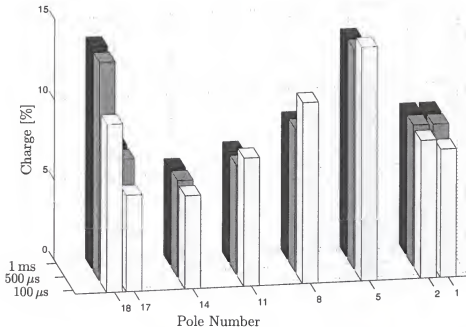


Figure I.7: Percentage of total charge transferred to ground at different poles, calculated at three different instants of time ($100 \mu\text{s}$, $500 \mu\text{s}$, and 1 ms from the beginning of the return stroke), for stroke 1 of flash FPL0034 (See Table I.32). Lightning strike point is between poles 9 and 10.

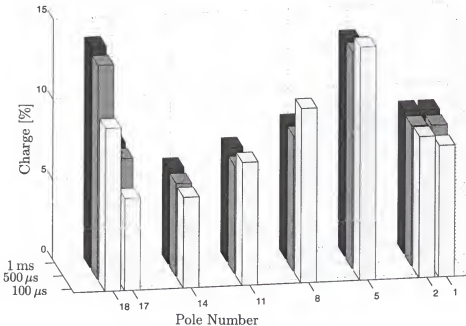


Figure I.8: Percentage of total charge transferred to ground at different poles, calculated at three different instants of time ($100 \mu\text{s}$, $500 \mu\text{s}$, and 1 ms from the beginning of the return stroke), for stroke 2 of flash FPL0034 (See Table I.34). Lightning strike point is between poles 9 and 10.

Table I.37: Power spectrum density of measured current waveforms integrated over four different frequency ranges as a percentage of its power spectrum density integrated over the bandwidth of the measurement for stroke 3 of flash FPL0034.

| ID | Δf_1 | Δf_2 | Δf_3 | Δf_4 |
|------------|--------------|--------------|--------------|--------------|
| I_i | 79.24 | 7.80 | 0.92 | 0.52 |
| I_{M_i} | - | - | - | - |
| I_{L_i} | - | - | - | - |
| I_{CN1} | 49.31 | 47.73 | 1.45 | 0.22 |
| I_{G1} | 86.17 | 1.95 | 0.06 | 0.03 |
| I_{CN2} | 27.37 | 66.77 | 1.32 | 2.96 |
| I_{N2} | 85.83 | 2.73 | 0.01 | 0.02 |
| I_{G2} | 85.59 | 2.62 | 0.22 | 0.04 |
| I_{CN5} | 13.16 | 67.91 | 11.13 | 6.54 |
| I_{A5} | 6.24 | 41.01 | 22.86 | 29.80 |
| I_{B5} | 1.28 | 2.89 | 18.17 | 77.49 |
| I_{C5} | 34.86 | 60.95 | 0.82 | 1.94 |
| I_{G5} | 81.84 | 6.99 | 0.39 | 0.05 |
| I_{AN8} | 6.82 | 30.97 | 26.48 | 35.09 |
| I_{BN8} | 5.02 | 23.79 | 31.84 | 38.67 |
| I_{CN8} | 34.60 | 3.10 | 13.78 | 42.74 |
| I_{N8} | 85.10 | 3.41 | 0.01 | 0.01 |
| I_{G8} | 51.38 | 32.10 | 10.18 | 0.98 |
| I_{A9} | 5.33 | 9.50 | 21.30 | 63.22 |
| I_{B9} | 3.62 | 8.01 | 58.68 | 29.34 |
| I_{C9} | 84.00 | 3.48 | 0.34 | 0.03 |
| I_{CN11} | 24.24 | 59.27 | 13.77 | 1.33 |
| I_{G11} | 50.12 | 29.84 | 11.95 | 1.56 |
| I_{CN14} | 39.60 | 52.91 | 3.47 | 1.58 |
| I_{G14} | 72.81 | 13.61 | 2.45 | 0.31 |
| I_{CN17} | 51.83 | 44.50 | 0.21 | 0.37 |
| I_{G17} | 82.44 | 3.84 | 0.38 | 0.11 |
| I_{G18} | 83.98 | 2.87 | 0.03 | 0.03 |

$100 \text{ Hz} \leq \Delta f_1 < 10 \text{ kHz}$; $10 \text{ kHz} \leq \Delta f_2 < 100 \text{ kHz}$

$100 \text{ kHz} \leq \Delta f_3 < 1 \text{ MHz}$; $1 \text{ MHz} \leq \Delta f_4 < 10 \text{ MHz}$

Table I.38: Peak current and charge transferred at different points in the system calculated at three different instants of time (100 μ s, 500 μ s, and 1 ms) for stroke 4 of flash FPL0034.

| ID | Peak [kA] | Charge calculated in different time windows | | | | | | Saturation | |
|------------|--------------|---|-------|-------------|-------|--------|-------|------------|--|
| | | 100 μ s | | 500 μ s | | 1 ms | | | |
| | | [C] | % | [C] | % | [C] | % | | |
| I_i | -18.86 | -0.59 | 100.0 | -1.14 | 100.0 | -1.41 | 100.0 | - | |
| I_{Mi} | <-19.03 | <-0.58 | >97.6 | <-1.11 | >97.6 | <-1.38 | >97.6 | Severe | |
| I_{La} | - | - | - | - | - | - | - | - | |
| I_{CN1} | -0.18 | -0.00 | 0.3 | -0.00 | 0.2 | -0.00 | 0.2 | - | |
| I_{G1} | -0.68 | -0.05 | 8.1 | -0.10 | 8.8 | -0.13 | 8.9 | - | |
| I_{CN2} | -0.41 | -0.00 | 0.7 | -0.00 | 0.4 | -0.00 | 0.3 | - | |
| I_{N2} | -1.24 | -0.08 | 14.3 | -0.18 | 16.1 | -0.23 | 15.9 | - | |
| I_{G2} | -1.30 | -0.05 | 8.7 | -0.10 | 8.8 | -0.13 | 8.9 | - | |
| I_{CN5} | -0.79 | -0.00 | 0.5 | -0.00 | 0.3 | -0.00 | 0.2 | - | |
| I_{A5} | -0.34 | -0.00 | 0.1 | -0.00 | 0.1 | -0.00 | 0.1 | - | |
| I_{B5} | - | - | - | - | - | - | - | - | |
| I_{C5} | -0.57 | -0.01 | 1.0 | -0.01 | 0.7 | -0.01 | 0.7 | - | |
| I_{G5} | -2.35 | -0.09 | 14.6 | -0.16 | 13.6 | -0.19 | 13.6 | - | |
| I_{AN8} | -0.08 | 0.00 | 0.3 | 0.00 | 0.2 | 0.00 | 0.0 | - | |
| I_{BN8} | -0.70 | 0.00 | 0.3 | 0.00 | 0.2 | 0.00 | 0.2 | - | |
| I_{CN8} | -0.07 | -0.00 | 0.2 | -0.01 | 1.1 | -0.03 | 1.8 | - | |
| I_{N8} | -2.56 | -0.17 | 29.1 | -0.34 | 30.0 | -0.41 | 29.4 | - | |
| I_{G8} | -7.92 | -0.07 | 11.0 | -0.10 | 8.7 | -0.12 | 8.7 | - | |
| I_{A9} | -0.15 | 0.00 | 0.1 | 0.00 | 0.0 | -0.00 | 0.0 | - | |
| I_{B9} | -1.02 | 0.00 | 0.0 | 0.00 | 0.0 | 0.00 | 0.0 | Slight | |
| I_{C9} | -7.79 | -0.38 | 63.9 | -0.79 | 69.6 | -0.98 | 69.6 | - | |
| I_{CN11} | -7.78 | -0.04 | 6.1 | -0.04 | 3.3 | -0.04 | 2.6 | - | |
| I_{G11} | -6.47 | -0.05 | 7.7 | -0.08 | 6.8 | -0.10 | 7.1 | - | |
| I_{CN14} | -0.87 | -0.01 | 1.4 | -0.01 | 0.8 | -0.01 | 0.6 | - | |
| I_{G14} | -2.17 | -0.03 | 5.6 | -0.07 | 5.9 | -0.09 | 6.0 | - | |
| I_{CN17} | -0.67 | -0.01 | 2.5 | -0.01 | 1.3 | -0.02 | 1.1 | - | |
| I_{G17} | -1.20 | -0.03 | 5.7 | -0.08 | 7.4 | -0.11 | 7.6 | - | |
| I_{G18} | -0.94 | -0.05 | 9.1 | -0.13 | 11.2 | -0.16 | 11.6 | - | |

Table I.39: Power spectrum density of measured current waveforms integrated over four different frequency ranges as a percentage of its power spectrum density integrated over the bandwidth of the measurement for stroke 4 of flash FPL0034.

| ID | Δf_1 | Δf_2 | Δf_3 | Δf_4 |
|------------|--------------|--------------|--------------|--------------|
| I_i | 78.66 | 7.18 | 1.31 | 0.65 |
| I_{Mi} | - | - | - | - |
| I_{Li} | - | - | - | - |
| I_{CN1} | 46.86 | 49.20 | 1.96 | 0.42 |
| I_{G1} | 85.69 | 1.65 | 0.10 | 0.04 |
| I_{CN2} | 22.84 | 67.15 | 2.78 | 5.77 |
| I_{N2} | 85.44 | 2.34 | 0.02 | 0.02 |
| I_{G2} | 85.00 | 2.23 | 0.43 | 0.06 |
| I_{CN5} | 10.28 | 63.64 | 17.24 | 8.00 |
| I_{A5} | 5.55 | 35.31 | 28.00 | 30.98 |
| I_{B5} | 2.61 | 2.57 | 18.65 | 75.86 |
| I_{C5} | 32.92 | 60.20 | 1.68 | 3.41 |
| I_{G5} | 81.47 | 6.22 | 0.64 | 0.07 |
| I_{AN8} | 5.72 | 26.43 | 31.64 | 35.79 |
| I_{BN8} | 4.96 | 14.09 | 49.29 | 30.99 |
| I_{CN8} | 44.48 | 2.05 | 11.00 | 34.33 |
| I_{N8} | 84.74 | 2.99 | 0.02 | 0.01 |
| I_{G8} | 48.14 | 29.74 | 15.02 | 1.28 |
| I_{A9} | 3.32 | 6.23 | 25.18 | 64.86 |
| I_{B9} | 1.21 | 7.01 | 73.64 | 18.04 |
| I_{C9} | 83.62 | 2.97 | 0.43 | 0.03 |
| I_{CN11} | 18.99 | 57.76 | 20.33 | 1.79 |
| I_{G11} | 47.18 | 27.18 | 16.95 | 1.82 |
| I_{CN14} | 32.84 | 56.61 | 5.99 | 2.53 |
| I_{G14} | 72.31 | 12.03 | 3.66 | 0.42 |
| I_{CN17} | 46.56 | 49.59 | 0.41 | 0.69 |
| I_{G17} | 82.33 | 3.04 | 0.56 | 0.15 |
| I_{G18} | 83.13 | 3.27 | 0.06 | 0.05 |

$100 \text{ Hz} \leq \Delta f_1 < 10 \text{ kHz}$; $10 \text{ kHz} \leq \Delta f_2 < 100 \text{ kHz}$

$100 \text{ kHz} \leq \Delta f_3 < 1 \text{ MHz}$; $1 \text{ MHz} \leq \Delta f_4 < 10 \text{ MHz}$

Table I.40: Peak current and charge transferred at different points in the system calculated at three different instants of time ($100\ \mu s$, $500\ \mu s$, and 1 ms) for stroke 5 of flash FPL0034.

| ID | Peak [kA] | Charge calculated in different time windows | | | | | | Saturation | |
|------------|--------------|---|-------|-------------|-------|--------|-------|------------|--|
| | | 100 μs | | 500 μs | | 1 ms | | | |
| | | [C] | % | [C] | % | [C] | % | | |
| I_i | -27.14 | -0.94 | 100.0 | -2.27 | 100.0 | -3.07 | 100.0 | - | |
| I_{Mi} | <-19.11 | <-0.90 | >96.6 | <-2.20 | >96.6 | <-2.95 | >96.3 | Severe | |
| I_{Li} | - | - | - | - | - | - | - | - | |
| I_{CN1} | -0.22 | -0.00 | 0.3 | -0.00 | 0.1 | -0.00 | 0.2 | Slight | |
| I_{G1} | -0.97 | -0.07 | 8.0 | -0.20 | 8.7 | -0.27 | 8.8 | - | |
| I_{CN2} | -0.68 | -0.01 | 1.1 | -0.01 | 0.5 | -0.01 | 0.3 | - | |
| I_{N2} | -1.79 | -0.13 | 13.5 | -0.36 | 16.0 | -0.49 | 16.1 | - | |
| I_{G2} | -1.62 | -0.08 | 8.6 | -0.20 | 8.8 | -0.27 | 8.8 | Slight | |
| I_{CN5} | -1.10 | -0.01 | 0.7 | -0.01 | 0.3 | -0.01 | 0.2 | - | |
| I_{A5} | -0.44 | -0.00 | 0.1 | -0.00 | 0.1 | -0.00 | 0.0 | - | |
| I_{B5} | - | - | - | - | - | - | - | - | |
| I_{C5} | -0.85 | -0.01 | 1.4 | -0.01 | 0.6 | -0.02 | 0.5 | - | |
| I_{G5} | -3.26 | -0.14 | 14.6 | -0.31 | 13.7 | -0.42 | 13.6 | Slight | |
| I_{AN8} | -0.08 | 0.00 | 0.4 | 0.00 | 0.2 | 0.00 | 0.1 | - | |
| I_{BN8} | -1.42 | 0.00 | 0.3 | 0.00 | 0.2 | 0.00 | 0.1 | - | |
| I_{CN8} | -0.12 | -0.00 | 0.1 | -0.01 | 0.6 | -0.03 | 0.9 | - | |
| I_{N8} | -3.52 | -0.26 | 27.9 | -0.68 | 30.0 | -0.79 | 25.7 | Slight | |
| I_{G8} | -10.89 | -0.11 | 11.3 | -0.20 | 8.7 | -0.26 | 8.4 | Slight | |
| I_{A9} | -0.21 | 0.00 | 0.1 | 0.00 | 0.0 | 0.00 | 0.0 | - | |
| I_{B9} | <-1.50 | <0.00 | >0.1 | <0.00 | >0.0 | <0.00 | >0.0 | Severe | |
| I_{C9} | -10.76 | -0.58 | 62.2 | -1.59 | 69.9 | -2.17 | 70.9 | Slight | |
| I_{CN11} | <-10.64 | <-0.06 | >6.9 | <-0.06 | >2.8 | <-0.06 | >2.1 | Severe | |
| I_{G11} | -8.77 | -0.07 | 7.8 | -0.15 | 6.6 | -0.20 | 6.7 | - | |
| I_{CN14} | -1.13 | -0.02 | 1.8 | -0.02 | 0.8 | -0.02 | 0.6 | - | |
| I_{G14} | -3.09 | -0.05 | 5.7 | -0.13 | 5.8 | -0.18 | 5.9 | - | |
| I_{CN17} | -1.01 | -0.03 | 3.4 | -0.03 | 1.4 | -0.03 | 1.0 | - | |
| I_{G17} | -1.58 | -0.05 | 5.7 | -0.17 | 7.3 | -0.23 | 7.6 | - | |
| I_{G18} | -1.27 | -0.08 | 8.6 | -0.24 | 10.6 | -0.34 | 11.2 | - | |

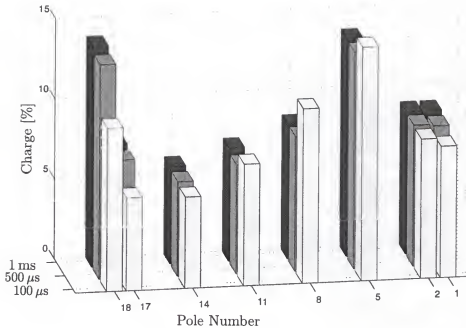


Figure I.9: Percentage of total charge transferred to ground at different poles, calculated at three different instants of time ($100\ \mu\text{s}$, $500\ \mu\text{s}$, and $1\ \text{ms}$ from the beginning of the return stroke), for stroke 3 of flash FPL0034 (See Table I.36). Lightning strike point is between poles 9 and 10.

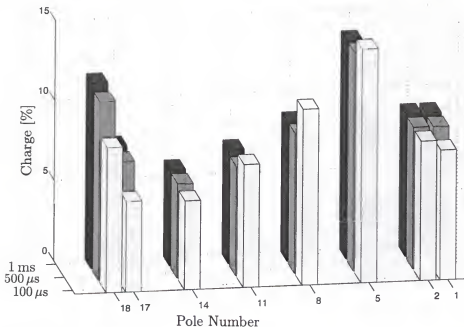


Figure I.10: Percentage of total charge transferred to ground at different poles, calculated at three different instants of time ($100\ \mu\text{s}$, $500\ \mu\text{s}$, and $1\ \text{ms}$ from the beginning of the return stroke), for stroke 4 of flash FPL0034 (See Table I.38). Lightning strike point is between poles 9 and 10.

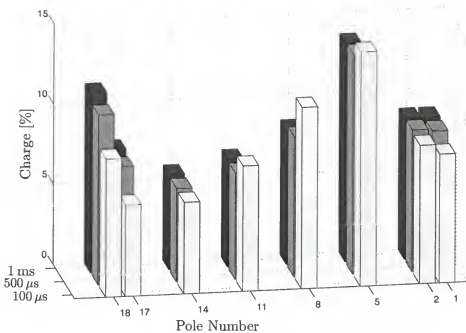


Figure I.11: Percentage of total charge transferred to ground at different poles, calculated at three different instants of time ($100 \mu\text{s}$, $500 \mu\text{s}$, and 1 ms from the beginning of the return stroke), for stroke 5 of flash FPL0034 (See Table I.40). Lightning strike point is between poles 9 and 10.

Table I.41: Power spectrum density of measured current waveforms integrated over four different frequency ranges as a percentage of its power spectrum density integrated over the bandwidth of the measurement for stroke 5 of flash FPL0034.

| ID | Δf_1 | Δf_2 | Δf_3 | Δf_4 |
|------------|--------------|--------------|--------------|--------------|
| I_i | 81.06 | 4.27 | 0.81 | 0.19 |
| I_{Mi} | - | - | - | - |
| I_{Li} | - | - | - | - |
| I_{CN1} | 58.64 | 37.18 | 1.57 | 0.33 |
| I_{G1} | 85.23 | 0.91 | 0.05 | 0.01 |
| I_{CN2} | 34.87 | 61.15 | 0.66 | 1.25 |
| I_{N2} | 85.30 | 1.14 | 0.01 | 0.01 |
| I_{G2} | 84.86 | 1.27 | 0.22 | 0.02 |
| I_{CN5} | 15.33 | 72.78 | 8.01 | 2.78 |
| I_{A5} | 10.70 | 54.98 | 20.82 | 13.40 |
| I_{B5} | 1.52 | 2.60 | 18.69 | 77.03 |
| I_{C5} | 41.46 | 54.91 | 0.54 | 0.93 |
| I_{G5} | 83.07 | 3.37 | 0.37 | 0.02 |
| I_{AN8} | 10.01 | 41.01 | 28.22 | 19.80 |
| I_{BN8} | 5.08 | 22.40 | 59.15 | 12.78 |
| I_{CN8} | 49.69 | 2.56 | 9.40 | 29.63 |
| I_{N8} | 85.04 | 1.46 | 0.01 | 0.01 |
| I_{G8} | 58.80 | 20.97 | 11.27 | 0.49 |
| I_{A9} | 6.88 | 8.96 | 28.32 | 54.85 |
| I_{B9} | - | - | - | - |
| I_{C9} | 84.12 | 1.38 | 0.26 | 0.01 |
| I_{CN11} | - | - | - | - |
| I_{G11} | 55.39 | 21.89 | 13.05 | 0.61 |
| I_{CN14} | 47.21 | 45.53 | 3.40 | 0.88 |
| I_{G14} | 76.72 | 7.72 | 2.16 | 0.15 |
| I_{CN17} | 61.87 | 33.96 | 0.12 | 0.17 |
| I_{G17} | 82.99 | 1.95 | 0.27 | 0.05 |
| I_{G18} | 83.32 | 2.20 | 0.03 | 0.02 |

$100 \text{ Hz} \leq \Delta f_1 < 10 \text{ kHz}$; $10 \text{ kHz} \leq \Delta f_2 < 100 \text{ kHz}$

$100 \text{ kHz} \leq \Delta f_3 < 1 \text{ MHz}$; $1 \text{ MHz} \leq \Delta f_4 < 10 \text{ MHz}$

Table I.42: Peak current and charge transferred at different points in the system calculated at three different instants of time (100 μ s, 500 μ s, and 1 ms) for stroke 1 of flash FPL0036.

| ID | Peak [kA] | Charge calculated in different time windows | | | | | | Saturation | |
|------------|--------------|---|-------|-------------|-------|--------|-------|------------|--|
| | | 100 μ s | | 500 μ s | | 1 ms | | | |
| | | [C] | % | [C] | % | [C] | % | | |
| I_i | -26.72 | -1.39 | 100.0 | -3.34 | 100.0 | -3.71 | 100.0 | - | |
| I_{Mi} | <-19.11 | <-1.34 | >95.8 | <-3.21 | >96.1 | <-3.56 | >96.1 | Severe | |
| I_{Li} | - | - | - | - | - | - | - | - | |
| I_{CN1} | -0.23 | -0.01 | 0.7 | -0.05 | 1.4 | -0.08 | 2.3 | Slight | |
| I_{G1} | -1.48 | -0.09 | 6.3 | -0.20 | 6.0 | -0.24 | 6.4 | - | |
| I_{CN2} | -1.47 | -0.11 | 7.9 | -0.24 | 7.2 | -0.24 | 6.4 | - | |
| I_{N2} | -1.80 | -0.12 | 8.5 | -0.65 | 19.3 | -0.81 | 21.9 | - | |
| I_{G2} | -1.73 | -0.10 | 7.2 | -0.21 | 6.2 | -0.24 | 6.5 | Slight | |
| I_{CN5} | -1.67 | -0.09 | 6.8 | -0.22 | 6.6 | -0.23 | 6.1 | - | |
| I_{A5} | -0.45 | -0.00 | 0.2 | -0.00 | 0.1 | -0.00 | 0.1 | - | |
| I_{B5} | -0.38 | -0.00 | 0.1 | -0.00 | 0.1 | -0.00 | 0.1 | - | |
| I_{C5} | -1.63 | -0.12 | 8.9 | -0.31 | 9.2 | -0.35 | 9.5 | - | |
| I_{G5} | -3.14 | -0.18 | 12.7 | -0.33 | 10.0 | -0.37 | 9.9 | - | |
| I_{AN8} | -0.08 | 0.00 | 0.2 | 0.00 | 0.1 | 0.00 | 0.1 | - | |
| I_{BN8} | -1.54 | 0.00 | 0.1 | 0.00 | 0.1 | 0.00 | 0.0 | - | |
| I_{CN8} | - | - | - | - | - | - | - | - | |
| I_{N8} | -2.83 | -0.21 | 15.2 | -0.80 | 23.9 | -0.99 | 26.7 | Slight | |
| I_{G8} | -10.60 | -0.14 | 9.9 | -0.23 | 6.8 | -0.24 | 6.4 | Slight | |
| I_{A9} | -0.25 | -0.00 | 0.1 | -0.00 | 0.0 | -0.00 | 0.0 | - | |
| I_{B9} | <-1.50 | <-0.00 | >0.1 | <-0.00 | >0.1 | <-0.00 | >0.1 | Severe | |
| I_{C9} | -10.65 | -0.55 | 39.2 | -1.33 | 39.7 | -1.44 | 39.0 | Slight | |
| I_{CN11} | -10.11 | -0.33 | 23.9 | -0.81 | 24.3 | -0.91 | 24.4 | Slight | |
| I_{G11} | -8.39 | -0.11 | 8.0 | -0.18 | 5.5 | -0.19 | 5.2 | - | |
| I_{CN14} | -1.12 | -0.07 | 4.9 | -0.17 | 4.9 | -0.18 | 4.8 | - | |
| I_{G14} | -2.75 | -0.09 | 6.1 | -0.16 | 4.9 | -0.17 | 4.7 | - | |
| I_{CN17} | -1.56 | -0.11 | 7.5 | -0.20 | 5.9 | -0.21 | 5.7 | - | |
| I_{G17} | -1.45 | -0.09 | 6.4 | -0.21 | 6.3 | -0.22 | 6.1 | - | |
| I_{G18} | -2.09 | -0.15 | 11.0 | -0.37 | 11.1 | -0.39 | 10.6 | Slight | |

Table I.43: Power spectrum density of measured current waveforms integrated over four different frequency ranges as a percentage of its power spectrum density integrated over the bandwidth of the measurement for stroke 1 of flash FPL0036.

| ID | Δf_1 | Δf_2 | Δf_3 | Δf_4 |
|------------|--------------|--------------|--------------|--------------|
| I_i | 82.30 | 3.62 | 0.28 | 0.09 |
| I_{Mi} | - | - | - | - |
| I_{Li} | - | - | - | - |
| I_{CN1} | 83.76 | 0.36 | 0.05 | 0.01 |
| I_{G1} | 82.92 | 4.38 | 0.05 | 0.01 |
| I_{CN2} | 85.26 | 1.62 | 0.01 | 0.02 |
| I_{N2} | 84.32 | 0.26 | 0.01 | 0.00 |
| I_{G2} | 82.24 | 5.50 | 0.20 | 0.02 |
| I_{CN5} | 81.76 | 4.68 | 0.11 | 0.04 |
| I_{A5} | 12.17 | 64.36 | 11.49 | 11.00 |
| I_{B5} | 7.19 | 57.29 | 15.93 | 18.95 |
| I_{C5} | 85.05 | 1.42 | 0.01 | 0.01 |
| I_{G5} | 81.64 | 6.15 | 0.25 | 0.02 |
| I_{AN8} | 8.26 | 33.01 | 32.71 | 24.98 |
| I_{BN8} | 3.54 | 5.21 | 77.39 | 13.28 |
| I_{CN8} | - | - | - | - |
| I_{N8} | 83.93 | 1.05 | 0.01 | 0.00 |
| I_{G8} | 60.22 | 23.97 | 6.51 | 0.40 |
| I_{A9} | 4.76 | 25.39 | 25.52 | 43.72 |
| I_{B9} | - | - | - | - |
| I_{C9} | 82.47 | 3.45 | 0.31 | 0.01 |
| I_{CN11} | 79.96 | 5.55 | 0.88 | 0.05 |
| I_{G11} | 59.50 | 24.29 | 6.87 | 0.42 |
| I_{CN14} | 83.37 | 2.70 | 0.19 | 0.07 |
| I_{G14} | 78.63 | 8.10 | 0.95 | 0.08 |
| I_{CN17} | 84.85 | 3.23 | 0.02 | 0.03 |
| I_{G17} | 84.77 | 1.72 | 0.14 | 0.02 |
| I_{G18} | 85.35 | 1.50 | 0.01 | 0.01 |

$100 \text{ Hz} \leq \Delta f_1 < 10 \text{ kHz}$; $10 \text{ kHz} \leq \Delta f_2 < 100 \text{ kHz}$

$100 \text{ kHz} \leq \Delta f_3 < 1 \text{ MHz}$; $1 \text{ MHz} \leq \Delta f_4 < 10 \text{ MHz}$

Table I.44: Peak current and charge transferred at different points in the system calculated at three different instants of time ($100\ \mu s$, $500\ \mu s$, and 1 ms) for stroke 2 of flash FPL0036.

| ID | Peak [kA] | Charge calculated in different time windows | | | | | | Saturation | |
|------------|--------------|---|-------|-------------|-------|--------|-------|------------|--|
| | | 100 μs | | 500 μs | | 1 ms | | | |
| | | [C] | % | [C] | % | [C] | % | | |
| I_i | -27.14 | -1.19 | 100.0 | -3.27 | 100.0 | -3.95 | 100.0 | - | |
| I_{L4} | - | - | - | - | - | - | - | - | |
| I_{CN1} | -0.25 | -0.01 | 0.8 | -0.05 | 1.5 | -0.09 | 2.2 | Slight | |
| I_{G1} | -1.40 | -0.08 | 6.6 | -0.19 | 5.9 | -0.24 | 6.2 | - | |
| I_{CN2} | -1.38 | -0.09 | 7.5 | -0.09 | 2.9 | -0.09 | 2.2 | - | |
| I_{N2} | -1.55 | -0.10 | 8.6 | -0.59 | 18.0 | -0.86 | 21.8 | - | |
| I_{G2} | -1.93 | -0.09 | 7.4 | -0.20 | 6.1 | -0.25 | 6.2 | Slight | |
| I_{CN5} | -1.65 | -0.09 | 7.2 | -0.25 | 7.5 | -0.28 | 7.0 | - | |
| I_{A5} | -0.47 | -0.00 | 0.2 | -0.00 | 0.1 | -0.00 | 0.1 | - | |
| I_{C5} | -1.54 | -0.11 | 9.1 | -0.32 | 9.8 | -0.38 | 9.7 | - | |
| I_{G5} | -3.41 | -0.15 | 12.6 | -0.33 | 10.0 | -0.38 | 9.6 | Slight | |
| I_{BN8} | -2.03 | 0.00 | 0.1 | 0.00 | 0.0 | -0.00 | 0.0 | Slight | |
| I_{CN8} | - | - | - | - | - | - | - | - | |
| I_{N8} | -2.64 | -0.18 | 14.8 | -0.64 | 19.6 | -0.63 | 15.9 | - | |
| I_{G8} | -11.26 | -0.12 | 10.4 | -0.27 | 8.1 | -0.30 | 7.5 | Slight | |
| I_{A9} | -0.26 | -0.00 | 0.1 | -0.00 | 0.0 | -0.00 | 0.0 | - | |
| I_{B9} | <-1.50 | <-0.00 | >0.2 | <-0.00 | >0.1 | <-0.00 | >0.1 | Severe | |
| I_{C9} | -10.83 | -0.46 | 38.8 | -1.28 | 39.3 | -1.52 | 38.4 | Slight | |
| I_{CN11} | -10.34 | -0.27 | 22.9 | -0.73 | 22.4 | -0.89 | 22.4 | Slight | |
| I_{G11} | -8.97 | -0.09 | 7.6 | -0.18 | 5.6 | -0.20 | 5.1 | - | |
| I_{CN14} | -1.17 | -0.06 | 5.3 | -0.19 | 5.8 | -0.23 | 5.8 | - | |
| I_{G14} | -3.10 | -0.07 | 6.0 | -0.16 | 4.9 | -0.18 | 4.6 | - | |
| I_{CN17} | -1.48 | -0.09 | 7.3 | -0.10 | 2.9 | -0.09 | 2.3 | - | |
| I_{G17} | -1.62 | -0.08 | 6.5 | -0.21 | 6.3 | -0.23 | 5.9 | - | |
| I_{G18} | -1.95 | -0.13 | 11.1 | -0.35 | 10.8 | -0.40 | 10.0 | Slight | |

Table I.45: Power spectrum density of measured current waveforms integrated over four different frequency ranges as a percentage of its power spectrum density integrated over the bandwidth of the measurement for stroke 2 of flash FPL0036.

| ID | Δf_1 | Δf_2 | Δf_3 | Δf_4 |
|------------|--------------|--------------|--------------|--------------|
| I_i | 82.08 | 4.07 | 0.36 | 0.11 |
| I_{Li} | - | - | - | - |
| I_{CN1} | 83.76 | 0.34 | 0.05 | 0.01 |
| I_{G1} | 82.93 | 4.90 | 0.06 | 0.02 |
| I_{CN2} | 86.98 | 4.21 | 0.03 | 0.05 |
| I_{N2} | 84.09 | 0.30 | 0.01 | 0.00 |
| I_{G2} | 82.20 | 6.21 | 0.25 | 0.03 |
| I_{CN5} | 82.16 | 4.32 | 0.12 | 0.04 |
| I_{A5} | 10.85 | 61.50 | 14.45 | 12.36 |
| I_{C5} | 84.66 | 1.77 | 0.01 | 0.02 |
| I_{G5} | 81.29 | 7.26 | 0.36 | 0.02 |
| I_{BN8} | 2.01 | 3.86 | 83.62 | 10.21 |
| I_{CN8} | - | - | - | - |
| I_{N8} | 84.13 | 1.79 | 0.01 | 0.01 |
| I_{G8} | 63.28 | 19.77 | 7.55 | 0.39 |
| I_{A9} | 3.47 | 18.58 | 29.83 | 47.71 |
| I_{B9} | - | - | - | - |
| I_{C9} | 82.26 | 3.95 | 0.40 | 0.02 |
| I_{CN11} | 79.24 | 6.59 | 1.27 | 0.06 |
| I_{G11} | 58.27 | 24.34 | 9.21 | 0.50 |
| I_{CN14} | 83.53 | 2.24 | 0.18 | 0.07 |
| I_{G14} | 77.96 | 9.11 | 1.43 | 0.10 |
| I_{CN17} | 85.39 | 5.89 | 0.03 | 0.04 |
| I_{G17} | 84.42 | 2.21 | 0.21 | 0.03 |
| I_{G18} | 85.09 | 2.07 | 0.02 | 0.01 |

$100 \text{ Hz} \leq \Delta f_1 < 10 \text{ kHz}$; $10 \text{ kHz} \leq \Delta f_2 < 100 \text{ kHz}$

$100 \text{ kHz} \leq \Delta f_3 < 1 \text{ MHz}$; $1 \text{ MHz} \leq \Delta f_4 < 10 \text{ MHz}$

Table I.46: Peak current and charge transferred at different points in the system calculated at three different instants of time ($100\ \mu s$, $500\ \mu s$, and $1\ ms$) for stroke 3 of flash FPL0036.

| ID | Peak [kA] | Charge calculated in different time windows | | | | | | Saturation | |
|------------|--------------|---|-------|-------------|-------|--------|-------|------------|--|
| | | 100 μs | | 500 μs | | 1 ms | | | |
| | | [C] | % | [C] | % | [C] | % | | |
| I_i | -24.50 | -1.17 | 100.0 | -2.36 | 100.0 | -2.64 | 100.0 | Slight | |
| I_{Li} | - | - | - | - | - | - | - | - | |
| I_{CN1} | -0.22 | -0.01 | 0.9 | -0.05 | 1.9 | -0.07 | 2.5 | Slight | |
| I_{G1} | -1.44 | -0.08 | 6.8 | -0.15 | 6.4 | -0.18 | 6.7 | - | |
| I_{CN2} | -1.36 | -0.07 | 6.2 | -0.06 | 2.7 | -0.06 | 2.2 | - | |
| I_{N2} | -1.26 | -0.10 | 8.4 | -0.38 | 16.0 | -0.36 | 13.6 | - | |
| I_{G2} | -1.64 | -0.09 | 7.6 | -0.15 | 6.5 | -0.18 | 6.8 | Slight | |
| I_{CN5} | -1.61 | -0.09 | 7.5 | -0.18 | 7.8 | -0.19 | 7.0 | - | |
| I_{A5} | -0.41 | -0.00 | 0.1 | -0.00 | 0.1 | -0.00 | 0.1 | - | |
| I_{C5} | -1.52 | -0.11 | 9.1 | -0.24 | 10.1 | -0.28 | 10.7 | - | |
| I_{G5} | -2.96 | -0.15 | 12.8 | -0.24 | 10.3 | -0.27 | 10.3 | - | |
| I_{BN8} | -1.42 | 0.00 | 0.1 | 0.00 | 0.0 | -0.00 | 0.0 | - | |
| I_{CN8} | - | - | - | - | - | - | - | - | |
| I_{N8} | -2.58 | -0.17 | 14.3 | -0.33 | 14.1 | -0.31 | 11.9 | - | |
| I_{G8} | -9.98 | -0.11 | 9.4 | -0.16 | 6.8 | -0.18 | 6.7 | Slight | |
| I_{A9} | -0.25 | -0.00 | 0.1 | -0.00 | 0.0 | -0.00 | 0.0 | - | |
| I_{B9} | <-1.50 | <-0.00 | >0.1 | <-0.00 | >0.0 | <-0.00 | >0.1 | Severe | |
| I_{C9} | -9.88 | -0.46 | 39.0 | -0.92 | 38.8 | -0.99 | 37.5 | - | |
| I_{CN11} | -9.45 | -0.26 | 22.4 | -0.50 | 21.3 | -0.55 | 20.7 | Slight | |
| I_{G11} | -7.77 | -0.09 | 7.6 | -0.13 | 5.6 | -0.14 | 5.4 | - | |
| I_{CN14} | -1.08 | -0.07 | 5.7 | -0.15 | 6.4 | -0.16 | 6.1 | - | |
| I_{G14} | -2.64 | -0.07 | 6.0 | -0.12 | 4.9 | -0.13 | 4.8 | - | |
| I_{CN17} | -1.46 | -0.06 | 5.0 | -0.05 | 2.2 | -0.05 | 1.9 | - | |
| I_{G17} | -1.42 | -0.08 | 6.6 | -0.15 | 6.4 | -0.16 | 6.2 | - | |
| I_{G18} | -1.94 | -0.13 | 11.2 | -0.26 | 10.9 | -0.27 | 10.4 | - | |

Table I.47: Power spectrum density of measured current waveforms integrated over four different frequency ranges as a percentage of its power spectrum density integrated over the bandwidth of the measurement for stroke 3 of flash FPL0036.

| ID | Δf_1 | Δf_2 | Δf_3 | Δf_4 |
|------------|--------------|--------------|--------------|--------------|
| I_i | 81.38 | 5.58 | 0.46 | 0.16 |
| I_{Li} | - | - | - | - |
| I_{CN1} | 83.87 | 0.46 | 0.06 | 0.01 |
| I_{G1} | 82.86 | 6.04 | 0.08 | 0.02 |
| I_{CN2} | 84.02 | 9.30 | 0.03 | 0.05 |
| I_{N2} | 84.71 | 0.69 | 0.01 | 0.01 |
| I_{G2} | 82.16 | 7.31 | 0.24 | 0.02 |
| I_{CN5} | 82.07 | 5.19 | 0.13 | 0.05 |
| I_{A5} | 9.75 | 60.66 | 14.08 | 14.83 |
| I_{C5} | 84.93 | 2.15 | 0.01 | 0.02 |
| I_{G5} | 81.11 | 8.35 | 0.33 | 0.03 |
| I_{BN8} | 2.11 | 4.78 | 76.01 | 16.77 |
| I_{CN8} | - | - | - | - |
| I_{N8} | 83.86 | 3.44 | 0.02 | 0.01 |
| I_{G8} | 55.27 | 29.23 | 8.44 | 0.58 |
| I_{A9} | 3.73 | 17.04 | 27.02 | 51.73 |
| I_{B9} | - | - | - | - |
| I_{C9} | 81.70 | 5.43 | 0.47 | 0.02 |
| I_{CN11} | 77.02 | 9.89 | 1.58 | 0.10 |
| I_{G11} | 55.68 | 29.05 | 7.91 | 0.63 |
| I_{CN14} | 83.76 | 2.58 | 0.20 | 0.08 |
| I_{G14} | 76.88 | 11.09 | 1.37 | 0.12 |
| I_{CN17} | 76.24 | 18.98 | 0.03 | 0.07 |
| I_{G17} | 84.74 | 2.67 | 0.20 | 0.04 |
| I_{G18} | 85.55 | 2.45 | 0.02 | 0.01 |

$100\text{ Hz} \leq \Delta f_1 < 10\text{ kHz}$; $10\text{ kHz} \leq \Delta f_2 < 100\text{ kHz}$

$100\text{ kHz} \leq \Delta f_3 < 1\text{ MHz}$; $1\text{ MHz} \leq \Delta f_4 < 10\text{ MHz}$

Table I.48: Peak current and charge transferred at different points in the system calculated at three different instants of time (100 μ s, 500 μ s, and 1 ms) for stroke 4 of flash FPL0036.

| ID | Peak [kA] | Charge calculated in different time windows | | | | | | Saturation | |
|------------|--------------|---|-------|-------------|-------|-------|-------|------------|--|
| | | 100 μ s | | 500 μ s | | 1 ms | | | |
| | | [C] | % | [C] | % | [C] | % | | |
| I_i | -7.29 | -0.24 | 100.0 | -0.40 | 100.0 | -0.42 | 100.0 | - | |
| I_{Mi} | -7.24 | -0.23 | 100.0 | -0.38 | 100.0 | -0.40 | 100.0 | - | |
| I_{La} | - | - | - | - | - | - | - | - | |
| I_{CN1} | -0.13 | -0.01 | 3.8 | -0.03 | 9.1 | -0.04 | 10.5 | - | |
| I_{G1} | -0.31 | -0.02 | 8.0 | -0.03 | 8.9 | -0.04 | 9.0 | - | |
| I_{CN2} | -0.25 | -0.01 | 4.6 | -0.01 | 2.9 | -0.01 | 2.5 | - | |
| I_{N2} | -0.22 | -0.01 | 6.2 | -0.01 | 2.8 | 0.00 | 0.2 | - | |
| I_{G2} | -0.36 | -0.02 | 8.7 | -0.03 | 9.0 | -0.04 | 9.2 | - | |
| I_{CN5} | -0.38 | -0.01 | 5.0 | -0.01 | 3.0 | -0.01 | 2.1 | - | |
| I_{A5} | -0.10 | 0.00 | 0.0 | 0.00 | 0.0 | 0.00 | 0.1 | - | |
| I_{B5} | -0.03 | -0.00 | 0.1 | -0.00 | 0.0 | -0.00 | 0.0 | - | |
| I_{C5} | -0.37 | -0.02 | 8.7 | -0.05 | 13.0 | -0.06 | 15.1 | - | |
| I_{G5} | -0.70 | -0.03 | 13.4 | -0.05 | 13.3 | -0.05 | 13.4 | - | |
| I_{AN8} | -0.08 | -0.00 | 0.2 | 0.00 | 0.0 | 0.00 | 0.0 | - | |
| I_{BN8} | -0.08 | -0.00 | 0.0 | -0.00 | 0.0 | -0.00 | 0.1 | - | |
| I_{CN8} | - | - | - | - | - | - | - | - | |
| I_{N8} | -0.57 | -0.03 | 15.2 | -0.05 | 13.2 | -0.04 | 10.0 | - | |
| I_{G8} | -2.85 | -0.02 | 9.8 | -0.03 | 9.1 | -0.04 | 9.3 | - | |
| I_{A9} | -0.06 | 0.00 | 0.0 | 0.00 | 0.1 | 0.00 | 0.0 | - | |
| I_{B9} | -0.04 | 0.00 | 0.1 | 0.00 | 0.1 | -0.00 | 0.1 | - | |
| I_{C9} | -2.85 | -0.08 | 36.2 | -0.13 | 33.5 | -0.12 | 30.3 | - | |
| I_{CN11} | -2.84 | -0.05 | 22.9 | -0.07 | 19.6 | -0.06 | 15.4 | - | |
| I_{G11} | -1.94 | -0.02 | 7.5 | -0.02 | 6.4 | -0.03 | 6.4 | - | |
| I_{CN14} | -0.36 | -0.01 | 4.4 | -0.01 | 2.9 | -0.01 | 2.1 | - | |
| I_{G14} | -0.69 | -0.01 | 5.8 | -0.02 | 5.8 | -0.02 | 6.0 | - | |
| I_{CN17} | -0.27 | -0.01 | 5.2 | -0.01 | 3.6 | -0.01 | 3.2 | - | |
| I_{G17} | -0.42 | -0.01 | 6.5 | -0.03 | 7.6 | -0.03 | 7.8 | - | |
| I_{G18} | -0.46 | -0.03 | 11.7 | -0.05 | 14.0 | -0.06 | 14.4 | - | |

Table I.49: Power spectrum density of measured current waveforms integrated over four different frequency ranges as a percentage of its power spectrum density integrated over the bandwidth of the measurement for stroke 4 of flash FPL0036.

| ID | Δf_1 | Δf_2 | Δf_3 | Δf_4 |
|------------|--------------|--------------|--------------|--------------|
| I_i | 74.02 | 8.75 | 2.01 | 4.12 |
| I_{Mi} | 76.72 | 9.27 | 1.48 | 0.73 |
| I_{Li} | - | - | - | - |
| I_{CN1} | 83.97 | 0.71 | 0.06 | 0.01 |
| I_{G1} | 83.08 | 4.38 | 0.15 | 0.29 |
| I_{CN2} | 74.96 | 14.70 | 0.80 | 2.31 |
| I_{N2} | 84.88 | 2.62 | 0.29 | 0.75 |
| I_{G2} | 81.54 | 6.18 | 0.30 | 0.34 |
| I_{CN5} | 70.77 | 16.86 | 1.91 | 2.66 |
| I_{A5} | 0.84 | 3.96 | 27.05 | 68.08 |
| I_{B5} | 3.09 | 3.22 | 18.21 | 75.17 |
| I_{C5} | 81.31 | 4.94 | 0.22 | 0.50 |
| I_{G5} | 78.22 | 9.28 | 0.62 | 0.61 |
| I_{AN8} | 3.28 | 2.86 | 20.29 | 73.32 |
| I_{BN8} | 0.41 | 2.68 | 23.67 | 73.20 |
| I_{CN8} | - | - | - | - |
| I_{N8} | 83.44 | 4.07 | 0.17 | 0.34 |
| I_{G8} | 38.09 | 31.55 | 15.98 | 8.86 |
| I_{A9} | 1.62 | 1.97 | 19.42 | 76.69 |
| I_{B9} | 2.74 | 2.25 | 17.77 | 76.69 |
| I_{C9} | 76.32 | 10.12 | 1.75 | 0.81 |
| I_{CN11} | 71.08 | 11.46 | 4.26 | 2.25 |
| I_{G11} | 37.90 | 29.23 | 14.60 | 13.03 |
| I_{CN14} | 74.54 | 9.00 | 2.66 | 4.26 |
| I_{G14} | 67.40 | 16.63 | 3.13 | 2.81 |
| I_{CN17} | 77.10 | 11.47 | 0.83 | 2.13 |
| I_{G17} | 82.59 | 3.62 | 0.44 | 0.68 |
| I_{G18} | 84.11 | 2.99 | 0.10 | 0.21 |

$100\text{ Hz} \leq \Delta f_1 < 10\text{ kHz}$; $10\text{ kHz} \leq \Delta f_2 < 100\text{ kHz}$

$100\text{ kHz} \leq \Delta f_3 < 1\text{ MHz}$; $1\text{ MHz} \leq \Delta f_4 < 10\text{ MHz}$

Table I.50: Peak current and charge transferred at different points in the system calculated at three different instants of time ($100\ \mu s$, $500\ \mu s$, and 1 ms) for stroke 5 of flash FPL0036.

| ID | Peak [kA] | Charge calculated in different time windows | | | | | | Saturation | |
|------------|--------------|---|-------|-------------|-------|-------|-------|------------|--|
| | | 100 μs | | 500 μs | | 1 ms | | | |
| | | [C] | % | [C] | % | [C] | % | | |
| I_i | -8.64 | -0.29 | 100.0 | -0.49 | 100.0 | -0.53 | 100.0 | - | |
| I_{Mi} | -8.42 | -0.27 | 100.0 | -0.47 | 100.0 | -0.50 | 100.0 | - | |
| I_{Li} | - | - | - | - | - | - | - | - | |
| I_{CN1} | -0.14 | -0.01 | 3.2 | -0.04 | 7.8 | -0.04 | 8.6 | - | |
| I_{G1} | -0.38 | -0.02 | 8.2 | -0.04 | 8.8 | -0.04 | 8.8 | - | |
| I_{CN2} | -0.33 | -0.01 | 5.4 | -0.02 | 3.5 | -0.02 | 3.1 | - | |
| I_{N2} | -0.28 | -0.02 | 6.7 | -0.02 | 4.2 | -0.01 | 1.9 | - | |
| I_{G2} | -0.43 | -0.02 | 8.9 | -0.04 | 9.0 | -0.05 | 9.2 | - | |
| I_{CN5} | -0.49 | -0.02 | 5.8 | -0.02 | 3.7 | -0.02 | 3.0 | - | |
| I_{A5} | -0.13 | -0.00 | 0.0 | -0.00 | 0.0 | -0.00 | 0.1 | - | |
| I_{B5} | -0.05 | 0.00 | 0.0 | 0.00 | 0.1 | 0.00 | 0.2 | - | |
| I_{C5} | -0.44 | -0.02 | 8.8 | -0.06 | 12.4 | -0.07 | 14.1 | - | |
| I_{G5} | -0.87 | -0.04 | 13.8 | -0.06 | 13.4 | -0.07 | 13.3 | - | |
| I_{AN8} | -0.08 | 0.00 | 0.0 | 0.00 | 0.1 | 0.00 | 0.1 | - | |
| I_{BN8} | -0.08 | 0.00 | 0.1 | -0.00 | 0.0 | -0.00 | 0.1 | - | |
| I_{CN8} | - | - | - | - | - | - | - | - | |
| I_{N8} | -0.69 | -0.04 | 15.6 | -0.07 | 14.0 | -0.06 | 11.3 | - | |
| I_{G8} | -3.52 | -0.03 | 9.9 | -0.04 | 8.8 | -0.05 | 9.0 | - | |
| I_{A9} | -0.09 | 0.00 | 0.0 | 0.00 | 0.0 | 0.00 | 0.1 | - | |
| I_{B9} | -0.04 | -0.00 | 0.0 | -0.00 | 0.1 | -0.00 | 0.1 | - | |
| I_{C9} | -3.54 | -0.10 | 37.7 | -0.16 | 35.0 | -0.16 | 31.5 | - | |
| I_{CN11} | -3.51 | -0.06 | 23.1 | -0.09 | 20.3 | -0.08 | 16.7 | - | |
| I_{G11} | -2.48 | -0.02 | 7.7 | -0.03 | 6.7 | -0.03 | 6.7 | - | |
| I_{CN14} | -0.45 | -0.01 | 4.9 | -0.02 | 3.5 | -0.01 | 2.9 | - | |
| I_{G14} | -0.82 | -0.02 | 6.0 | -0.03 | 6.0 | -0.03 | 6.1 | - | |
| I_{CN17} | -0.34 | -0.02 | 5.9 | -0.02 | 4.2 | -0.02 | 3.9 | - | |
| I_{G17} | -0.48 | -0.02 | 6.6 | -0.04 | 7.6 | -0.04 | 7.7 | - | |
| I_{G18} | -0.54 | -0.03 | 11.9 | -0.06 | 13.7 | -0.07 | 13.6 | - | |

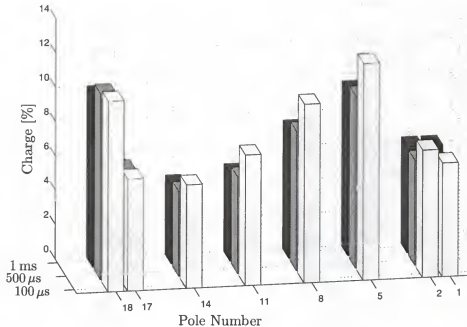


Figure I.12: Percentage of total charge transferred to ground at different poles, calculated at three different instants of time ($100\ \mu s$, $500\ \mu s$, and $1\ ms$ from the beginning of the return stroke), for stroke 2 of flash FPL0036 (See Table I.44). Lightning strike point is between poles 9 and 10.

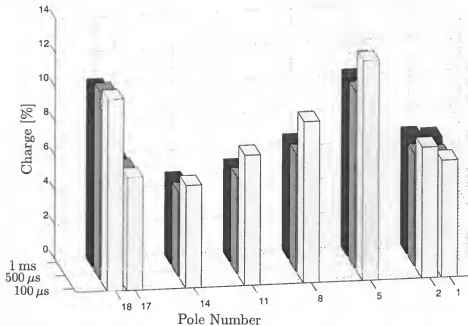


Figure I.13: Percentage of total charge transferred to ground at different poles, calculated at three different instants of time ($100\ \mu s$, $500\ \mu s$, and $1\ ms$ from the beginning of the return stroke), for stroke 3 of flash FPL0036 (See Table I.46). Lightning strike point is between poles 9 and 10.

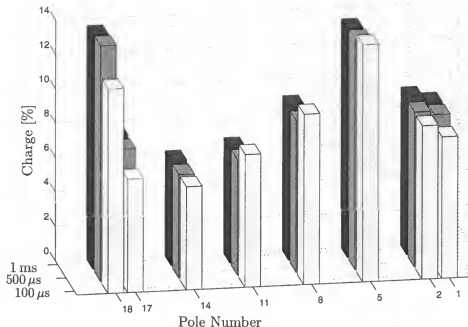


Figure I.14: Percentage of total charge transferred to ground at different poles, calculated at three different instants of time ($100 \mu\text{s}$, $500 \mu\text{s}$, and 1 ms from the beginning of the return stroke), for stroke 5 of flash FPL0036 (See Table I.50). Lightning strike point is between poles 9 and 10.

Table I.51: Power spectrum density of measured current waveforms integrated over four different frequency ranges as a percentage of its power spectrum density integrated over the bandwidth of the measurement for stroke 5 of flash FPL0036.

| ID | Δf_1 | Δf_2 | Δf_3 | Δf_4 |
|------------|--------------|--------------|--------------|--------------|
| I_i | 75.63 | 8.36 | 1.72 | 2.97 |
| I_{Mi} | 77.30 | 9.28 | 1.35 | 0.49 |
| I_{L1} | - | - | - | - |
| I_{CN1} | 83.96 | 0.68 | 0.05 | 0.01 |
| I_{G1} | 83.32 | 4.48 | 0.14 | 0.19 |
| I_{CN2} | 78.58 | 11.75 | 0.50 | 1.27 |
| I_{N2} | 84.99 | 2.76 | 0.20 | 0.48 |
| I_{G2} | 82.12 | 5.90 | 0.26 | 0.24 |
| I_{CN5} | 74.92 | 13.57 | 1.45 | 1.48 |
| I_{A5} | 0.94 | 5.13 | 30.11 | 63.78 |
| I_{B5} | 3.38 | 3.21 | 19.14 | 73.75 |
| I_{C5} | 81.88 | 4.97 | 0.16 | 0.33 |
| I_{G5} | 78.71 | 9.13 | 0.59 | 0.39 |
| I_{AN8} | 1.32 | 3.37 | 22.33 | 72.81 |
| I_{BN8} | 1.48 | 2.63 | 24.93 | 70.80 |
| I_{CN8} | - | - | - | - |
| I_{N8} | 83.36 | 4.24 | 0.13 | 0.22 |
| I_{G8} | 39.73 | 31.71 | 16.71 | 6.23 |
| I_{A9} | 0.53 | 2.55 | 18.75 | 78.04 |
| I_{B9} | 1.36 | 2.58 | 18.59 | 77.19 |
| I_{C9} | 77.30 | 9.58 | 1.57 | 0.52 |
| I_{CN11} | 71.42 | 11.71 | 4.24 | 1.62 |
| I_{G11} | 41.56 | 29.68 | 14.25 | 8.75 |
| I_{CN14} | 77.83 | 7.35 | 2.04 | 2.38 |
| I_{G14} | 69.86 | 15.29 | 2.76 | 1.82 |
| I_{CN17} | 79.18 | 10.06 | 0.46 | 1.14 |
| I_{G17} | 82.82 | 3.64 | 0.41 | 0.47 |
| I_{G18} | 84.37 | 3.04 | 0.07 | 0.14 |

$100 \text{ Hz} \leq \Delta f_1 < 10 \text{ kHz}$; $10 \text{ kHz} \leq \Delta f_2 < 100 \text{ kHz}$

$100 \text{ kHz} \leq \Delta f_3 < 1 \text{ MHz}$; $1 \text{ MHz} \leq \Delta f_4 < 10 \text{ MHz}$

Table I.52: Peak current and charge transferred at different points in the system calculated at three different instants of time (100 μ s, 500 μ s, and 1 ms) for stroke 1 of flash FPL0037.

| ID | Peak [kA] | Charge calculated in different time windows | | | | | | Saturation | |
|------------|--------------|---|-------|-------------|-------|---------|-------|------------|--|
| | | 100 μ s | | 500 μ s | | 1 ms | | | |
| | | [C] | % | [C] | % | [C] | % | | |
| I_i | -47.43 | -1.97 | 100.0 | -4.59 | 100.0 | -11.07 | 100.0 | Slight | |
| I_{Mi} | <-19.11 | <-1.62 | >82.2 | <-4.18 | >91.0 | <-10.60 | >95.8 | Severe | |
| I_{Li} | <-3.96 | <-0.37 | >18.6 | <-1.83 | >39.8 | <-3.73 | >33.7 | Severe | |
| I_{CN1} | -0.18 | -0.00 | 0.3 | -0.01 | 0.1 | -0.01 | 0.1 | - | |
| I_{G1} | - | - | - | - | - | - | - | - | |
| I_{CN2} | -1.41 | -0.04 | 2.0 | -0.04 | 0.9 | -0.04 | 0.4 | - | |
| I_{N2} | <-2.80 | <-0.20 | >10.4 | <-0.69 | >15.0 | <-0.89 | >8.0 | Severe | |
| I_{G2} | <-2.26 | <-0.17 | >8.6 | <-0.41 | >8.9 | <-1.01 | >9.1 | Severe | |
| I_{CN5} | -1.99 | -0.02 | 1.1 | -0.02 | 0.5 | -0.02 | 0.2 | - | |
| I_{A5} | -0.81 | -0.01 | 0.3 | -0.01 | 0.1 | -0.00 | 0.0 | - | |
| I_{B5} | -0.63 | -0.02 | 1.1 | -0.02 | 0.5 | -0.02 | 0.2 | - | |
| I_{C5} | -0.29 | -0.00 | 0.0 | -0.00 | 0.0 | -0.00 | 0.0 | - | |
| I_{G5} | <-4.49 | <-0.28 | >14.4 | <-0.63 | >13.7 | <-1.55 | >14.0 | Severe | |
| I_{AN8} | -0.09 | 0.02 | 1.0 | 0.02 | 0.5 | 0.03 | 0.2 | - | |
| I_{BN8} | <-3.00 | <-0.00 | >0.2 | <-0.00 | >0.1 | <0.00 | >0.0 | Severe | |
| I_{CN8} | -0.36 | -0.00 | 0.0 | -0.00 | 0.1 | -0.00 | 0.0 | - | |
| I_{N8} | <-3.96 | <-0.34 | >17.5 | <-0.64 | >14.0 | <-0.69 | >6.2 | Severe | |
| I_{G8} | <-13.79 | <-0.23 | >11.5 | <-0.42 | >9.2 | <-1.03 | >9.3 | Severe | |
| I_{A9} | -0.08 | 0.01 | 0.4 | 0.01 | 0.2 | 0.01 | 0.1 | - | |
| I_{B9} | <-1.50 | <-0.04 | >2.2 | <-0.03 | >0.7 | <-0.03 | >0.2 | Severe | |
| I_{C9} | <-14.10 | <-1.12 | >56.9 | <-3.16 | >68.7 | <-7.03 | >63.6 | Severe | |
| I_{CN11} | <-11.20 | <-0.11 | >5.7 | <-0.11 | >2.4 | <-0.10 | >0.9 | Severe | |
| I_{G11} | <-12.88 | <-0.16 | >8.2 | <-0.32 | >7.0 | <-0.78 | >7.0 | Severe | |
| I_{CN14} | -1.55 | -0.04 | 1.9 | -0.04 | 0.8 | -0.04 | 0.3 | - | |
| I_{G14} | <-4.37 | <-0.12 | >5.9 | <-0.28 | >6.1 | <-0.69 | >6.2 | Severe | |
| I_{CN17} | -1.79 | -0.10 | 4.9 | -0.10 | 2.1 | -0.10 | 0.9 | - | |
| I_{G17} | -2.02 | -0.12 | 5.9 | -0.34 | 7.4 | -0.81 | 7.4 | Slight | |
| I_{G18} | <-2.72 | <-0.20 | >9.9 | <-0.57 | >12.4 | <-1.40 | >12.6 | Severe | |

Table I.53: Power spectrum density of measured current waveforms integrated over four different frequency ranges as a percentage of its power spectrum density integrated over the bandwidth of the measurement for stroke 1 of flash FPL0037.

| ID | Δf_1 | Δf_2 | Δf_3 | Δf_4 |
|------------|--------------|--------------|--------------|--------------|
| I_i | 82.76 | 2.52 | 0.28 | 0.03 |
| I_{Mi} | - | - | - | - |
| I_{Li} | - | - | - | - |
| I_{CN1} | 77.66 | 16.28 | 0.46 | 0.05 |
| I_{G1} | 5.23 | 7.65 | 22.84 | 63.92 |
| I_{CN2} | 60.29 | 35.69 | 0.12 | 0.13 |
| I_{N2} | - | - | - | - |
| I_{G2} | - | - | - | - |
| I_{CN5} | 34.51 | 59.68 | 3.21 | 0.38 |
| I_{A5} | 24.70 | 68.94 | 3.97 | 1.58 |
| I_{B5} | 62.18 | 33.78 | 0.18 | 0.32 |
| I_{C5} | 10.70 | 12.84 | 23.33 | 52.37 |
| I_{G5} | - | - | - | - |
| I_{AN8} | 25.98 | 59.94 | 10.52 | 1.49 |
| I_{BN8} | - | - | - | - |
| I_{CN8} | 9.46 | 4.53 | 20.92 | 63.77 |
| I_{N8} | - | - | - | - |
| I_{G8} | - | - | - | - |
| I_{A9} | 26.22 | 57.47 | 9.94 | 4.06 |
| I_{B9} | - | - | - | - |
| I_{C9} | - | - | - | - |
| I_{CN11} | - | - | - | - |
| I_{G11} | - | - | - | - |
| I_{CN14} | 63.28 | 31.41 | 0.98 | 0.20 |
| I_{G14} | - | - | - | - |
| I_{CN17} | 82.97 | 10.45 | 0.03 | 0.03 |
| I_{G17} | 83.70 | 0.92 | 0.06 | 0.00 |
| I_{G18} | - | - | - | - |

$100 \text{ Hz} \leq \Delta f_1 < 10 \text{ kHz} ; 10 \text{ kHz} \leq \Delta f_2 < 100 \text{ kHz}$

$100 \text{ kHz} \leq \Delta f_3 < 1 \text{ MHz} ; 1 \text{ MHz} \leq \Delta f_4 < 10 \text{ MHz}$

Table I.54: Peak current and charge transferred at different points in the system calculated at three different instants of time (100 μ s, 500 μ s, and 1 ms) for stroke 2 of flash FPL0037.

| ID | Peak [kA] | Charge calculated in different time windows | | | | | | Saturation | |
|------------|--------------|---|-------|-------------|-------|--------|-------|------------|--|
| | | 100 μ s | | 500 μ s | | 1 ms | | | |
| | | [C] | % | [C] | % | [C] | % | | |
| I_i | -20.36 | -0.64 | 100.0 | -1.39 | 100.0 | -1.76 | 100.0 | - | |
| I_{Mi} | <-19.11 | <-0.62 | >97.4 | <-1.33 | >96.0 | <-1.69 | >95.9 | Severe | |
| I_{Li} | <-3.96 | <-0.35 | >55.3 | <-0.92 | >66.5 | <-1.21 | >68.8 | Severe | |
| I_{CN1} | -0.14 | -0.00 | 0.3 | -0.00 | 0.2 | -0.00 | 0.2 | - | |
| I_{G1} | - | - | - | - | - | - | - | - | |
| I_{CN2} | -0.53 | -0.01 | 0.9 | -0.01 | 0.4 | -0.01 | 0.3 | - | |
| I_{N2} | -1.29 | -0.09 | 14.4 | -0.22 | 16.1 | -0.29 | 16.2 | - | |
| I_{G2} | -1.55 | -0.06 | 9.1 | -0.13 | 9.0 | -0.16 | 9.1 | - | |
| I_{CN5} | -0.97 | -0.00 | 0.7 | -0.00 | 0.3 | -0.00 | 0.2 | - | |
| I_{A5} | -0.38 | -0.00 | 0.1 | -0.00 | 0.1 | -0.00 | 0.1 | - | |
| I_{B5} | -0.11 | -0.00 | 0.1 | -0.00 | 0.0 | -0.00 | 0.0 | - | |
| I_{C5} | -0.05 | -0.00 | 0.0 | -0.00 | 0.0 | -0.00 | 0.0 | - | |
| I_{G5} | -2.92 | -0.09 | 14.8 | -0.19 | 13.6 | -0.24 | 13.6 | - | |
| I_{AN8} | -0.10 | 0.00 | 0.4 | 0.00 | 0.2 | 0.00 | 0.1 | - | |
| I_{BN8} | -0.59 | 0.00 | 0.4 | 0.00 | 0.3 | 0.00 | 0.2 | - | |
| I_{CN8} | -0.37 | -0.00 | 0.1 | -0.00 | 0.2 | -0.00 | 0.2 | - | |
| I_{N8} | -2.65 | -0.19 | 29.2 | -0.42 | 30.3 | -0.53 | 30.0 | - | |
| I_{G8} | -10.02 | -0.07 | 11.4 | -0.12 | 8.6 | -0.15 | 8.4 | Slight | |
| I_{A9} | -0.05 | 0.00 | 0.2 | 0.00 | 0.1 | 0.00 | 0.1 | - | |
| I_{B9} | -0.67 | 0.00 | 0.2 | 0.00 | 0.1 | 0.00 | 0.0 | - | |
| I_{C9} | -9.95 | -0.42 | 65.9 | -0.97 | 70.1 | -1.24 | 70.4 | - | |
| I_{CN11} | -6.86 | -0.03 | 4.3 | -0.03 | 2.0 | -0.03 | 1.6 | - | |
| I_{G11} | -5.53 | -0.05 | 7.7 | -0.09 | 6.6 | -0.12 | 6.6 | - | |
| I_{CN14} | -0.86 | -0.01 | 1.0 | -0.01 | 0.5 | -0.01 | 0.3 | - | |
| I_{G14} | -2.19 | -0.04 | 5.7 | -0.08 | 5.9 | -0.11 | 6.1 | - | |
| I_{CN17} | -0.83 | -0.02 | 2.6 | -0.02 | 1.2 | -0.02 | 0.9 | - | |
| I_{G17} | -1.16 | -0.03 | 5.5 | -0.10 | 7.2 | -0.13 | 7.4 | - | |
| I_{G18} | -0.82 | -0.05 | 8.0 | -0.13 | 9.5 | -0.17 | 9.6 | - | |

Table I.55: Power spectrum density of measured current waveforms integrated over four different frequency ranges as a percentage of its power spectrum density integrated over the bandwidth of the measurement for stroke 2 of flash FPL0037.

| ID | Δf_1 | Δf_2 | Δf_3 | Δf_4 |
|------------|--------------|--------------|--------------|--------------|
| I_i | 78.88 | 6.54 | 1.06 | 0.53 |
| I_{Mi} | - | - | - | - |
| I_{Li} | - | - | - | - |
| I_{CN1} | 46.84 | 49.27 | 1.55 | 0.25 |
| I_{G1} | 2.94 | 5.94 | 23.55 | 67.02 |
| I_{CN2} | 25.89 | 68.07 | 1.38 | 3.11 |
| I_{N2} | 85.30 | 1.77 | 0.01 | 0.02 |
| I_{G2} | 84.46 | 2.02 | 0.49 | 0.04 |
| I_{CN5} | 13.65 | 71.28 | 10.39 | 3.63 |
| I_{A5} | 6.87 | 41.51 | 26.09 | 25.47 |
| I_{B5} | 3.76 | 33.97 | 20.46 | 41.66 |
| I_{C5} | 2.09 | 3.42 | 22.85 | 71.40 |
| I_{G5} | 80.83 | 5.93 | 0.78 | 0.06 |
| I_{AN8} | 7.51 | 40.67 | 30.25 | 21.03 |
| I_{BN8} | 9.15 | 27.42 | 42.30 | 19.78 |
| I_{CN8} | 2.63 | 2.87 | 22.30 | 71.83 |
| I_{N8} | 84.62 | 2.32 | 0.02 | 0.01 |
| I_{G8} | 46.65 | 31.06 | 15.00 | 1.00 |
| I_{A9} | 7.15 | 27.30 | 27.95 | 36.84 |
| I_{B9} | 3.39 | 12.09 | 64.10 | 20.08 |
| I_{C9} | 82.94 | 2.93 | 0.52 | 0.02 |
| I_{CN11} | 16.79 | 58.52 | 20.78 | 2.90 |
| I_{G11} | 56.93 | 21.12 | 11.54 | 1.60 |
| I_{CN14} | 26.49 | 62.72 | 5.99 | 3.29 |
| I_{G14} | 76.23 | 8.36 | 2.27 | 0.33 |
| I_{CN17} | 47.66 | 48.76 | 0.27 | 0.55 |
| I_{G17} | 82.76 | 2.29 | 0.36 | 0.12 |
| I_{G18} | 83.36 | 2.65 | 0.04 | 0.05 |

$100 \text{ Hz} \leq \Delta f_1 < 10 \text{ kHz}$; $10 \text{ kHz} \leq \Delta f_2 < 100 \text{ kHz}$

$100 \text{ kHz} \leq \Delta f_3 < 1 \text{ MHz}$; $1 \text{ MHz} \leq \Delta f_4 < 10 \text{ MHz}$

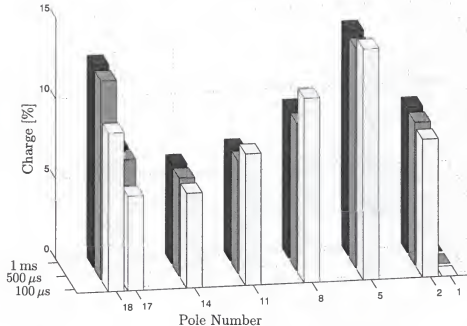


Figure I.15: Percentage of total charge transferred to ground at different poles, calculated at three different instants of time ($100 \mu\text{s}$, $500 \mu\text{s}$, and 1 ms from the beginning of the return stroke), for stroke 1 of flash FPL0037 (See Table I.52). Lightning strike point was at pole 9.

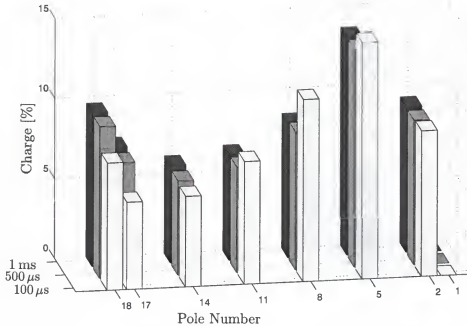


Figure I.16: Percentage of total charge transferred to ground at different poles, calculated at three different instants of time ($100 \mu\text{s}$, $500 \mu\text{s}$, and 1 ms from the beginning of the return stroke), for stroke 2 of flash FPL0037 (See Table I.54). Lightning strike point was at pole 9.

BIBLIOGRAPHY

M. Abramowitz and I. Stegun. *Handbook of Mathematical Functions With Formulas, Graphs, and Mathematical Tables*. National Bureau of Standards, Applied Mathematics Series 55, Washington, DC, tenth edition, 1972.

A. Ametani. Highly efficient method for calculating transmission line transients. *IEEE Transactions on Power Apparatus and Systems*, PAS-95(5):1545–1551, Sep-Oct 1976.

H. Andoh, S. Nishiaki, H. Suzuki, S. Boggs, and J. Kuang. Failure mechanisms and recent improvements in ZnO arrester elements. *IEEE Electrical Insulation Magazine*, 16(1):25–31, January/February 2000.

P. Barker, T. Short, H. Mercure, S. Cyr, and J. O'Brien. Surge arrester energy duty considerations following from triggered lightning experiments. *1998 Winter Power Meeting, Panel Session on Transmission Line Surge Arrester Application Experience*, 1998.

E. M. Bazelyan, B. N. Gorin, and V. I. Levitov. Physical and engineering foundations of lightning protection. *Gidrometeoizdat*, St. Petersburg, Russia, 1978.

P. W. Berg and J. L. McGregor. *Elementary Partial Differential Equations*. Holden-Day, Inc., Oakland, California, 1966.

K. Berger, R. B. Anderson, and H. Kroninger. Parameters of lightning flashes. *Electra*, (41):23–27, July 1975.

K. Berger and E. Vogelsanger. Photographische blitzuntersuchungen der Jahre 1955–1965 auf dem Monte San Salvatore. *Bull. Schweiz. Elektrotech. Ver.*, 57:1–22, 1966.

G. W. Bowdler. *Measurements in High-Voltage test circuits*. Pergamon Press, Oxford, New York, 1973.

F. H. Branin. Transient analysis of lossless transmission lines. *Proc. IEEE*, 55:2012–2013, November 1967.

A. Budner. Introduction of frequency-dependent line parameters into an electromagnetic transients program. *IEEE Transactions on Power Apparatus and Systems*, PAS-89(1):88–97, January 1970.

Alternative Transients Program (ATP) Rule Book. Can-Am EMTP User Group, Portland, OR, 1987–1998.

D. P. Carroll and F. Nozari. Efficient computer method for simulating transients on transmission lines with frequency dependent parameters. *IEEE Transactions on Power Apparatus and Systems*, PAS-94(4):1167–1176, Jul-Aug 1975.

J. R. Carson. Wave propagation in overhead wires with ground returns. *Bell System Technical Journal*, 5:539–554, 1926.

Jack Cartinhour. *Digital Signal Processing: An Overview of Basic Principles*. Prentice Hall, Upper Saddle River, New Jersey, 1998.

CIGRE. Guide to procedures for estimating the lightning performance of transmission lines. *CIGRE Working Group 33-01 (Lightning) of Study Committee 33 (Overvoltages and Insulation Coordination)*, Paris, October 1991.

R.A.W. Connor and R.A. Parkins. Operations statistics in the management of large distribution system. *Proc. IEE*, 133, 1966.

F. C. Creed. *The Generation and Measurement of High Voltage Impulses*. Center Book Publishers, Inc., Princeton, New Jersey, 1989.

E. G. da Costa, A. G. da Lima, and S.R. Naidu. Electrothermal model for complete metal oxide surge arresters. In *IEE Conference Publication*, volume 2, pages 2.242.S13–2.245.S13, London, UK, 1999.

C. Dang, T. M. Parnell, and P. J. Price. Response of metal oxide surge arresters to steep fronted current impulses. *IEEE Transactions on Power Delivery*, PWRD-1(1):157–163, Jan 1986.

Power System Analysis Using EMTP/ATP. Department of Electrical Engineering, University of Florida, Gainesville, Florida, March 1999.

H. W. Domme. Digital computer solution on electromagnetic transients in single- and multiphase networks. *IEEE Transactions on Power Apparatus and Systems*, PAS-88(4):388–399, April 1969.

H. W. Domme. *Electromagnetic Transients Program Reference Manual (EMTP theory book)*. Bonneville Power Administration, Portland, OR, 1986.

C. Drilling, M. Droidner, E. G. Jordan, and J. Meppelink. A device for correct measurement of the residual voltage of low voltage surge arresters and spark gaps during the application of high rate of rise current impulses. *ICLP'98*, pages 899–904, 1998.

D. W. Durbak. Zinc-oxide arrester model for fast surges. *EMTP Newsletter*, 5(1), January 1985.

P. M. Embree and D. Danieli. *C++ Algorithms for Digital Signal Processing*. Prentice Hall PTR, Upper Saddle River, NJ, second edition, 1999.

A. J. Eriksson. Lightning and tall structures. *Trans. SA Inst. Electr. Eng.*, (69):2–16, August 1978.

A. J. Eriksson, M. F. Stringfellow, and D. V. Meal. Lightning-induced overvoltages on overhead distribution lines. *IEEE Transactions on Power Apparatus and Systems*, PAS-101(4):960–968, April 1982.

M. I. Fernandez. Responses of an unenergized test power distribution system to direct and nearby lightning strikes. Master's thesis, University of Florida, Gainesville, Florida, 1997.

M. I. Fernandez, C. T. Mata, V. A. Rakov, M. A. Uman, K. J. Rambo, M. V. Stapleton, and M. Bejleri. Improved Lightning Arrester Protection Results, Final Results. Technical Report TR-109670-R1, Electric Power Research Institute (EPRI), Palo Alto, CA, December 1998.

M. I. Fernandez, V. A. Rakov, and M. A. Uman. Overvoltages in Underground Systems, Phase I Results. Technical Report TR-109669, Electric Power Research Institute (EPRI), Palo Alto, CA, Dec 1997a.

M. I. Fernandez, V. A. Rakov, and M. A. Uman. Testing of Lightning Arresters and Improved Lightning Protection, Preliminary Results. Technical Report TR-109670, Electric Power Research Institute (EPRI), Palo Alto, CA, Dec 1997b.

R. J. Fisher, G. H. Schnetzer, R. Thottappillil, V. A. Rakov, M. A. Uman, and J. D. Goldberg. Parameters of triggered-lightning flashes in Florida and Alabama. *Journal of Geophysical Research*, 98(D12):22887–22902, December 1993.

Distribution Construction Standards. FPL, West Palm Beach, 1996 edition, August 1996.

N. Georgiadis, M. Rubinstein, M. A. Uman, P. J. Medullas, and E. M. Thomson. Lightning-induced voltages at both ends of a 448-m power-distribution line. *IEEE Transactions on Electromagnetic Compatibility*, 34(4):452–460, November 1992.

A. Greenwood. *Electrical Transients in Power Systems*. John Wiley & Sons, Inc., second edition, 1991.

E. Groschupf. *Simulation of transient phenomena in system with HVDC and ac transmission lines*. PhD thesis, Technical University, Darmstadt, Germany, 1976.

T. Hagiwara, T. Funabashi, H. Watanabe, N. Takeuchi, and T. Ueda. Metal-oxide surge arrester model with active v-i characteristics. *Electrical Engineering in Japan*, 121(1):35–42, Oct. 1997.

J. F. Hauer. State-space modeling of transmission line dynamics via nonlinear optimization. *IEEE Transactions on Power Apparatus and Systems*, PAS-100(12): 4918–4925, December 1981.

IEEE. *IEEE guide for measuring earth resistivity, ground impedance, and earth surface potentials of a ground system*. Institute of Electrical and Electronics Engineers, Inc., An American National Standard, ANSI/IEEE Std 81-1983, 1983.

IEEE. *IEEE Standard Techniques for High-Voltage Testing*. IEEE Power Engineering Society, New York, New York, October 1995. IEEE Std 4-1995.

IEEE-EEI. Report of Joint IEEE-EEI Subject Committee on EHV Line Outages. *Trans. IEEE*, 86, 1967.

IEEE Working Group 3.4.11. Modeling of metal oxide surge arresters. *IEEE Transactions on Power Delivery*, 7(1):302-308, Jan. 1992.

A. F. Imece, D. W. Durbak, H. Elahi, S. Kolluri, A. Lux, D. Mader, T. E. McDermott, A. Morched, A. M. Mousa, R. Natarajan, L. Rugeles, and E. Tarasiewicz. Modeling guidelines for fast front transients. *IEEE Transactions on Power Delivery*, 11(1):493-501, Jan 1996.

A. Jeffrey. *Handbook of Mathematical Formulas and Integrals*. Academic Press, Inc., San Diego, California, 1995.

M. Khalifa. *High-Voltage Engineering*. Marcel Dekker, Inc., New York, New York, 1990.

Ikmo Kim, Toshihisa Funabashi, Haruo Sasaki, Toyohisa Hagiwara, and Misao Kobayashi. Study of zno arrester model for steep front wave. *IEEE Transactions on Power Delivery*, 11(2):834-841, April 1996.

M. Kobayashi, H. Sasaki, and K. Nakamura. Rocket-triggered lightning experiments on zinc oxide arresters and their applications to power transmission lines. *Electrical Engineering in Japan*, 122(4):25-33, March 1998.

E. Kuffel. *High-Voltage Engineering: Fundamentals*. Pergamon Press, Oxford, New York, 1984.

C. Leteinturier, J. H. Hamelin, and A. Eybert-Berard. Submicrosecond characteristics of lightning return-stroke currents. *ieeemc*, 33(4):351-357, November 1991.

J. R. Lucas and P. G. McLaren. A computationally efficient mov model for series compensation studies. *IEEE Transactions on Power Delivery*, 6(4):1491-1497, Oct 1991.

P. C. Magnusson. Traveling waves on multi-conductor open-wire lines em dash a numerical survey of the effects of frequency dependence of modal composition. *IEEE Transactions on Power Apparatus and Systems*, PAS-92(3):999-1008, May-Jun 1973.

J. R. Marti. *The problem of frequency dependence in transmission line modelling*. PhD thesis, The University of British Columbia, Vancouver, Canada, April 1981.

J. R. Marti. Accurate modelling of frequency-dependent transmission lines in electromagnetic transient simulations. *IEEE Transactions on Power Apparatus and Systems*, PAS-101(1):147–157, January 1982.

M. J. Master, M. A. Uman, W. H. Beasley, and M. Darveniza. Lightning induced voltages in power lines: Experiment. *IEEE Transactions on Power Apparatus and Systems*, PAS-103(9):2519–2529, September 1984.

M. J. Master, M. A. Uman, W. H. Beasley, and M. Darveniza. Voltages induced in an overhead line by the lightning stepped leader. *IEEE Transactions on Electromagnetic Compatibility*, EMC-28(3):158–161, August 1986.

C. T. Mata, M. I. Fernandez, V. Rakov, and M. A. Uman. EMTP modeling of a triggered-lightning strike to the phase conductor of an overhead distribution line. *IEEE Transactions on Power Delivery*, 2000a. In press.

C. T. Mata, M. I. Fernandez, V. A. Rakov, M. A. Uman, M. Bejleri, K. J. Rambo, and M. V. Stapleton. Overvoltages in Underground Systems, Phase 2 Results. Technical Report TR-109669-R1, Electric Power Research Institute (EPRI), Palo Alto, CA, December 1998a. Co-sponsored by Duquesne Light Co., Pittsburgh, PA.

C. T. Mata, M. I. Fernandez, V. A. Rakov, M. A. Uman, K. J. Rambo, and M. V. Stapleton. Investigation of lightning entry into a secondary service, using rocket triggered lightning. Technical Report TR-110418, EPRI, Palo Alto, CA, April 1998b.

C. T. Mata, V. A. Rakov, K. J. Rambo, M. V. Stapleton, and M. A. Uman. UF/FPL study of triggered lightning strikes to FPL distribution lines. Technical report, Florida Power and Light, Miami, Florida, September 1999a. Preliminary Report.

C. T. Mata, V. A. Rakov, K. J. Rambo, M. V. Stapleton, and M. A. Uman. UF/FPL study of triggered lightning strikes to FPL distribution lines. Technical report, Florida Power and Light, Miami, Florida, December 1999b. Final Report.

C. T. Mata, V. A. Rakov, K. J. Rambo, and M. A. Uman. UF/FPL study of triggered lightning strikes to FPL distribution lines. Technical report, Florida Power and Light, Miami, Florida, December 2000b. Final Report, Supplement 1, Flash FPL0011.

C. T. Mata, V. A. Rakov, K. J. Rambo, and M. A. Uman. UF/FPL study of triggered lightning strikes to FPL distribution lines. Technical report, Florida Power and Light, Miami, Florida, December 2000c. Final Report, Supplement 2, Flash FPL0014.

C. T. Mata, V. A. Rakov, K. J. Rambo, and M. A. Uman. UF/FPL study of triggered lightning strikes to FPL distribution lines. Technical report, Florida Power and Light, Miami, Florida, December 2000d. Final Report, Supplement 3, Flash FPL0018.

C. T. Mata, V. A. Rakov, K. J. Rambo, and M. A. Uman. UF/FPL study of triggered lightning strikes to FPL distribution lines. Technical report, Florida Power and Light, Miami, Florida, December 2000e. Final Report, Supplement 4, Flash FPL0032.

C. T. Mata, V. A. Rakov, K. J. Rambo, and M. A. Uman. UF/FPL study of triggered lightning strikes to FPL distribution lines. Technical report, Florida Power and Light, Miami, Florida, December 2000f. Final Report, Supplement 5, Flash FPL0033.

C. T. Mata, V. A. Rakov, K. J. Rambo, and M. A. Uman. UF/FPL study of triggered lightning strikes to FPL distribution lines. Technical report, Florida Power and Light, Miami, Florida, December 2000g. Final Report, Supplement 6, Flash FPL0034.

C. T. Mata, V. A. Rakov, K. J. Rambo, and M. A. Uman. UF/FPL study of triggered lightning strikes to FPL distribution lines. Technical report, Florida Power and Light, Miami, Florida, December 2000h. Final Report, Supplement 8, Flash FPL0037.

C. T. Mata, V. A. Rakov, K. J. Rambo, and M. A. Uman. UF/FPL study of triggered lightning strikes to FPL distribution lines. Technical report, Florida Power and Light, Miami, Florida, December 2000i. Final Report.

C. T. Mata, V. A. Rakov, K. J. Rambo, and M. A. Uman. UF/FPL study of triggered lightning strikes to FPL distribution lines. Technical report, Florida Power and Light, Miami, Florida, December 2000j. Final Report, Supplement 7, Flash FPL0036.

R. E. Matick. *Transmission Lines for Digital and Communication Networks. An Introduction to Transmission Lines, High-frequency and High-speed Pulse Characteristics and Applications*. IEEE PRESS, New York, New York, 1995.

MATLAB. *Signal Processing Toolbox*. The Mathworks, Inc., Natick, MA, 4 edition, 1996.

Y. Matsumoto, O. Sakuma, K. Shinjo, M. Saiki, T. Wakai, T. Sakai, H. Nagasaka, H. Motoyama, and M. Ishii. Measurement of lightning surges on test transmission line equipped with arresters struck by natural and triggered lightning. *IEEE Transactions on Power Delivery*, 11(2):996–1002, Apr 1996.

W. S. Meyer and H. W. Domme. Numerical modelling of frequency-dependent transmission-line parameters in an electromagnetic transients program. *IEEE Transactions on Power Apparatus and Systems*, PAS-93(5):1401–1409, October 1974.

1999 Short Course on High Voltage Measuring Techniques. Mississippi State University, Mississippi, USA, April 1999.

H. Motoyama, Y. Matsumoto, and N. Itamoto. Observation and analysis of multi-phase back flashover on the okushishiku test transmission line caused by winter lightning. *IEEE Transactions on Power Delivery*, 13(4):1391–1398, Oct 1998.

K. Mukae, K. Tsuda, and S. Shiga. Zinc oxide-praseodymium oxide elements for surge arresters. In *1987. IEEE, New York, NY, USA. 8p 87WM219-9*, New Orleans, LA, 1987. IEEE Power Engineering Society.

M. S. Naidu and V. Kamaraju. *High Voltage Engineering*. McGraw-Hill, 1995.

T. Noda. *User Instructions of Noda Setup in ATP*, March 1997.

T. Noda and A. Ametani. *User instructions of Noda Ssetup in ATP*, July 1998. Original manuscript was prepared in March 1997 and revised by A. Ametani in Jly 1998.

T. Noda, N. Nagaoka, and A. Ametani. Phase domain modeling of frequency-dependent transmission lines by means of an ARMA model. *IEEE Transactions on Power Delivery*, 11(1):401–407, January 1996.

M. Pereira, K. Sadek, and G. Lafond. Development and synthetic tests of a MOV thermal model for series compensation. In *International Conference on Digital Power System Simulators, Proceedings, ICDS 1995*, pages 227–232, Piscataway, NJ, 1995. IEEE.

A. Petit, X. D. Do, and G. St-Jean. An experimental method to determine the electro-thermal model parameters of metal oxide surge arresters. *IEEE Transactions on Power Delivery*, 6(2):715–721, April 1991.

P. Pinceti and M. Giannettoni. Simplified model for zinc oxide surge arresters. *IEEE Transactions on Power Delivery*, 14(2):393–398, April 1999.

F. Rachidi, M. Rubinstein, S. Guerrieri, and C. A. Nucci. Voltages induced on overhead lines by dart leaders and subsequent return strokes in natural and triggered lightning. *IEEE Transactions on Electromagnetic Compatibility*, 39(2):160–166, May 1997.

V. A. Rakov and M. A. Uman. Long continuing current in negative lightning ground flashes. *Journal of Geophysical Research*, 95(D5):5455–5470, 1990.

V. A. Rakov, M. A. Uman, M. I. Fernandez, C. T. Mata, K. J. Rambo, and M. V. Stapleton. Direct lightning strikes to the lightning protective system of a residential building: Triggered-lightning experiments. *IEEE Transactions on Power Delivery*, 2000, to be published.

V. A. Rakov, M. A. Uman, K. J. Rambo, M. I. Fernandez, R. J. Fisher, G. H. Schnetzer, R. Tottappillil, A. Eybert-Berard, J. P. Berlandis, P. Lalande, A. Bonamy, P. Laroche, and A. Bondiou-Clergerie. New insights into lightning processes gained from triggered-lightning experiments in Florida and Alabama. *Journal of Geophysical Research*, 103:14,117–14,130, 1998.

V. A. Rakov, M. A. Uman, and R. Thottappillil. Review of lightning properties from electric field and TV observations. *Journal of Geophysical Research*, 99(D5):10745–10759, May 1994.

M. Rubinstein, M. A. Uman, P. J. Medelius, and E. M. Thomson. Measurements of the voltage induced on an overhead power line 20 m from triggered lightning. *IEEE Transactions on Electromagnetic Compatibility*, 36(2):134–140, May 1994.

H. M. Ryan. *High Voltage Engineering and Testing*. Peter Peregrinus Ltd., United Kingdom, 1994.

M. N. O. Sadiku. *Numerical Techniques in Electromagnetics*. CRC Press, Boca Raton, Florida, 1992.

W. Schmidt, J. Meppelink, B. Richter, K. Feser, L. E. Kehl, and D. Qiu. Behaviour of mo-surge-arrester blocks to fast transients. *IEEE Transactions on Power Delivery*, 4(1):292–300, Jan 1989.

H. M. Schneider and H. R. Stillwell. Measurement of lightning current waveshapes on distribution systems. *IEEE PES Summer Meeting*, Paper A 79 526-5, July 15–20 1979.

A. J. Schwab. *High-Voltage Measurement Techniques*. M.I.T. Press, Cambridge, Mass., 1972.

A. Semlyen and A. Dabuleanu. Fast and accurate switching transient calculations on transmission lines with ground return using recursive convolutions. *IEEE Transactions on Power Apparatus and Systems*, PAS-94(2):561–571, Mar-Apr 1975.

G. A. Shneerson. *Field and Transients in Superhigh Pulse Current Devices*. Nova Science Publishers, Inc., New York, 1997. Horizons in World Physics, Volume 223.

G. Simpson and F. J. Scrase. The distribution of electricity in the thunderclouds. *Proc. R. Soc. London Ser. A*, 161:309–352, 1937.

J. K. Snelson. Propagation of travelling waves on transmission lines. frequency dependent parameters. *IEEE Transactions on Power Apparatus and Systems*, PAS-91(1):Jan–Feb, January 1972.

R. Soler, A. Rousseau, and M. Serrano. Modelling of thermal phenomena in zinc-oxide surge arresters. *Electr Fr Bull Dir Etud Rech*, Ser A(1):63–79, 1991.

F.R. Stockum. Simulation of the nonlinear thermal behavior of metal oxide surge arresters using a hybrid finite difference and empirical model. *IEEE Transactions on Power Delivery*, 9(1):306–313, January 1994.

M. Stolzenburg, W. D. Rust, and T. C. Marshall. Electrical structure in thunderstorm convective regions 3. Syntesys. *Journal of Geophysical Research*, 103(D12):14,097–14,108, June 1998.

E. J. Tarasiewicz, F. Rimmer, and A. S. Morched. Transmission line arrester energy, cost, and risk of failure analysis for partially shielded transmission lines. *IEEE Transactions on Power Delivery*, 15(3):919–924, July 2000.

R.S. Thallam, J.L. Koepfinger, G.E. Lee, D.J. Melvold, D.W. Lenk, J.B. Posey, D. Worden, D. Dawson, S.G. Whisenant, K.B. Stump, and R. Odenberg. Bibliography of metal oxide surge arresters, 1990-1992. *IEEE Transactions on Power Delivery*, 10(3):1285–1300, July 1995.

R. Thottappillil, J. D. Goldberg, V. A. Rakov, and M. A. Uman. Properties of M components from currents measured at triggered lightning channel base. *Journal of Geophysical Research*, 100(D12):25711–25720, December 1995.

M. A. Uman. *The Lightning Discharge*. Academic Press, San Diego, California, 1987.

M. A. Uman, V. A. Rakov, K. J. Rambo, T. W. Vaught, M. I. Fernandez, D. J. Cordier, R. M. Chandler, R. Bernstein, and C. Golden. Triggered-lightning experiments at Camp Blanding, Florida (1993-1995). *Trans. IEE Japan, Special Issue on Artificial Rocket Triggered Lightning*, 117-B(4):446–452, 1997.

D. Wang, V. A. Rakov, M. A. Uman, N. Takaggi, T. Watanabe, D. E. Crawford, K. J. Rambo, G. H. Schnetzer, R. J. Fisher, and Z. I. Kawasaki. Attachment process in rocket triggered lightning strokes. *Journal of Geophysical Research*, 104:2143–2150, 1999.

R. K. Wangsness. *Electromagnetic Fields*. John Wiley & Sons, Inc., second edition, 1986.

R. G. Wasley and S. Selvavinayagamoorthy. Approximate frequency-response values for transmission-line transient analysis. *Proceedings of the Institute of Electrical Engineering*, 121(4):281–286, April 1974.

J.J. Woodworth and R.S. Thallam. Bibliography of metal oxide surge arresters, 1989-1990. *IEEE Transactions on Power Delivery*, 8(3):1000–1034, July 1993.

BIOGRAPHICAL SKETCH

Carlos T. Mata received his bachelor's degree from the "Universidad Simón Bolívar" (USB), Venezuela in 1993, and his master's and Ph.D. degrees at the University of Florida (UF) in 1997 and 2000, respectively. Mr. Mata is involved in the area of computer modeling of different lightning processes and responses of power distribution systems to direct and nearby lightning strikes. Since 1997 he has held a graduate research assistantship in the UF Lightning Research Laboratory, conducting experiments at the International Center for Lightning Research and Testing, (ICLRT). Mr. Mata has also taught several graduate and undergraduate courses in the Electrical and Computer Engineering Department at UF, and the Power System Analysis (EMTP Short Course) offered every year as part of the Division of Continuing Education at UF. In 1998 Mr. Mata was awarded with the GAANN program (Graduate Assistance in Areas of National Need). He is author or coauthor of five journal publications and six technical reports. Mr. Mata is a student member of the American Geophysical Union (AGU), the Institute of Electrical and Electronics Engineers (IEEE) and the Power Engineering Society (PES). Mr. Mata was in charge of the design, installation, and calibration of measuring equipment on the distribution lines tests in 1999 and 2000 at the ICLRT. He also wrote a series of computer-oscilloscope interface programs for data acquisition automation, control, plotting, and analysis of the acquired data.

I certify that I have read this study and that in my opinion it conforms to acceptable standards of scholarly presentation and is fully adequate, in scope and quality, as a dissertation for the degree of Doctor of Philosophy.



Vladimir A. Rakov, Chairman
Professor of Electrical and Computer
Engineering

I certify that I have read this study and that in my opinion it conforms to acceptable standards of scholarly presentation and is fully adequate, in scope and quality, as a dissertation for the degree of Doctor of Philosophy.



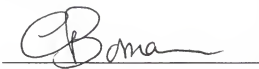
Martin A. Uman, Cochairman
Professor of Electrical and Computer
Engineering

I certify that I have read this study and that in my opinion it conforms to acceptable standards of scholarly presentation and is fully adequate, in scope and quality, as a dissertation for the degree of Doctor of Philosophy.



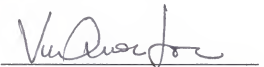
Dennis P. Carroll
Professor of Electrical and Computer
Engineering

I certify that I have read this study and that in my opinion it conforms to acceptable standards of scholarly presentation and is fully adequate, in scope and quality, as a dissertation for the degree of Doctor of Philosophy.



Gijs Bosman
Professor of Electrical and Computer
Engineering

I certify that I have read this study and that in my opinion it conforms to acceptable standards of scholarly presentation and is fully adequate, in scope and quality, as a dissertation for the degree of Doctor of Philosophy.



Loc Vu-Quoc
Professor of Aerospace Engineering,
Mechanics and Engineering Science

This dissertation was submitted to the Graduate Faculty of the College of Engineering and to the Graduate School and was accepted as partial fulfillment of the requirements for the degree of Doctor of Philosophy.

December 2000



M. J. Ohanian
Dean, College of Engineering

Winfred M. Phillips
Dean, Graduate School

LD
1780
2000
M425

UNIVERSITY OF FLORIDA



3 1262 08555 0423